DISS. ETH NO. 24040

Dendronized Polymers with Tailored Intermolecular Interactions: Synthesis and Thermomechanical Characterization

A thesis submitted to attain the degree of

DOCTOR OF SCIENCES of ETH ZURICH

(Dr. sc. ETH Zurich)

presented by

LEON FLORIAN SCHERZ

M.Sc. in Chemistry, Technical University of Munich

born on 21.06.1988

citizen of Germany

accepted on the recommendation of

Prof. Dr. A. D. Schlüter, examiner

Prof. Dr. D. Vlassopoulos, co-examiner

Prof. Dr. J. Vermant, co-examiner

2017

"Les questions les plus intéressantes restent des questions. Elles enveloppent un mystère. A chaque réponse, on doit joindre un «peut-être». Il n'y a que les questions sans intérêt qui ont une réponse définitive."

(Eric-Emmanuel Schmitt, 2002)

Acknowledgement

First and foremost, I would like to thank **Prof. A. Dieter Schlüter** for providing me with the chance to earn my PhD at the Institute of Polymers and to perform research in the field of dendronized polymers. Throughout my doctoral studies, he was always very reassuring and his balanced personality made for an enjoyable working atmosphere. Moreover, I would like to thank him for the opportunity to present my work at conferences and the chance to engage in diverse projects and collaborations. Finally, I would like to thank Prof. Schlüter for conveying to me the importance of communication and diplomacy.

A particular motivation for this thesis has been the rheological characterization of dendronized polymers in the melt. This has been advanced in collaboration with the group of **Prof. Dimitris Vlassopoulos** (Foundation for Research & Technology – Hellas (FORTH), Heraklion, Crete, Greece). Therefore, I would like to express my sincerest gratitude to Prof. Vlassopoulos for sharing his great expertise in rheology and his dedication to this undertaking. Throughout my PhD, his immeasurable pursuit of high-quality research and fine scientific writing has always been very motivating and inspiring. Moreover, I would like to thank **Salvatore Costanzo** for performing the rheological measurements on the bulk dendronized polymer samples, his commitment to this project and the many enlightening discussions we had. His ability to handle even the lowest amounts of samples with great care as well as his patience at explaining the obtained results have always been highly appreciated.

An additional motivation for this thesis has been to investigate the behavior of dendronized polymers at the air-water interface in collaboration with the group of **Prof. Jan Vermant** (Laboratory of Soft Materials, ETH Zurich). Therefore, I would like to thank Prof. Vermant for sharing his expertise in the field of soft matter and valuable discussions regarding the behavior of polymers at the air-water interface. In particular, I would like to thank **Martina Pepicelli** for performing the surface rheological characterization of dendronized polymers on the Langmuir trough. I am very thankful for her efforts and her detailed updates on the progress of the measurements, even though the results obtained will not be discussed in greater detail in this work.

Moreover, I would like to thank **Prof. Martin Kröger** (Polymer Physics, ETH Zurich) for his atomistic simulations on dendronized polymer interactions and encouraging and motivating discussions.

Many thanks go to **Dr. Mona Abdel-Rahman** (Department of Chemistry, Assiut University, Egypt) for the opportunity to work on an interesting topic that, unfortunately, is outside the scope of this thesis and therefore not mentioned further in this work. Nevertheless, her enthusiasm for science and her dedication to our project has been very inspiring.

Additionally, I would like to thank **Dr. Thomas Schweizer**. Thomas provided excellent technical support and managed to repair machines whenever they were broken in a minimum amount of time. I would also like to thank Thomas for taking the time to discuss results from gel permeation chromatography, differential scanning calorimetry and thermogravimetric analyses. In addition, I would like to acknowledge his contribution to the characterization of dendronized polymers by nonlinear rheology and his custom built CPP3 device, which will also not presented to a greater detail in this thesis.

Throughout my PhD, I had the privilege to present my research to **Prof. Gerhard Wegner** (Max Planck Institute for Polymer Research, Mainz, Germany) during his annual stays in our group. I would like to thank Prof. Wegner for showing interest in my work and for sharing his vast and interdisciplinary scientific knowledge in many intense and fruitful discussions.

I would like to thank **Sabrina Sant** and **Constantin Sahm**, who carried out semester projects within the framework of this thesis. In particular, I would like to acknowledge their contributions to the efficient synthesis and characterization of macromonomers bearing ureido pyrimidinone moieties and photolabile protecting groups. I would also like to thank **Simon Leu**, who carried our his Bachelor's thesis under my supervision. In addition to his contributions to the development of novel hybrid dendronized polymers, I am also grateful for his trust and motivation throughout his thesis.

Prof. Nicolas Spencer (Laboratory for Surface Science and Technology, ETH Zurich) and **Dr. Shivaprakash Ramakrishna** are thanked for providing access to their atomic force microscope and training on the machine. **Prof. Lucio Isa** (Laboratory for Interfaces, Soft matter and Assembly, ETH Zurich) is thanked for granting access to the dynamic light scattering machine.

Many thanks go to **Dr. Damir Bozic** (Department of Materials, ETH Zurich), who supported the group in all IT-related matters in an excellent way.

The **Swiss National Fund** is acknowledged for financial support under the framework of the grant 143211.

Special thanks go to **Daniela Zehnder** for taking excellent care of organizational matters and for her ever-present kind and supportive attitude.

My labmates, **Richard Bernitzky**, **Dr. Bernd Deffner**, **Dr. Chiara Gstrein**, **Philipp Tanner** and **Dr. Wei Wang** are thanked for the nice working atmosphere, cordial relation, support in the lab, and many fruitful discussions. In this context, I would also like to express special thanks to **Daniel Messmer** for sharing his extensive knowledge related to dendronized polymers, many helpful discussions, and for proofreading both my research plan and this thesis. In addition, I would like to thank all former and present members of the **Schlüter Group**, particularly **Deguang Zhang**, **Dr. Katja Junker**, **Ralph Lange**, **Sandra Luginbühl**, **Stan van de Pol**, **Dr. Tim Hunger-**

land, **Vivian Müller**, **Wenyang Dai**, **Dr. Xiaoyu Sun**, and **Prof. Yingjie Zhao** for friendly relations, many helpful discussions and esteemed support.

Moreover, I would like to express my sincerest gratitude to my parents, **Elvira** and **Slavo**, and my sister, **Livia**, for their continuing support, particularly in testing times.

Finally, I would like to cordially thank my girlfriend, **Michaela**, for putting in great efforts to make our long-distance relationship work throughout my PhD. Her caring and encouraging nature has always been a strong support over the years.

Abstract

Dendronized polymers (DPs) represent an intriguing class of macromolecules that combines the concepts of dendrimers and polymers. By tailoring their cross-sectional thickness and persistence length through the generation number (g) and backbone degree of polymerization (P_n), respectively, DPs can be endowed with a wide range of conformations, spanning from flexible polymers to shape-persistent molecular objects.

In this work, several key structural parameters of DPs, including P_n, g, and the ability to engage in intermolecular hydrogen bonding interactions, have been systematically varied to arrive at a matrix of 44 different DPs, the thermomechanical properties of which have been investigated to explore the intrinsic properties of these interesting materials. More specifically, a series of well-studied, i.e. "classic", DPs was modified through hybridization with first- and second-generation oligo(ethylene glycol)-based dendrons to suppress intermolecular hydrogen bonding. Moreover, a series of DPs with enhanced hydrogen bonding interactions was prepared via controlled radical copolymerization of the "classic" macromonomer with a ureidopyrimidinone (UPy)-containing analogue. Apart from the "hybrid" DPs, which could not be fully redissolved from a non freeze dried state, the average molecular weights of all synthesized polymers were determined by gel permeation chromatography (GPC) against poly(methyl methacrylate) standards. In addition, labeling experiments proved the high degrees of structure perfection of the synthesized DPs (>99%). For the "classic" DPs, the determined degrees of structure perfection were confirmed by thermogravimetric analysis (TGA), which also proved applicable for the UPy-functionalized DPs. Here, it could be shown that both Boc and UPy moieties contribute to the initial weight loss up to $\approx 300\,^\circ\mathrm{C}$ and that the initial degradation temperatures decreased with increasing UPy content from $\approx 223\,^\circ\mathrm{C}$ to $\approx 209\,^\circ\mathrm{C}$, consistently, irrespective of g. This led to the proposition of a mechanism in which UPy catalyzed the thermolysis of Boc moieties. However, due to the relatively large errors of the method ($\pm 3\%$) that rendered the comparatively small molar mass differences of the repeating units statistically invariant, TGA could not be established as a complementary method to ^{1}H NMR spectroscopy for the determination of the composition ratios of Boc and UPy-functionalized macromonomers in the respective copolymers. For the synthesized UPy-functionalized DPs, a combination of dynamic light scattering (DLS), GPC, and ^{1}H NMR spectroscopy was employed to investigate their collapse into single-chain polymeric nanoparticles (SCPNs) in aprotic solvents such as $CHCl_3$. Thereby, it could be shown that the cohesive strength of the formed SCPNs is governed by the concentration of UPy moieties along the polymer backbone and that intramolecular UPy-UPy dimerization in higher-generation DPs remains possible in the realm of close spatial proximity of the UPy-moieties, only. The glass-liquid transition of the prepared DPs was investigated using differential scanning calorimetry (DSC), which revealed that the DPs are amorphous materials, the glass transition temperature (T_g) of which is affected by g, P_n, the chemical

properties of the peripheral end groups, and the strength of bonding interactions. The T_g values of the "classic" DPs approach a final value of $\approx 70\,^{\circ}\mathrm{C}$ with increasing g and P_n, whereas the higher segmental mobility of the "hybrid" DPs results in significantly lower T_g values (as low as $T_g \approx -45\,^{\circ}\mathrm{C}$). In contrast, at comparable P_n, the T_g values of the UPy-functionalized DPs increase in a linear fashion as a function of the UPy content from $\approx 40\,^{\circ}\mathrm{C}$ (0 mol% UPy) to $\approx 130\,^{\circ}\mathrm{C}$ (50 mol% UPy) and the formation of supramolecular DP networks, respectively. Upon immersing the UPy moieties in higher-generation DPs, the T_g values of DPs containing high and low amounts of UPy moieties converged, which was ascribed to a shift of the UPy-dimerization from inter- to intramolecular. All studied DPs underwent very slow ageing in the region of hours owing to the reduced global mobility of these bulky molecules. Even so, the segmental mobility was found to be increased in the "hybrid" DPs and constrained in the UPy-functionalized DPs, which translated into vastly different equilibration times (few hours to hundreds of hours), as inferred from oscillatory time sweep measurements. The very large entanglement molecular weight of the "classic" DPs was found to cause a frequency dependent rheological response, which is typically characterized by low values of the entanglement plateau modulus in the low frequency regime, similar to bottlebrush polymers but tuneable through both g and P_n. More specifically, the origin of the elastic plateau was ascribed to the interpenetration of neighboring molecules in the melt and hydrogen bonding interactions, which effectively enhanced the "molecular friction" between DPs. Increasing g and P_n both enhance the contact areas and the backbone-to-backbone correlation between individual DPs, as was also suggested by small-angle X-ray scattering. In contrast, the shielded hydrogen bonding interactions in the "hybrid" DPs significantly reduce the molecular friction between DPs and result in a weak gel-like behavior with no apparent onset of an elastic plateau, irrespective of P_n. On the other hand, it could be demonstrated that the incorporation of UPy-moieties in DPs can further broaden the scope of rheological responses, as exemplified by the transition from liquid-like to solid-like behavior observed for short-chained DPs with increasing UPy-content. The rheological data obtained from higher-generation UPy-functionalized DPs supports the findings obtained from DSC and indicates that already one layer of dendrons suffices to effectively reduce the probability for intermolecular UPy-dimerization and prevent the formation of the supramolecular DP network. The combined results have demonstrated remarkable effects of the chemical structure on the viscoelastic properties of such super soft elastomers with ultra-high molar mass and pave the way into applications such as concrete plasticization or priming.

Kurzfassung

Dendronisierte Polymere (DPs) stellen eine faszinierende Polymerklasse dar, welche die Konzepte von Dendrimeren und Polymeren verbindet. Da sich ihre Querschnittsdicke und Persistenzlänge durch die Generation (g) und den Polymerisationsgrad (P_n) einstellen lässt, können DPs ein breites Spektrum an Konformationen annehmen, welches von flexiblen Polymeren bis hin zu formstabilen molekularen Objekten reicht.

Im Rahmen der vorliegenden Arbeit wurden verschiedene strukturelle Parameter, im Speziellen P_n, g, sowie die Möglichkeit zur Ausbildung intermolekularer Wasserstoffbrückenbindungen, systematisch variiert, um anhand eines Probensatzes von 44 verschiedenen DPs ihre thermomechanischen Eigenschaften zu untersuchen und die intrinsischen Eigenschaften dieser interessanten Materialien näher zu beleuchten. Ausgehend von umfangreich charakterisierten "klassischen" DPs wurden durch das Anbringen von Oligoethylenglykol-basierten Dendronen "Hybridpolymere" hergestellt, die keine intermolekularen Wasserstoffbrücken eingehen können. Darüber hinaus wurde durch Copolymerisation des "klassischen" Macromonomers mit einem Ureidopyrimidinon (UPy)-haltigen Analogon eine Reihe von UPy-funktionalisierten DPs (UPy-DPs) hergestellt, welche extrem starke Wasserstoffbrücken ausbilden können. Mit Ausnahme der "Hybridpolymere", welche ohne vorangegangene Gefriertrocknung nicht erneut vollständig gelöst werden konnten, wurden die durchschnittlichen Molekulargewichte aller DPs mittels Größenausschlusschromatographie (GPC) gegen Polymethylmethacrylat Standards bestimmt. Darüber hinaus wurde die hohe Strukturintegrität der synthetisierten Polymere (>99%) durch UV-Markierungsexperimente bestimmt und für die "klassischen" Polymere mit den zwei längsten P_ns exemplarisch mittels thermogravimetrischer Analyse (TGA) bestätigt. TGA wurde ebenfalls für die UPy-DPs eingesetzt, wobei gezeigt werden konnte, dass Boc- und UPy-Gruppen gemeinsam zum Masseverlust bis zu einer Temperatur von $\approx 300\,^\circ\mathrm{C}$ beitragen und die anfängliche Zersetzungstemperatur - unabhängig von g - mit steigendem UPy-Gehalt von $\approx 223\,^\circ\mathrm{C}$ auf $\approx 209\,^\circ\mathrm{C}$ sinkt. In diesem Zusammenhang wurde ein Mechanismus zur UPy-katalysierten thermischen Abspaltung der Boc Gruppen vorgeschlagen. Aufgrund des relativ großen Messfehlers der Methode ($\pm 3\%$) und den vergleichsweise kleinen Molmassenunterschieden der verschiedenen UPy-DPs war es jedoch nicht möglich, die Copolymerzusammensetzung thermogravimetrisch zu bestimmen und TGA als komplementäre Methode zur ^{1}H NMR Spektroskopie erfolgreich einzusetzen. Zur Untersuchung der sich aus UPy-DPs bildenden polymeren Nanopartikeln, welche aus einzelnen Ketten bestehen (SCPNs), wurde eine Kombination aus dynamischer Lichtstreuung (DLS), GPC, und ^{1}H NMR Spektroskopie eingesetzt. Dadurch konnte gezeigt werden, dass der Zusammenhalt der SCPNs durch die Konzentration der UPy-Gruppen entlang der Hauptkette bestimmt wird und dass die UPy-Gruppen in DPs mit höheren g lediglich dann intramolekular dimerisieren können, wenn sie sich in direkter räumlicher Nähe zueinander befinden. Der Wärmeübergang der hergestellten DPs wurde mittels

dynamischer Differenzkalorimetrie (DSC) untersucht. Bei den vorgestellten Polymeren handelt es sich um amorphe Materialien, deren Glasübergangstemperatur (T_g) durch g, P_n, die chemischen Eigenschaften der Endgruppen und die Stärke der anziehenden Wechselwirkungen bestimmt wird. Die T_g-Werte der "klassischen" DPs näherten sich mit zunehmender g und P_n einem Wert von $\approx 70\,°C$ an, wohingegen die höhere Kettensegmentbeweglichkeit der "Hybridpolymere" zu deutlich niedrigeren T_g-Werten (bis zu $T_g \approx -45\,°C$) führte. Dagegen stiegen die T_g-Werte der UPy-DPs durch die Ausbildung eines supramolekularen Netzwerkes bei gleichbleibendem P_n mit steigendem UPy-Gehalt annähernd linear von $\approx 40\,°C$ (0 mol% UPy) auf $\approx 130\,°C$ (50 mol%) an. Die Abschirmung der UPy-Gruppen in höheren g führte zur Annäherung der T_g-Werte von stark und geringfügig UPy-funktionalisierten DPs, was durch den Wechsel von inter- zu intramolekularer UPy-Dimerisierung erklärt werden kann. Die physikalische Alterung der untersuchten DPs erfolgte sehr langsam, über einen Zeitraum von Stunden, was mit ihrer eingeschränkten Beweglichkeit zusammenhängt. Dennoch führten die Unterschiede in der jeweiligen Kettensegmentbeweglichkeit im Fall der "Hybridpolymere" sowie der UPy-DPs zu stark unterschiedlichen Zeiten (wenige Stunden bis zu hunderte von Stunden) bis zur Gleichgewichtseinstellung. Es konnte gezeigt werden, dass das sehr hohe Verschlaufungsmolekulargewicht "klassischer" DPs ein frequenzabhängiges rheologisches Verhalten hervorruft, welches üblicherweise durch das Auftreten eines elastischen Plateaus bei niedrigen Frequenzen gekennzeichnet ist und dem von Polymerbürsten ähnelt, jedoch durch g und P_n einstellbar ist. Der Ursprung des elastischen Plateaus ist auf die Verzahnung von benachbarten Molekülen in der Schmelze sowie Wasserstoffbrückenbindungen zurückzuführen, welche die Reibung zwischen den DPs erhöhen. Kleinwinkel-Röntgenstreuung bestätigte, dass dabei sowohl die Kontaktfläche als auch die wechselseitige Ausrichtung der Hauptketten mit zunehmender g und P_n zunehmen. Im Gegensatz dazu führt das Ausschalten der intermolekularen Wasserstoffbrücken in den "Hybridpolymeren" dazu, dass die Reibung zwischen den DPs stark herabgesetzt ist und das rheologische Verhalten - unabhängig von P_n - dem eines schwachen Gels ähnelt. Ebenfalls konnte gezeigt werden, dass die Bandbreite des rheologischen Verhaltens von DPs durch den Einbau von UPy-Gruppen nochmals deutlich erweitert werden kann, wie am Beispiel von kurzkettigen Proben mit steigendem UPy-Gehalt und dem dadurch hervorgerufenen Übergang von viskosem zu elastischem Verhalten gezeigt wurde. Die für höhere g erhaltenen Resultate werden durch die DSC-Ergebnisse gestützt und deuten darauf hin, dass bereits eine weitere Generation ausreicht, um intermolekulare UPy-Wechselwirkungen und die Ausbildung eines supramolekularen Netzwerkes zu unterbinden. Die gewonnenen Erkenntnisse belegen den Einfluss der chemischen Struktur auf die rheologischen Eigenschaften dieser superweichen Elastomere mit sehr hohen Molekulargewichten und ebnen den Weg hin zu Anwendungen, z.B. in der Betonverflüssigung oder in Grundierungen.

Contents

1 Introduction

1.1 Polymers

1.1.1 Concept

1.1.1.1 Classification by macromolecular composition

Since the seminal studies by Staudinger et al. in the early 1920s, the modern understanding of polymers has much evolved. Historically, polymers have commonly been understood as large yet relatively simple structures composed of covalently connected building blocks called repeating units. In the simplest case, the repeating units are connected to each other to form a linear homopolymer, as illustrated in Figure 1-1(a). If there are two or more structural units involved, the term copolymer is used (cf. Figure 1-1(b) – (e)). In both cases, the average number of repeating units present in the polymeric main chain is referred to as the degree of polymerization (P_{n}). Today, the spectrum of polymers that can be prepared encompasses virtually any desired distribution of repeating units along the polymer main chain or within any specific segment in a copolymer. Hence, linear copolymers can be divided into random copolymers (b), alternating copolymers (c), gradient copolymers (d), as well as block copolymers (e) comprising covalently joined homopolymer sequences.[1]

Figure 1-1: Schematic representation of linear polymer microstructures encompassing homo- (**a**) and copolymers (**b** – **e**). Copolymers can be further divided into random (**b**), alternating (**c**), gradient (**d**), or block (**e**) copolymers.

1.1.1.2 Classification by macromolecular structure

Apart from linear chains, both homo- and copolymers can also comprise branched structures. Branching can arise through several routes, such as chain transfer to polymer by which the activity of a growing polymer chain is transferred to another existing polymer

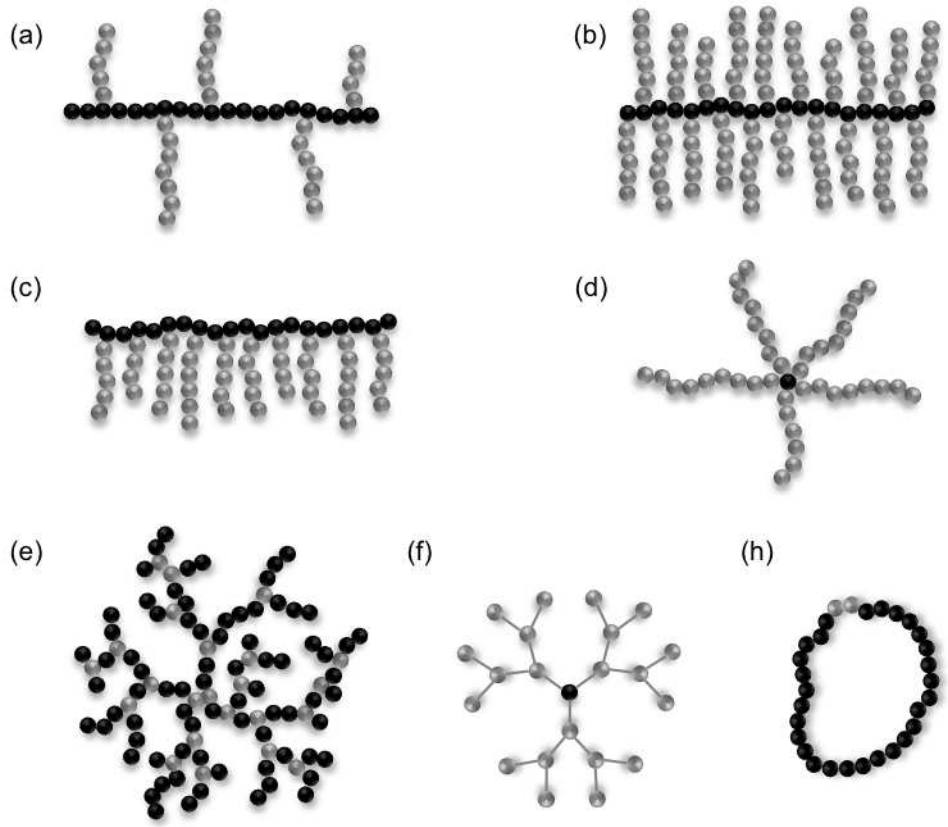

Figure 1-2: Schematic representation of a selection of macromolecular structures, including graft (**a**), bottle brush (**b**), comb (**c**), star (**d**), hyperbranched (**e**), dendrimers (**f**), and cyclic polymers (**h**).

chain.[2] Further examples include the deliberate use of multifunctional monomers directly in the polymerization reaction or grafting of either preformed polymer chains to- ("graft to") or monomers from ("graft from") sites along an existing backbone.[1] As depicted in Figure 1-2, several macromolecular structures can be distinguished depending on the density, furcation and location of the junction points. Nominally, the term "graft polymer" is used for polymers in which one or more of the linear side chains are structurally and/or configurationally different from the backbone (cf. Figure 1-2(a)). In this context, a distinction between "graft" and "bottle brush" polymers can be made according to the graft density, with higher graft densities affecting both the conformation and physical properties of the resulting brush-like macromolecules (b).[3] In the "comb polymers", branches emanate from three-way branch points, two of which are involved in the formation of a linear backbone (c).[4] In "star" polymers (d),[5] all branches radiate from a single branch point. Moreover, extensive branching may even lead to the formation of giant three-dimensional, cross-linked polymer networks, provided that the concentration of branching points is high enough. Since the cohesiveness in these molecules is brought about by covalent bonds, the cross-links in these networks are permanent. This is in contrast to transient networks comprising reversible cross-links by intermolecular forces.

However, cross-linking can also be suppressed in such a way that the highly branched molecules, i.e. hyperbranched polymers (e), remain discrete entities.[6] Dendrimers represent another important class of highly branched molecules (f).[7] Due to their step-wise mode of synthesis, these tree-like molecules feature well-defined molecular structures and - ideally - uniform molecular masses. Although they are currently of academic interest rather than of commercial importance, cyclic polymers depict a final class of non-linear polymers, in which linear chains form loops (h).[8]

1.1.2 Polymer synthesis

The previous section addressed the concept of polymers and presented various macromolecular structures in which polymers can be classified. In the following, Section 1.1.2.1 aims at providing an overview over the conceptual approaches used for the preparation of polymers in general, complemented by a more detailed description of the free and controlled radical chain-growth polymerization mechanisms in Sections 1.1.2.2 and 1.1.2.3, respectively.

1.1.2.1 Classification of polymerization reactions

In the late 1920s, Carothers suggested a classification of polymers into addition and condensation polymers as per the reactions underlying their preparation.[9, 10] Accordingly, polymers prepared by condensation lack certain atoms from the monomer units, which are usually liberated as small byproducts. In contrast, the numbers of atoms in the repeating units of addition polymers are identical to the monomers from which they are derived. In 1953, Flory proposed a superior definition based on the reaction mechanism involved in the formation of polymers, i.e. a classification into step growth polymers and chain growth polymers (cf. Figure 1-3).[2] According to this definition, macromolecules prepared by chain growth polymerization are formed in chain propagating reactions, i.e. by the addition of monomers to the reactive sites of growing chains. In such reactions, high molar mass polymers are achieved quickly, whereby longer reaction times result in higher degrees of conversion but do not affect much the (average) molecular weight of the polymers if a (self-)termination step exists. Monomers are present throughout the polymerization and their concentration decreases steadily with increasing reaction time (cf. Figure 1-3(a)). Furthermore, different stages, i.e. initiation, propagation, termination, and chain transfer, exist in chain growth polymerizations, which all feature distinct mechanisms and very different rate constants (cf. Section 1.1.2.2). In contrast, macromolecules originating from step growth polymerizations are formed in discrete steps (cf. Figure 1-3(b)). The important features of step growth polymerizations include rapid conversion of monomer early in the reaction, while the increase in molecular weight at low conversion occurs only slowly due to the formation of statistically distributed low oligomers. Unlike in chain growth reactions, the molar masses of the formed species build up slowly

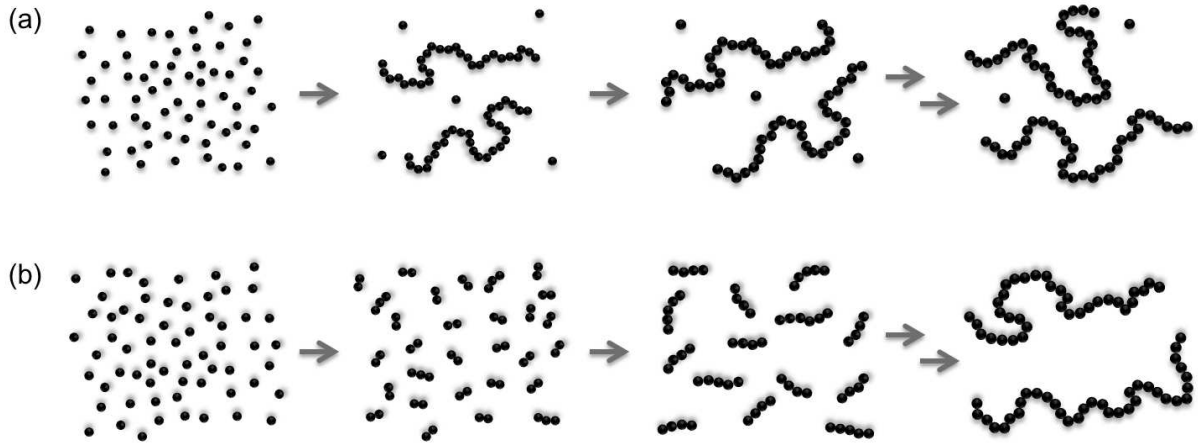

Figure 1-3: Schematic representation of the conversion dependence of polymer molar mass in chain growth polymerizations (**a**) and step growth polymerizations (**b**). The four cartoons in each row depict snapshots of the polymerization mixtures over the course of the polymerizations.

through the entire polymerization and products comprising high molecular weights are only formed after sufficiently long reaction times and when high conversions of typically >98% have been reached. Owing to the lack of a termination step, the end groups of step growth polymers remain active throughout the polymerization. Moreover, step-growth polymerizations do not require the use of initiators and the same reaction mechanism applies throughout the polymerization. Figure 1-4 qualitatively illustrates the degrees of conversion required to obtain polymers with high average molecular weights for different polymerization mechanisms.

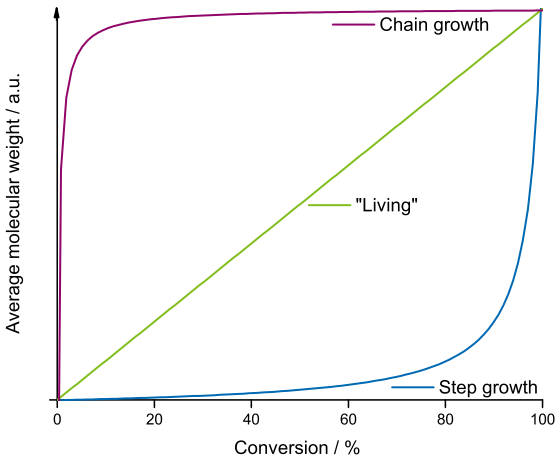

Figure 1-4: Qualitative plot of the average molecular weight of polymers as a function of monomer conversion for chain growth polymerizations (with self-termination), step growth polymerizations, and ”living” polymerizations.

1.1.2.2 Free-radical chain growth polymerization

Polymerizations following a free-radical mechanism are typical chain growth reactions that feature three distinct reaction phases, i.e. initiation, propagation, and termination, as illustrated in Scheme 1-1. In the initiation stage, the formation of initiating radicals can be achieved in manifold ways, including thermal- or light-induced decomposition of compounds, redox reactions, or ionizing radiation, and represents the rate-determining step. The decomposition of compounds containing peroxo or azo groups represents arguably the most prominent approach. Once the initiating radicals are formed, the addition reaction to the monomer competes with other possible secondary reactions such as the recombination of radicals promoted by the "cage effect" of the solvent molecules,[11] which reduces the initiator's efficiency. In this regard, it has been shown that the viscosity of the reaction medium is inversely proportional to the efficiency of initiators due to the concomitantly enhanced cage-effect.[12] Moreover, the reaction between a radical and another molecule can either lead to the formation of a different initiating species or constitute a dead end for the polymerization reaction. After the initiating radical has diffused into

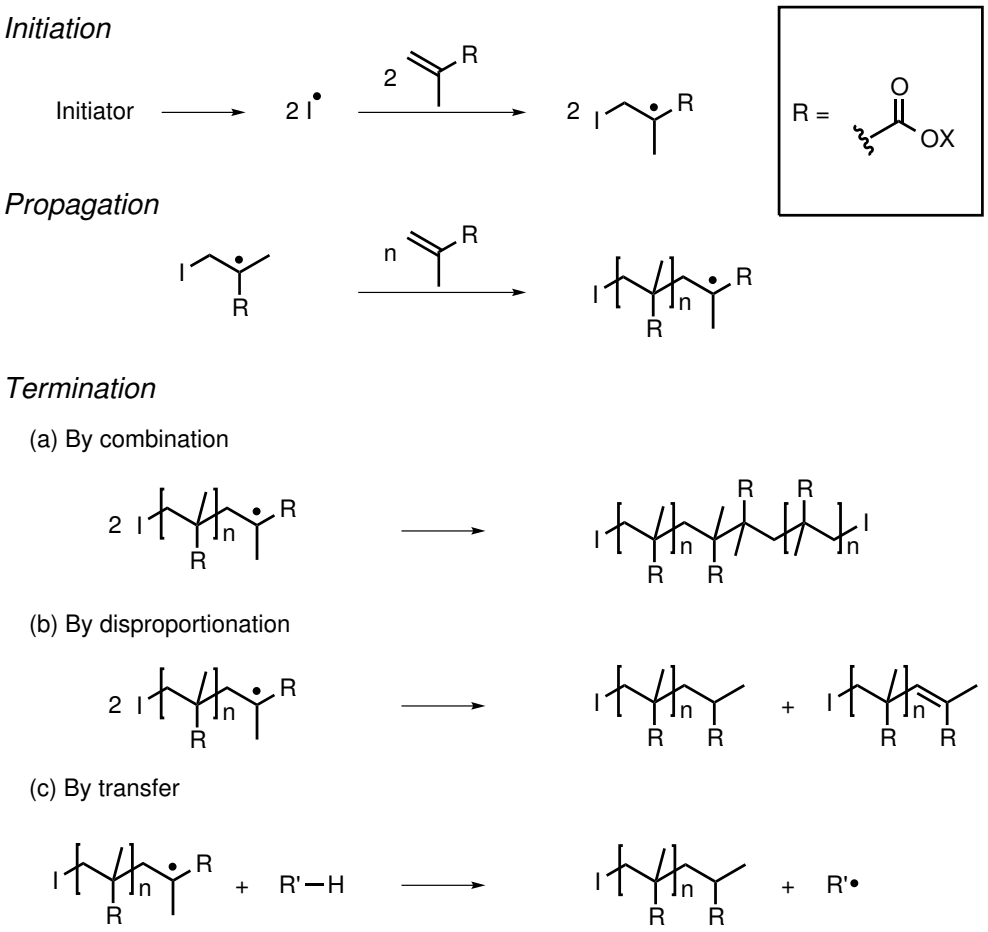

Scheme 1-1: Generic mechanism for the free-radical chain growth polymerization (FRP) of methacrylate monomers reproduced from reference [13].

the proximity of the monomer, the capture of the free radical by the monomer completes the initiation reaction. Subsequently, the propagation stage is characterized by fast and repeated monomer additions to macroradicals carrying an unpaired electron at the active polymer chain end. The interaction between the active chain end and the monomer takes place between the p-orbitals of both species and results in the formation of a σ-bond at the expense of a double bond, whereby the loss of unsaturation constitutes the key driving force. Finally, the free-radical propagation stage can be terminated by three types of reactions: Firstly, two radicals that are located on the active chain ends of different macroradicals can combine to form a covalent bond and a larger polymer chain, respectively (cf. Scheme 1-1(a)). Secondly, the two macroradicals can also react in a disproportionation reaction, whereby one of them abstracts an atom (usually hydrogen) from the other one. This results in the formation of two inactive polymer molecules differing from each other in that one has a terminal saturated structure and the other one has a terminal double bond (cf. Scheme 1-1(b)). Generally, the higher activation energies required for disproportionation reactions favor termination by recombination, especially at lower temperatures. On a related note, high monomer concentrations in solution or in bulk polymerizations may give rise to auto-accelerated polymerization rates and the so-called "Trommsdorff" effect. Here, the underlying cause is that the termination rates decrease due to the increased viscosity of the reaction medium caused by the formed polymers. More specifically, the increased viscosity restricts the mobility of large polymer radicals and hampers their ability to undergo termination reactions while, at the same time, the comparably small monomers can still diffuse to the active chain ends and propagate the chain growth. Thirdly, termination can also proceed via transfer reactions, which result in the formation of a terminated polymer molecule and, often, a new free radical capable of new initiation (cf. Scheme 1-1(c)). Thereby, the molecules that participate in chain transferring can be any of those present in the reaction medium, including solvents, monomers, inactive polymeric chains, and initiators. Moreover, transfer reactions can also occur from the active polymer chain end to a location on the polymeric backbone in a process known as "backbiting". In principle, the same reaction can also take place between a macroradical and a location on another polymer chain. In either case, the resulting free-radical site on the polymer backbone can give rise to fresh chain growth and the formation of a branch, respectively.

1.1.2.3 Reversible addition-fragmentation chain transfer (RAFT) polymerization

In an ideal polymerization, all chains are initiated simultaneously, grow at the same rate, and do not undergo termination reactions. As a consequence, polymerization reactions matching these characteristics are commonly referred to as controlled or "living" polymerizations.[14] Characteristics often associated with living polymerizations include significantly narrowed molecular weight distributions compared to FRP, the lack of self-

termination, and molecular weights that can be predicted from the monomer-to-initiator ratio and increase linearly with conversion, as illustrated in Figure 1-4. In radical polymerizations, the propensity of free radicals to undergo recombination makes it necessary to suppress (or at least render insignificant) all processes that terminate chains irreversibly. Thus, living characteristics can be conferred on radical polymerizations by reagents that react with the propagating radicals, either through reversible coupling or by reversible chain transfer, in a way that the majority of living chains are maintained in a "dormant form". Despite the intermittent growth characteristics associated with these so-called reversible deactivation radical polymerizations (RDRPs),[15] rapid equilibration between the active and dormant forms yields equal chances for chain growth and enables the linear increase of molecular weights with conversion. Among the RDRP techniques that have received the most attention recently are nitroxide-mediated polymerization (NMP),[16] atom transfer radical polymerization (ATRP),[17] and reversible addition-fragmentation transfer (RAFT).[18] In this regard, the RAFT process has been widely recognized as one of the most convenient and versatile methods to impart control on radical polymerizations since the first reports concerning this topic in the 1980s.[19] More specifically, the advantages of the RAFT process encompass the compatibility with a very wide range of monomers and functional groups as well as with the conditions used in conventional free-radical polymerizations. However, it should be noted that RAFT polymerizations suffer from rate retardation and that the control is lost for high molar masses. Moreover, depending on the concentration of RAFT-derived end groups in the polymers, the products tend to be milky with a pink touch, which may represent an undesirable property.

Scheme 1-2 delineates the reactions and equilibria associated with the RAFT process, which exist on top of those originating from conventional radical polymerization, i.e. initiation, propagation and termination (cf. Section 1.1.2.2). The generic structure of RAFT agents **R1** and **R2** contains a reactive double bond, which is capable of undergoing radical addition. Hence, the effectiveness of a RAFT agent strongly depends on the monomer being polymerized as well as on the properties of the radical leaving group "R" and the "Z" group, which can be chosen to activate or deactivate the double bond (C=X) and to modify the stability of the intermediate radicals **Int1** and **Int2**. In terms of moiety "A", common examples are CH_2,CH_2=$CHCH_2$, O, or S. "R" serves as the leaving group, which, upon homolytic cleavage, must be capable of re-initiating the polymerization efficiently. The properties of RAFT agents can be discussed by looking at the addition rate coefficients (k_{add}) and the fragmentation rate coefficients (k_b) associated with the addition of radicals to the double bond in these compounds and the scission of the resulting intermediates, respectively. In this context, the overall reactions and equilibria pertaining to the RAFT process can generally be divided into two sets of reactions, i.e. the so-called pre-equilibrium involving the initial reversible chain transfer step and the main equilibrium associated with the chain equilibration process. In the pre-equilibrium, which takes place in the early stages of the RAFT polymerization, propagating (oligomeric) macroradicals $P_n\bullet$ add to the double bond of the initial RAFT agent **R1**, resulting in a

carbon-centered intermediate RAFT radical **Int1** (K_1=$k_{add,1}/k_{b,1}$). Subsequently, **Int1** undergoes β-scission, either yielding back the reactants ($P_n\bullet$, **R1**) or releasing an initiating leaving group radical R• under concomitant formation of a polymeric RAFT agent **R2**, which constitutes the dormant species (K_2=$k_{add,2}/k_{b,2}$). A similar set of reactions is operating in the main equilibrium. Here, a propagating macroradical $P_m\bullet$ reacts with the polymeric RAFT agent **R2** to form intermediate RAFT radical **Int2**, whereby recurring RAFT events establish the equilibrium between growing and dormant polymer chains (K_P=k_{addP}/k_b). Accordingly, several requirements must be met in order for a RAFT polymerization to proceed efficiently: Firstly, the RAFT agents **R1** and **R2** have to possess a reactive double bond featuring a high addition rate constant (k_{add}). Secondly, the intermediate radicals **Int1** and **Int2** should possess weak bonds, which are capable of undergoing rapid fragmentation (large (k_b) with no side reactions. Thirdly, the intermediate **Int1** should partition in favor of products ($k_{b,2} \geq k_{b,1}$). Finally, the expelled radicals (R•) must be able to re-initiate the polymerization efficiently.[20]

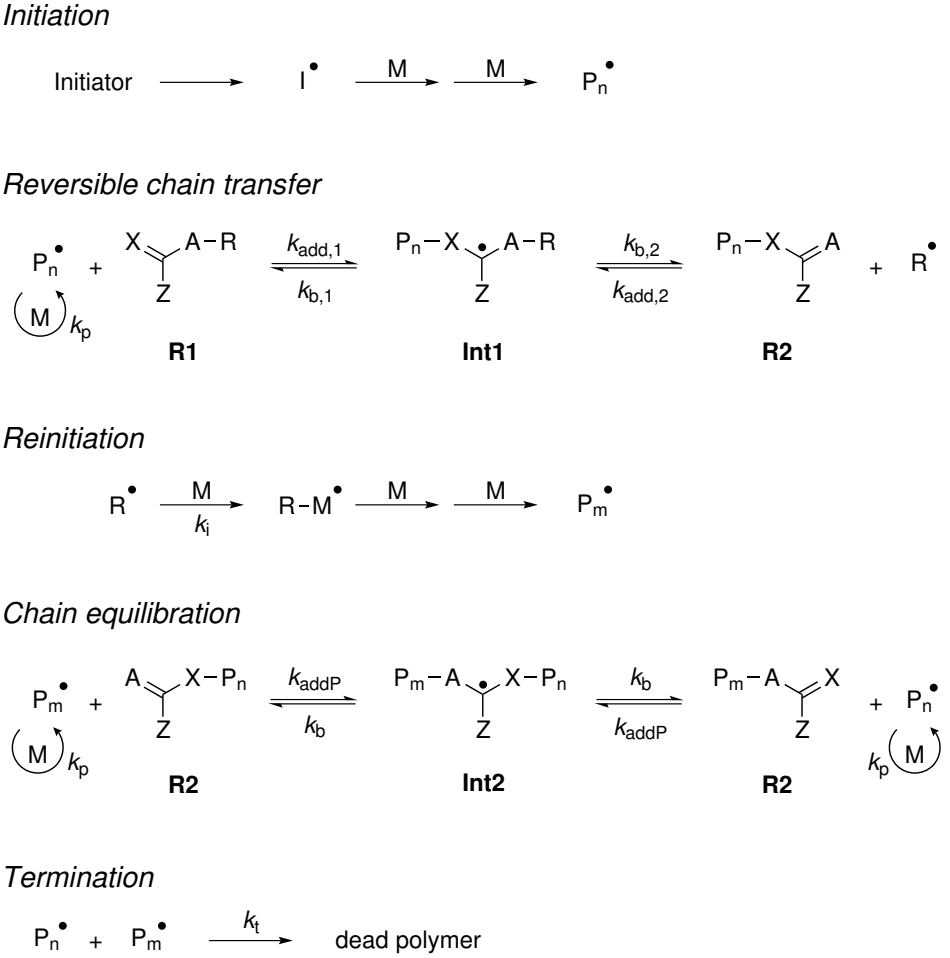

Scheme 1-2: Generic mechanism for the reversible addition-fragmentation transfer (RAFT) polymerization reproduced from reference [18].

Due to their compatibility with a broad range of monomers and good functional group tolerance, thiocarbonylthio compounds (X, A = S in Scheme 1-2) depict one of the most versatile and well-known transfer agents in RAFT polymerizations[21, 22] and a selection of frequently used thiocarbonylthio RAFT agents is depicted in Figure 1-5. Their mechanism follows the sequential addition-fragmentation equilibria depicted in Scheme 1-2.[23] Thereby, initiation occurs as in conventional radical polymerization, followed by addition of a propagating radical ($P_n\bullet$) to the thiocarbonylthio compound **R1** and fragmentation of the intermediate radical **Int1** to form a polymeric thiocarbonylthio compound **R2** and a new radical (R•). R• subsequently reacts with monomers to form a new propagating radical ($P_m\bullet$). In the following, rapid equilibration between the active propagating radicals ($P_n\bullet$ and $P_m\bullet$) and the dormant polymeric thiocarbonylthio compounds **R2** ensures that all chains possess an equal probability for growth and allows for the production of low dispersity polymers. Although the vast majority of chains retain the thiocarbonylthio end group and can be isolated as stable materials upon completion of the polymerization, the presence of polymers lacking such end groups may not be ruled out since the possibility for termination via radical-radical recombination is not excluded by the RAFT process.

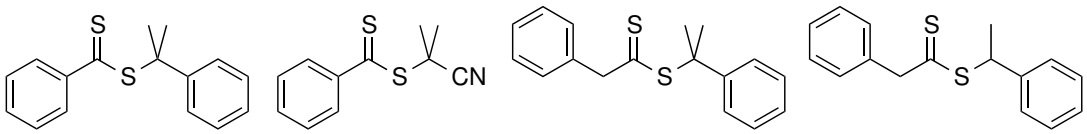

CDB **CPDB** **PPPDTA** **PEPDTA**

Figure 1-5: Chemical structures of commonly used thiocarbonylthio RAFT agents: Cumyl dithiobenzoate (**CDB**), 2-(2-cyanopropyl) dithiobenzoate (**CPDB**), 2-phenylprop-2-yl phenyldithioacetate (**PPPDTA**), 1-phenylethyl phenyldithioacetate (**PEPDTA**).

1.1.2.4 Reactivity ratios of monomers in copolymerizations

The mere presence of more than one monomer species in a polymerization mixture does not necessarily lead to the formation of a copolymer (cf. Section 1.1.1.1). In fact, the outcome of the polymerization, i.e. whether the product will consist of copolymers or a mixture of homopolymers, is predominantly governed by the reactivity of the used monomers. In this context, the kinetic analysis of radical copolymerizations can be simplified by assuming that the reactivity of macroradicals is solely determined by the terminal monomer units. This makes it possible to satisfactorily predict the behavior of many monomer mixtures.[24] In light of the above, the copolymerization of a pair of monomers

(M_1 and M_2) involves four distinct growth reactions and two types of polymer radicals ($P-M_1\bullet$ and $P-M_2\bullet$), which can be written as illustrated in Scheme 1-3.

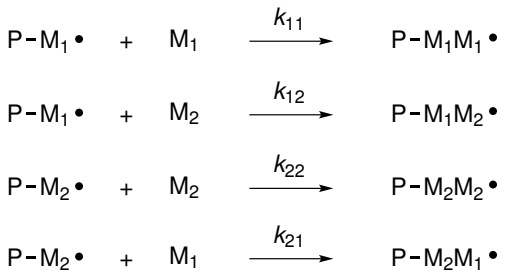

Scheme 1-3: Summary of the four different reactions that can take place for two monomers at the reactive chain end and the corresponding rate constants.

Consequently, the reaction rate constants (k_{11}, k_{12}, k_{22}, k_{21}) can be used to calculate the monomer reactivity ratios (r_1, r_2) according to Equations 1-1 and 1-2:

$$r_1 = \frac{k_{11}}{k_{12}} \tag{1-1}$$

$$r_2 = \frac{k_{22}}{k_{21}} \tag{1-2}$$

The reactivity ratios represent the relative reaction rates of polymer radicals, which are terminated with either M_1 or M_2, with their own monomers or the comonomers, respectively. Thereby, large r values indicate a tendency to add the same monomer, while small r values are indicative of the preferred incorporation of the comonomer. From this definition, it follows that several limiting cases can be derived. For instance, when $r_1 = r_2 = 1$, both monomers react as fast with themselves as with each other and hence, a random copolymer is formed. On the other hand, when $r_1 > 1$, the macroradical $P-M_1\bullet$ is reacting with monomer M_1 faster than it is with the comonomer (M_2). Hence, homopolymerization of M_1 is favored. In contrast, when the values for r_1 and r_2 are equal to or approach zero, the polymer radicals react preferentially with the comonomer and an alternating copolymer is formed, regardless of the monomer mixture. Based on the r values and the respective monomer concentrations ($[M_1]$ and $[M_2]$), the composition of the copolymers can be calculated from the Mayo-Lewis Equation 1-3:[13]

$$\frac{d[M_1]}{d[M_2]} = \frac{[M_1] \cdot (r_1[M_1] + [M_2])}{[M_2] \cdot ([M_1] + r_2[M_2])} \tag{1-3}$$

In practice, the reactivity of monomers is frequently determined experimentally, e.g. by carrying out several polymerizations at varying monomer ratios and analyzing the copolymers' composition using ^{1}H NMR spectroscopy. Notably, the polymerizations are stopped already at low conversions in order to ensure the equal availability of both monomers for

the incorporation in the copolymers and allow for the assumption that the monomer concentrations remained constant during the polymerization. Since all the other parameters in Equation 1-3 are known, the monomers' reactivity ratios r_1 and r_2 can be calculated, accordingly.

1.1.3 Post-polymerization modification

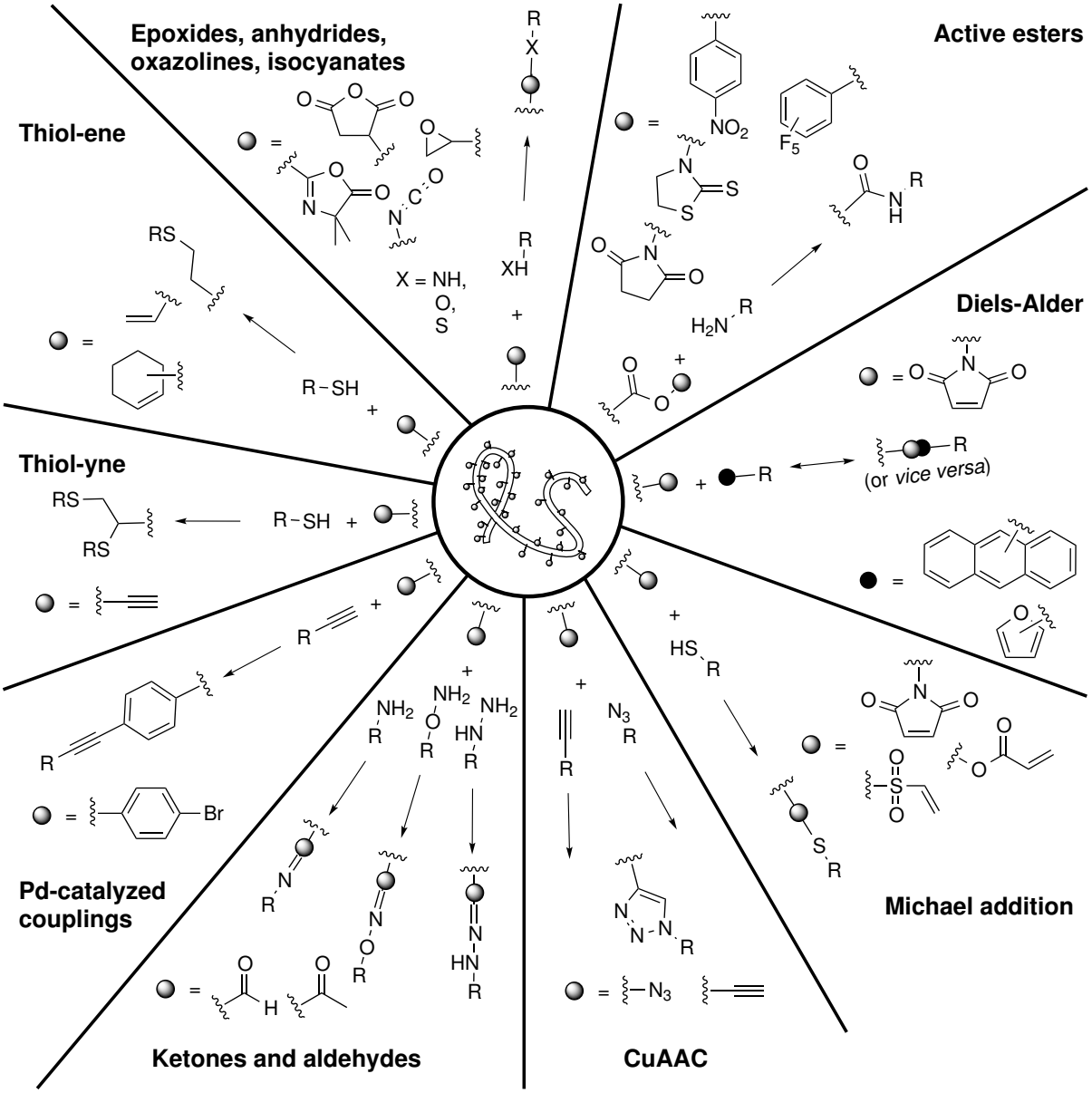

Scheme 1-4: Overview over different reactions that are used for the preparation of functionalized polymers via post-polymerization modifications. Drafted in the style of reference [25].

The history of post-polymerization modifications (PPMs) is arguably as long as the history of polymer science itself. Some of the earliest reports include the transformation of natural rubber into a tough and elastic material on treatment with sulfur,[26] the preparation of nitrocellulose by exposing cellulose to nitric acid,[27] or cellulose acetate, which was prepared by heating cellulose with acetic anhydride in a sealed tube and has found common use, e.g. in photographic films, artificial silk and membrane materials.[28] However, despite their widespread use for the preparation of functional materials since the late 19th and early 20th centuries, these materials and their underlying PPMs were only poorly understood.[29] As illustrated in Scheme 1-4, today, a wide range of tools for PPMs is available. This has also been made possible by the emergence of "living" and controlled radical polymerization techniques, such as reversible addition-fragmentation chain transfer (cf. Section 1.1.2.3),[21] which exhibit improved functional group tolerance compared to conventional polymerization techniques. This way, well-defined polymers bearing a variety of functional groups have become accessible. In this context, the discovery of several efficient reactions, which are capable of producing a wide catalogue of synthetic materials and are now commonly referred to as "Click" reactions, helped to increase the value of post-modification reactions even further and provided the basis for their explosive growth in use and versatility since the 1990s[25].

The characteristics of these "Click" reactions include high yields with no (or easily removable) by-products, regio- and stereospecificity, insensitivity to oxygen or water, mild reaction conditions and orthogonality with other common reactions of organic synthesis.[30] In addition, a wide variety of readily available starting materials may be used in these reactions. In light of the synthetic methodology applied in this work, which heavily relies on the formation of amide bonds in the dendritic growth reactions (dendronizations), emphasis is placed on activated esters (cf. top-right corner in Scheme 1-4).

Activated esters represent reactive groups that are readily available, do not require an additional deprotection step before post-polymerization modification, and are prone to react with a wide range of nucleophiles. More importantly, they react with amines cleanly and under mild conditions by forming amide bonds (cf. Scheme 1-5). The synthesis and PPMs of active ester polymers was pioneered by Ferruti and Ringsdorf, who examined the suitability of reactive esters as precursors for pharmacologically active polymers in the 1970s.[31, 32] Since then, a broad variety of active ester polymers has been developed and the reaction of active esters with amines has become one of the most frequently used PPM-strategies. The predominant use of amines is due to the fact that they can react selectively even in the presence of weaker nucleophiles, such as alcohols. Although *N*-hydroxysuccinimidyl active ester polymers are most commonly employed, the solubility of these polymers is limited to dimethylformamide (DMF) and dimethyl sulfoxide (DMSO) which, together with possible side reactions, such as succinimide ring-opening or the formation of *N*-substituted glutarimide groups, imposes a drawback of these polymers.[33] However, these side reactions can be suppressed by using an excess of amine or proton acceptors such as triethyl amine (TEA) or N,N-dimethylaminopyridine (DMAP).[34]

Moreover, the limited solubility can be addressed by inter-exchanging the location of the mounted functional groups, i.e. the PPM of amine-bearing polymers with activated esters. In this context, Schlüter and co-workers demonstrated the high coupling efficacy of activated NHS derivatives with DPs bearing primary amines for a variety of chemically different and sterically encumbered systems.[35–42]

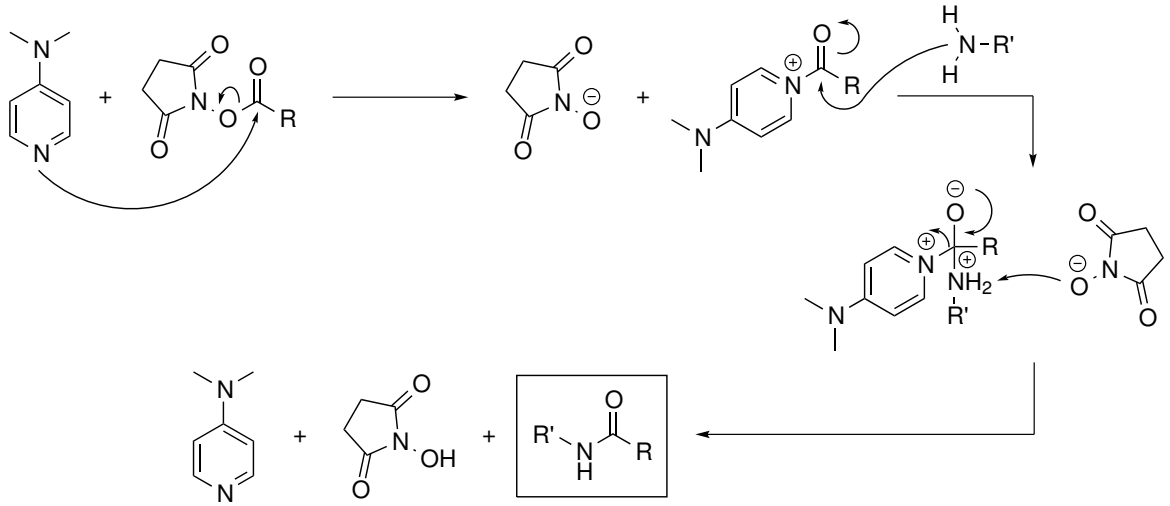

Scheme 1-5: Mechanism of the N,N-dimethylaminopyridine-catalyzed coupling reaction between activated succinimidyl esters and primary amines.

1.2 Dendronized polymers (DPs)

1.2.1 Concept

Polymer synthesis and technology have matured into one of the main fields in materials science with applications of polymers ranging from cheap commodity materials to highly sophisticated and "smart" materials.[43, 44] Dendrimers, on the other hand, constitute repeatedly branched molecular structures which have been developed in the past decades and paved the way for a new class of materials with promising applications, *e.g.* in biochemistry,[45] catalysis,[46] or microelectronics.[47] However, due to the inherent confinement of space, the size accessible with classical dendrimers is limited to a few nanometers. By contrast, polymers are the largest covalently linked synthetic molecular structures, at least with respect to their contour length. This being the case, fusing the concepts of polymers and dendrimers can be considered a promising approach towards novel, sophisticated materials with manifold potential applications (cf. Figure 1-6).

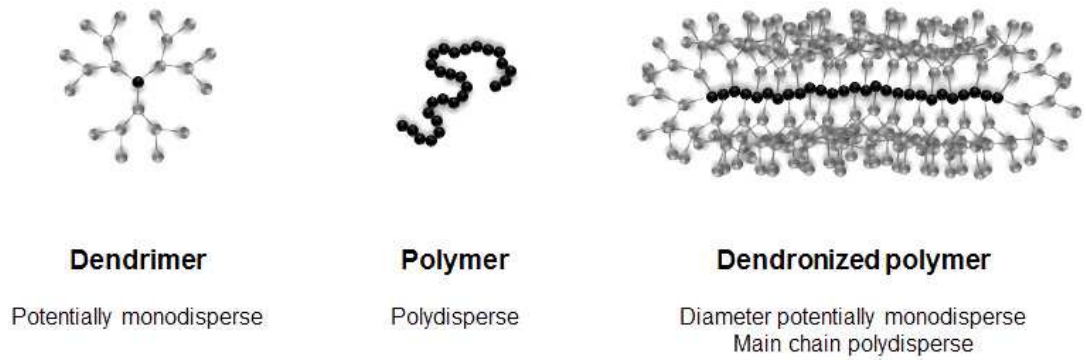

Figure 1-6: Schematic representation of the concept of dendronized polymers.

Polymers with dendritic side chains radiating from the polymer backbone were first described in a patent by Tomalia *et al.* in 1987.[48] One major structural characteristic of such polymers is their thickness, which is determined by the number of branching points between the polymer backbone and the periphery, i.e. the dendron generation number *g*. Consequently, the polymer also exhibits a polymer generation, which is normally referred to as PG*g*. Numerous reports in the literature have demonstrated that the decoration of polymer backbones with dendritic appendices results in certain features that distinguish them from conventional polymers, including a large number of functional peripheral end groups, a defined surface and loadable interior, potentially monodisperse diameters, and highly dense structures, which render these molecules resistant against main chain collapse. Moreover, it has been shown that crowding around the polymer backbone leads to stiffening and elongation of the polymer backbone with increasing dendron generation in the realm of high degrees of polymerization (cf. Figure 1-7).[49, 50] Qualitatively, similar results were obtained for polymers with linear side chains.[51] However, unlike conventional

linear polymers, dendrons become more bulky with increasing molar mass due to their repeatedly branched structure. In this regard, the fixed distance between two consecutive dendrons along the polymer backbone results in a tighter packing of the dendrons and increases the interaction between neighboring dendrons. Thus, deformations require rearrangements in the dendritic shell, especially for higher generation numbers, which links the flexibility of the whole polymer to the mobility of the dendron and gives rise to effects such as viscoelasticity and plasticity that go beyond the wormlike chain (WLC) model, which describes a polymer that is stiff over short distances and flexible at longer ones.[52] Hence, the chain thickness can be seen as a new variable in polymer chemistry influencing the properties of such polymers in addition to the effects originating from the particular chemical structures and backbone chain lengths, respectively. Over the years, the term "dendronized" polymers (DPs) was coined by SCHLÜTER and co-workers, who showed that these polymers can be considered cylindrical, "molecular objects".[42, 53, 54]

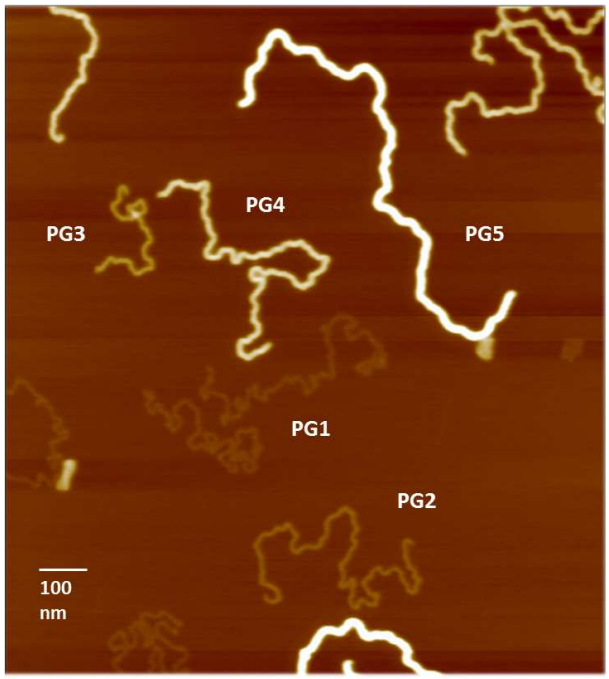

Figure 1-7: AFM height image (tapping mode) taken from reference [50] illustrating the flexible chain – wormlike chain – molecular object transition of DPs with increasing polymer generation.

Previous atomistic models reported in the literature for a particularly well-studied series of DPs, which are hence called "classic" DPs in the following, have provided information on the density variation in these DPs as a function of the radial distance from the polymer backbone.[55] As illustrated in Figure 1-8, the highest density is located in the region close to the backbone, with values ranging between roughly $1.3 - 1.8\,\mathrm{g\,cm^{-1}}$. Upon moving further towards the periphery, the density drops to approximately $1.2\,\mathrm{g\,cm^{-1}}$ and remains virtually constant over a length scale depending on the respective generation, before a

relatively sharp and progressive decrease can be observed until the outermost layer of the cylindrical section has been reached. Albeit well-defined, this drop in density cannot be described by a step-function, which implies that DPs feature a less densely-packed volume fraction towards their ”surface” that allows for intermolecular penetration of DPs, e.g. in order to reduce local density gradients in the molten state (cf. patterned area in Figure 1-8). Accordingly, the topologically peripheral functional groups of dendritic polymers play an important role for the physical properties of these materials. In this regard, the large number of terminal end groups and the overall dimensions of these macromolecules imply that secondary interactions, such as van der Waals forces and hydrogen bonding, play much greater roles in influencing the physical properties compared to the situation in small organic molecules.

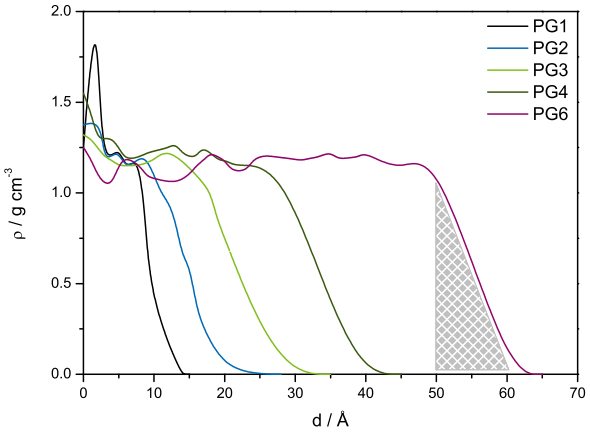

Figure 1-8: MD simulated density profiles for **PG1** – **PG6** (**PG5** excluded) *in vacuo* reproduced from reference [55]. The density (ρ) is plotted against the distance (d) to the backbone measured using the vector perpendicular to the helix axis. For **PG6**, the patterned inset represents the fraction of reduced density where intermolecular interdigitation may take place.

1.2.2 Synthetic approaches

Owing to the fact that DPs combine the concepts of polymers and dendrimers, their preparation involves both organic synthesis of the dendrons and methods of polymer synthesis. Hence, the general synthetic strategies may be conceptually divided into three categories (cf. Figure 1-9), i.e. the graft-to route, the graft-from route and the macromonomer route, with each strategy possessing distinct advantages and disadvantages.[56] However, the lines between these routes are blurred to some extent and combinations may be applied successfully.

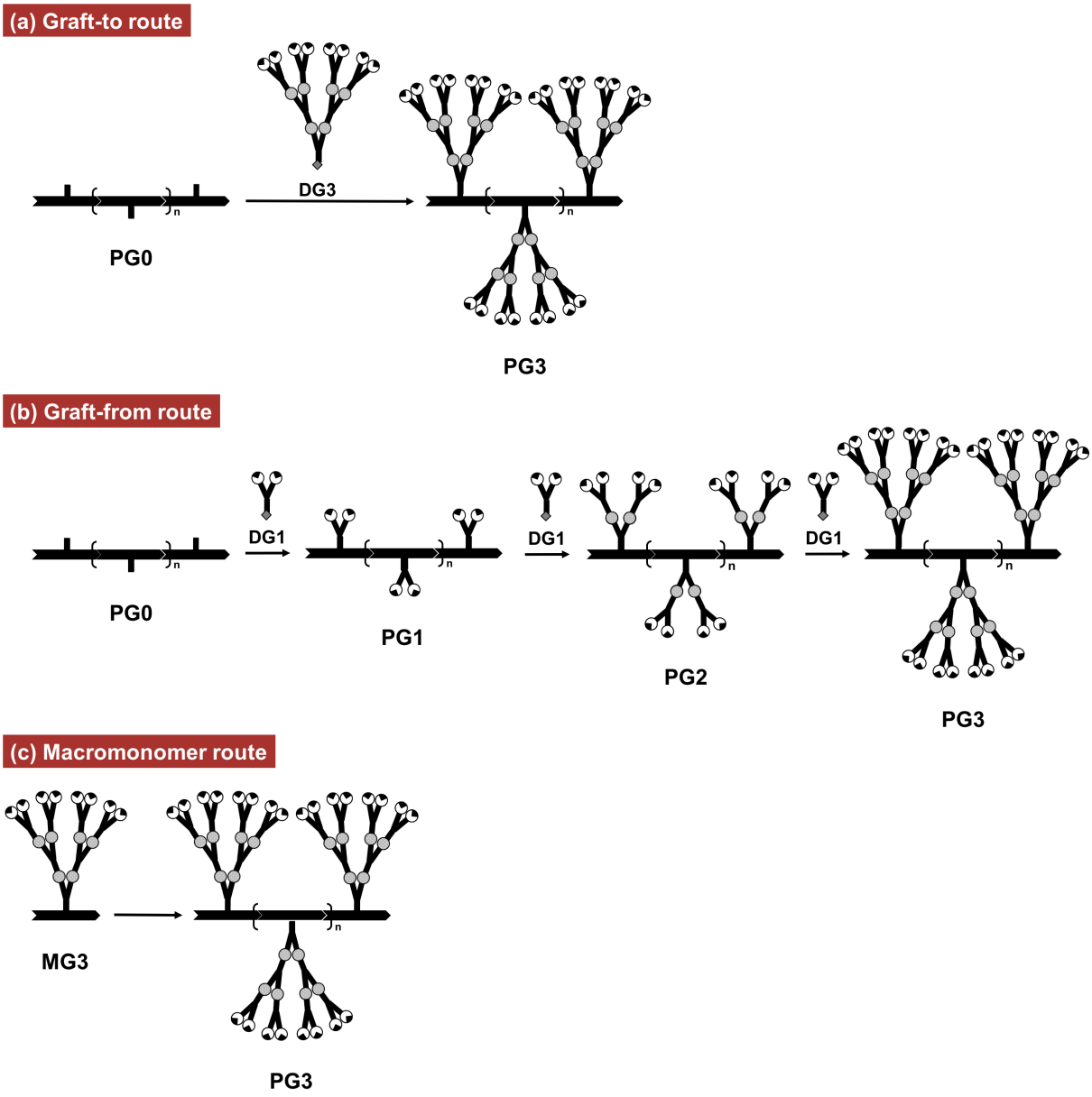

Figure 1-9: Schematic representation of the conceptual synthetic approaches towards third-generation dendronized polymers.

A common feature of all three synthetic protocols is the inherent molecular weight distribution, which is inevitably associated with any type of polymerization reaction and generally distinguishes DPs from their monodisperse dendrimer-counterparts.

- The coupling of preformed dendrons of the desired generation to the preformed polymer is referred to as the **graft-to strategy** (cf. Figure 1-9(a)), which is also termed "convergent route". Because dendrons with desirably high generations can be prepared analogously to dendrimers, synthetic solutions are abundant. On the downside, the random coil conformation of polymer chains does not allow for an easy access to functional groups along the backbone and focal points of large dendrons may likewise be immersed inside the dendritic branches. This way, an entropically disfavored unfolding of the polymer chains would be required and thus, high degrees of dendronization are inherently difficult to achieve by means of such post-polymerization reactions. Nonetheless, the adverse unfolding of chains may be mitigated by other contributions in the system.
- The **graft-from strategy** (or "divergent route") involves the successive attachment of $g = 1$ dendrons to the preformed polymer chain to grow higher generations, typically following a two-step deprotection-coupling protocol (cf. Figure 1-9(b)). In principle, the difficulties encountered at it are similar to those in a divergent synthesis. However, the use of sterically less demanding first-generation dendronization units facilitates both diffusion into the coiled chains and dendronization reactions, compared to higher generation dendrons. As the synthesis of higher-generations DPs requires a vast number of simultaneous coupling reactions to take place, the synthesis is susceptible to structural defects. Because of the similarity in structure and size, the resulting species will be inseparable since any kind of structural defect will only contribute to the overall polydispersity. This explains the need for highly efficient coupling reactions and, even more importantly, reliable methods to quantify the degree of dendronization, e.g. by UV-labeling.[57]
- In the **macromonomer strategy**, dendrons of the desired generation are equipped with a polymerizable group at their focal point and polymerized (cf. Figure 1-9(c)). Since this strategy does not require any post-polymerization reactions, a quantitative degree of dendron attachment is guaranteed and thus, DPs with complete structural perfection are obtained as long as no chain transfer to polymer or macromonomer occurs. Even so, the dendritic nature of the used macromonomers often implicates a considerable molecular weight, which may render their purification difficult. More importantly, steric hindrance imposes a large effect on the polymerization kinetics, i.e. crowded dendrons may inhibit polymerizations completely or lead to undesired results such as oligomeric products or very broad molecular weight distributions.

2 Motivation

Ever since the discovery of dendronized polymers (DPs) in the late 1980s, considerable research has been devoted to the development of new and more efficient synthetic routes to these intriguing macromolecules. However, considerably less attention has been paid to the investigation of their bulk mechanical properties, which are thought to depend mainly on three molecular characteristics: The degree of polymerization (P_n) of the backbone, the dendron generation (g), and the chemical characteristics of their structures.[41, 58–60] In this regard, atomistic calculations of the radial density profiles from the polymer backbone to the peripheral groups suggested that the density in the interior of DPs is relatively evenly distributed, before it drops markedly upon reaching the surface of DPs.[55] Despite being relatively clear-cut, this density drop is not a step function and, hence, the interpenetration of the outermost layers of neighboring DPs becomes possible. Accordingly, the surface functional groups of dendritic macromolecules play a pivotal role in determining their intermolecular interactions and physical properties.

In an effort to investigate the influence of polymer structure, hydrogen bond shielding peripheral moieties, and supramolecular binding motifs on the thermal and viscoelastic properties of DPs, novel DPs featuring chemical modifications to the known "classic" DPs are envisaged.[50] To this end, first-generation "classic" DPs (**PG1**) with a range of distinct P_n values to capture the effects emerging upon the transition from the oligomeric to the polymeric regime have to be prepared. Since these samples represent the "reference materials" against which comparisons are made as well as the base polymers for the synthesis of both higher-generation "classic" DPs (**PG2, PG3**) and "hybrid" DPs featuring two concentric layers of different dendron motifs around the backbone, the preparation of sufficient amounts of **PG1** is necessary. A recent MD simulation study concluded that intramolecular interactions are significantly more abundant in these "classic" DPs than intermolecular ones, which were detected only upon considerable interdigitation of two molecules.[61] These results were supported by previous rheological studies, which pointed towards a scenario in the melt that could be the result of inter-chain hydrogen bonding and/or $\pi - \pi$-stacking.[62] To further probe these interactions, "hybrid" DPs bearing oligo(ethylene glycol) (OEG)-based dendrons in the periphery are envisaged, which depict ideal candidates since the outer shells of these "hybrid" DPs do not participate in such interactions while, at the same time, the structure forming characteristics of the underlying "classic" DPs are maintained. Thus, two OEG-based dendrons ($g = 1, 2$) applicable in the dendronization reaction need to be developed and synthesized. In order to achieve a minimum degree of structural change and retain the amide connectivity between generations, these novel dendrons should bear succinimidyl esters at their focal points. Moreover, their stability and activity towards primary amines, as present in the deprotected "classic" DPs, needs to be established, followed by the preparation of a series of "hybrid" **H[1+1]** and **H[1+2]** DPs based on the aforementioned "classic" **PG1** base polymers. On the other

hand, the feasibility of preparing DPs with the potential to engage in strong secondary interactions via either a post-modification or a copolymerization approach should be investigated. Following the arguments raised with the "classic" DPs, first-generation DPs (**PG1-UPy**) featuring varied concentrations of strongly hydrogen-bonding UPy moieties at the $g = 1$ level and a range of P_n values are envisaged. In addition, a subset of three **PG1-UPy** samples comprising 5, 25, and 50 mol% UPy at the $g = 1$ level will be dendronized to obtain second- and third-generation DPs (**PG2-UPy**, **PG3-UPy**), which are expected to provide insights about the depth of intermolecular interactions and the mobility of the UPy groups inside the DPs. Finally, the synthesized polymers will be systematically characterized by differential scanning calorimetry and, with the help of collaborators, rheological measurements.

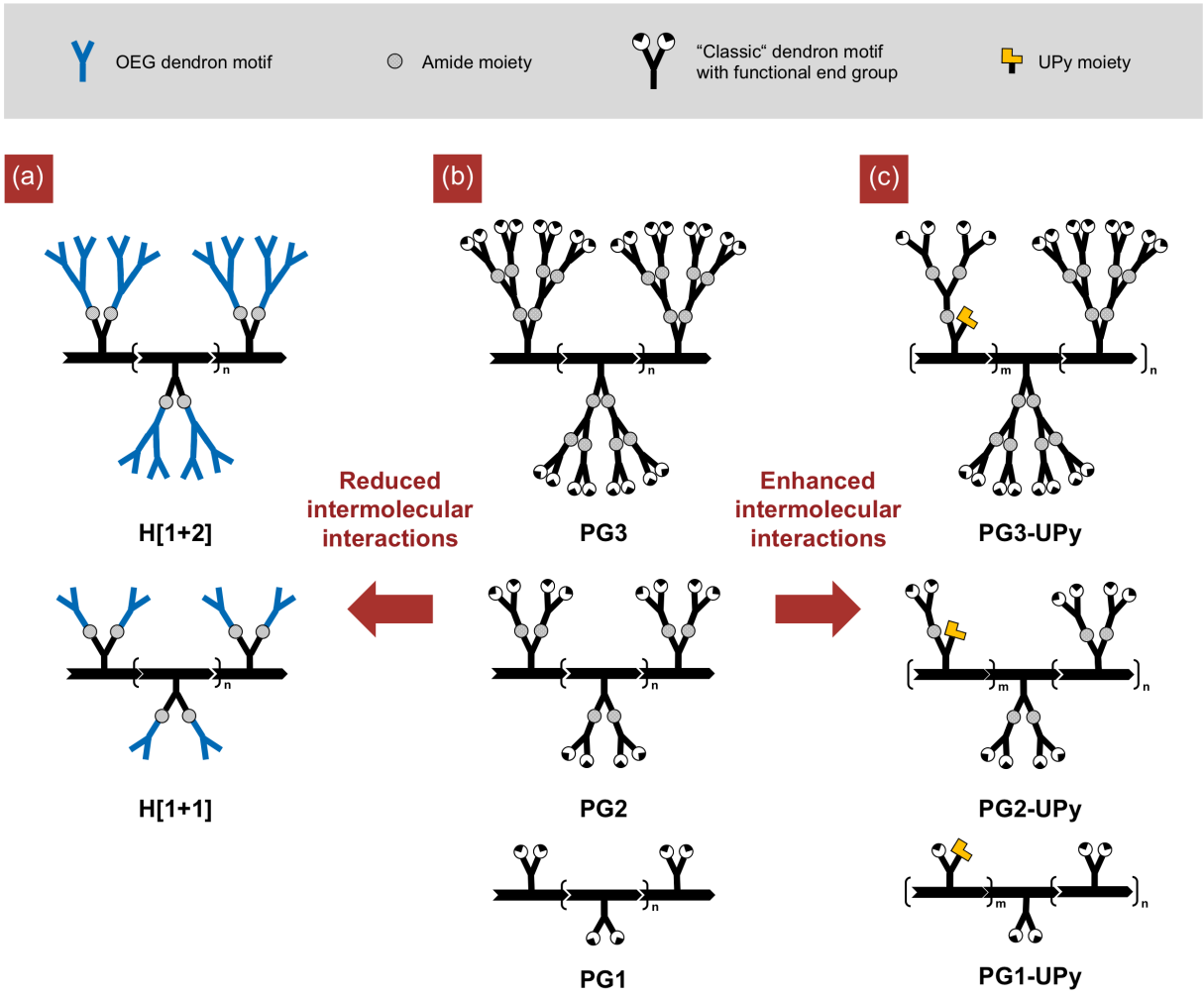

Figure 2-1: Schematic representation of the DPs in this work. "Hybrid" DPs (**a**) are discussed in Section 3.2; "Classic" DPs (**b**) are described in Section 3.1; UPy-functionalized DPs are presented in Section 3.3 (**c**).

3 Results and discussion

3.1 "Classic" DPs

3.1.1 Synthesis of first-generation "classic" DPs

Macromonomer **1c** bearing two Boc-protected amines was prepared in an overall yield of 85% in two steps from the commercially available methyl ester **1a** as delineated in Scheme 3-1. Although the synthesis was described previously in the literature,[50] the revised protocol reported herein offers some improvements in terms of efficacy and scalability. First, methyl ester **1a** was reduced to the corresponding alcohol **1b** using lithium aluminium hydride (LAH) at −10 °C. Performing the reduction at low temperatures is crucial since warming of the reaction to room temperature led to partial cleavage of the Boc groups. In addition, quenching of excess LAH was preferably accomplished by the Fieser workup,[63] which resulted in a granular precipitate that could easily be removed from the reaction mixture by filtration. This way, the extraction step could be significantly improved compared to the previous protocol. Subsequently, alcohol **1b** was esterified with freshly distilled methacryloyl chloride (MAC) to give macromonomer **1c**, which was obtained as a white solid in high purity after column chromatography and overlaying of the oily residue with hexane.

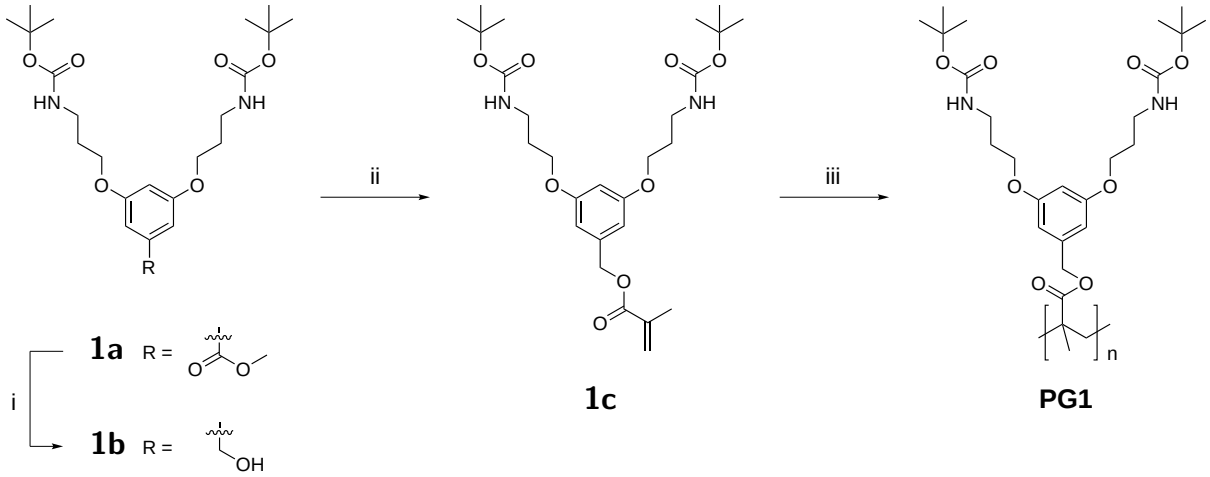

Scheme 3-1: Synthesis of macromonomer **1c** and **PG1**. Reagents and conditions: i) LAH, THF, −10 °C, 2 h, *87%*; ii) MAC, Et_3N, CH_2Cl_2, 0 °C, 3 h, *94%*; iii) AIBN, (CDB,) 65 °C, 14 – 23 h, *62 – 81%*.

Subsequently, a series of first-generation base polymers (**PG1**) comprising different degrees of polymerization (P_n) was prepared by using different radical polymerization techniques. Thereby, polymer samples with relatively small degrees of polymerization ($P_n \approx 50$,

300) were obtained with narrow molecular weight distributions (M_w/M_n) of approximately 1.2 – 1.5 by controlled radical polymerization using azo-*bis*-isobutyronitrile (AIBN) as the initiator and cumyl dithiobenzoate (CDB) as the RAFT reagent (Entries 1, 2 in Table 3-2). Although previously reported protocols for the RAFT polymerization of macromonomer **1c** state a temperature of 60 °C,[50, 64] a slightly higher temperature (65 °C) was chosen for the polymerization reaction due to evidence in the literature that retardation with dithiobenzoates is reduced at higher temperatures.[65] Moreover, higher temperatures should allow for higher polymerization rates and achieve given conversions at shorter reaction times, respectively.[18]

Table 3-1: Polymerization conditions[a] for the radical polymerization of monomer **1c** to give **PG1**.

Entry	Polymer	AIBN, mol%	CDB, mol%	Time, h	Yield, g	Yield, %
1	PG1-50	2	2	23	4.49	70
2	PG1-300	0.4	0.4	18	2.02	67
3	PG1-1000	0.2	-	13	1.61	81
4	PG1-1500	0.2	-	14	1.24	62
5	PG1-2000	0.2	-	16	1.39	73
6	PG1-3000	0.1	-	14	1.36	68

[a]Carried out at a concentration of 1.0 g mL^{-1} in DMF at 65 °C.

The somewhat longer polymerization times required in the presence of higher RAFT agent concentrations listed in Table 3-1 can be explained by the formation of ketenimines, which are derived from the decomposition of AIBN.[66] These unstable intermediates can be intercepted by RAFT agents and converted to by-products, which reduce the initiator efficiency and cause retardation. As mentioned earlier, higher temperatures may also result in narrower molecular weight distributions,[65] which is consistent with the rate constants for the fragmentation of the RAFT intermediates and the transfer coefficients of RAFT agents that both increase with reaction temperature.[67] In the present case, the slight increase of the polymerization temperature did not lead to any noticeable increase in undesired side reactions, accordingly. Polymer samples featuring longer backbone chain lengths (Entries 3 – 6 in Table 3-2) were synthesized by free radical polymerization using AIBN as the initiator, which naturally resulted in somewhat broader molecular weight distributions ($M_w/M_n \approx 1.4 - 1.8$). Here, the RAFT protocol was not applicable as it is generally accepted that livingness in reversible-deactivation radical polymerization is diminished when high-molecular weight polymers are targeted. This is due to longer reaction times, increased termination and unavoidable side reactions, which generate a significant fraction of dead chains (cf. Section 1.1.2.3).[68] Moreover, an upper limit for achievable degrees of polymerization of roughly 600 repeating units, which corresponds to a number-average molecular weight (M_n) of approximately 320 kDa, has also been

reported for structurally related DPs, beyond which a marked loss of control over the molecular weight distribution was observed.[64]

Table 3-2: Summary of the experimentally determined molar masses[a] of **PG1**.

Entry	Polymer	M_w, kDa	M_n, kDa	M_w/M_n	P_n
1	PG1-50	28	23	1.21	44
2	PG1-300	210	140	1.50	260
3	PG1-1000	900	520	1.73	1002
4	PG1-1500	760	1090	1.43	1448
5	PG1-2000	1030	1530	1.49	1975
6	PG1-3000	1600	2900	1.81	3060

[a]Determined by GPC in DMF at 45 °C.

The degrees of polymerization of the synthesized DPs were determined by gel permeation chromatography (GPC) measured on 1 mg ml^{-1} solutions of **PG1** in DMF and the molecular weights given in Table 3-2 were calculated based on the data obtained from the on-line light scattering detectors. Poly(methyl methacrylate) standards with peak molecular weights (M_p) of 0.10, 0.212, 0.66, 0.981, and 2.73 MDa were used for calibration and the molecular weight standard closest to the theoretical molecular weight of the respective polymer was used as reference. Figure 8-5 on page 174 of the Appendix depicts the obtained GPC elution traces of the prepared "classic" **PG1** samples listed in Table 3-2. Since light scattering (LS) is derived from first principles and does not rely on any assumptions, in principle, this method can be regarded as a tool for the direct determination of molecular weights. Thus, GPC-LS has frequently been used for the characterization of both semi-flexible and rod-like polymers, as reported in the literature.[69, 70] However, it is important to note that the scattering curves need to be fitted with a model and that poly(methyl methacrylate) is not an ideal standard for DPs, as the hydrodynamic volume of DPs depends strongly on the generation number *g*. In this regard, it is known that very large appendices, such as in DPs, can result in discrepancies between the theoretical and experimental molecular weights. These may be explained by the opposing effects of (i) chain thickening, i.e. the polymer's mass per repeat unit length being much larger than the molar mass of the calibration standard's repeat unit, which leads to an underestimation of molecular weights, and (ii) chain stiffening with increasing *g*, which leads to an overestimation of hydrodynamic volume and molecular weight, accordingly.

In an attempt to overcome this limitation, Zhang et al. investigated the potential of first-generation DPs comprising similar chemical structures to the herein investigated DPs for the determination of absolute molar masses by GPC calibrated with values obtained from light scattering on the respective samples.[71] However, the obtained *absolute* light scattering calibration curve yielded correct molar masses and molar mass distributions only for the first-generation DP samples. When applied to higher DP generations, the obtained

molar masses were most probably smaller than the true ones. For these higher DP generations, i.e. up to **PG4**, all attempts to prepare absolute light scattering calibration curves failed because of irreproducible results caused by the tendency of these polymers to form aggregates. Hence, the encountered solubility issues were one motivation for moving to the present DP structures comprising ether linkages in their branches (cf. Scheme 3-1), which greatly facilitate the dissolution in solvents such as MeOH, DMF, or THF and, thus, reduce the tendency for aggregate formation. However, a comprehensive investigation on the refractive index increments of "classic" DPs has not been conducted to this point in time. In essence, the true molar masses are difficult to estimate as the effect of chain thickening is somewhat counterbalanced by the increase in chain stiffness. Nevertheless, the results of the GPC analyses presented herein are in good agreement with existing reports on DPs and are deemed suitable for a reliable comparison of different samples in terms of relative molecular weights and backbone chain lengths, respectively.[42, 62]

3.1.2 Synthesis of higher-generation "classic" DPs

Table 3-3: Summary of the experimentally determined molar masses[a] of **PG2** and **PG3**.

Entry	Polymer	M_w, kDa	M_n, kDa	M_w/M_n	P_n
1	PG2-50	58	54	1.07	44
2	PG2-300	500	310	1.61	255
3	PG2-1000	1690	1150	1.47	942
4	PG2-1500	2100	1740	1.20	1422
5	PG2-2000	2790	2350	1.19	1924
6	PG2-3000	4000	3610	1.11	2950
7	PG3-50	123	113	1.09	43
8	PG3-300	860	630	1.37	238
9	PG3-1000	3140	2440	1.29	930
10	PG3-1500	4320	3570	1.21	1359
11	PG3-2000	6040	5000	1.21	1910
12	PG3-3000	13600	7560	1.80	2880

[a]Determined by GPC in DMF at 45 °C.

A series of "classic" DPs was synthesized from **PG1** (cf. Section 3.1.1) in a divergent approach (cf. Section 1.2.2) up to generation number $g = 3$ by employing $g = 1$-dendron **1d** bearing a succinimidyl ester at its focal point. As stated in Table 3-4 and illustrated in Scheme 3-2, the dendronization procedure involves repeated deprotection-coupling steps and prolonged reaction times following a protocol which has been developed earlier.[50] This mode of synthesis was chosen in order to reduce the impact of the growth reaction on

the backbone degree of polymerization and molar mass distribution. Thus, the obtained **PG2** and **PG3** samples can be referred to as homologous DPs, which allow for systematic studies of generation-dependent effects as they comprise virtually identical backbone chain lengths.

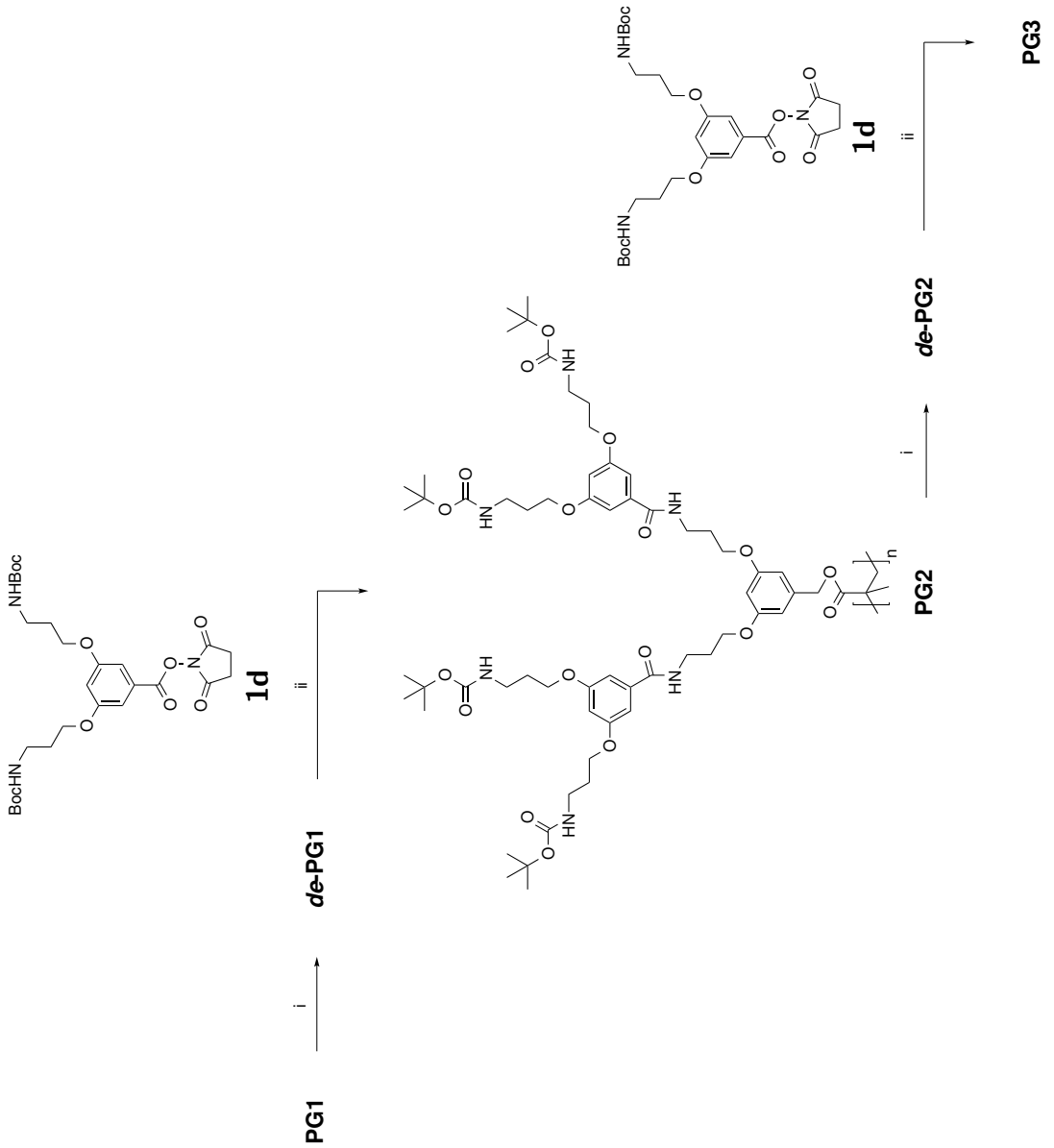

Scheme 3-2: Synthesis of higher-generation "classic" DPs. Reagents and conditions: i) TFA, −10 °C to RT, 14 h, *quant.*; ii) Et_3N, 4-DMAP, DMF, RT, *60 – 80%*.

Purification of the "classic" DPs involved precipitation into ice-cold diethyl ether to remove the added surplus of dendronization agent **1d** and DMF prior to column chromatography. Fractions containing polymer were lyophilized from 1,4-dioxane to yield the **PG2** and **PG3** samples listed in Table 3-3 as fibrous foams. The moderate yields of 60 – 80% for each step may be caused by the strong adhesion of DPs to glass surfaces and/or retention of aggregated or substantially defective DPs upon column chromatography. For

PG2 and **PG3** with $P_n \approx 2000$, 3000, the dendronization conversions were determined by UV-labeling experiments using 2,4-dinitrofluorobenzene to tag unreacted amines, followed by spectrophotometric quantification of these labeled moieties.[42, 57] The obtained degrees of structure perfection were calculated to be close to 100% for each step, resulting in an overall perfection of ≫99% for the respective **PG3** representatives (cf. Table 3-4).

Table 3-4: Conditions for the divergent growth of **PG1** and **PG2** to give **PG2** and **PG3**.

Entry	Polymer	Dendronization[a] Time, d	Coverage[b], %	Yield, %
1	PG2-50	16	-	72
2	PG2-300	7	-	71
3	PG2-1000	10	-	79
4	PG2-1500	7	-	76
5	PG2-2000	8	99.8	64
6	PG2-3000	9	99.9	82
7	PG3-50	8	-	81
8	PG3-300	16	-	63
9	PG3-1000	47	-	45
10	PG3-1500	20	-	64
11	PG3-2000	48	99.3	65
12	PG3-3000	22	99.9	73

[a]Carried out in DMF at room temperature. [b]Determined by UV-labeling with 1-fluoro-2,4-dinitrofluorobenzene.

3.1.3 Summary of Section 3.1

A series of "classic" DPs comprising six different backbone chain lengths and generation numbers $g = 1-3$ was prepared by a combination of macromonomer- and divergent approaches according to the literature. This mode of synthesis has been shown to impose the least possible impact on P_n and M_w/M_n, which renders the prepared series "homologous". Although *absolute* molar mass determination of DPs is complicated by the counterbalancing effects of chain stiffening and thickening with increasing g, the values obtained by GPC calibrated with PMMA standards should at least allow for reliable comparisons between the different samples with P_n values ranging from $\approx 50-3000$. For the longest backbone chain lengths ($P_n \approx 2000$, 3000), the structure perfection was determined by UV-labeling experiments to be ≫99% for the respective $g = 3$-representatives.

3.2 DPs with suppressed intermolecular interactions

3.2.1 Concept of ”hybridization”

Although the term ”hybrid” may be equally used for materials comprising inorganic and (dendritic) organic components[72] or diblock copolymers possessing linear-dendritic structures,[73] the herein described concept of ”hybrid” dendronized polymers builds upon furnishing DPs with chemically or structurally different dendritic motifs (cf. Figure 3-1). In principle, this represents a convenient strategy to fuse distinct properties in one macromolecule and allows for the preparation of multi-functional and responsive materials.[74, 75] Ideally, the microstructure of this kind of DP features two (or more) concentric layers of different dendrons around the linear polymer backbone. Put another way, radially segregated cylinders are obtained, whereby the individual layer sizes are determined by the underlying constituents and in the order of a few nanometers. Following this definition, hybrid DPs possess an all-dendritic structure and may even offer the possibility for further growth reactions.

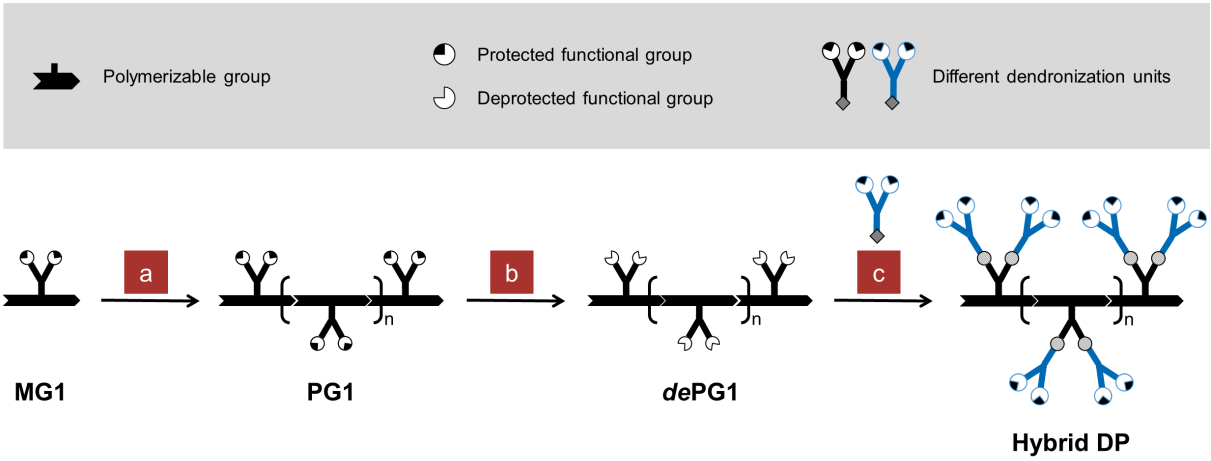

Figure 3-1: Divergent synthesis of hybrid dendronized polymers: (**a**) Polymerization; (**b**) Deprotection; (**c**) Dendronization with chemically or structurally different dendronization units.

One of the first examples of such ”hybrid” dendronized polymers was reported by Mynar *et al.*, who referred to these macromolecules as ”doubly-dendronized” polymers.[74] Their synthesis involved the preparation of linear poly(*p*-hydroxystyrene) (PHS), which was subsequently grafted with dendritic poly(aliphatic ester)s based on bishydroxy propionic acid up to generation three in a divergent protocol. Pentynoic acid was used to post-modify the hydroxy end groups and provide terminal alkyne groups. In a final step, copper-catalyzed azide-alkyne cycloaddition (CuAAC) was applied to link third-generation dendrons featuring azido focal points to the periphery of these DPs, which gave sixth-generation DPs

with nearly quantitative CuAAC reaction as judged by SEC and spectroscopic analysis. In another example, Zhang *et al.* prepared poly(ethylenimine) (PEI) dendronized with poly(amidoamine) (PAMAM)-type dendrons of varied generation, which were end-capped using hexyl acrylate.[76] The resulting macromolecular amphiphiles performed as unimolecular nanocontainers that were capable of encapsulating a water-soluble Rhodamine dye in their interiors. Furthermore, generation-dependent encapsulation properties were found, with higher generations exhibiting higher loading capacities and more localized cavities due to the increasingly dense packing of the dendrons. Further reports in the literature demonstrated the possibility to induce hydrophobic dendronized polymers with water-solubility by end-capping hydrophobic terminal functionalities with solubilizing appendices.[77, 78]

In this context, water-soluble polymers are attractive for many fields of application, including construction,[79] food science,[80] and pharmaceuticals.[81] Among non-toxic and biocompatible water-soluble polymers, especially non-charged polymers experience a demand since they do not cause problems with cell lysis and normally do not show complex aggregation behavior. Thus, both linear oligo(ethylene glycol) (OEG) and branched glycerol (BGL) containing compounds are frequently used to render otherwise hydrophobic materials water-soluble.[82–87] At it, OEGs offer certain beneficial chemical features:[88–92] Owing to their terminal, neutral alkoxy functionality, OEGs and their dendritic analogues are water soluble under a wider range of pH conditions compared to compounds comprising charged end groups such as ammonium cations or sulfonate anions. Second, the capped terminal hydroxyl groups and ether functionalities in OEGs render these molecules amphiphilic and effect good solubility in both water and a wide range of organic solvents. Third, the absence of asymmetric centers in symmetrically branched OEGs prevents the formation of diastereomeric mixtures when the hybridized molecules contain asymmetric centers.[93] Unsurprisingly, owing to their non-toxicity and generally good biocompatibility, OEG units have been incorporated into polymers and dendritic macromolecules for various bio-related applications.[45, 94] In addition, OEG moieties can be used to endow polymers with thermoresponsive behavior. In this regard, the lower critical solution temperatures (LCSTs) are usually above 100 °C but tunable by the overall hydrophilic-lipophilic balance of the macromolecule (composition effect)[95, 96] and by the arrangement of hydrophilic and hydrophobic moieties in the macromolecule (structure effect).[97]

In light of the well-defined structure and beneficial properties of symmetrically branched OEGs, it was of obvious interest to extend the concept of hybridization to the "classic" dendronized polymers and prepare novel "hybrid" polymers. These novel representatives should not only allow for exploring the structure effect very systematically but also offer new insights into how the shielding of $\pi-\pi$ stacking- and hydrogen bonding moieties influences intermolecular interactions depending on the bulkiness of the OEG appendices. Stimulated by these perspectives, a series of novel "hybrid" DPs comprising a core-shell structure with a hydrophobic interior and a hydrophilic periphery was synthesized via a "graft to" route (cf. Section 1.2.2). More specifically, the core of these novel polymers

consists of "classic" DPs (cf. Section 3.1.1), which are decorated with OEG dendrons forming the outer shell. Section 3.2.2 describes the synthesis of oligo(ethylene glycol)-based dendrons of generation numbers $g = 1$ and $g = 2$. Subsequently, the preparation and characterization of the "hybrid" dendronized polymers is discussed in Section 3.2.3. In addition to the more general aspects given above, one further concrete motivation for synthesizing these novel polymers was to investigate their rheological behavior in comparison to the "classic" DPs, which will be the topic of Section 3.7.

3.2.2 Synthesis of oligo(ethylene glycol) (OEG)-based dendrons

3.2.2.1 Syntheses of first-generation OEG dendrons

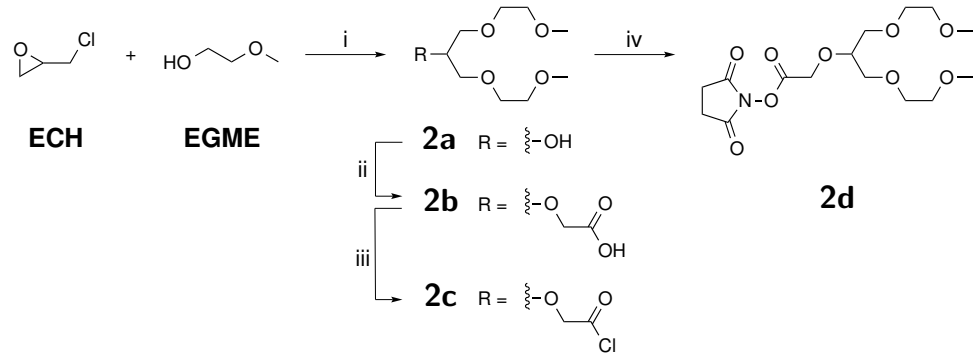

Scheme 3-3: Synthesis of dendronization unit **2d**. Reagents and conditions: i) 50% NaOH, 80 °C, 14 h, *61%;* ii) MBA, NaH, KI, THF, 70 °C, 14 h, *87%*; iii) $SOCl_2$, DMF, CH_2Cl_2, RT, 14 h, *quant.*; iv) **2c**, NHS, Et_3N, −10 °C to RT, 12 h, *89%*.

The synthetic route towards 2-hydroxy-1,3-*bis*(methoxyethoxy)-propane (**2a**) serving as the first-generation ethylene glycol dendron with a single branching point and the corresponding succinimidyl ester **2d** is delineated in Scheme 3-3. Starting from the readily available starting materials epichlorohydrine (ECH) and 2-methoxyethanol (EGME), secondary alcohol **2a** was prepared by slowly adding 50% aqueous sodium hydroxide solution to a mixture of ECH and EGME at 50 °C. The mixture was heated to 70 °C and maintained at that temperature for about 4 h, followed by acidification with concentrated hydrochloric acid. The workup involved removal of precipitated sodium chloride by filtration, evaporation of excess EGME from the product mixture at a rotary evaporator and vacuum distillation of the remaining crude to afford pure **2a** in large scale (up to 120 g) in moderate yields (55-68%). Under optimized conditions, the excess of alcohol (3.5 – 4 equivalents) and elevated temperature (70 – 80 °C) keep the self-condensation of ECH at a tolerable amount without rendering reaction mixture too bulky for convenient handling. Also, purification of the crude product mixture in a single vacuum distillation step using a 30 cm Vigreux column was incomplete and did not afford alcohol **2a** in pure form.

This was solved by the aforementioned removal of starting materials at a rotary evaporator prior to vacuum distillation. Thereafter, **2a** was condensed with *mono*-chloroacetic acid (MCA) under nucleophilic displacement conditions, followed by purification of the carboxylic acid **2b** by acid-base extraction. Under optimized conditions using *mono*-bromoacetic acid (MBA), potassium iodide to help with the nucleophilic displacement, and a minimum excess of sodium hydride, the coupling proceeded in near-quantitative yields. When MCA and a large excess of base (more than 3 equivalents based on **2a**) were employed, acetic acid was identified as the main by-product, which could easily be removed by gentle heating in high vacuum. The resulting product was obtained as a brown-reddish oil and attempts to discolor **2b** with activated charcoal, washing with ethylenediaminetetraacetic acid (EDTA) solution, or column chromatography using various solvent mixtures were unsuccessful. Therefore, acyl chloride **2c** was generated from the acid **2b** by treatment with thionyl chloride and DMF, which was used as a catalyst to generate the Vilsmeier-Haack reagent *in situ*. In this context, the inability of acyl chloride **2c** to form a hydrogen-bonded dimer resulted in a significantly lower boiling point and allowed for further purification by distillation, in contrast to the corresponding carboxylic acid **2b**. Since only gaseous by-products are formed in the preparation of the acyl chloride, the reaction proceeds smoothly and pure **2c** was obtained as a slightly yellow liquid after vacuum distillation under inert atmosphere ($\approx$70% yield after distillation). In principle, compound **2c** constitutes an activated species, which was effectively employed in test coupling reactions with amine-bearing (dendritic) compounds. However, given the long dendronization reaction times, the moisture sensitive nature of acyl chlorides compared to activated esters is certainly unfavorable (cf. Section 3.2.3 for a discussion on the stability and activity of succinimidyl esters vs. acyl chlorides). Hence, compound **2c** was converted into the corresponding succinimidyl ester **2d** by treatment with a stoichiometric amount of *N*-hydroxysuccinimide (NHS) and obtained in high yield (89%) after stirring overnight and extraction with ether.

3.2.2.2 Syntheses of second-generation OEG dendrons

In order to identify suitable synthetic pathways for the preparation of second-generation alcohol **3b** in high yield and at sufficiently large scale, various routes towards compound **3b** starting from its first-generation homologue **2a** were investigated, as depicted in Scheme 3-4. Since, apart from 3-chloro-2-chloromethyl-1-propene (MDC), all materials used in the synthesis were available in large quantities and at reasonable cost, initial efforts focused on its replacement or independent synthesis, respectively. In this regard, reactions to prepare MDC from cheap and readily available chemicals were successful,[98] however, the reported yield could not be fully reproduced (36% vs. 55%), which lowered the calculated savings margin. In addition, the procedure turned out to be tedious and time consuming due to multiple heating and cooling steps as well as the evolution of large amounts of gaseous by-products. Further attempts to prepare **3b** analogously to the first generation, i.e.

from ECH and **2a**, gave only low product yields. This held true irrespective of whether a two-step procedure involving first the nucleophilic displacement of chloride using a stoichiometric amount of **2a** under anhydrous conditions and subsequent ring opening of the epoxide **2e** under either anhydrous or aqueous conditions (8% vs. 32% overall yield) or a one-pot reaction (11% anhydrous vs. 23% aqueous) was performed.

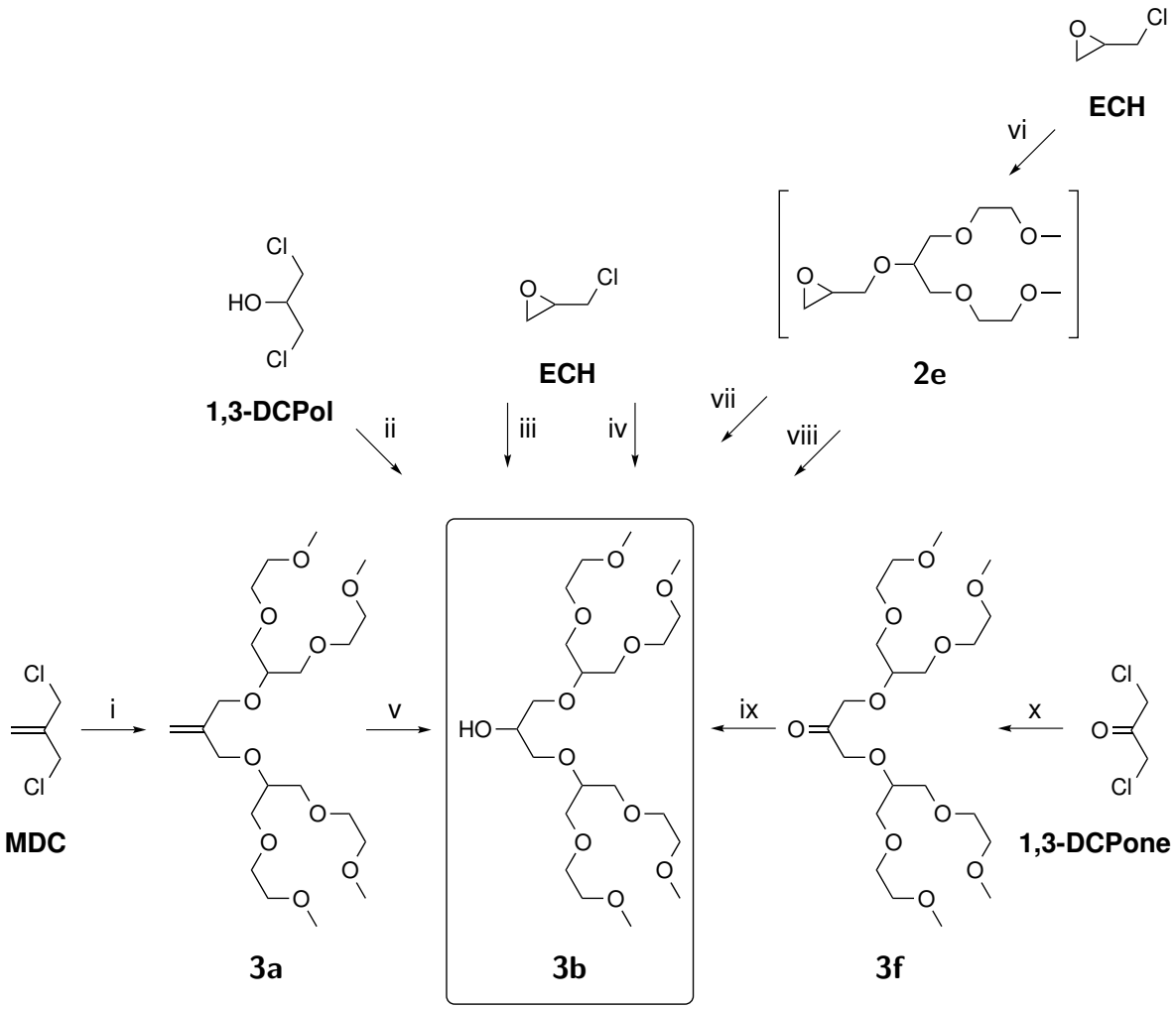

Scheme 3-4: Different synthetic routes towards dendron **3b**. Reagents and conditions: i) **2a**, NaH, KI, THF, 80 °C, 4 d, *61%*; ii) **2a**, NaH, KI, THF, 80 °C, 4 d, *31%*; iii) **2a**, NaH, THF, 80 °C, 4 d, *11%*; iv) **2a**, 50% KOH, H_2O, 80 °C, 2 d, *23%*; v) 1. O_3, CH_2Cl_2/MeOH, −78 °C, 30 min, 2. $NaBH_4$, −78 °C to RT, 14 h, *99%*; vi) **2a**, NaH, THF, 70 °C, 20 h; vii) **2a**, 50% NaOH, H_2O, 60 °C, 24 h, *32%*; viii) Sodium alcoholate of **2a**, THF, 80 °C, 24 h, *8%*; ix) $NaBH_4$, THF, −10 °C to RT, 14 h, *94%*; x) **2a**, NaH, KI, THF, 80 °C, 4 d, *21%*. All reactions were performed on a 2 g scale (based on **2a**).

Evidently, the hydroxyl group formed in the ring opening of ECH acts as a nucleophile in successive reactions and causes the loss of control, which is reflected by the low yields and the large amount of formed by-products, including partial and complete generations.

In addition, the similar polarity of all formed products hampered purification by column chromatography, which turned out to be non-trivial. Nevertheless, pure OEG dendrons up to generation number $g = 3$ could be isolated and identified using eluent-mixtures of dichloromethane and methanol. Further screening of reactants and conditions towards **3b** involved 1,3-dichloro-2-propanol (1,3-DCPol) and 1,3-dichloro-2-propanone (1,3-DCPone), which led to no significant improvements with regard to the yield of the desired product **3b**. For the same reasons discussed earlier, the formation of by-products came as no real surprise in case of 1,3-dichloro-2-propanol, whereas the low yields found with ketone 1,3-dichloro-2-propanone might be explained by enolate formation under the strongly basic, anhydrous conditions and, hence, deactivation of the electrophilic β-carbon, which prevented the nucleophilic displacements from running to completion. After subjection of the crude product mixture to chromatographic purification and reduction of the isolated ketone **3f** with sodium borohydride, the overall yield of **3b** amounted to 20%. This being the case, the reaction of MDC with **2a** using anhydrous conditions and 5 mol% of potassium iodide to promote the nucleophilic displacements followed by ozonolysis of the double bond and subsequent reductive workup with sodium borohydride has given the best results so far.[99] The synthetic route to the second-generation dendron **3b** and the corresponding activated ester **3e** is delineated in Scheme 3-5, accordingly.

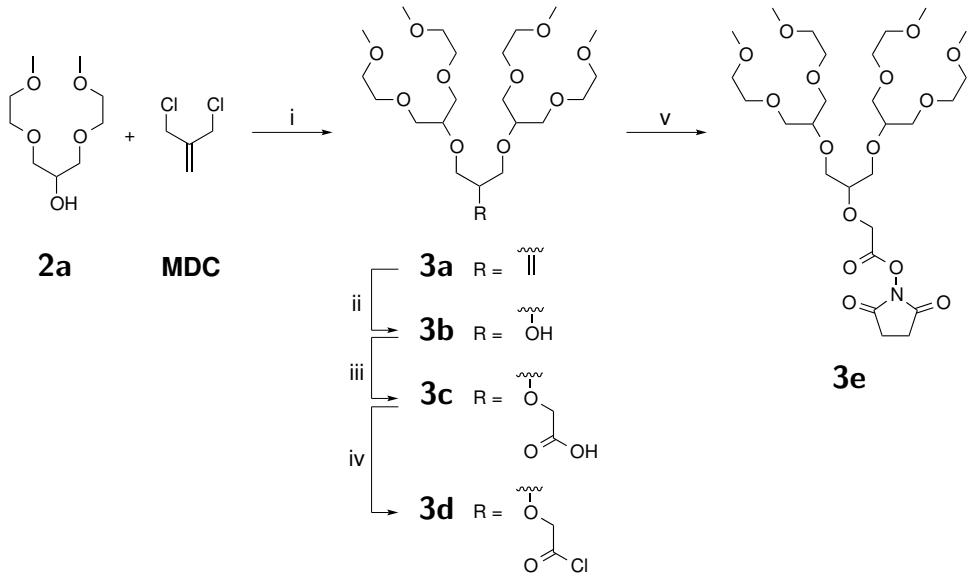

Scheme 3-5: Synthesis of dendronization unit **3e**. Reagents and conditions: i) NaH, KI, THF, 65 °C, 4 d, *67%*; ii) 1. O_3, CH_2Cl_2/MeOH, -78 °C, 30 min, 2. $NaBH_4$, -78 °C to RT, 14 h, *99%*; iii) MBA, NaH, KI, THF, 70 °C, 14 h, *93%*; iv) $SOCl_2$, DMF, CH_2Cl_2, RT, 14 h, *quant.*; v) NHS, Et_3N, CH_2Cl_2, -10 °C to RT, 14 h, *84%*.

In light of the difficulties encountered with the separation of OEG species (*vide supra*), the double bond in MDC is beneficial as it prevents the formation of generation numbers higher than two. Although chromatographic purification of the crude mixture after

reaction of MDC with **2a** remained delicate, separation of **3a** from excess **2a** is facilitated by the different polarity imposed by the double bond in **3a**. Moreover, efforts to remove sufficiently volatile products, including excess **2a**, from the product mixture by vacuum distillation in an inert atmosphere prior to chromatographic purification led to unprecedentedly high yields of **3a** and **3b** (95% and 90% yield from **2a**, respectively). As a result, future attempts may also be directed to the application of this procedure, i.e. removal of excess **2a** *in vacuo* prior to column chromatography, to reactions starting from ECH and 1,3-dichloro-2-propanol, which would offer the potential for considerable cost and time savings. The follow-up reactions towards the activated ester were mostly performed as described previously with the first-generation analogue **2d**, i.e. coupling with **6** and conversion to the corresponding succinimidyl ester **3e** in a two-step protocol. The products following the alcohol **3b** were colored. However, owing to the high molecular weight of the second-generation acyl chloride **3d**, purification by means of vacuum distillation was not feasible anymore and therefore, **3e** was obtained as a brownish oil. One may speculate that the crown ether-like structure of the second-generation OEG dendritic motif promotes the complexation of metal ions such as Na^+ or K^+, which may give rise to charge-transfer effects in these regularly colorless compounds. So far, however, all attempts to address this issue were unsuccessful.

3.2.3 Synthesis of "hybrid" DPs

3.2.3.1 Hydrolysis stability and reactivity of OEG dendrons

The comparatively long reaction times involved in the preparation of dendritic macromolecules renders the stability, selectivity and reactivity of reagents applied in these reactions highly important. Therefore, the applicability of the novel oligo(ethylene glycol)-based dendrons synthesized in this work (cf. Section 3.2.2) with regard to the above-mentioned properties had to be investigated in preliminary studies. In this context, ^{1}H NMR experiments revealed that the addition of D_2O (≈ 10 vol%) to a solution of acyl chloride **2c** in $CDCl_3$ led to complete hydrolysis within 12 h, which could easily be identified by the upfield shift of the β-methylene protons (cf. Figure 8-7 on page 175 of the Appendix). In contrast, the ^{1}H NMR spectra of the corresponding activated esters **2d** and **3e** recorded in DMSO-d6 exhibited significantly slower decomposition after addition of the aforementioned amount of water (cf. Figures 8-8 and 8-9 on page 176 of the Appendix) and no signs of degradation could be observed during regular storage of the compounds under N_2 at $-20\,^\circ$C over the course of at least 5 months. In this context, it should be noted that the solubility of water in chloroform is very limited and, hence, the rate of hydrolysis is limited by the rate of diffusion of the species towards the liquid-liquid interface in the NMR tubes. Hence, the hydrolysis of acyl chlorides should proceed even faster in water-miscible solvents such as DMSO. In a next step, the reactivity of succinimidyl esters **2d** and **3e** towards primary amines was tested using benzylamine

($BnNH_2$) as delineated exemplarily for compound **2d** in Scheme 3-6. Benzylamine was chosen due to its aromatic signals, which allowed for an easy assignability in the respective ^{1}H NMR spectra as they do not coincide with resonances originating from the aliphatic oligo(ethylene glycol) dendrons. By using a two-fold excess of **7** based on activated ester **2d**, the amount of **2f** formed directly reflects the efficacy of the reaction and the activity of the succinimidyl ester, respectively. The coupling product **2f** was obtained with high purity and in quantitative yield within one minute after completion of the addition and simple acid-base extraction to remove excess **7** and *N*-hydroxysuccinimide. The resulting ^{1}H NMR spectra of coupling products **2f** and **3g** are shown in Figures 8-10 and 8-11 on page 177 of the Appendix.

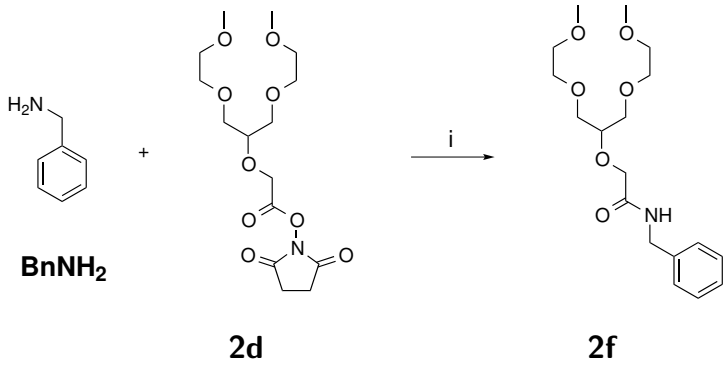

Scheme 3-6: Experimental determination of succinimidyl ester reactivity towards primary amines (exemplarily shown for dendronization unit **2d**). Reagents and conditions: i) 1,4-dioxane, Et_3N, RT, 1 min, *quant.*

3.2.3.2 Coupling of OEG dendrons with "classic" DPs

The syntheses of "hybrid" DPs were performed as delineated in Scheme 3-7. Therein, the terms **x** and **y** in **H[x+y]** denote the generation numbers g of the underlying "classic" DPs ($\mathbf{x} = g_{\text{polymer}}$) and the oligo(ethylene glycol)-based dendrons ($\mathbf{y} = g_{\text{OEG-dendron}}$), respectively. Hence, "hybrid" DPs with a desired generation number g_{target} were prepared by deprotecting "classic" DPs of target generation number $g_{\text{target}} - 1$ or $g_{\text{target}} - 2$ in neat TFA, followed by coupling with dendronization units **2d** and **3e** in analogy to the "classic" DPs. This way, a matrix of twelve nominally second- and third-generation "hybrid" polymers, i.e. **H[1+1]** and **H[1+2]** comprising six different backbone chain lengths, was prepared based on the respective first-generation "classic" polymers (cf. Section 3.1.1 and Table 3-2 on page 23) as summarized in Table 3-5.

For purification, the "classic" protocol was changed from column chromatography to repeated precipitation of the "hybrid" polymers into diethyl ether. In a final step, the "hybrid" DPs were subjected to filtration through a short silica pad (path length ≈ 3 cm) to remove salts originating from the synthesis. This way, yields of 50 – 90% could be achieved, whereby the significant differences between the individual samples likely result

from potentially incomplete dissolution of the respective samples prior to filtration and/or the relatively low sample weights, which are prone to weighing errors. When purification was performed by proper column chromatography, the yields dropped to 0 – 30% due to pronounced clogging of the column, which has also been reported by Zhang et al. for conceptually similar DPs.[77] Subsequently, lyophilization from 1,4-dioxane afforded the "hybrid" DPs as gummy, sticky solids, which were fully soluble in water (by visual inspection) and in a wide range of organic solvents, including DMF, CH_2Cl_2, $CHCl_3$, and methanol, but insoluble in hexane and diethyl ether. Since freeze-drying of the "hybrid"

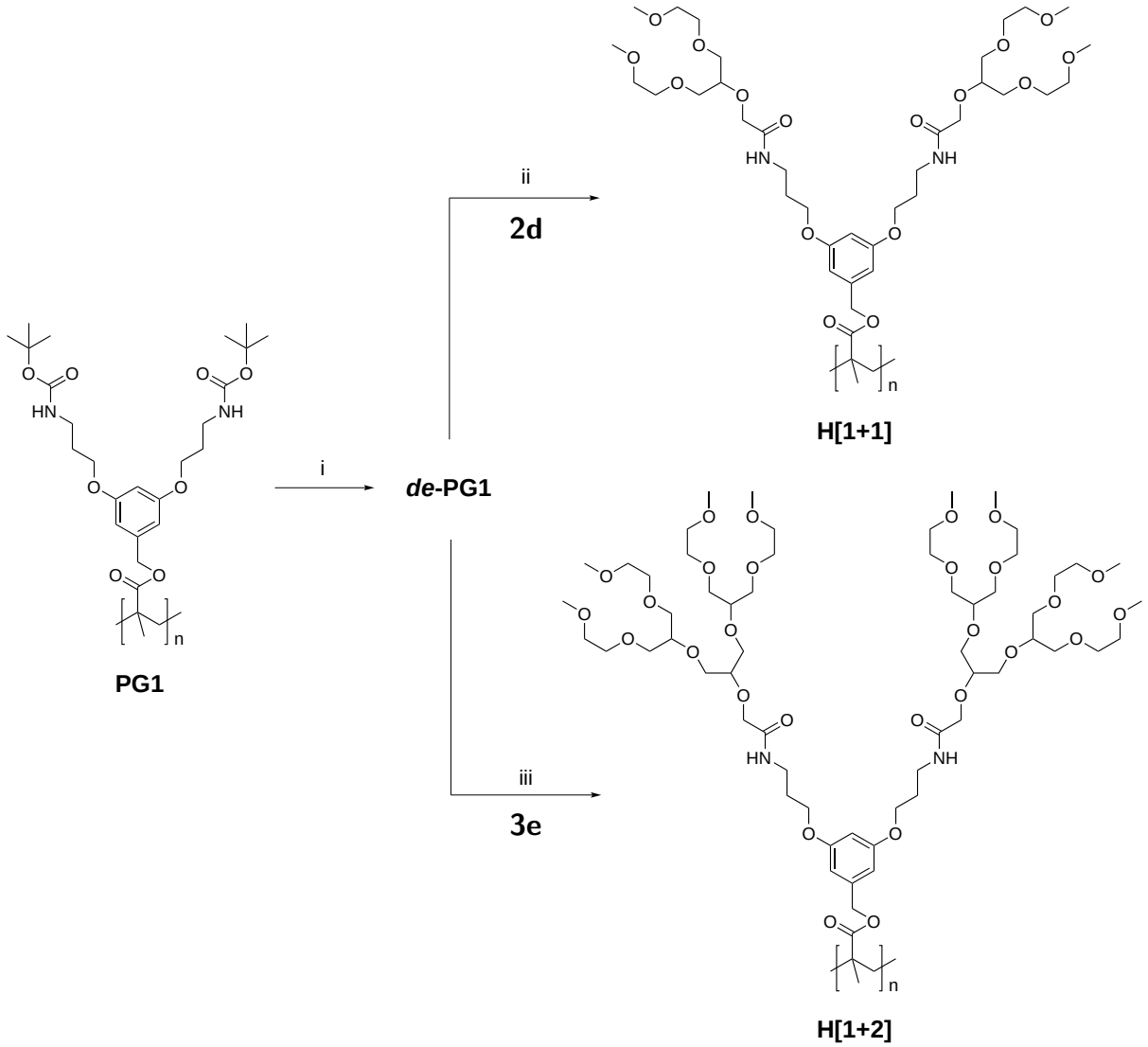

Scheme 3-7: Synthesis of "hybrid" **H[1+1]** and **H[1+2]** DPs. Reagents and conditions: i) TFA, −10 °C to RT, 14 h, *quant.*; ii) Et_3N, 4-DMAP, RT, *60 – 90%*; iii) Et_3N, 4-DMAP, RT, *50 – 80%*.

DPs did not yield fibrous foams as with the "classic" DPs, the freeze-drying step was abandoned in subsequent purifications. This turned out to be detrimental to the "hy-

brid" polymers' solubility at a later stage in the project. More precisely, polymers which had been obtained by evaporation of the solvent and drying to completion could not be fully re-dissolved anymore. A solvent effecting the complete dissolution of these samples could not be identified, and the affected samples could only be partially swollen, even with the help of agitation, elevated temperatures and prolonged duration of exposure. Solubility issues were particularly encountered with samples comprising larger backbone chain lengths ($P_n > 50$). Attempts to store the "hybrid" DPs in aqueous or methanolic solutions proved equally inadequate, since the solutions turned turbid after a few days, indicating the formation of aggregates. Although these precipitates have not been the topic of further investigations, one may speculate that the behavior of the "hybrid" DPs presented herein is similar to the aggregation behavior of charged DPs in aqueous solution, for which duplex formation has been proposed.[100] According to the underlying theoretical model, the formation of duplexes enables the hydrophobic interior of the "classic" DPs to better protect themselves against the aqueous surrounding.[101, 102] A similar mechanism may apply to the non-charged "hybrid" DPs discussed herein.

Table 3-5: Conditions applied for the synthesis of **H[1+1]** and **H[1+2]**.

Entry	Polymer	Dendronization time,[a] d	Coverage,[b] %	Yield, %
1	H[1+1]-50	9	-	85
2	H[1+1]-300	8	-	66
3	H[1+1]-1000	12	-	62
4	H[1+1]-1500	8	-	78
5	H[1+1]-2000	14	-	67
6	H[1+1]-3000	9	-	89
7	H[1+2]-50	8	99.1	77
8	H[1+2]-300	37	-	49
9	H[1+2]-1000	30	99.0	74
10	H[1+2]-1500	14	-	50
11	H[1+2]-2000	13	-	72
12	H[1+2]-3000	21	-	79

[a]Carried out in DMF at room temperature. [b]Determined by UV-labeling with 1-fluoro-2,4-dinitrofluorobenzene (Sanger's reagent) where possible.

In general, the handling of the **H[1+2]** samples was somewhat less delicate compared to their **H[1+1]** counterparts as far as solubility issues are concerned. Nevertheless, the described solution behavior and particularly the fact that once-dried polymers were not re-dissolvable both hampered the further characterization of the "hybrid" polymers. This way, GPC analyses could not be conducted properly and, hence, no experimental molecular weights can be stated. While this indicates some uncertainty, the well-defined

chemical structures and the established high reactivity of succinimidyl esters **2d** and **3e** leave little doubt about the ability of these compounds to participate efficiently in the dendronization reactions and give "hybrid" DPs, whose backbone chain lengths and molecular weights are determined by the respective underlying "classic" DPs and the chemical structures of the "hybridized" repeating units, respectively. Also, the limited number of freeze-dried samples available implied that the degrees of structure perfection of "hybrid" DPs could not be determined with the same rigorousness and comprehensiveness applied in the case of the "classic" DPs (cf. Section 3.1.1). Nevertheless, labeling of two samples (Entries 7 and 9 in Table 3-5) with Sanger's reagent confirmed that the dendronization reactions with compound **3e** were near-quantitative. Given the sterically more encumbered structure of **3e** as compared with **2d**, the values obtained for **H[1+2]** can be regarded as lower thresholds for the degrees of structure perfection to be expected for **H[1+1]**.[103] In this regard, the somewhat reduced reactivity of the second-generation dendronization unit **3e** compared to its first-generation analogue **2d** is substantiated by the results obtained from ^{1}H NMR spectroscopy and the observed hydrolysis rates of both compounds, respectively (cf. Figures 8-8 and 8-9 on page 176 of the Appendix). In addition, ^{1}H NMR spectra of representative **H[1+1]** and **H[1+2]** samples also indicated a high coverage, as evidenced by the integrated peak ratios of signals corresponding to the oligo(ethylene glycol) moieties and the aromatic protons, which were in good agreement with the theoretically expected values (cf. Figures 8-12 and 8-13 on page 178 of the Appendix). Hence, it can be argued that identical chemical structures and high degrees of structure perfection prevail throughout the two "hybrid" DP series described herein, irrespective of whether their purification involved freeze-drying or not. Unfortunately, the replication of all experiments to yield freeze-dried **H[1+1]** and **H[1+2]** samples was not possible due to the limited amount of "classic" first-generation base polymers, which were used for the preparation of the homologous series (cf. Section 3.1.1).

3.2.4 Summary of Section 3.2

The preparation of DPs with different dendronization units provides a convenient strategy to fuse distinct properties in one macromolecule. To this end, two novel oligo(ethylene glycol)-based dendronization units of $g = 1$, 2 bearing succinimidyl esters at their focal points were synthesized. The activity and stability of these dendrons were investigated and established in model coupling reactions with benzylamine and hydrolysis studies, which were both followed by ^{1}H NMR spectroscopy. The synthesized OEG dendrons were subsequently coupled to the first-generation "classic" DPs described in Section 3.1 to yield amphiphilic nanocylinders that combine the water-solubilizing properties of the OEG dendrons with the structure-forming characteristics of "classic" DPs. It was found that freeze-drying of these "hybrid" DPs is crucial for their re-dissolvability, as the polymers obtained after simple evaporation of solvents could only be swollen after some storage time.

3.3 DPs with enhanced supramolecular interactions

3.3.1 Concept of transient networks

Supramolecular polymers are assembled from monomeric building blocks through the formation of non-covalent, directional interactions, such as ionic associations, π-π stacking, ligand-metal complexation, or hydrogen bonding.[104] Thereby, the reversible and dynamic nature of these non-covalent interactions renders many supramolecular polymers responsive to external stimuli, such as temperature, solvents, or the presence of chemicals. For reasons of directionality and versatility, especially hydrogen bonds hold a prominent place in supramolecular chemistry and, consequently, a plethora of hydrogen bonding moieties have been developed and employed for the synthesis of supramolecular polymers.

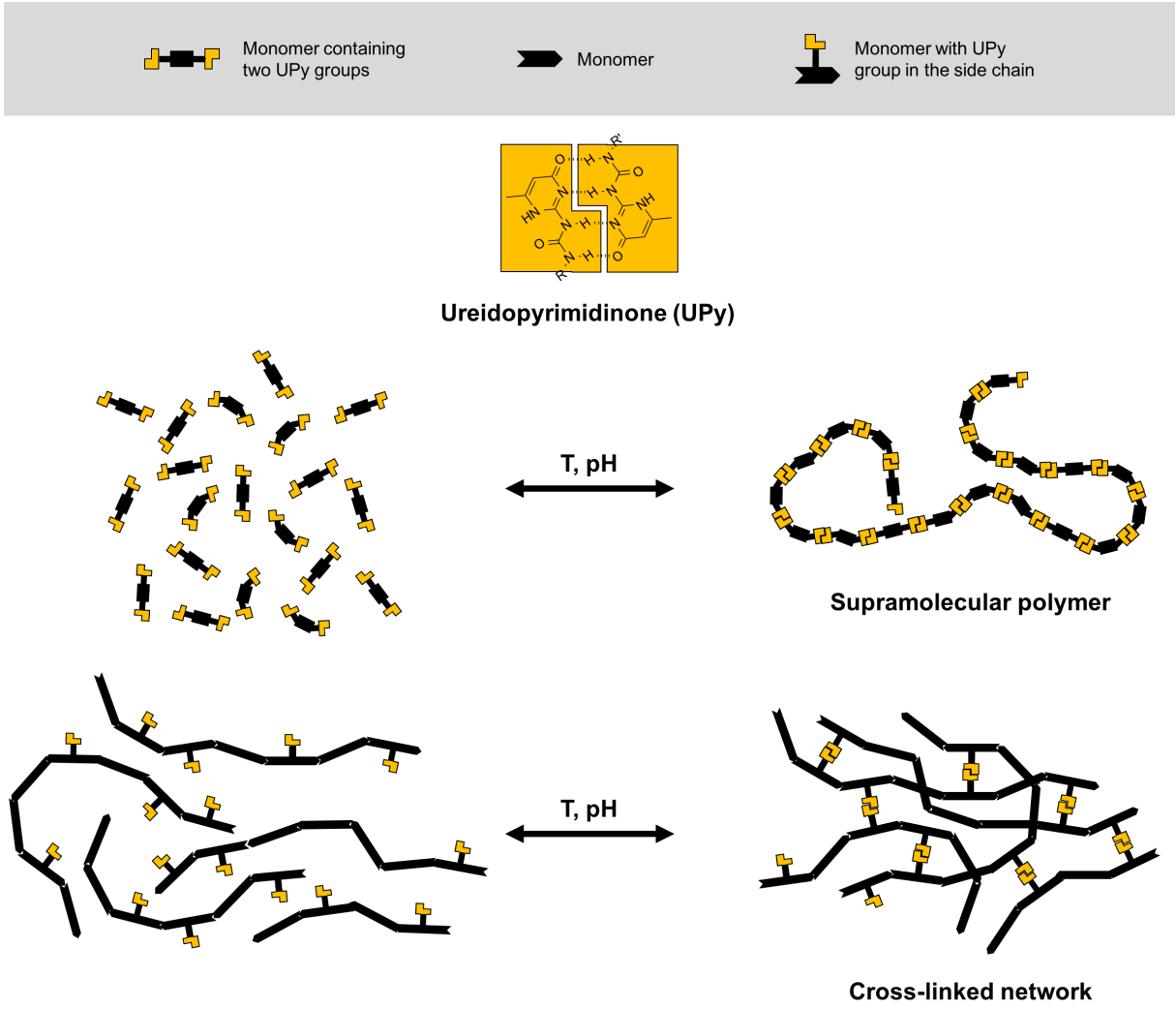

Figure 3-2: Schematic representation of supramolecular polymers (top) or cross-linked supramolecular structures (bottom) originating from self-complementary quadruple hydrogen bonding interactions between UPy groups.

The strength and specificity of hydrogen bonding interactions described in the literature ranges from weakly complementary pyridine-phenol pairs[105] to extremely strong, self-complementary sixfold hydrogen-bonded dimers.[106] In this regard, one of the most investigated and frequently used hydrogen bonding moieties is the 2-ureido-4[1*H*]-pyrimidinone (UPy) group, which was first reported by Sijbesma *et al.* in the context of highly thermally responsive polymeric materials in the late 1990s.[107] The synthetic accessibility and exceptionally high association constant ($K_{\mathrm{dim}} \approx 10^7\,\mathrm{M}^{-1}$ in $CHCl_3$) of this self-complementary, quadruple hydrogen bonding group have greatly contributed to its success. As illustrated schematically in Figure 3-2, the equilibrium of such a supramolecular assembly can be reversibly shifted to the monomer side, with a concomitant change in properties due to the resulting increase in chain mobility and decrease in viscosity, respectively, before the original material is re-formed by shifting the equilibrium back to the assembled state. Depending on the location and the number of moieties that are capable of undergoing directional secondary interactions in the employed building blocks, in principle, the range of achievable structures encompasses supramolecular assemblies and cross-linked networks.

Linear supramolecular assemblies are formed if the non-covalent binding motifs function as end groups in bifunctional molecules. In the realm of high degrees of polymerization, the resulting supramolecular polymers feature a polymer-like behavior (cf. top half of Figure 3-2).[108] The properties of these materials have been shown to improve significantly upon UPy-functionalization, even though Van Beek *et al.* could show that their mechanical stability does not result merely from pairwise UPy – UPy association and large apparent molecular weights. Instead, a strong dependency of the enhanced properties on crystallization of UPy dimers into long stacks could be identified.[109] In this context, the nature of the linker connecting the UPy moieties to the underlying building block was also shown to affect the binding strength of the supramolecular motif, with bulky substituents preventing such crystallization while additional urea or urethane groups enhance lateral hydrogen bonding between the UPy dimers.[110, 111] Furthermore, de Greef *et al.* investigated the effect of competitive intramolecular hydrogen bonding exerted by oligo(ethylene glycol)-substituents attached to the UPy groups on the dimerization constant of the respective dimers.[112] Their studies revealed that the ether oxygens of sufficiently long OEG chains could back-fold to the hydrogen bond donor atoms of the UPy group and strongly reduce its dimerization strength.

Moreover, the presence of multiple supramolecular binding motifs in the side chains along a polymeric backbone gives rise to the formation of so-called "transient networks", in which the cross-links can be reversibly formed and broken, as illustrated in the bottom half of Figure 3-2. Studies in the literature have demonstrated the ability to incorporate UPy groups in the side chains of higher molecular weight polymers via either copolymerization of UPy-functionalized monomers[113] or a post-modification approach.[114] In principle, both strategies were successfully applied to prepare supramolecular materials, the bulk properties of which were primarily determined by the concentration of UPy groups incor-

porated along the polymer chain. However, in the case of the copolymerization approach, the low solubility of UPy monomers usually limited their incorporation to a few mol%, which also reduced the scope of obtainable properties.[115, 116] The post-polymerization modification approach imposes some downsides, too, including a lower degree of control over the exact amount of UPy-functionalization owing to the fact that full conversion cannot be guaranteed *a priori*. This holds especially true for polymers comprising a considerable degree of complexity, for which performing post-polymerization modifications selectively and quantitatively becomes increasingly challenging.

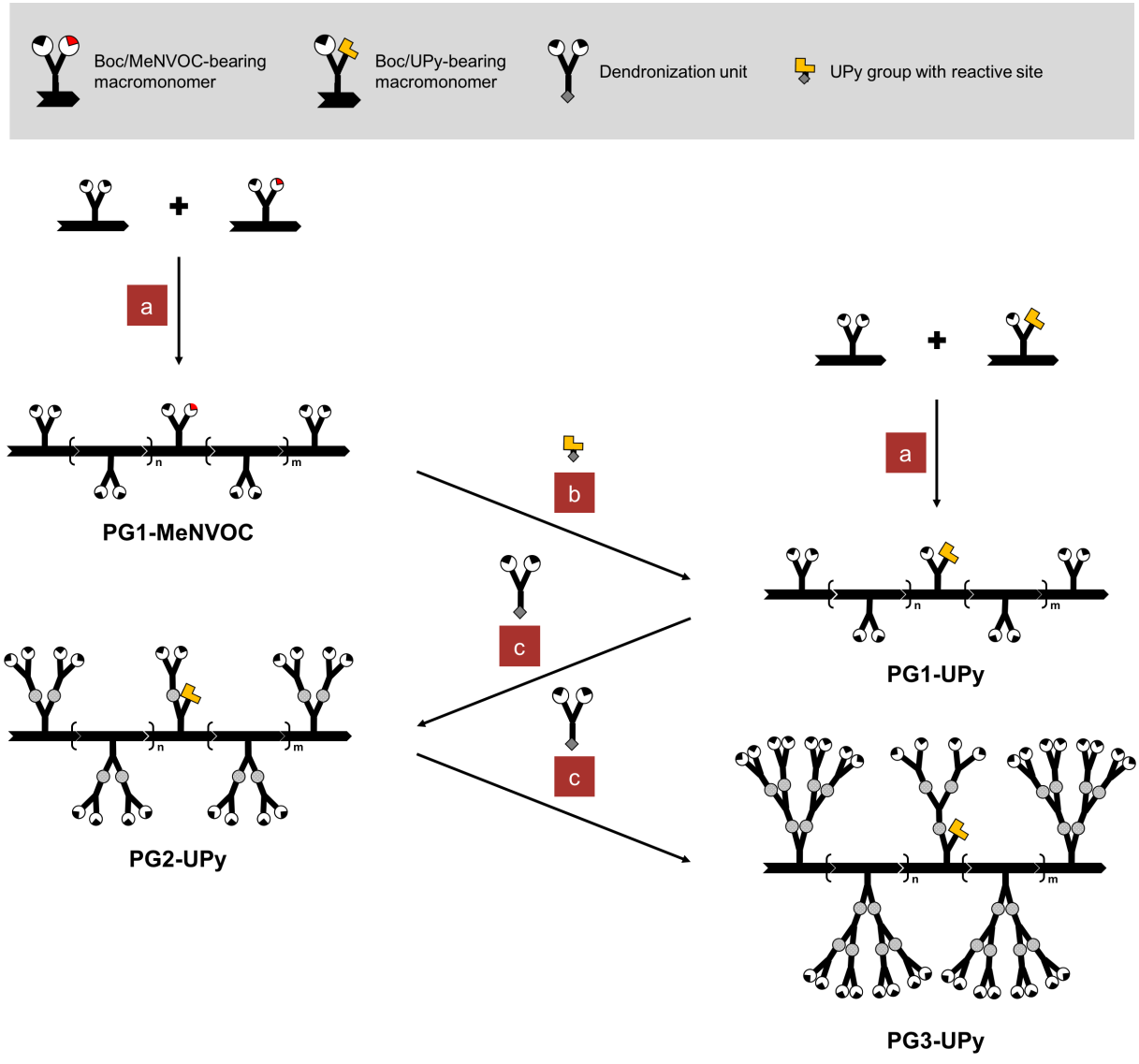

Figure 3-3: Schematic representation of the conceptual synthetic approaches towards UPy-functionalized dendronized polymers via post modification or copolymerization. (**a**) Copolymerization of macromonomers; (**b**) Selective deprotection and PPM using UPy-precursors; (**c**) Deprotection and PPM using dendritic building blocks.

In this context, most of the dendritic building blocks reported in the literature carry only one sort of peripheral functional group each, which is typically uniformly protected with a single kind of protecting group. Consequently, the options available for "surface" engineering are obviously limited,[117–120] i.e. potential pathways include either the modification of all functional groups at once or the modification of a portion of randomly distributed functional groups over the entire macromolecule. To overcome this limitation and increase the options for surface- and interior modifications, there is an obvious demand for synthetic strategies leading to compounds with individually addressable functionalities, which would not only allow for a higher degree of control over the structure and chemistry of DPs, but also considerably widen their scope of application.

In this section, the preparation of transient DP networks using the two conceptionally different pathways illustrated in Figure 3-3 will be discussed. First of all, the initial approach to prepare UPy-functionalized DPs in a post-polymerization modification approach will be presented in Section 3.3.2. Existing orthogonal protecting group strategies reported in the literature on DPs will be introduced and the potential of photolytically cleavable protecting groups will be highlighted. In this regard, a particular focus will be placed on the eminently promising class of *o*-nitrobenzene derivatives, including mechanistic aspects of the photolysis reaction. Moreover, the synthetic approach to a dendronized macromonomer bearing two orthogonally protected amines (MeNVOC/Boc) will be described. Finally, the performance of the synthesized macromonomer and a polymer prepared thereof in preliminary photolysis studies will be discussed and evaluated against the direct use of UPy-bearing macromonomers in a copolymerization approach, which will be the topic of Section 3.3.3. More specifically, the preparation of a UPy-bearing dendronized macromonomer will be presented, followed by the synthesis and characterization of a homologous series of DPs comprising varied degrees of UPy-functionalization and generation numbers $g = 1 - 3$.

3.3.2 Post-polymerization modification approach

3.3.2.1 Orthogonal protecting groups in "classic" DPs

Current research on the "classic" DPs largely relies on the commercially available, doubly Boc-protected first-generation methyl and succinimidyl esters described in Section 3.1 and their complete deprotection using trifluoroacetic acid.[119] Naturally, this strategy imposes inherent restrictions on the feasibility and sequence of successive reactions. Hence, a more sophisticated approach, such as the employment of orthogonal protecting groups, appears desirable. Previous studies in the literature reported on the *tert*-butyloxycarbonyl (Boc) / benzyloxycarbonyl (Cbz) and the Boc / 2,7-di(*tert*-butyl)-9-fluorenyloxycarbonyl (Fmoc*) protecting group systems, which offer a high degree of orthogonality regarding the conditions applied for their deprotection.[121–123] However, their use in dendronized polymers comprising chemical structures that resemble the present "classic" DPs (cf.

Figure 3-4 for Cbz- (dendron **8**) and Fmoc*- (macromonomer **9**) as examples) was found to be unsuitable. In the case of the Cbz protecting group, partial de-dendronization, i.e. cleavage of dendrons directly at the benzylic ester functions connecting the dendrons to the backbone, was observed under the conditions applied for the cleavage of peripheral Cbz protecting groups by hydrogenolysis.[120]

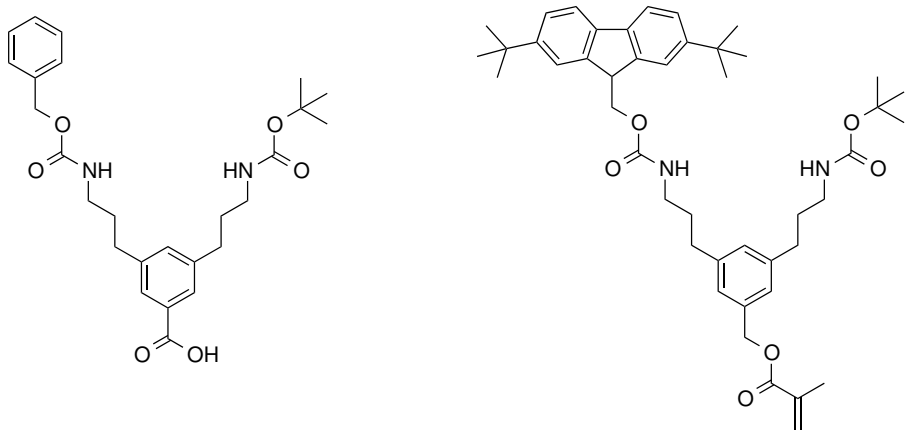

8 **9**

Figure 3-4: Previous examples by Al-Hellani et al. on dendritic structures comprising Cbz/Boc (compound **8**)[124] and Fmoc*/Boc (compound **9**)[119] orthononally protected amines.

In the case of Fmoc*, the poor solubility of many Fmoc-protected amino compounds in organic solvents as well as difficulties to remove the by-product originating from its deprotection[125] are overcome by the introduction of *tert*-butyl groups in the 2,7-positions of fluorene[126] and deprotection of amines at the polymer level was found to proceed selectively and quantitatively in the presence of Boc.[120] Nevertheless, this system has certain limitations as well: Although, in the first step, the two *tert*-butyl groups can be introduced by Friedel-Crafts alkylation in high yield,[121] the addition of the hydroxymethyl group in the second step involves mono-lithiation and reaction with paraformaldehyde.[127] This reaction was shown to be sensitive to the exact stoichiometry of the reactants, with small surpluses resulting in substantially diminished yields of the desired hydroxymethyl product along with the fulvene elimination product and recovered di-*tert*-butylfluorene.[121] In addition, the deprotection sequence of the Boc / Fmoc*-system is rather pre-determined as the presence of free amines during dendronizations - or under amine-coupling conditions in general - may lead to inadvertent deprotection of Fmoc* by the latter.

Because of the aforementioned reasons, the need for a protecting group strategy providing both true orthogonality and facile large-scale synthesis becomes apparent. In this context, photolabile protecting groups, which are by nature orthogonal to traditional protecting groups, have recently drawn considerable attention in synthetic chemistry.[128] At it, the mild and neutral conditions involved in their deprotection render photolytically

cleavable protecting groups popular in the field of "Green Chemistry" as well.[129] The general requirements imposed on photolytically cleavable protecting groups include rapid and complete release upon irradiation with light, high quantum efficiencies and reasonable light-sensitivity. Furthermore, the generated photo-products should be inert enough to tolerate the presence of active functional groups in the respective system, i.e. they should not undergo any undesired side reactions. Usually, light-induced reactions are very fast, which - in combination with the ability to temporally and spatially control the exposure to light in a precise manner - can be exploited in manifold ways, such as in the light-triggered release of previously "caged" compounds in biokinetic studies[130] or the generation of patterned images in polymer films.[131] Notably, even "photoorthogonality", i.e. a differentiation between multiple photocleavable protecting groups in one system based on distinct excitation wavelengths, has been demonstrated.[132, 133] A considerable number of studies in the literature describes carbamoyl derivatives based on benzoins,[134–136] *o*-nitrobenzyl,[137–139] 9-fluorenone,[140] or 7-hydroxycoumarin-4-ylmethyl[141–144] as photolabile protecting groups for amines. In this context, a focus on *o*-nitrobenzyl alcohol derivatives can be observed and among the many reports in the literature, a study by Cameron and Fréchet is particularly noteworthy.[138] Therein, the authors suggest that the photosensitivity of *o*-nitrobenzyl systems is determined by a complex combination of both steric and electronic effects inherent in the structure of the chromophores. More specifically, it was shown that quantum efficiencies varied depending on the number of nitro groups in the *ortho*-position of the benzene ring, the electronic nature of the aromatic moiety, and the bulkiness of the α-substituent in the benzylic position.

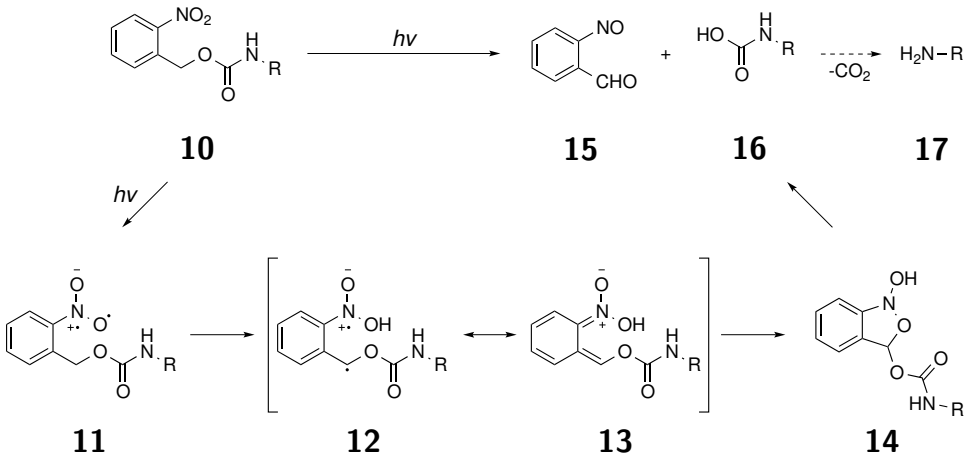

10 **15** **16** **17**

11 **12** **13** **14**

Scheme 3-8: Proposed mechanism for the photolysis of *o*-nitrobenzyl carbamates according to Cameron et al. [138]

The underlying photoinduced internal oxidation-reduction reaction of aromatic nitro compounds containing a C-H bond in *ortho*-position to a nitro group has been the subject of extensive research.[138, 145] As a result, a number of intramolecular photorearrangements are known in which the nitro group is reduced to a nitroso group and an oxygen atom is inserted into the ortho benzylic C-H bond. The proposed mechanism is illustrated in

Scheme 3-8. Thereby, the primary photochemical process and the rate-determining step is the intramolecular H-abstraction by the excited nitro group in compound **10**, followed by an electron-redistribution process to the aci-nitro form **13**, which then rearranges to the nitroso product **15**. In the case of carbamates, spontaneous decarboxylation of **16** frees carbon dioxide and the respective amine **17**. Noteworthy, the fact that the *o*-nitrobenzyl photorearrangement proceeds via an intramolecular pathway represents a particularly attractive feature, as it allows for carrying out the photolysis reaction both in solution and in the solid state. In general, aliphatic amines are released from *o*-nitrobenzylcarbamates upon photolysis in good yield. At it, the undesired occurrence of imine byproducts originating from the reaction of the released amine **17** with the aldehyde photoproduct **15** can be suppressed by the addition of a carbonyl scavenger to the reaction mixture, or through alkyl or aryl substitution at the benzylic position. In the latter case, a ketone is generated as the photoproduct, which is much less prone to imine formation compared to the nitroso aldehyde **15** formed in the absence of a substituent at the benzylic position. Moreover, the introduction of two methoxy groups in the benzene ring results in an increased absorbance at wavelengths longer than 320 nm. As a consequence, the α-methylnitroveratryloxycarbonyl (MeNVOC) photolabile protecting group has been widely used, e.g. in peptide synthesis or light stimuli-responsive materials.[146, 147]

3.3.2.2 Synthesis of MeNVOC-bearing macromonomer 4b

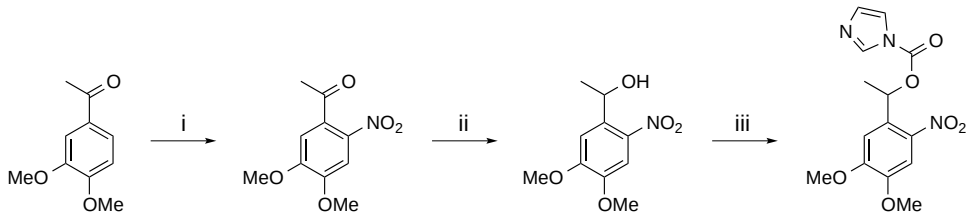

18 **19** **20** **21**

Scheme 3-9: Synthesis of CDI-activated 4,5-dimethoxy-2-nitrobenzyl alcohol **21**. Reagents and conditions: i) HNO_3, $NaNO_2$, 0 °C, 30 min, *69%*; ii) $NaBH_4$, THF/MeOH, −15 °C, 2 h, *96%*; iii) CDI, CH_2Cl_2, RT, *98%*.

The synthesis of imidazole-activated MeNVOC precursor **21** is delineated in Scheme 3-9. Starting from commercially available 3,4-dimethoxyacetophenone (**18**), nitration using nitric acid and sodium nirite gave the desired product **19** in moderate yield (69% yield).[148] Compound **19** precipitated from the reaction mixture and was obtained in high purity after simple washing of the residue with ice cold water. Notably, the selectivity of the nitration reaction to give the desired *ortho*-substituted product was confirmed by ^{1}H-^{1}H nuclear Overhauser effect spectroscopy (NOESY) and the existence of a cross-peak originating from the spatial proximity of the acetophenone methyl protons and the aromatic proton in *ortho*-position to the acetophenone group (cf. Figure 8-15 on page 179 of the

Appendix). Subsequent reduction of the ketone in compound **19** to give the corresponding alcohol **20** proceeded smoothly using sodium borohydride (96% yield).[131] By using a stoichiometric amount of the reducing agent and careful reaction monitoring (TLC), no reduction of the nitro group was observed. In a final step, the obtained alcohol was activated with 1,1'-carbonyldiimidazole (CDI) to give the corresponding novel CDI-activated MeNVOC precursor **21** in an excellent yield of 98%.

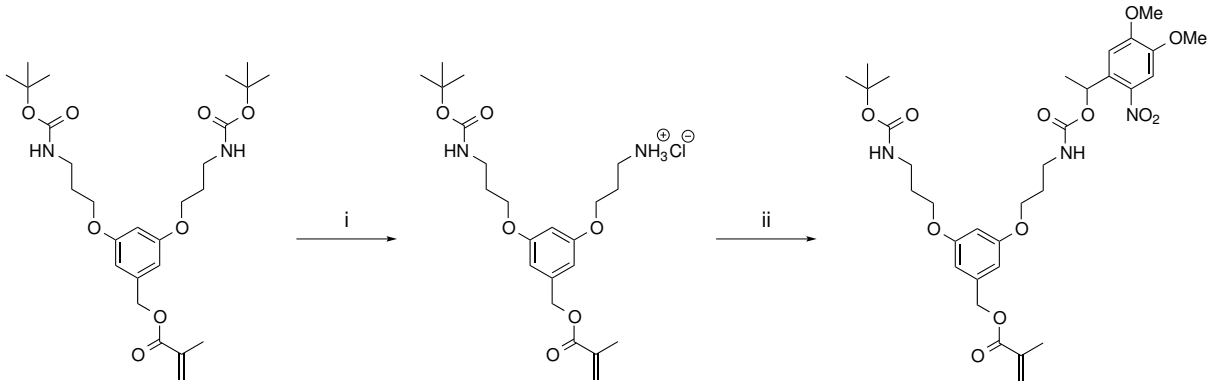

Scheme 3-10: Synthesis of macromonomer **4b**. Reagents and conditions: i) TFA, CH_2Cl_2, RT, 6 d, *57%*; ii) **21**, Et_3N, DMF, RT, 3 d, *70%*.

The synthetic approach towards the orthogonally protected, first-generation macromonomer **4b** is delineated in Scheme 3-10. Starting from the doubly Boc-protected, first-generation macromonomer **1c** (cf. Section 3.1.1), reaction with trifluoroacetic acid afforded a statistical mixture of singly and doubly deprotected species, along with unreacted starting material. Due to the vastly different polarities of these compounds, the desired mono deprotected product **4a** was easily isolated by column chromatography and obtained on a multi-gram scale, albeit in moderate yields (50-60%). Subsequently, the previously described MeNVOC-precursor **21** was coupled to the mono-deprotected amine in the style of a procedure described in the literature.[149] The MeNVOC-functionalized macromonomer **4b** was purified by column chromatography and obtained in good yield (70%).

3.3.2.3 Photolysis of MeNVOC-containing compounds

In order to establish the usability of the α-methylnitroveratryloxycarbonyl (MeNVOC) moiety, it was helpful to determine its sensitivity to the exposure of light under standard laboratory conditions, as dealing with highly light-sensitive compounds can be tedious and frustrating due to unwanted decomposition. Hence, a preliminary study on the photolytic stability of the MeNVOC group under various conditions was performed first. To this end, compound **22** (cf. page 136 of the Experimental) was synthesized, starting from the previously described alcohol **20** (*vide supra*). At it, the last two steps of the synthesis, i.e. the reduction of the ketone in compound **19** and the activation with N,N'-disuccinimidyl

carbonate to give compound **22**, including the all work-up procedures, were performed under rigorous exclusion of light. Model compound **22** was recrystallized twice from ethanol to obtain a very clean NMR spectrum. Then, aliquots of compound **22** ($\approx 15\,\mathrm{mg}$) were placed in Schlenk tubes under an atmosphere of nitrogen in order to prevent any side reactions due to the presence of oxygen or moisture, and the samples were exposed to various lighting conditions, including sunlight next to a window, a standard halogen lamp inside the fume hood, and the UV lamp used for TLC inspection. In addition, different time frames and states of matter were considered, including the material in its solid form and in solution. After exposure to the above-described conditions, the samples were examined by NMR spectroscopy and the spectra were compared to the original clean spectrum.

As apparent from Figure 8-16 on page 180 of the Appendix, the samples placed near the window and in the fume hood with the lighting turned on appear to be stable even after prolonged exposure to these conditions (up to 8 d). However, after several days, the color of the solid samples that were exposed to sun and UV light started to darken from bright yellow to orange-brown. Surprisingly, the corresponding NMR spectra still looked clean and showed no noticeable signs of decomposition. This may be explained by the fact that the decomposition proceeds more efficiently on the surface, whereas the light transparency inside the solid granules is significantly reduced. Hence, the decomposition of the MeNVOC groups located inside the granules was hardly detectable by standard NMR spectroscopy. Even in the case of exposure to low-intensity UV light matching the excitation maximum of the MeNVOC moiety ($\lambda = 365\,\mathrm{nm}$), no significant decomposition could be deduced from the respective ^{1}H NMR spectra. In the case of the dissolved samples that were exposed to the conditions described above, a few additional signals could be identified in the corresponding ^{1}H NMR spectra and TLC analyses, the intensity of which was very small though. This observation is convincing as the photoreaction is likely to be more efficient in a system that is more transparent to the incoming light and offers increased conformational mobility compared to the solid state.[150] All in all, the findings from the preliminary photolysis study demonstrate that the MeNVOC protecting group provides reasonable stability under normal laboratory working conditions. Consequently, synthesis and storage require only a minimum of light-related precautions, such as wrapping reaction vessels in aluminium foil and storage in the dark.

In a next step, the rate and the efficiency of the MeNVOC protecting group in the dendritic system under consideration, i.e. the "classic" DPs, was investigated using the MeNVOC-bearing macromonomer **4b** as a model compound for the final polymer. At it, the unimolecular character of the macromonomer arguably allows for a more precise investigation of the photolysis reaction and easier determination of the decomposition products derived therefrom compared with the polydisperse mixture obtained after polymerization. As previous reports in the literature point towards a strong dependency of both the feasibility and the efficiency of the photolysis reaction on the respective compound-solvent-system,[151] initial efforts were focused on the identification of suitable solvents for the

photolysis reaction in the present dendritic system. Figure 3-5 illustrates the recorded UV-Vis spectra of macromonomer **4b** as a function of irradiation time for four different solvents, i.e. THF (a), DMF (b), MeOH (c), and $CHCl_3$ (d).

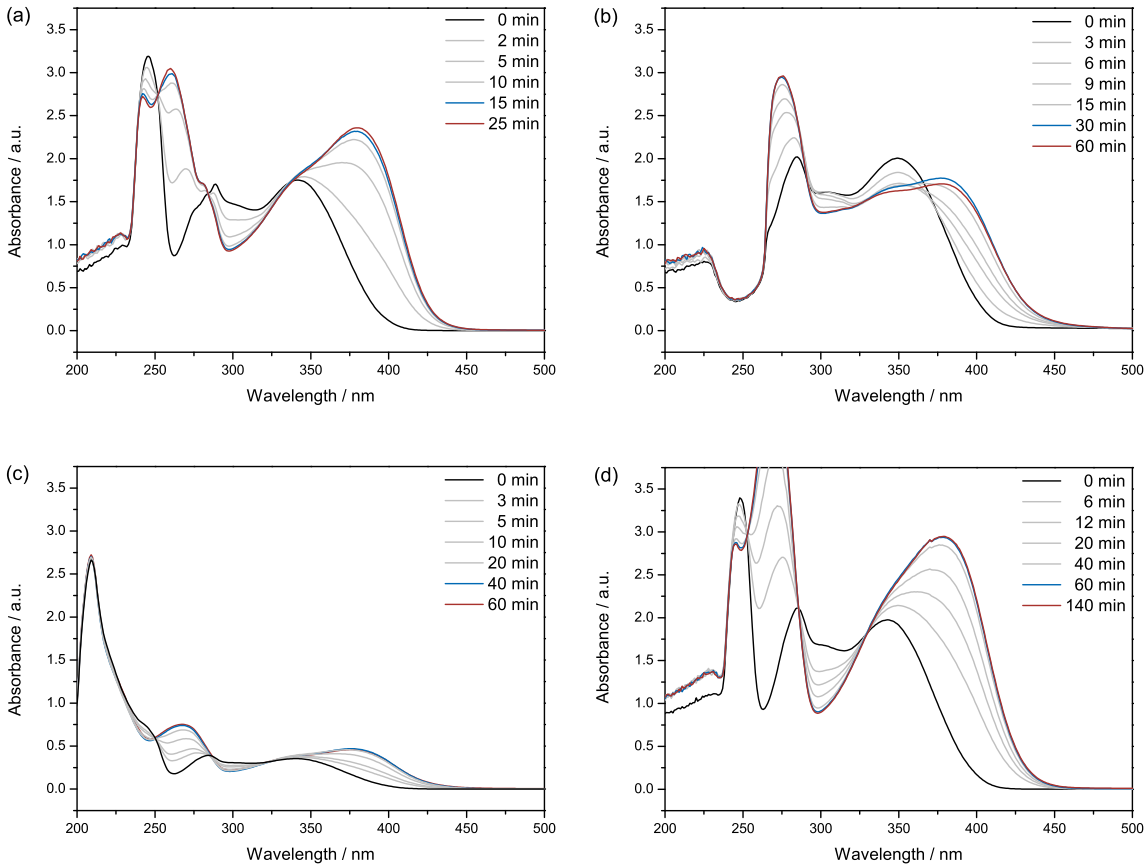

Figure 3-5: UV-Vis spectra of **4b** recorded in (**a**) THF, (**b**) DMF, (**c**) MeOH, and (**d**) $CHCl_3$ as a function of irradiation time. All irradiation experiments were performed on solutions of similar concentration ($c \approx 3.5 \cdot 10^{-4}$ M) at $\lambda_{max} = 365$ nm and a nominal power output by the used LED light source of $P = 200$ mW.

The UV-Vis spectra corresponding to the approximate endpoints of the photolysis reactions, i.e. the irradiation times after which additional irradiation effected no further changes in the resulting spectra, are drawn in blue and red, respectively. The actual experiments were performed on solutions of macromonomer **4b** in the respective solvents ($c \approx 3.5 \cdot 10^{-4}$ M) that were irradiated with a LED light source featuring an emission wavelength maximum (λ_{max}) of 365 nm and a maximum nominal output power (P) of 250 mW. By carrying out the irradiation experiments directly in the quartz cuvettes used for the spectrophotometric measurements, the individual UV-Vis spectra series could be obtained in a time-efficient manner by subsequent irradiation of a single sample.

The time-dependent UV-Vis measurements of macromonomer **4b** in THF are illustrated in Figure 3-5(a). Irradiation with UV light of a wavelength $\lambda_{max} = 365\,nm$ resulted in a noticeable red shift of the observable absorption maxima, i.e. the short-wavelength absorption peak at $\lambda \approx 245\,nm$ decreased as the absorption peak at $\lambda \approx 260\,nm$ increased, consistently. In addition, the absorption peak centered around $\lambda \approx 340\,nm$ in the spectrum prior to irradiation shifts to $\lambda \approx 380\,nm$ and increases in intensity with increasing irradiation time. Moreover, the light-induced changes of the spectra revealed the emergence of three isosbestic points located at 252 nm, 284 nm, and 336 nm, which point towards a successful photoreaction. In this context, the term isosbestic point is usually employed with reference to a set of absorption spectra plotted on the same chart, which all intersect at one wavelength at least.

From a physical chemistry point of view, an isosbestic point has been defined as a wavelength occurring in the absorption spectra during a chemical reaction, where at least two chemical species, e.g. the reactant A and the product B, have identical molar absorption coefficients, which remain constant as the reaction proceeds.[152, 153] In this regard, a stable isosbestic point is often taken as evidence that a reaction proceeds without the formation of a persistent intermediate or multiple products. However, from previous experimental work and computer simulations in the literature,[154] it is known that more complex reactions can also exhibit isosbestic points and that even the wavelength of the isosbestic point may change. Hence, it follows that the mere appearance of one or more clean isosbestic points in spectrophotometric studies on (photo-)chemical reactions cannot be taken as evidence for the clean or quantitative conversion of a precursor to a single given product. Rather, the existence of an isosbestic point implies a constant fractional yield of products. For instance, an isosbestic point may also occur if a product mixture comprising both colorless and chromogenic products are formed. In the system at hand, one may argue that the photocleavage reaction is clean, which is in line with the well-understood photolysis mechanism of *o*-nitrobenzenes[138, 145] and further examples in the literature reporting on virtually quantitative cleavage yields.[137] Under the applied photolysis conditions, the end point of the performed irradiation experiments in THF was reached after $\approx 15\,min$ as inferred from a separate irradiation experiment, in which continuous irradiation for 25 min resulted in a virtually superimposable UV-Vis spectrum. Although these initial results were promising from a theoretical point of view, a direct translation to the actual goal, i.e. the photolysis of MeNVOC moieties at the polymer-level, was not feasible as the generation of a large number of free amines in THF would most likely result in the irreversible precipitation of the polymer from the deprotection mixture.

Hence, the photolysis reaction was further investigated in DMF, which is the solvent of choice for dendronization reactions with the "classic" DPs. Contrary to the time-dependent spectra of **4b** in THF, the respective spectra obtained in DMF did not show well-defined isosbestic points, as illustrated in Figure 3-5(b). The progressively changing intersection wavelengths of the absorption curves around $\lambda \approx 360\,nm$ are indicative of the

simultaneous formation of a reaction intermediate ($A \longrightarrow C \longrightarrow B$) or side products in addition to the desired photolysis reaction.[155]

To this end, further efforts were directed to identify the suitability of MeOH for use in the photocleavage reactions, as the free amine-induced solubility issues could also be overcome by the ability of MeOH to engage in hydrogen boding. As apparent from Figure 3-5(c), three sharp isosbestic points could be observed at 249 nm, 286 nm, and 323 nm over the complete irradiation time, whereby the end point of the photolysis reaction was reached after $\approx$ 20 min.

Since, to this point, all NMR spectroscopic measurements on macromonomer **4b** and its precursors were performed in $CDCl_3$, it was of obvious interest to follow the photolysis reaction not only spectrophotometrically but also via NMR spectroscopy. Hence, the evolution of the UV-Vis spectra of **4b** as a function of irradiation time were also investigated in $CHCl_3$, as illustrated in Figure 3-5(d). Similar to the previously described UV-Vis spectra obtained in THF and MeOH, three distinct isosbestic points could be identified at 253 nm, 286 nm, and 329 nm. However, the time required to reach the end point of the photolysis reaction was somewhat larger compared to the irradiation times that were previously identified with THF and MeOH ($\approx$ 60 min vs. $\approx$ 15 min and $\approx$ 40 min, respectively). Moreover, at the same concentration ($c \approx 3.5 \cdot 10^{-4}$ M), the intensities of the UV-Vis absorption bands in $CHCl_3$ were significantly higher compared to the absorption bands recorded in the other solvents. Although solvent dependencies in absorption spectra are generally a result of physical intermolecular solute-solvent interaction forces such as ion-dipole, dipole-dipole, or hydrogen bonding, which tend to alter the energy difference between ground and excited state of the absorbing species containing the chromophore, it should be noted that solvent effects on the intensity of UV-Vis absorption bands cannot be interpreted in a simple qualitative fashion as is the case for the band position shifts.[156] Nevertheless, the results obtained from the time-dependent UV-Vis measurements performed in $CHCl_3$ provide conclusive evidence that the photolysis reaction yields a constant fraction of products, which can (in principle) be identified and followed in the respective NMR spectra (*vide infra*). In this context, the feasibility to perform the photolysis reaction at the polymer-level was investigated with the help of a first-generation "classic" DP containing approximately 10 mol% MeNVOC-protected amines (cf. page 139 of the Experimental). To this end, the polymer was dissolved in $CDCl_3$ and subjected to irradiation for two and a half days directly in an NMR tube. As apparent from the comparison of the respective ^{1}H NMR spectra before and after irradiation shown in Figures 8-20 and 8-19 on page 182 of the Appendix, the broad signals originating from polymer-bound MeNVOC moieties disappeared virtually completely and new narrow signals emerged in the process, which can likely be ascribed to the formed nitroso by-product **23**. The combined results demonstrate that the photolysis of MeNVOC groups can, in principle, be performed cleanly on the "classic" DPs at hand.

In order to further investigate the photolysis of MeNVOC-protected macromonomer **4b**, ^{1}H NMR spectra were recorded as a function of irradiation time. The irradiation of larger

sample quantities was attempted with the objective to enable the structural analysis of the species formed in the reaction. In this regard, the irradiation of larger amounts of substance was also expected to facilitate the recovery of useful product quantities and address the question whether the conversion of the MeNVOC deprotection reaction proceeded virtually quantitatively. This would be a prerequisite for the purpose of synthesizing DPs with high degrees of structure perfection. To this end, approximately 200 mg of **4b** were placed in a glass vial, dissolved in $CDCl_3$ ($c \approx 6 \cdot 10^{-2}$ M) and mixed on a magnetic stirrer, continuously. Irradiations were performed by shining UV light of $\lambda_{max} = 365$ nm and a nominal output power $P = 250$ mW from the top directly into the solution. After predetermined irradiation times, aliquots were taken from the reaction mixture for ^{1}H NMR analyses and filled back in the vial for subsequent irradiation. Due to the evolution of heat and the lack of cooling in the open experimental setup, evaporated solvent was replaced prior to the ^{1}H NMR measurements. As illustrated in Figure 8-18 on page 181 of the Appendix, the progress of the photolysis reaction was determined from the integrated peak areas corresponding to the Boc (1.487 – 1.343 ppm) and the α-methyl (1.638 – 1.535 ppm) groups in macromonomer **4b**. These integral ranges amount to exactly 9 and 3 protons in the starting material. Upon irradiation, the intensity of the doublet corresponding to the α-methyl group decreases and a singlet centered around 2.5 ppm emerges, which corresponds to the acetyl moiety in the *o*-nitrobenzene species **23** formed as one of the primary products of the photocleavage reaction (cf. Scheme 3-11). Hence, the conversion of unphotolyzed starting material (β) can be calculated from the integrated peak area corresponding to the α-methyl protons in macromonomer **4b** ($I_{\alpha\text{-Me, t}}$) according to Equation 3-2:

$$\beta = \frac{I_{\alpha-\text{Me, t}}}{I_{\alpha-\text{Me, t}\,=\,0}} \cdot 100\% \tag{3-1}$$

$$\widehat{=} \frac{I_{\alpha-\text{Me, t}}}{3} \cdot 100\% \tag{3-2}$$

Figure 3-6 illustrates the calculated α-values as a function of irradiation time. As apparent from the plot, the initially observed, relatively fast photolysis rate started to converge from an irradiation time of approximately one day onwards, which resulted in a conversion of approximately 90% after four and a half days (cf. lowest image section in Figure 8-18 on page 181 of the Appendix). This result shows that a quantitative deprotection could not be realized under the applied experimental conditions over the time-scale of the experiment. Notably, the color of the solution changed from light yellow to red, which may be explained by the formation of primary and secondary photoproducts, as exemplarily illustrated in Scheme 3-11. In this context, previous reports in the literature pointed out that the *o*-nitroso aromatic ketones produced as primary photoproducts usually absorb more strongly than the parent photocleavable protecting group at the irradiation wavelength.[144] Thus, both species compete for the incoming photons, which ultimately leads to the drastically prolonged times required to achieve complete pho-

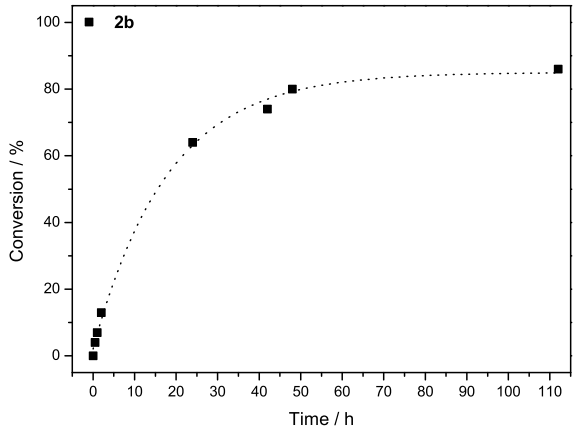

Figure 3-6: Relative conversion of macromonomer **4b** ($c \approx 6 \cdot 10^{-2}$ M in $CDCl_3$) upon irradiation with UV light ($\lambda_{max} = 365$ nm, $P = 250$ mW) calculated based on Equation 3-2. The dotted line is drawn to guide the eye.

tolysis. Moreover, *o*-nitroso aromatic ketones have been reported to undergo extensive secondary photochemistry, i.e. dimerization of the nitroso species to generate the corresponding azobenzenes, especially upon prolonged irradiation.[150] In this regard, it is worth noting that the photolysis of MeNVOC groups was apparently not affected by the presence of oxygen, as inferred from measurements performed on degassed solutions of compound **4b** in THF and irradiation times that were virtually identical to the ones of the untreated solutions. Even though the isolation of all species formed in the present photolysis reaction was not feasible by column chromatography, the desired MeNVOC-deprotected macromonomer **24**, nitrosoacetophenone **23**, and its dimeric form **25** could be unambiguously identified in the crude reaction mixture by mass spectrometry, alongside uncleaved starting macromonomer **4b** (cf. Scheme 3-11).

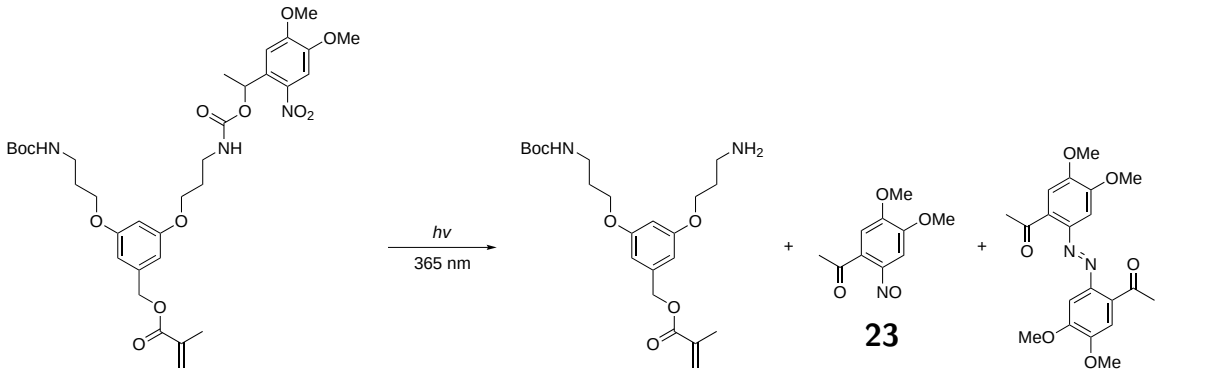

Scheme 3-11: Molecular structures of the proposed and HRMS-identified primary (compounds **23** and **24**) and secondary (compound **25**) photoproducts formed upon irradiation of macromonomer **4b**.

In order to investigate the influence of the experimental setup, specifically with regard to the irradiation power, further tests were performed on a stock solution of macromonomer **4b** in THF ($c \approx 3.34 \cdot 10^{-4}$ M) that was used in irradiations with either the above-described LED or a Rayonet reactor designed specifically for photochemical reactions. On the one hand, the intensity of the above-described LED ($\lambda_{max} = 365$ nm) was reduced to 20% of its maximum output power of 250 mW (nominal) in order to lower the heat build-up in the sample and provide relatively mild conditions for the photolysis reaction, respectively. On the other hand, the Rayonet photoreactor was equipped with eight UV light bulbs with an emission maximum centered around 350 nm (no band-pass filter) mounted concentrically around the sample holder. The power of each light source in the photoreactor was 8 W, resulting in a total nominal output power of 64 W.

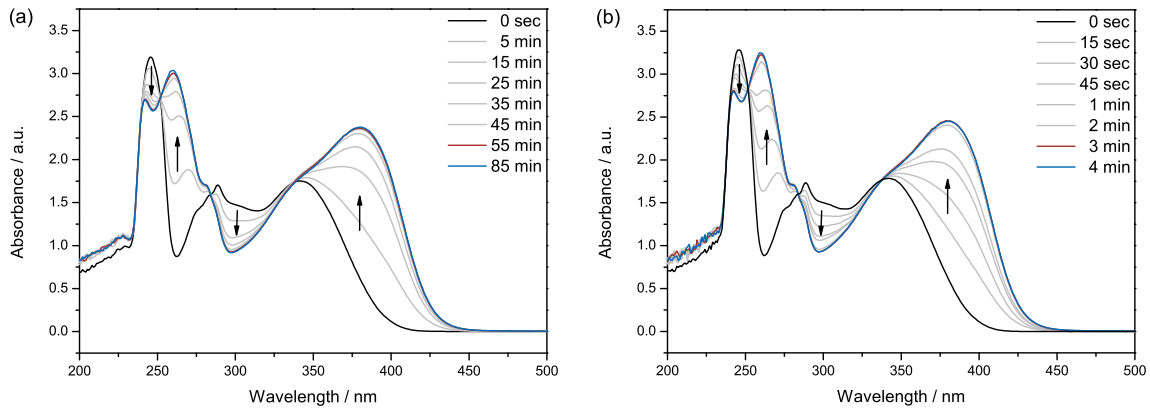

Figure 3-7: UV-Vis spectra of **4b** recorded in THF as a function of irradiation time at (**a**) $\lambda_{max} = 365$ nm, $P = 50$ mW (nominal) and (**b**) $\lambda_{max} = 350$ nm, $P = 64$ W (nominal). Both irradiation experiments were performed using aliquots of the same stock solution ($c \approx 3.34 \cdot 10^{-4}$ M in THF).

As evident from the comparison of the time-dependent UV-Vis spectra obtained with each setup shown in Figure 3-7, the time required to reach the end point of the photolysis reaction by using the photoreactor was at least five times shorter (3 min vs. 15 min) than the one required using the LED. As the conditions were not optimized, it appears reasonable to assume that the photocleavage reaction can proceed quantitatively and within an viable time frame under optimized conditions in the photoreactor. This is underlined by the fact that - apart from the significantly reduced time required to reach the end point of the photolysis reaction - no changes could be identified upon comparison of the respective time-dependent UV-Vis spectra obtained from the LED- and the photoreactor-experiments.

3.3.3 Copolymerization approach

3.3.3.1 Synthesis of UPy-bearing macromonomer 4c

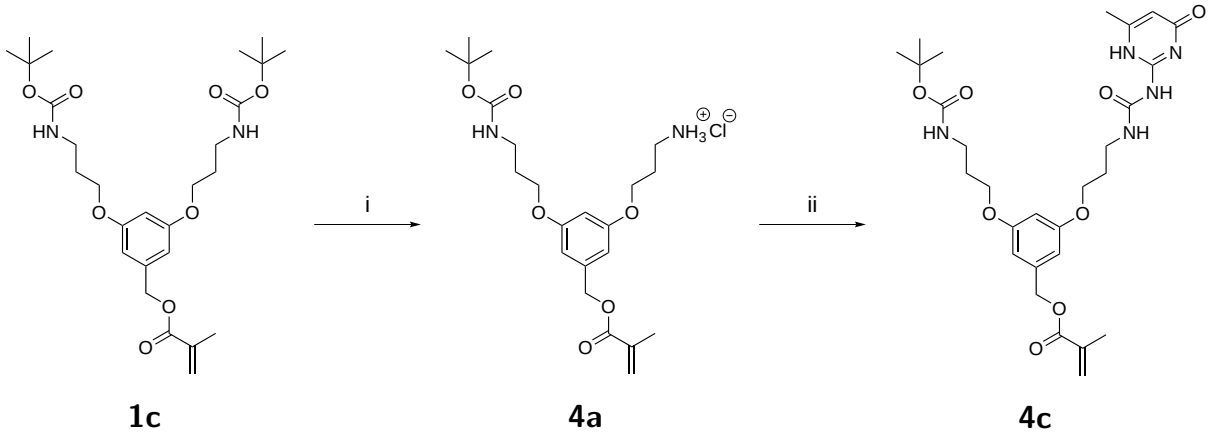

Scheme 3-12: Synthesis of macromonomer **4c**. Reagents and conditions: i) TFA, CH_2Cl_2, RT, 6 d, *57%*; ii) **5**, Et_3N, DMF, RT, 12 h, *quant.*

The synthetic approach towards UPy-bearing macromonomer **4c** is outlined in Scheme 3-12. Analogously to the MeNVOC-functionalized macromonomer **4b** (*vide supra*), doubly Boc-protected, first-generation macromonomer **1c** was reacted with trifluoroacetic acid to afford a statistical mixture of singly and doubly deprotected species, along with unreacted starting material. After separation of the desired, mono-deprotected product **4a** by column chromatography, the UPy moiety was introduced into the mono-deprotected amine.

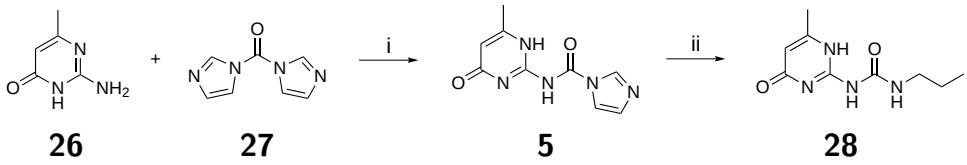

Scheme 3-13: Synthesis of UPy-precursor **5**. Reagents and conditions: i) THF, 70 °C, 17 h, *97%*; ii) *n*-Propylamine, $CHCl_3$, 55 °C, 18 h, *92%*.

To this end, 6-methylisocytosine (**26**) was activated with 1,1'-carbonyldiimidazole (**27**) in one step according to the literature, as delineated in Scheme 3-13.[149]. This way, compound **5**, which was found to be stable for at least 6 months when stored at −20 °C under an atmosphere of nitrogen, was obtained in near-quantitative yield. However, its strongly associating nature prohibited characterization by NMR spectroscopy. Hence, a combination of IR spectroscopy and MALDI-TOF mass spectrometry was used successfully to identify the product of the synthesis. In addition to the characterization data existing in the literature, the high purity of compound **5** obtained this way and its melting point were determined *inter alia* by combustion analysis. Previous studies demonstrated the high

reactivity of **5** with primary amines.[157] Accordingly, the reaction of **5** with *n*-propylamine gave compound **28**, which is soluble and allowed for NMR spectroscopic characterization, in excellent yield (92%) (cf. Scheme 3-13). Subsequently, the target compound **4c** was obtained quantitatively from **4a** in a coupling reaction with **5**.

3.3.3.2 Synthesis of first-generation UPy-functionalized DPs

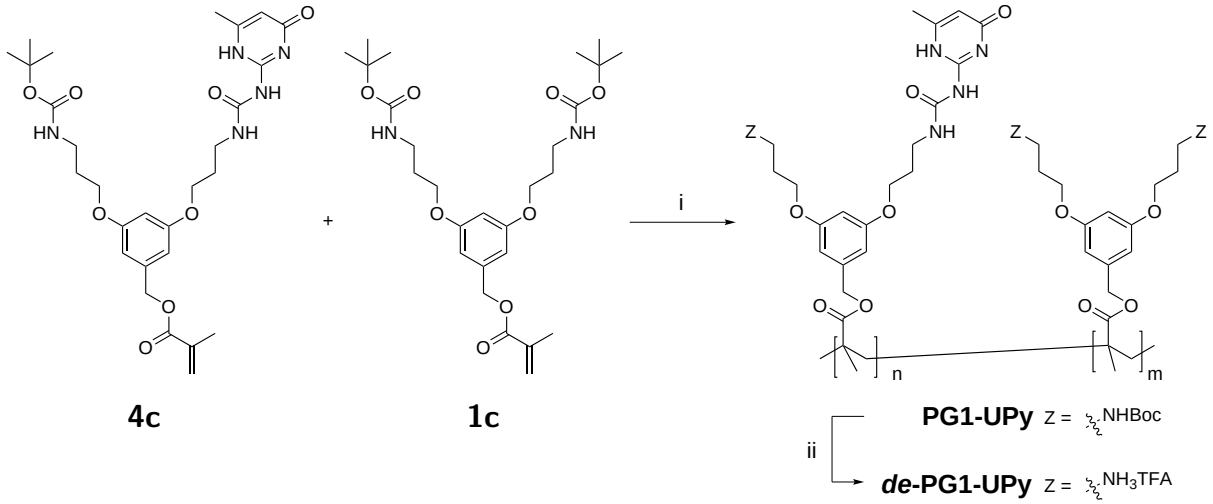

Scheme 3-14: Synthesis of **PG1-UPy**. Reagents and conditions: i) AIBN, (CDB,), DMF, 65 °C, 14 – 20 h, *87 – 97 %*; ii) TFA, 0 °C, 12 h, *quant.*

The two synthesized monomers, i.e. **1c** bearing two Boc-protected amines and **4c** comprising one Boc and UPy motif each in the side chains, were subjected to radical polymerization at 65 °C in DMF using azobisisobutyronitrile (AIBN) as the initiator (cf. Scheme 3-14). Two UPy DP series were synthesized as specified in Table 3-6: On the one hand, polymers comprising similar degrees of polymerization ($P_n \approx 40$) but varying molar feed ratios of monomers **1c** and **4c** to give first-generation DPs comprising 0 – 50 mol% UPy (Entries 1-6 in Tables 3-6 and 3-7) were prepared in controlled radical polymerizations (RAFT) using cumyl dithiobenzoate (CDB) as the chain transfer agent. On the other hand, polymers with larger degrees of polymerization ($P_n \approx 130$, 710, 1200) but a constant UPy loading of 25 mol% (Entries 7-9 in Tables 3-6 and 3-7) were prepared by free radical polymerization (FRP) to study the influence of both the extent of UPy-functionalization and backbone chain length on the thermomechanical properties of UPy-bearing DPs (cf. Sections 3.5.3, 3.6.3, 3.6.4 and 3.7). The backbone chain lengths in these two DP series were carefully chosen in order to obtain both short-chained samples lacking the ability for entanglements and samples with longer backbone chain lengths in order to capture potential effects arising upon the transition from the oligomeric to the polymeric regime.

For ease of assignment, the term χ in **PG*g*-UPy**χ was introduced to denote the theoretical molar fraction of UPy at the $g = 1$-level in the respective copolymers. The precise extent of UPy-functionalization was determined by ^{1}H NMR spectroscopy in $CDCl_3$

and calculation of the UPy-to-Boc ratio as delineated in Equation 3-3, with N_{UPy} and N_{Boc} denoting the relative number of UPy and Boc functionalities in the first-generation copolymers, respectively. Figure 8-23 on page 184 of the Appendix illustrates the ^{1}H NMR spectra of macromonomers **1c** and **4c** and their corresponding equimolar random copolymer **PG1-UPy25**. Thereby, the spectrum of **4c** reveals the existence of extensive fourfold hydrogen bonding via the 4[1*H*]-pyrimidinone dimer, as is evident from the presence of characteristic peaks at 13.11, 11.86 and 10.01 ppm corresponding to the UPy-N*H* signals.[158] However, the concomitant broadening of these signals is not only indicative of the reduced mobility of the UPy dimer but makes them useless for the determination of the copolymer compositions. Hence, the signals associated with the allylic proton in the pyrimidinone ring of **4c** and the proton resonances originating from the peripheral Boc groups in **1c** and **4c** were used instead. The number of UPy groups per extended repeating unit (N_{UPy}) was calculated from the integrated peak area of the allylic proton at 5.7 ppm (I_{UPy}), which was set to unity as one allylic proton exists in each UPy group. Hence, N_{UPy} is equal to I_{UPy} around 5.7 ppm. Moreover, the number of Boc groups per extended repeating unit (N_{Boc}) was calculated by dividing the integrated peak area I_{Boc} around 1.4 ppm, with contributions from both **1c** and **4c** (cf. Figure 8-23), by nine (as there are nine protons in each Boc group) to give Equation 3-5:

$$\chi = \frac{N_{\mathrm{UPy}}}{N_{\mathrm{UPy}} + N_{\mathrm{Boc}}} \cdot 100\% \tag{3-3}$$

$$\widehat{=} \frac{I_{\mathrm{UPy}}}{I_{\mathrm{UPy}} + \dfrac{I_{\mathrm{Boc}}}{9}} \cdot 100\% \tag{3-4}$$

$$= \frac{1}{1 + \dfrac{I_{\mathrm{Boc}}}{9}} \cdot 100\% \tag{3-5}$$

As apparent from the results summarized in Table 3-6, in all cases, the observed polymer composition was found to be within a very narrow range compared to the feed molar ratio, which suggests a statistical distribution of both monomers in the copolymers due to virtually identical monomer reactivity ratios. In this regard, the generally high degrees of conversion in the copolymerization given in Table 3-6 call for a second characterization method to substantiate the claimed statistical incorporation of both macromonomers in the UPy-functionalized copolymers. This was addressed by the performed dynamic light scattering measurements, and the results are discussed in Section 3.4.

Table 3-6: Polymerization conditions for the radical polymerization of monomers **1c** and **4c** to give **PG1-UPy**.

Entry	Polymer	Method[a]	Feed, **1c:4c**	$\chi_{\mathbf{4c},\mathrm{th}}$, mol%	$\chi_{\mathbf{4c},\mathrm{exp}}$[b], mol%	Yield, %
1	PG1-UPy0	RAFT	1:0	0.0	0.0	83
2	PG1-UPy5	RAFT	9:1	5.0	5.5	88
3	PG1-UPy10	RAFT	4:1	10.0	10.1	82
4	PG1-UPy25	RAFT	1:1	25.0	25.1	80
5	PG1-UPy33	RAFT	1:2	33.3	33.4	92
6	PG1-UPy50	RAFT	0:1	50.0	50.0	87
7	PG1-UPy25a	FRP	1:1	25.0	25.2	97
8	PG1-UPy25b	FRP	1:1	25.0	25.2	91
9	PG1-UPy25c	FRP	1:1	25.0	25.2	97

[a]Carried out at a concentration of $1.0\,\mathrm{g\,mL^{-1}}$ (Entries 1 – 6), $0.25\,\mathrm{g\,mL^{-1}}$ (Entry 7), $0.39\,\mathrm{g\,mL^{-1}}$ (Entry 8), and $0.50\,\mathrm{g\,mL^{-1}}$ (Entry 9) in DMF at 65 °C using AIBN as the initiator and CDB as the chain transfer agent in RAFT. [b]Determined by ^{1}H NMR spectroscopy.

Table 3-7: Summary of the experimentally determined molar masses[a] of **PG1-UPy**.

Entry	Polymer	M_w, kDa	M_n, kDa	$M_\mathrm{w}/M_\mathrm{n}$	P_n
1	PG1-UPy0	24.4	21.4	1.14	41
2	PG1-UPy5	22.4	19.3	1.16	37
3	PG1-UPy10	28.1	23.2	1.21	43
4	PG1-UPy25	26.2	22.8	1.15	41
5	PG1-UPy33	23.4	20.5	1.14	37
6	PG1-UPy50	24.2	20.9	1.16	38
7	PG1-UPy25a	147.3	71.5	2.06	130
8	PG1-UPy25b	792.7	390.5	2.03	710
9	PG1-UPy25c	1162.8	668.3	1.74	1200

[a]Determined by GPC in DMF at 45 °C.

3.3.3.3 Synthesis of higher-generation UPy-functionalized DPs

In order to investigate the role of steric shielding and spatial proximity of UPy moieties on the resulting thermomechanical properties (cf. Sections 3.5.3, 3.6.3 and 3.7), higher generation numbers $g = 2,3$ were synthesized. The synthetic approach to **PG2-UPy** and **PG3-UPy** is depicted in Scheme 3-15 and relies on repetitive deprotection-coupling steps involving **1d**, analogous to the classic DPs (cf. Section 3.1.1).[50] More precisely, three first-generation base polymers were selected for the dendronization reactions, i.e. **PG1-UPy** comprising 5, 25, and 50 mol% UPy at the $g = 1$ level corresponding to entries 2, 4, and 6 in Table 3-6, respectively. The 5 mol% series was chosen due to the large average distance between UPy groups along the polymer backbone, which efficiently suppresses intramolecular UPy-UPy dimerization in unfolded chains, whereas intermolecular UPy-UPy dimerization may still exist depending on the extent and depth of interdigitation of neighbouring molecules. In contrast, the much more open dendritic structure of the 50 mol% series originating from the large fraction of UPy-blocked amines, which do not participate in dendritic growth reactions, is estimated to make both intra- and intermolecular UPy-UPy dimerization equally feasible, with a pronounced tendency for interdigitation to reduce local density gradients. Finally, the 25 mol% series was prepared to investigate the effects of both a relatively dense dendritic shell and a close average proximity of UPy moieties in the polymer, which should strongly favor intramolecular UPy-UPy dimerization as the generation number is increased. The 5, 25, and 50 mol% UPy-containing series were complemented by a series of UPy-unfunctionalized DPs for reasons of comparison (cf. Entry 1 in Table 3-6).

In an initial experiment, the chemical stability of the UPy moieties under the standard conditions for the deprotection reaction had to be ensured. To this end, monomer **4c** was subjected to TFA at −10 °C for 16 h, followed by quenching of excess TFA by repeated addition and evaporation of methanol. Deprotection at the monomer level was chosen over the corresponding polymer to simplify the evaluation of the experiment's outcome, i.e. to facilitate the allocation of signals in NMR spectra and to allow for a precise determination of potential side products by means of mass spectrometry. The ^{1}H NMR spectrum of the resulting product is depicted in Figure 8-21 on page 183 of the Appendix, which unambiguously demonstrates the complete deprotection of the NHBoc-bearing branch centering around ≈ 1.3 ppm. More importantly, the integrated peak area corresponding to the allylic proton in the pyrimidinone ring (at ≈ 5.7 ppm) remained unaffected and MALDI-TOF mass spectrometry confirmed the absence of species comprising two terminal ammonium triflate groups. Subsequently, **PG2-UPy** and **PG3-UPy** were prepared following the procedure applied with the "classic" DPs (cf. Section 3.1.1).

For all polymers, the degree of DP structure perfection was determined by labeling of unreacted amines with 1-fluoro-2,4-dinitrobenzene (Sanger's reagent) and quantification of the resulting absorbance at 357 nm via UV-Vis spectrophotometry, in analogy to the classic DPs.[42, 57] In this context, the characteristic absorbance band of UPy is centered

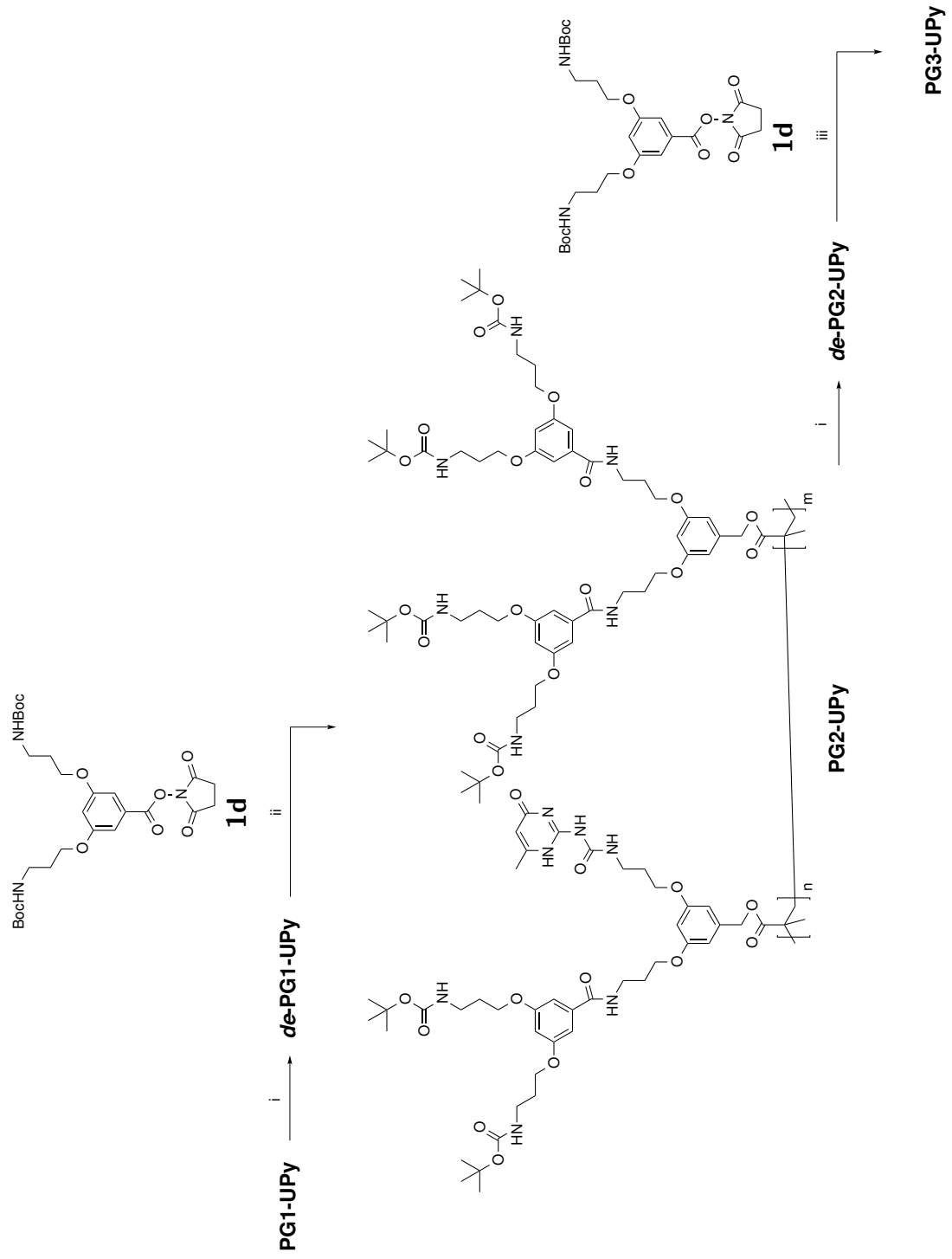

Scheme 3-15: Synthetic route towards higher-generation UPy DPs. Reagents and conditions: i) TFA, −10 °C to RT, 14 h, *quant.*; ii) Et_3N, 4-DMAP, RT, *60 – 70%*.

around 282 nm,[159, 160] and hence, no interference between UPy and Sanger-labeled sites was assumed. This way, the calculated degrees of structure perfection exceeded 99% for all g, as summarized in Table 3-8. As expected, the experimentally determined molar masses increased according to their theoretically calculated, extended repeat units, and their polydispersity and backbone chain lengths stayed approximately constant throughout the homologous series, as apparent from Table 3-9.

Table 3-8: Conditions for the divergent growth of **PG1-UPy** to give **PG2-UPy** and **PG3-UPy**. All polymers possess $P_n \approx 40$.

Entry	Polymer	Dendronization[a] Time, d	Coverage[b], %	Yield, %
1	PG2-UPy0	8	99.8	72
2	PG2-UPy5	14	99.8	70
3	PG2-UPy25	7	99.7	69
4	PG2-UPy50	8	99.1	70
5	PG3-UPy0	16	99.8	81
6	PG3-UPy5	30	99.9	77
7	PG3-UPy25	17	99.2	85
8	PG3-UPy50	21	99.1	78

[a]Carried out at a concentration of 1.0 g mL^{-1} in DMF at room temperature.
[b]Determined by labeling with 1-fluoro-2,4-dinitrofluorobenzene.

Table 3-9: Summary of the experimentally determined molar masses[a] of **PG2-UPy** and **PG3-UPy**.

Entry	Polymer	M_w, kDa	M_n, kDa	M_w/M_n	P_n
1	PG2-UPy0	57.1	50.1	1.14	41
2	PG2-UPy5	48.1	43.7	1.10	36
3	PG2-UPy25	50.5	43.5	1.16	40
4	PG2-UPy50	40.7	34.8	1.17	38
5	PG3-UPy0	115.5	105.0	1.10	40
6	PG3-UPy5	107.4	94.2	1.14	37
7	PG3-UPy25	105.3	86.3	1.22	41
8	PG3-UPy50	73.3	61.1	1.20	37

[a]Determined by GPC in DMF at 45 °C.

3.3.4 Summary of Section 3.3

The preceding sections discussed two conceptually different approaches for the preparation of DPs with enhanced supramolecular interactions. More specifically, the viability of a post-polymerization modification strategy involving a photocleavable α-methylnitroveratryloxycarbonyl (MeNVOC) amine protecting group in the "classic" DPs was compared to the feasibility of applying ureidopyrimidinone (UPy)-functionalized macromonomers directly in a copolymerization approach. To this end, the synthesis of the first-generation macromonomer **4b** bearing one Boc and one MeNVOC group was presented first, followed by a detailed investigation of the compound's photolysis behavior. In these investigations, the MeNVOC-protected macromonomer showed reasonable stability under standard working conditions and underwent photolysis upon irradiation with UV light in the range of $\lambda_{max} = 350 - 365$ nm. The photocleavage reaction was followed both spectroscopically (^{1}H NMR) and spectrophotometrically (UV-Vis) in a variety of organic solvents and using two different irradiation setups. Among the studied solvents, THF and MeOH gave the best results, as inferred from the time required to reach the end-point of the photolysis reaction and the evolution of clear isosbestic points in the UV-Vis spectra that were recorded as a function of irradiation time. Moreover, the power of the irradiation source was a major factor determining the progress of the photolysis reaction, whereby the photolysis reactions performed in a Rayonet photoreactor proceeded significantly faster compared to a weaker LED light source. Nevertheless, the occurrence of secondary photochemical reactions upon irradiation of larger amounts of substance and prolonged irradiation times led to relatively slow photolysis rates that have not permitted conclusive statements about the achievable conversions so far. Therefore, further studies were directed towards the synthesis of first-generation macromonomer **4c**, in which one of the amines is derivatized to a UPy group. In contrast to the generally accepted fact that the presence of UPy in small molecules and conventional monomers is detrimental to the solubility of the respective compounds, solubility issues are of no major concern in the present dendronized macromonomer **4c**. Accordingly, a series of five short-chained ($P_n \approx 40$), first-generation DPs containing 5 – 50 mol% UPy at the $g = 1$-level were prepared in controlled radical copolymerizations (RAFT) with macromonomer **1c**. Apart from the sample featuring 50 mol% UPy, all UPy-functionalized DPs were soluble in organic solvents such as 1,4-dioxane, DMF, and $CHCl_3$, which facilitated their characterization via GPC and the determination of the copolymer compositions by ^{1}H NMR spectroscopy. In addition, three copolymers comprising 25 mol% UPy at the $g = 1$-level but varied backbone chain lengths ($P_n \approx 130$, 710, 1200) were prepared by free radical polymerization. In this context, it is important to note that - in contrast to a post-polymerization route where the full conversion of end groups cannot be guaranteed - the copolymerization approach allowed for the maximum degree of control over the final concentration and sequence of UPy groups in these well-defined polymers. Finally, three distinct samples containing 5, 25, and 50 mol% UPy at the $g = 1$-level were subjected to repeated deprotection-dendronization reactions to afford UPy-functionalized DPs up to the third generation.

3.4 Single-chain polymeric nanoparticles from UPy-functionalized DPs

Single-chain polymeric nanoparticles (SCPNs), i.e. single polymer chains folded into a nanoparticle via intramolecular cross-linking triggered by self-assembling units in the polymers, constitute an emerging topic in the design of supramolecular polymers and have recently gained considerable attention due to their use in a variety of applications, such as artificial enzymes or drug delivery systems.[161–164] A number of examples exist in the literature showing that, under favorable conditions, the presence of pendent hydrogen bonding groups in polymers can induce the folding of individual polymer chains.[165, 166] Hence, it appeared reasonable that such a self-organizing process, which effectively leads to the formation of SCPNs, may also take place in the present UPy-functionalized DPs.

In the following sections, the combination of analytical techniques used to investigate the chain collapse of UPy-functionalized DPs into single-chain polymeric nanoparticles will be presented. Thereby, the use of ^{1}H NMR spectroscopy to obtain qualitative information on the existence of hydrogen bonding in a particular solvent is described. Moreover, the use of gel permeation chromatography (GPC) to gain qualitative information on the nature of these hydrogen bonds, i.e. whether they correspond to an intermolecular network or a coil-to-globule transition, will be discussed. As this method probes the hydrodynamic volume of the formed species, an increase in retention time indicates a reduction of the hydrodynamic volume of the polymer chain and *vice versa*. However, since the measurements are typically performed relative to a standard and interactions of the polymers' UPy-groups with the column cannot be excluded, the interpretation of the results is not always straightforward. Therefore, results from dynamic light scattering (DLS) will be presented in order to rule out potential interactions with the column material and substantiate the assumptions made based on the GPC results. Moreover, DLS gives a direct way to quantify the degree of chain collapse and highlight the unimolecular character of the SCPNs, respectively.

3.4.1 Influence of UPy-content

GPC measurements were conducted on solutions of first-generation DPs containing 0 – 50 mol% UPy in their side chains (cf. Entries 1 – 6 of Table 3-6 in Section 3.3.3.2) in both DMF and $CHCl_3$ ($c = 2.2\,mg\,mL^{-1}$) and the results are depicted in Figure 3-8(a) and (b). As an exception, **PG1-UPy50** could not be characterized in $CHCl_3$ due to the strongly associating nature of this polymer, which prevented adequate dissolution and filtration of the respective samples in this solvent. In this regard, the hydrogen bond disrupting nature of DMF weakened UPy-dimerization, as evidenced by the ill-defined broadening of hydrogen bonded protons in the corresponding NMR spectra, which are depicted exemplarily for **PG1-UPy25** in Figure 8-22 on page 183 of the Appendix. Consequently, the GPC

traces of all **PG1-UPy** samples in DMF showed similar characteristics ($M_n \approx 21$ kDa, PDI $\approx 1.14-1.21$). In contrast, GPC measurements performed in $CHCl_3$ revealed a consistent increase in the retention times of the UPy-containing DPs from 14.4 min ($M_n \approx 21$ kDA) to 15.1 min ($M_n \approx 8$ kDa) with increasing UPy-content, while the polydispersity remained almost constant (1.20 in DMF vs. 1.40 in $CHCl_3$). Since the recorded ^{1}H NMR spectra in $CDCl_3$, which is a weakly competing solvent, clearly indicated the formation of 4[1*H*]-pyrimidinone dimers, the observed decrease in hydrodynamic volumes can be ascribed to a collapse of the polymer chains as a result of intramolecular hydrogen bonding. At it, the observed reduction in apparent molecular weight up to roughly −60% is in good agreement with earlier reports on UPy-based SCPNs.[165, 166]

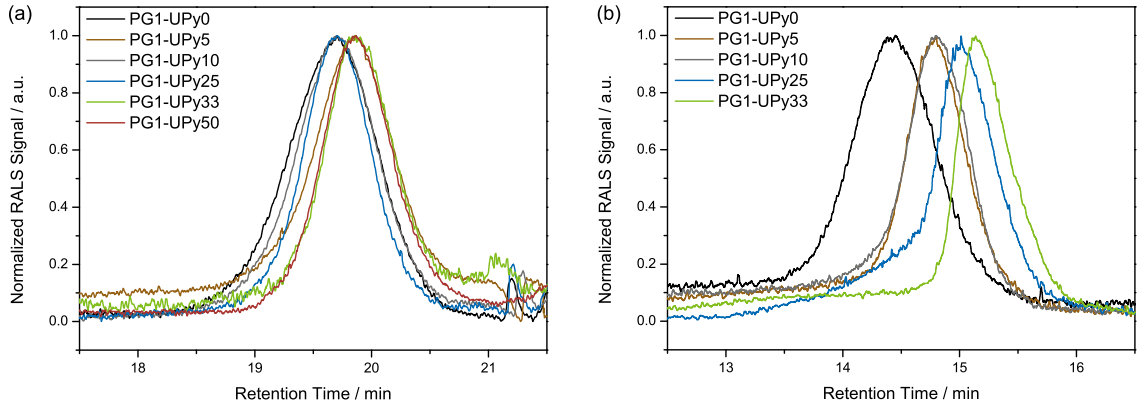

Figure 3-8: GPC elution traces of **PG1-UPy** samples featuring 0 – 50 mol% UPy in their side chains recorded in (**a**) DMF and (**b**) $CHCl_3$.

In order to assess if the UPy dimerization is indeed an intramolecular process, DLS measurements were performed on samples of the same concentrations as the ones used in GPC ($c = 2.2$ mg mL^{-1}), albeit at a lower temperature (25 °C vs. 35/45 °C in the case of $CHCl_3$/DMF GPC). Thereby, the hydrodynamic diameters (D_h) of the **PG1-UPy** samples dissolved in DMF and $CHCl_3$ were determined from the respective intensity distributions and the results are depicted in Figure 3-9. In the case of DMF, DLS revealed minor differences in the D_hs between the individual **PG1-UPy** samples, which generally correlate well with the results obtained from GPC and the overall dimensions expected for unimolecular chains comprising backbone chain lengths of approximately 37 – 43 repeating units. In contrast, the D_hs of the UPy-containing samples measured in $CHCl_3$ were significantly smaller compared to an unfunctionalized **PG1** of matching backbone chain length ($D_h \approx 4$ nm vs. 8 nm). This indicates that, under the described conditions, the UPy dimerization is indeed an intramolecular process. For both solvents, the observed monomodal peak distribution suggests the absence of significant inter-particle interactions, irrespective of the polarity of the solvent. Moreover, the combined results from GPC and DLS in $CHCl_3$ allow for further insights in terms of the qualitative stability sequence within this series of SCPNs. Thereby, the systematic decrease in hydrodynamic volumes with increasing UPy-content observed in GPC suggests that SCPNs from **PG1-**

UPy5 are more prone to unfolding due to shear forces in the column than their respective analogues containing higher UPy-contents. Again, this is supported by the findings from DLS showing that, in the absence of shear flow, all **PG1-UPy** samples collapse into SCPNs of similar dimension (*vide supra*). However, it should be noted that the small size of the particles involved renders these deviations hard to detect with regard to the uncertainty of the measurement.

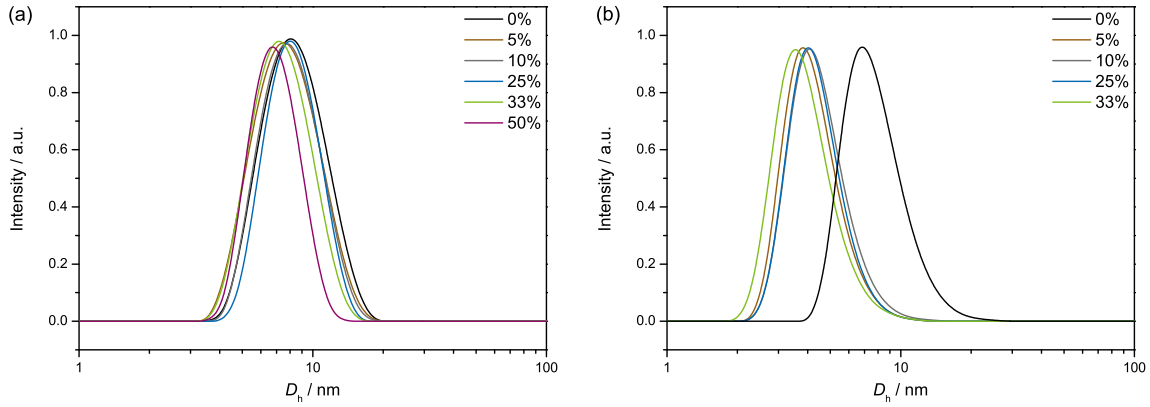

Figure 3-9: DLS intensity distribution vs. hydrodynamic diameters obtained for **PG1-UPy** samples with 0 – 50 mol% UPy recorded in (**a**) DMF and (**b**) $CHCl_3$.

3.4.2 Influence of backbone chain length

The **PG1-UPy** samples with longer backbone chain lengths ($P_n \approx 130$, 710, 1200) but a constant degree of 25 mol% UPy-functionalization (cf. Entries 7-9 in Table 3-7) were used to investigate the influence of molecular weight on the folding behavior of these polymers by DLS and compare the relative changes in D_h between the samples. Although the relative number of UPy moieties in the side chains of the aforementioned polymers is virtually identical, i.e. 25 mol% each, the absolute number of UPy groups per chain differs significantly due to the noticeable differences in their backbone chain lengths. Figure 3-10 compares the intensity distribution curves obtained by DLS measurements of the same polymers dissolved in $CHCl_3$ and DMF. Compared with the hydrodynamic diameters measured in DMF, the D_h values in $CHCl_3$ were found to be smaller by approximately 86%, irrespective of the backbone chain length ($P_n \approx 130$: −84%; $P_n \approx 710$: −89%, $P_n \approx 1200$: −88%). From this result, it can be concluded that increasing the polymer length evidently does not influence the ability of the polymer to form a SCPN. Perhaps even more importantly, the UPy moieties in the present UPy-functionalized DPs are arguably very evenly distributed along the polymer backbones, as a pronounced gradient of UPy moieties would result in the collapse of highly substituted segments, while segments void of UPy moieties would "stick out" of the nanoparticles and lead to generally larger D_h values. This also supports the assumption that the incorporation of macromonomers **1c** and **4c** into the corresponding copolymers proceeds in a highly statistical fashion.

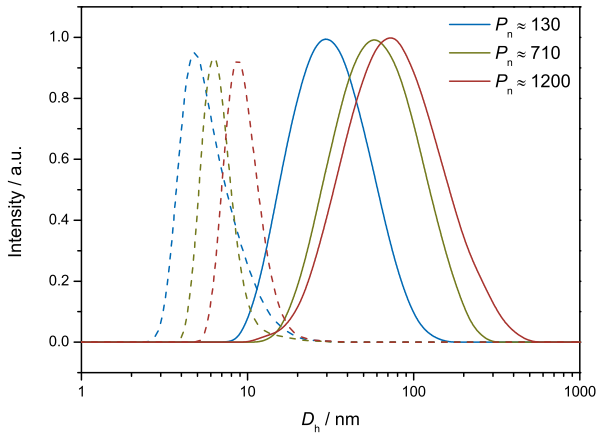

Figure 3-10: DLS intensity distribution vs. hydrodynamic diameters obtained for **PG1-UPy25** comprising $P_n \approx 130$ (blue), $P_n \approx 710$ (olive), $P_n \approx 1200$ (red) in DMF (solid line) and $CHCl_3$ (dashed line).

3.4.3 Influence of generation number

In order to investigate the influence of the average UPy-UPy distance in the polymer and the effect of dendron generation on the ability of the UPy groups to dimerize, ^{1}H NMR and DLS measurements were conducted on four homologous DP series comprising polymers with similar backbone chain lengths of approximately 40 repeating units but different UPy-contents at their respective $g = 1$ levels, i.e. 0, 5, 25, and 50 mol% (cf. Entries 1, 2, 4, and 6 in Table 3-7, Section 3.3.3.2, and Entries 1 – 8 in Table 3-9, Section 3.3.3.3). The

Table 3-10: Numeric summary of the D_h values[a] of **PG1 – 3-UPy** obtained from DLS measurements in DMF and $CHCl_3$.

		PG1 (a)		**PG2 (b)**		**PG3 (c)**	
		DMF	$CHCl_3$	DMF	$CHCl_3$	DMF	$CHCl_3$
Entry	χ_{UPy},[b] mol%	D_h, nm	D_h, nm	D_h, nm	D_h, nm	D_h, nm	D_h, nm
1(a)(b)(c)	0	8.0	7.9	9.5	9.2	11.5	11.3
2(a)(b)(c)	5	7.5	4.5	10.0	9.5	12.4	11.8
3(a)(b)(c)	25	8.0	4.0	9.9	7.1	11.6	11.0
4(a)(b)(c)	50	6.8	-	8.7	5.3	11.5	6.4

[a] Values obtained from averaging 3 measurements consisting of at least 13 individual recordings each; [b] Nominal UPy contents at the respective $g = 1$ levels.

recorded DLS intensity distribution curves are depicted in Figures 3-11 and 3-12. Also, a numerical summary of the hydrodynamic diameters obtained from the DLS measurements is provided in Table 3-10. DLS measurements on the UPy-unfunctionalized DPs (Entries

1a/b/c in Table 3-10) gave almost identical D_h values, irrespective of whether the measurements were conducted in DMF or $CHCl_3$ (cf. Figure 3-11). In contrast, the hydrodynamic diameters obtained from DLS of UPy-containing DPs in $CHCl_3$ were significantly smaller compared to values obtained with the same samples in DMF or their UPy-unfunctionalized analogues. Interestingly, the average UPy-UPy distance in the copolymers had a significant impact on the persistence of the SCPNs formed. Whereas **PG1-UPy5** exhibited an obvious chain collapse due to intramolecular UPy-UPy dimerization ($D_h \approx 4.5$ nm in $CHCl_3$ vs. ≈ 7.5 nm in DMF), the presence of larger, second-generation dendrons were sufficient to unfold the respective unimolecular aggregates and obtain hydrodynamic diameters that are similar to UPy-unfunctionalized analogues (cf. Entries 2b and 2c in Table 3-10).

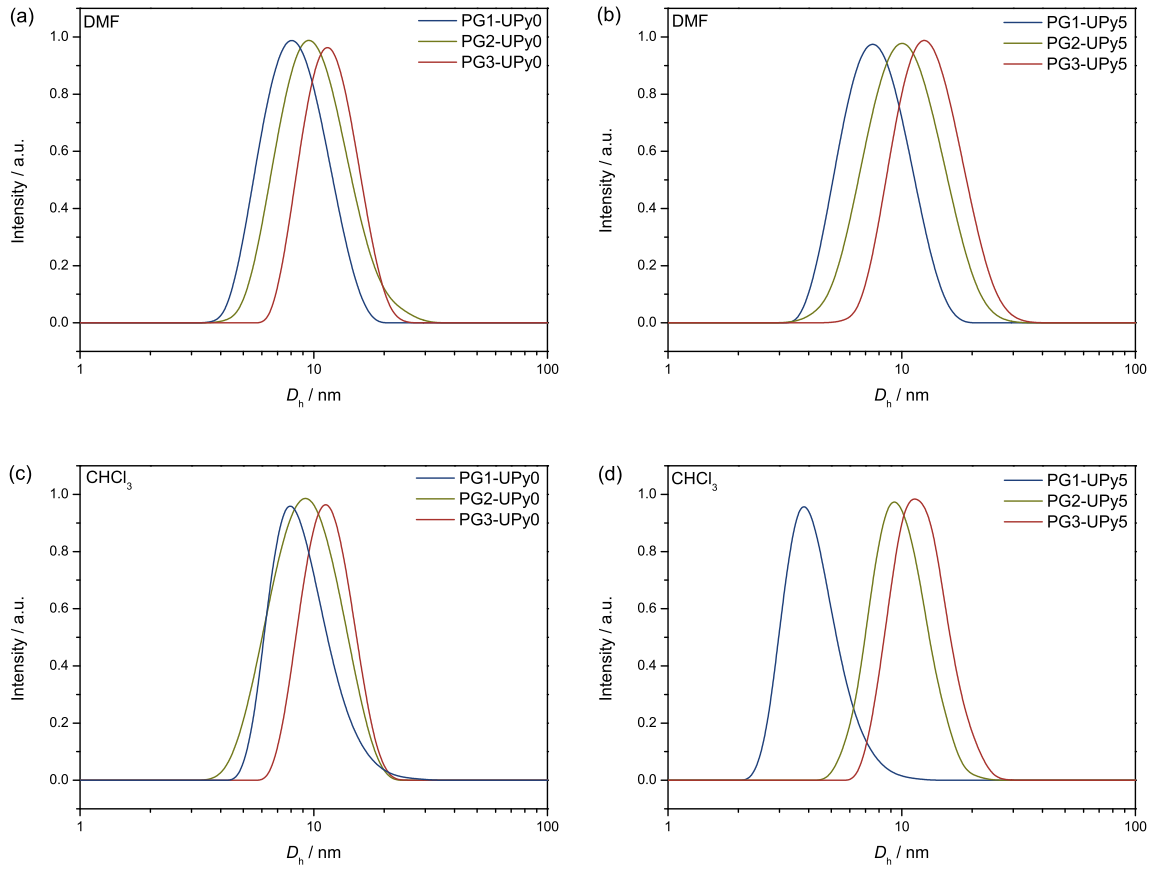

Figure 3-11: DLS intensity distribution vs. hydrodynamic diameters for DP samples of generation numbers $g = 1-3$ comprising 0 mol% UPy (**a**), (**c**), and 5 mol% UPy (**b**), (**d**) at the $g = 1$-level recorded in DMF and $CHCl_3$.

Since the average UPy-UPy distance in the 5 mol% UPy containing copolymers amounts to ten repeating units, the possibility for dimerization of adjacent UPy moieties within the interior of the DPs is virtually excluded. Hence, it can be argued that the second-generation dendrons already provide sufficient steric bulkiness to prevent selective intramolecular UPy-dimerization and to bury the UPy moieties inside the dendritic struc-

ture of these DPs. Accordingly, this renders the 5 mol% UPy containing DPs and their UPy-unfunctionalized analogues practically indistinguishable as of the second polymer generation (cf. Figure 3-11).

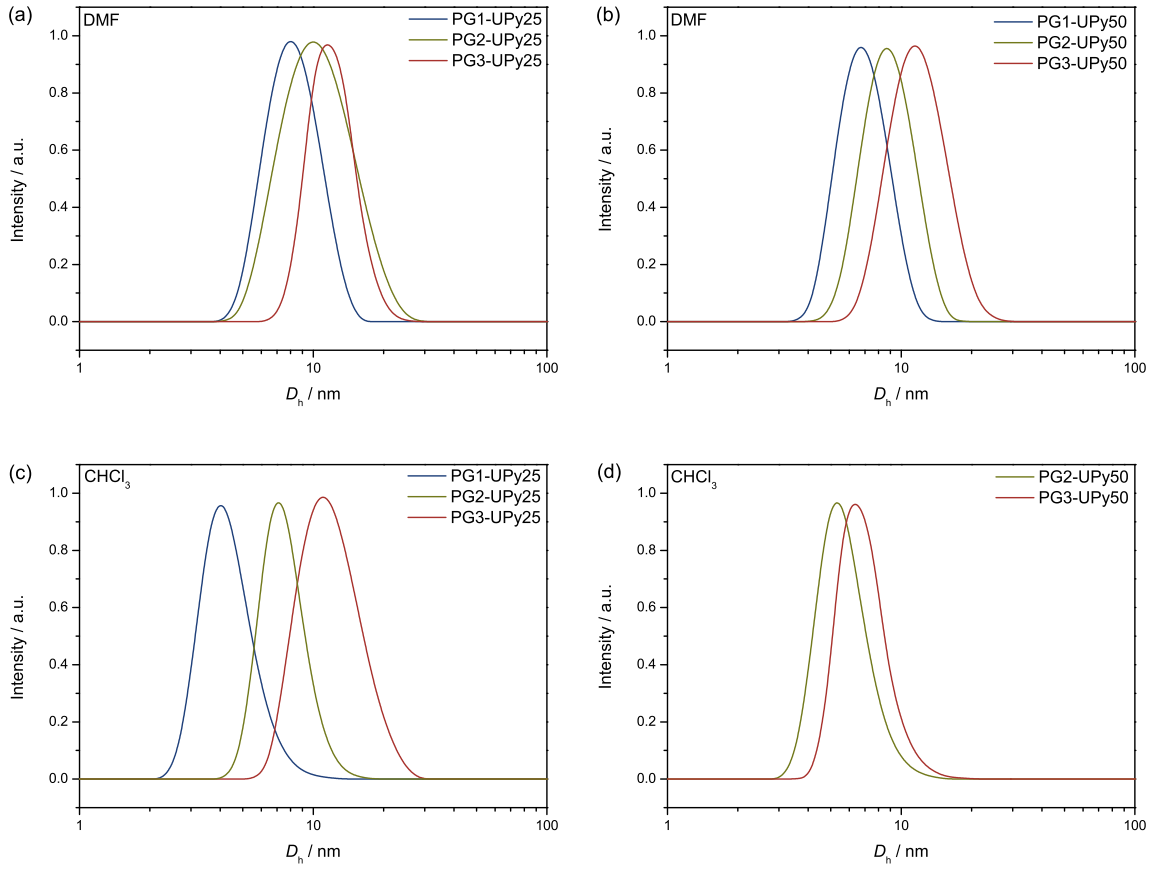

Figure 3-12: DLS intensity distribution vs. hydrodynamic diameters for DP samples of generation numbers $g = 1-3$ comprising 25 mol% UPy (**a**), (**c**), and 50 mol% UPy (**b**), (**d**) at the $g = 1$-level recorded in DMF and $CHCl_3$. The sample containing 50 mol% UPy could not be investigated in $CHCl_3$ due to the strongly associating nature of this polymer, which prevented adequate dissolution and filtration of the sample.

In contrast, the hydrodynamic diameters obtained for the 25 mol% and 50 mol% series in $CHCl_3$ were found to be noticeably smaller compared to the values recorded using the same samples in DMF (cf. Entries 3a/b and 4b/c in Table 3-10 and Figure 3-12). Arguably, the close proximity of the UPy moieties along the polymer backbone allows for UPy-dimerization inside the DPs, which is further facilitated by the more open dendritic structure caused by the higher degrees of dendron substitution with UPy groups, especially in the case of the 50 mol% UPy-bearing series. The existence of 4[1*H*]-pyrimidinone dimers in the higher-generation DPs is also evidenced by the ^{1}H NMR spectra of **PG2-UPy25** and **PG3-UPy25** recorded in $CDCl_3$, which are compiled in Figure 8-24 on page 185 of the Appendix. The integrated peak areas corresponding to the strongly downfield shifted

UPy-NH protons in **PG2-UPy25** and **PG3-UPy25** amount to roughly the same values that were determined with their corresponding first-generation homologue **PG1-UPy25**, respectively. The combined results from ^{1}H NMR spectroscopy and DLS demonstrate that the backbone rigidity and steric crowding in higher-generation DPs does impede intramolecular UPy-dimerization, consistently.

3.4.4 Influence of concentration

In order to investigate the formation and stability of the formed SCPNs, concentration-dependent DLS experiments were performed on chloroform solutions comprising various amounts of **PG1-UPy25** (cf. Entry 4 in Table 3-7, Section 3.3.3.2). Interestingly, at concentrations between $2 \cdot 10^{-2}$ mg mL^{-1} and $2 \cdot 10^{2}$ mg mL^{-1}, the results presented in Figure 3-13 suggest the presence of only a single species in solution, i.e. increasing the concentration of **PG1-UPy25** did not affect the measured D_h values over a wide range of concentrations. This observation indicates that the strength of the UPy dimers is sufficient to undergo stable intramolecular folding even at very dilute or high concentration. Evidently, the high local concentration of UPy moieties inside the polymer chain rather favors intramolecular dimerization of UPy groups into the four-fold hydrogen-bonded dimer in solution as no significant amounts of larger aggregates were observed, which would be observable in the case of significant degrees of intermolecular dimerization.

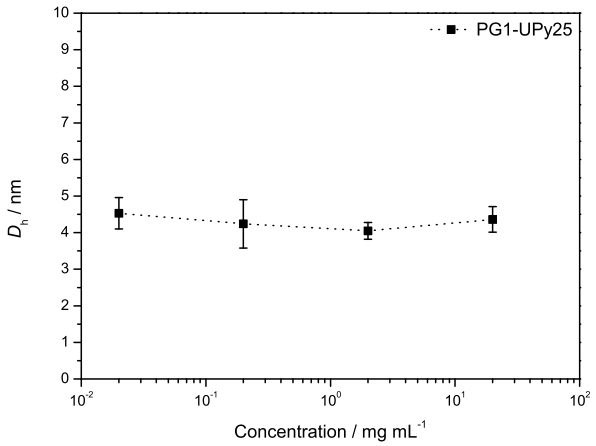

Figure 3-13: Hydrodynamic diameters (D_h) vs. concentration of **PG1-UPy25** obtained from DLS measurements in $CHCl_3$. The given error bars correspond to the standard deviation from the triplicate measurements and the dotted line is drawn to guide the eye.

3.4.5 Summary of Section 3.4

Section 3.4 discussed the collapse of ureidopyrimidinone (UPy)-functionalized DPs into single-chain polymeric nanoparticles (SCPNs), which are formed upon dissolution in apolar solvents due to intramolecular UPy-UPy dimerization. It was shown that the combination of ^{1}H NMR spectroscopy, gel permeation chromatography (GPC), and dynamic light scattering (DLS) represents a suitable set of analytic techniques to provide evidence for the existence of such SCPNs and for their characterization. Whereas the hydrodynamic diameters (D_hs) of short-chained DPs ($P_n \approx 40$) with $g = 1$ and 0 – 50 mol% UPy obtained by DLS in DMF showed only minor differences between the samples, the D_hs of the UPy-containing polymers were significantly smaller in $CHCl_3$ ($D_h \approx 4$ nm vs. 8 nm). This finding was substantiated by GPC measurements, which revealed that the hydrodynamic volumes of the UPy-functionalized samples in $CHCl_3$ decreased with increasing UPy content, consistently, as inferred from the increasing retention times. By comparing the results obtained from DLS and GPC, it was concluded that the concentration of UPy moieties per polymer chain directly affects the cohesion of the formed SCPNs: Whereas, in the absence of shear flow, all samples collapsed into SCPNs of similar dimension, samples comprising lower degrees of UPy-functionalization were more prone to unfolding due to shear forces in the column than their respective analogues containing higher UPy-contents. In this context, an influence of the degree of polymerization on the formation of SCPNs could not be observed for first-generation DPs with $P_n \approx 130$, 710, and 1200, whose D_hs decreased by roughly 86%, consistently. This hints towards an even distribution of UPy-moieties along the polymer backbone and substantiates the assumption that the incorporation of macromonomers **1c** and **4c** into the respective copolymers proceeds in a highly statistical fashion. In addition, the role of the average UPy-UPy distance in the copolymers and the influence of the dendron generation on the ability of the UPy groups to dimerize intramolecularly was investigated by a combination of ^{1}H NMR and DLS measurements, which were performed on four homologous DP series (g = 1 – 3) comprising similar backbone chain lengths ($P_n \approx 40$) but different UPy-contents at the $g = 1$ level (0, 5, 25, and 50 mol% UPy). Thereby, it was found that the backbone rigidity and steric crowding in higher-generation DPs does impede intramolecular UPy-dimerization, consistently. Nevertheless, in the realms of higher degrees of UPy substitution and concomitantly less sterically encumbered environments, the dimerization of UPy moieties can still take place in higher-generation DPs, as evidenced by the much smaller D_h values of the 50 mol% UPy-containing DPs, for which the signals corresponding to the 4[1*H*]-pyrimidinone dimers are also observable in the respective ^{1}H NMR spectra. Finally, the generally observed monomodal peak distributions suggest the lack of significant interparticle interactions in solution, irrespective of whether DMF or $CHCl_3$ is used as the solvent. Instead, the high local concentration of UPy groups inside the DPs favors intramolecular UPy-dimerization, as highlighted by the negligible concentration-dependence of the SCPN-formation.

3.5 Thermal transitions of DPs from differential scanning calorimetry

Calorimetry is a preferred technique used for the measurement of enthalpy changes during chemical processes and is frequently used in many fields of science, accordingly.[167] The sign and magnitude of the concomitant temperature change depend on the amount of heat released or absorbed, i.e. the enthalpy (H) of the process and the heat capacity (C_p) of the system. The general validity of the method endows calorimetrically determined values with a clear physical meaning, even though the interpretation of the obtained results with regard to the underlying phenomena is not always trivial.

In polymer science, calorimetry became a standard tool with the introduction of differential scanning calorimeters in the early 1960s,[168] the setup of which generally consists of two thermally controlled sample positions, one for the investigated sample and the other for a reference. In the simplest case, the reference may consist of just an empty crucible. In principle, the heat exchange of the sample in such a measuring system can take place through the heat flow sensor as well as with the surrounding oven. In the latter case, the heat flow is not detected by the heat flow sensor, which limits the accuracy in terms of absolute measurements.[169] However, the use of crucibles featuring identical heat-exchange coefficients and geometries for the encapsulation of both the sample and the reference allows for highly reproducible and, more importantly, constant losses for both positions. This makes it possible to include these losses in the calibration of the instrument. In one of the most common modes of operation, DSC is performed at a constant heating or cooling rate. In such an experiment, the primary outcome is a plot of the heat flow versus time. Typically, also the temperature is measured near the sample position and hence, the plot can also be represented as the heat flow versus temperature. This way, the heat flow associated with a material undergoing phase transitions such as melting, crystallization, or glass-liquid transition, can be studied by differential scanning calorimetry as a function of time and temperature. In this context, the glass transition temperature (T_g) of polymers is a materials property that generally represents a crucial parameter of both theoretical and practical interest, since it ultimately determines the temperature range for technical applications.

In the following sections, the glass transition temperatures of the prepared DPs will be discussed. Section 3.5.1 depicts the "starting point" of the discussion by pointing out the effects of both the backbone chain length and the generation number of the dendrons on the respective T_g values of "classic" DPs. Building thereon, Section 3.5.2 identifies the effects of oligo(ethylene glycol)-based dendrons as the outermost generation in "hybrid" DPs for the T_g values, whereas Section 3.5.3 highlights the changes caused by the presence of strongly hydrogen bonding moieties, also with regard to their topological location in the polymers.

3.5.1 Thermal properties of "classic" dendronized polymers

At room temperature, all "classic" DPs in this study (cf. Tables 3-2 and 3-3 in Section 3.1) are amorphous materials in a glassy state. Upon heating, the "classic" DPs show clearly visible enthalpy steps at the glass transition temperature. For each polymer generation, Figure 3-14 illustrates the respective T_g values, which were obtained from the second DSC heating runs, as a function of backbone chain length (P_n). Moreover, a numerical summary can be found in Table 8-1 on page 169 of the Appendix. For the series with nominal degrees of polymerization of approximately 50, 1500, and 3000 repeating units, the relative heat flows normalized by the weight of the sample and the initial heat value at low temperature as well as the respective differentiated DSC traces are illustrated in Figure 8-1 on page 170 of the Appendix. From the normalized heat flow traces, it can be deduced that the steps reflecting enthalpy changes decrease with increasing generation, consistently. This suggests that lower specific heat and smaller heat flows are involved in the glass transition of higher-generation DPs. In addition, the width of the glass transition temperatures appears to increase with generation, which is in accordance with respective data obtained for similar systems.[170]

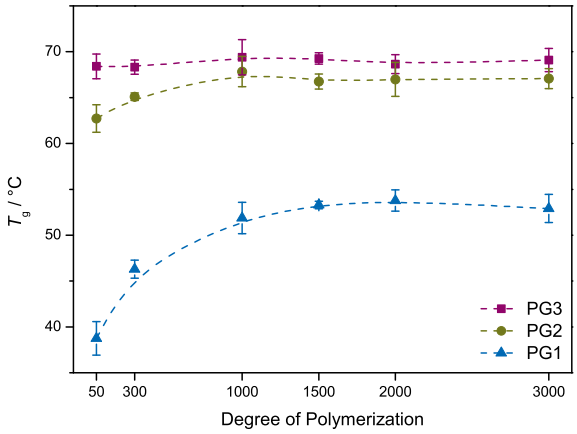

Figure 3-14: Compiled glass transition temperatures (T_g) of "classic" **PG1 – 3** samples as a function of degree of polymerization. The lines are drawn to guide the eye.

Previous molecular dynamics (MD) simulations suggested that the radial frequency distribution of the terminal Boc groups in the "classic" DPs around the backbone features a maximum, which shifts towards the periphery with increasing polymer generation.[62] Hence, it can be reasoned that the prevailing fraction of Boc groups resides near the surface, i.e. at the periphery of the DPs. In the following, the measured T_g values are attributed to the corresponding changes of the molecular structure. The results are rationalized in analogy to the trends observed for conventional hyperbranched polymers,[170–172] without accounting, however, for the facts that the segments between branching points in

the present DPs are very short and that the peripheral end groups are involved in bonding interactions.

For traditional amorphous polymers, the glass transition temperature originates from long-range segmental motions and reflects the rigidity of the backbone. In contrast, the glass transition temperature of DPs may be affected by various parameters, including the nature and number density of the branching points, the overall compactness of the structure, the number and chemical properties of the peripheral end groups, and the strength of bonding interactions (*vide infra*).[173] Here, both the number of branching points and the number of end groups increase as a function of the generation number. From a dynamic point of view, end groups and branching sites affect the glass temperature in opposite directions: On the one hand, increased branching reduces the local segmental mobility due to denser packing and, hence, contributes to an increase of the T_g values. On the other hand, a larger number of dangling end groups enhances local fluctuations, which results in a decrease of the T_g values.[170, 174, 175] In the "classic" **PG1 – 3** series at hand, the determined T_g values increase with the generation number and eventually level off, which is in line with existing reports showing that the glass temperature increases with g and approaches a final value of $\approx 70\,°C$, whereby no significant changes are observed after approximately the fourth generation.[62, 171, 175] The saturation of the glass transition temperature reflects the increasing backbone rigidity due to the bulky pendant side groups in these DPs. In this regard, it can also be considered analogous to the respective saturation with molar mass in linear polymers and dendrimers.[176–179] In addition, the presence of peripheral Boc and phenyl groups that engage in intra- and intermolecular bonding is arguably responsible for the increase of the T_g values as a function of generation. In fact, wide-angle X-ray scattering (WAXS) data on the present "classic" DPs hint to the presence of very broad short-range correlations (typically at a scale of about 0.35 nm), which provide indirect support for the argued role of supramolecular bonding interactions on the T_g values.[180] Moreover, various studies on the thermal behavior of dendrimers[174, 175] and other branched polymers[41, 181] have shown that the nature of the peripheral groups significantly affects the glass temperature of dendritic macromolecules. Thereby, increases in the polarity of peripheral groups generally cause an increase in T_g values due to the concomitant increase in cohesive energy density.

In addition to the role of the generation number and the peripheral end groups, the backbone chain length was found to influence the effective glass transition temperature as well. This holds unambiguously true for the **PG1** series, whereby the samples comprising the smallest degrees of polymerization (Entries 1 and 2 in Table 3-2 on page 23) are characterized by significantly lower T_g values compared to their longer-chained analogues. In order to minimize the influence of residual solvents causing softening and considerable fluctuations in the measured T_g values, especially in the case of the short-chained **PG1** representatives, sample aliquots were extensively dried to constant weight *in vacuo* at 60 °C before multiple DSC cycles were performed. This way, the heating traces generally overlapped as of the second DSC run, which was used for the evaluation. The reduced

glass transition temperature in samples with small backbone chain lengths is a well-known property of linear polymers and attributed to the enhanced backbone mobility due to a comparatively larger amount of main-chain ends.[176] In this respect, the **PG1** series behaves similar to linear polymers, as expected for low-generation DPs. However, in the **PG2** and even more so in the **PG3** series, the increase of T_g values as a function of the backbone chain length is absent, i.e. the glass transition temperature becomes independent of chain length. This is a consequence of the increased backbone rigidity, even in the case of samples with low degrees of polymerization.

3.5.2 Thermal properties of "hybrid" DPs

In contrast to the "classic" DPs, all hybrid DPs presented herein (cf. Section 3.2.3) are in a rubbery state at room temperature. Figure 3-15 illustrates the compiled T_g values of the "hybrid" polymers and a numerical summary is provided in Table 8-2 on page 169 of the Appendix. Compared to the "classic" DPs, the "hybrid" **H[1+1]** and **H[1+2]** series feature greatly reduced T_g values that decrease as the generation number of the pending oligo(ethylene glycol)-based dendrons increases. Interestingly, the T_g values determined for the "hybrid" DP series range in between the T_g values of the "classic" DPs and the T_g values found for recently reported, structurally related purely oligo(ethylene-glycol)-based DPs.[99]

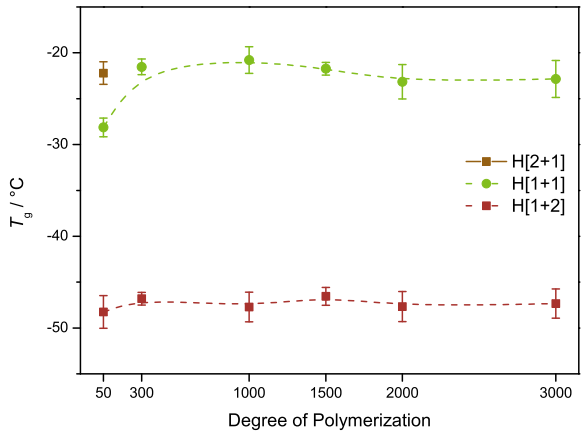

Figure 3-15: Compiled glass transition temperatures of "hybrid" **H[1+1]**, **H[1+2]**, and **H[2+1]** samples as a function of degree of polymerization. The lines are drawn to guide the eye.

Although a saturation of the glass transition temperature with increasing generation could not be determined unambiguously due to the limited set of hybridized polymer generations in this work, a noticeable increase of the T_g values as a function of backbone chain length was identified in the case of the **H[1+1]** series, similar to the "classic" **PG1** series. Accordingly, a decrease in the enthalpy steps and a broadening of the transition was ob-

served with increasing generation as well (cf. Figures 8-2 on page 171 of the Appendix). However, the "hybrid" DPs exhibit generally larger heat flows compared to their "classic" counterparts of matching polymer generation. In large parts, the interpretation of these results follows the line of argument used for the "classic" DPs as discussed in Section 3.5.1. In this context, previous reports have shown that the glass transition temperatures of hyperbranched polymers may be much lower compared to their linear counterparts or analogues with lower molecular weight, depending on their structural elements.[171, 182, 183] Likewise, the inner and outer branching units in the present "hybrid" DPs make different contributions to the overall polarity, stiffness and T_g values of the polymers. Evidently, the flexible oligo(ethylene glycol) side chains and methoxy-terminated end groups render the overall hybridized macromolecules more mobile than the Boc-terminated "classic" DPs that may engage in hydrogen bonding interactions.[174, 177, 178] In this regard, the influence of the terminal, flexible OEG side chains is further highlighted by the exemplarily prepared, short-chained **H[2+1]** sample ($P_n \approx 50$), which featured a significantly decreased T_g value compared to its third-generation "classic" counterpart, despite the effect of chain stiffening caused by the underlying second-generation "classic" dendron motif in **H[2+1]** (cf. Figure 3-15). Therefore, it can be reasoned that the boost of free volume resulting from the highly flexible oligo(ethylene glycol)-based end groups prevails over the contribution of branching points to molecular rigidity. Hence, the glass transition temperatures are significantly decreased and ultimately approach the T_g values of the purely oligo(ethylene glycol)-based DPs.

3.5.3 Thermal properties of UPy-functionalized DPs

All UPy-functionalized DPs prepared in this work (cf. Tables 3-7 and 3-9 in Sections 3.3.3.2 and 3.3.3.3) are amorphous materials and in a glassy state at room temperature. Analogously to the "classic" DPs, the materials softened upon heating and exhibited clearly visible enthalpy steps in DSC at their glass transition. Figure 3-16 depicts the compiled T_g values determined for the first-generation UPy-functionalized DPs with a backbone chain length of approximately 40 repeating units as a function of UPy content (a numerical summary can be found in Table 8-3 on page 172 of the Appendix).

Evidently, the glass temperature of the **PG1-UPy** samples increases almost linearly with the number of hydrogen bonding side groups, i.e. from $\approx 38\,^{\circ}C$ in **PG1-UPy0** to $\approx 127\,^{\circ}C$ in **PG1-UPy50**. The general trend of T_g values increasing with the number of hydrogen bonding moieties has been shown previously in the literature for other random UPy-functionalized copolymers.[114, 115, 184] However, the DPs reported herein distinguish themselves by their relatively high UPy contents and, more importantly, the relatively high T_g values. In contrast, the degree of UPy-functionalization in previously reported systems rarely exceeds 20 mol%. The enthalpy steps involved in the glass transition of these copolymers were found to decrease with increasing UPy-content, consistently. This can be inferred from the respective relative DSC heat flow traces, which were normalized

by the sample weight (cf. Figure 8-3 on page 172 of the Appendix). In this context, the concomitant broadening of the transition becomes particularly apparent from the respective differentiated DSC traces, which are also provided in Figure 8-3.

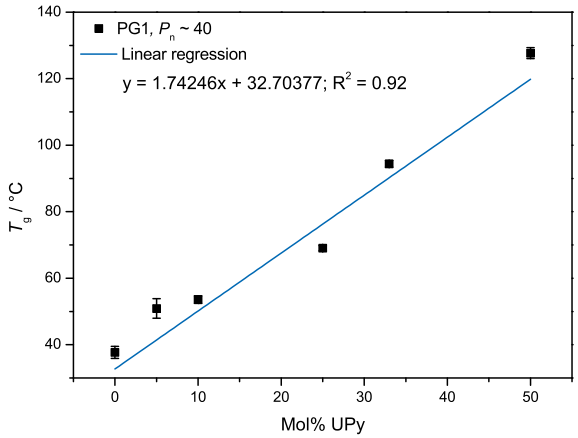

Figure 3-16: Compiled glass transition temperatures (T_g) of **PG1-UPy** samples of similar backbone chain lengths ($P_n \approx 40$) as a function of UPy-functionalization (mol% UPy). Uncertainties correspond to the standard deviation from triplicate measurements and the line depicts the linear regression.

The appearance of a single enthalpy step per DSC heating run suggests that the two macromonomers **1c** and **4c** form a homogeneous, compatible blend in the respective copolymers.[185] These findings can be rationalized by the formation of supramolecular networks based on strongly hydrogen bonding UPy dimers acting as temporary cross-links. Thereby, a larger number of UPy groups in the copolymers reduces the network's mesh size and, hence, slows down chain dynamics and reduces the available free volume, respectively. As a consequence, the T_g values increase as a function of the UPy content. In addition, a comparatively small dependence of the glass temperature on the backbone chain length was found by comparing the T_g values of **PG1-UPy25** samples featuring various backbone chain lengths (cf. Entries 7 – 9 in Table 3-7 on page 56). Thereby, the determined T_g values increased from $\approx 64\,°C$ (for $P_n \approx 40$) to $\approx 87\,°C$ (for $P_n \approx 1200$). Again, this may be explained analogously to the molar mass dependence of T_g on P_n found for conventional linear polymers, as discussed with the "classic" DPs in Section 3.5.1.

By comparison, the interpretation of the results obtained for the higher-generation DPs in this study is more complex. Here, the factor of segmental mobility becomes additionally related to the generation number, as previously discussed with the "classic" DPs in Section 3.5.1. In this regard, the segmental mobility may also be influenced by the average distance of UPy moieties in the copolymers, which determines the probability of intramolecular UPy dimerization and restricts this "reinforcement" of the DPs to the samples with large

UPy contents and short gaps between UPy groups. Figure 3-17 illustrates the compiled T_g values of DPs bearing 5, 25 and 50 mol% UPy at their respective $g = 1$ levels as a function of generation. For comparison, the data on comparable "classic" DPs are also included and a numerical summary of the T_g values obtained for the UPy-functionalized DPs featuring $g = 2,3$ can be found in Table 8-3 on page 172 of the Appendix. In addition, the relative heat flows normalized by the sample weight and their respective differentiated DSC traces are illustrated in Figure 8-4 on page 173. For **PG1-UPy0**, **PG1-UPy5** and **PG1-UPy25**, a saturation of the T_g values can be observed upon the transition from the first to the third generation, which is in line with previous reports demonstrating that the glass temperature of dendritic polymers increases with g before approaching a final value.[115, 170, 175]

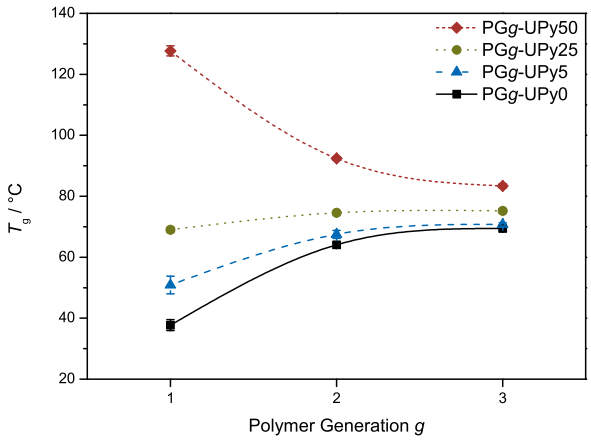

Figure 3-17: Glass transition temperatures of homologous **PG*g*-UPy** samples containing 0, 5, 25 and 50 mol% UPy at the $g = 1$ level as a function of generation (at $P_n \approx 40$). The lines are drawn to guide the eye.

The observed saturation of the T_g values is owed to the bulky pendent side groups of these DPs and reflects their enhanced backbone rigidity with increasing dendron generation. Qualitatively, the T_g values of the highly UPy-functionalized (50 mol%) and UPy-unfunctionalized DPs converge to intermediate temperatures with increasing DP generation. In the case of DPs comprising low to intermediate UPy contents (5 – 25 mol%), an increase of the recorded T_g values with g is also observable, albeit the differences in the T_g values between the first and third generation DPs of each series decrease with increasing UPy content. Nevertheless, larger UPy contents translate into higher T_g values throughout the present DP series, consistently. Arguably, these findings are both interesting and remarkable as they may provide valuable experimental information on the degree of backfolding of dendritic wedges and exposure of UPy groups to the environment, as well as insights into the nature of the hydrogen bonds. Based on the virtually identical T_g values of **PG3-UPy5** and **PG3-UPy0**, it can be reasoned that the UPy moieties in **PG3-UPy5** are completely sunk in the interior of the DPs. Hence, the possibility for intermolecular, specific hydrogen bonding interactions by the UPy moieties is effectively

excluded due to steric shielding by the surrounding dendrons (cf. Figure 3-18). In addition, the presumably highly statistical incorporation of the UPy-bearing monomer **4c** into the polymer combined with the large excess of unfunctionalized monomer **1c** (**1c**:**4c** = 9:1) makes it reasonable to assume that intramolecular UPy-dimerization is equally unlikely (cf. Figure 8-25 on page 185 of the Appendix). On the other hand, dendritic growth of **PG1-UPy50** to give **PG2-UPy50** greatly reduces the T_g value by $\approx 35\,^{\circ}\mathrm{C}$, despite the 50% lower grafting density compared to the UPy-unfunctionalized DPs.[50] Evidently, already a single dendron generation suffices to drastically decrease the amount of intermolecular UPy-dimerization. Subsequent dendronization of **PG2-UPy50** to give **PG3-UPy50** leads to a decrease in the glass temperature that is marked yet much smaller compared to the preceding dendronization ($\approx 9\,^{\circ}\mathrm{C}$). This could be an indication for the shift of the supramolecular UPy-interactions from an intermolecular DP network to intramolecularly reinforced DP chains, facilitated by the close proximity of UPy moieties in the homopolymer of macromonomer **4c**.

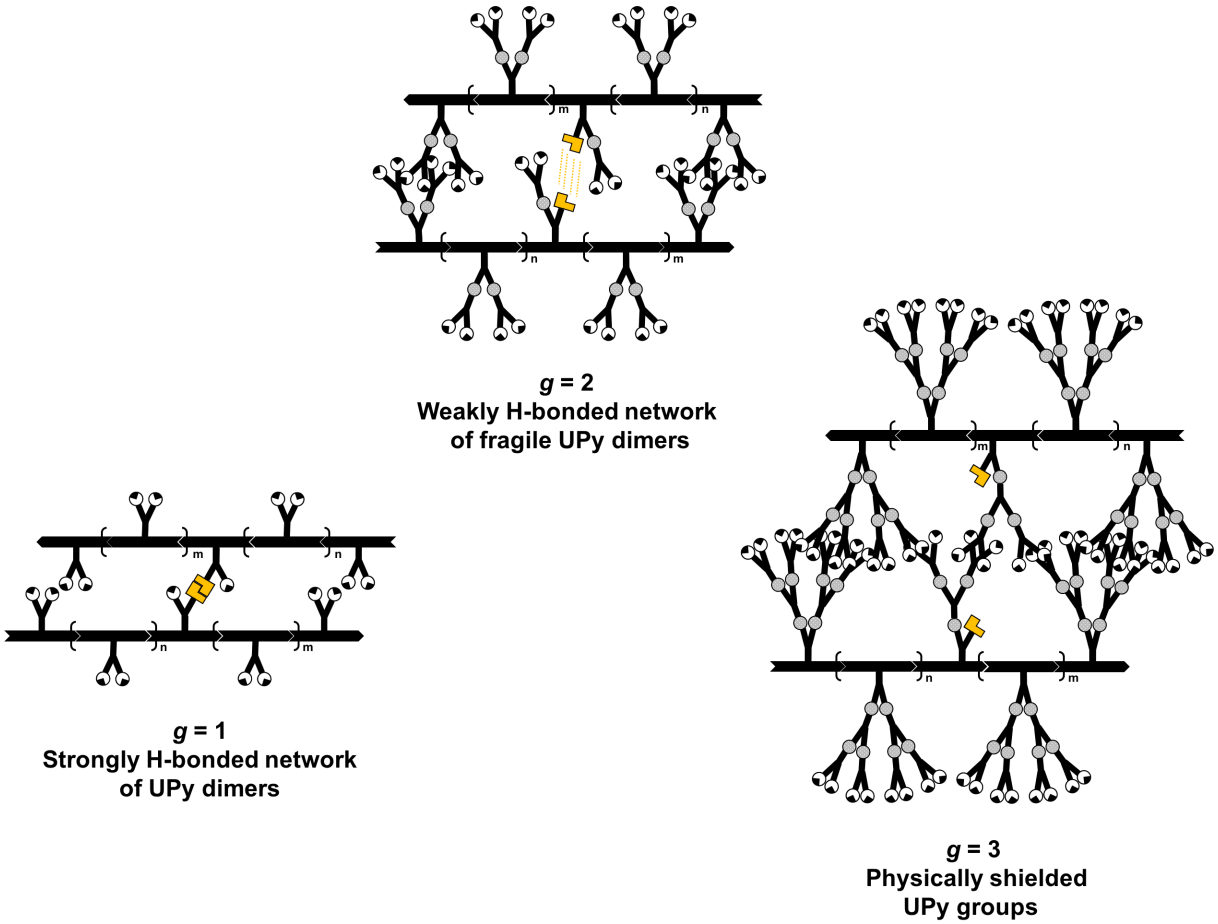

Figure 3-18: Schematic representation of the decreasing accessibility of UPy moieties in DPs with increasing dendron generation. Potential intramolecular dimerization is omitted for clarity.

3.5.4 Summary of Section 3.5

The thermal properties of DPs were investigated by DSC, with a particular focus on the parameters influencing the T_g of this class of polymers. Notably, the homologous character of the DPs studied herein offered the decisive advantage of virtually constant P_ns throughout the respective DP series, which allowed for systematic investigations of structure-property relationships as a function of *g*. By varying P_n, the influence of parameters changing upon the transition from the oligomeric to the polymeric regime, such as the number of free chain ends, could be identified as well. For conventional linear polymers, the glass transition originates from long-range segmental motion. In contrast, the three-dimensional, repeatedly branched structure of DPs renders the glass transition not a mere reflection of backbone stiffness but a consequence of many counterbalancing factors, including the number of end groups and branching sites, which both increase as a function of *g* and affect the T_g values of DPs in opposite directions. More specifically, increased branching leads to reduced local segmental mobility due to denser packing (increases T_g values) and more dangling end groups enhance local fluctuations (decreases T_g values). Based on these considerations, the data obtained with the "classic" DPs demonstrated that the T_g values approach a plateau with increasing P_n and *g*. Unsurprisingly, the molar mass dependence of the glass transition, which is well-known for conventional polymers, was best observable for the "classic" **PG1** series and diminished with increasing *g*. In this context, the heat flows involved in the glass transition of higher generations were found to decrease, consistently, which may be ascribed to the enhanced steric hindrance around the polymer backbone rendering differences in the segmental mobilities above and below the glass transition progressively more negligible. In addition, the presence of terminal NHBoc end groups, which are capable of undergoing hydrogen bonding interactions, restricts the conformational freedom of the molecules even further. In contrast, the T_g values of the "hybrid" **H[1+1]** and **H[1+2]** polymers were found to be significantly lower compared to their "classic" counterparts. Here, the gain of free volume caused by the flexible oligo(ethylene glycol) (OEG)-based terminal units prevails over the influence of the branching points. This was further highlighted by a **H[2+1]-50** sample, which featured a drastically reduced T_g value compared to its "classic" analogue, despite the backbone-stiffening effect caused by the underlying second-generation "classic" structural motif. Finally, the thermal properties of "classic" DPs comprising varied concentrations of strongly hydrogen bonding ureidopyrimidinone (UPy) groups at their $g = 1$ level were investigated as a function of P_n and *g*. At similar P_n, the studied **PG1-UPy** samples exhibited a linear relationship between UPy-content and T_g values, which was ascribed to the formation of supramolecular networks composed of UPy dimers and the successive reduction of free volume with decreasing mesh size. Depending on the average distance of UPy moieties in the copolymers and *g*, a shift from inter- to intramolecular UPy-dimerization was proposed based on the results obtained from DSC and ^{1}H NMR spectroscopy.

3.6 Thermal stability of DPs from thermogravimetric analysis

Thermogravimetric analysis (TGA) is a simple analytical technique for the characterization of materials that exhibit changes in weight due to decomposition, oxidation, or loss of volatiles such as traces of solvents or moisture. Thereby, TGA is frequently applied for the determination of characteristic decomposition patterns, studies of degradation mechanisms and reaction kinetics, and the determination of a sample's organic or inorganic contents in order to substantiate predicted material structures and properties.[186] In this regard, TGA represents an especially useful technique for the analysis of polymeric materials, whose large molar mass or complex molecular structure often restricts the applicability of more sophisticated analytical methods, e.g. due to the lack of adequate solubility.[187, 188] In this context, melt processing of polymers represents a desirable technique since it circumvents the use of solvents. However, conventional polymers generally require high temperatures to provide melts of sufficiently low viscosity for melt processing, which limits both the number of suitable polymers and the applicability of the technique itself.[189] In contrast, supramolecular polymers are expected to possess superior processing properties at relatively low temperatures due to the weakening of the non-covalent interactions upon heating (cf. Section 3.3.1). This way, supramolecular polymers combine good material properties with low-viscosity melts that are easy to handle.[107, 190] Nevertheless, the thermal stability of supramolecular polymers at the prospective processing temperature constitutes a prerequisite for the applicability of this technique.

In the following section, the usefulness of TGA for the characterization of dendronized polymers will be reviewed, particularly with respect to its applicability as an analysis technique to determine the degree of structure perfection of dendronized polymers. (cf. Section 5.3.5 of the Experimental for a description of the labeling procedure using Sanger's reagent). Furthermore, the feasibility of using TGA to confirm the composition ratio of dendronized macromonomers in their respective co- and homopolymers, which contain both Boc and UPy groups in their molecular structures, will be discussed.

3.6.1 Thermal stability of poly(methyl methacrylate) and "classic" DPs

Previous studies in the literature found that the thermal degradation of pure poly(methyl methacrylate) (PMMA), which constitutes the backbone in all the DPs presented in this work, is sensitive to a variety of factors, including the polymerization method, differences in the molecular structure of PMMA, the heating rate, and the presence of gas-phase oxygen during the heating run.[191] By way of example, thermal degradation of radically polymerized PMMA proceeds in three distinctive steps, as illustrated in Figure 3-19(a).

First, depolymerization is initiated from relatively weak head-to-head linkages at approximately 165 °C, followed by end-initiated depolymerization from unsaturated vinylidene chain ends and random scission of the main chain itself at approximately 270 °C and 360 °C, respectively. In contrast, due to the lack of irregular structures such as head-to-head linkages or unsaturated end groups, anionically polymerized PMMA features a single mass loss peak at approximately 360 °C. In general, higher heating rates tend to increase the peak temperatures of the individual degradation steps.[192] Furthermore, the presence of gas-phase oxygen plays a dual role in the degradation of radically polymerized PMMA: On the one hand, molecular oxygen traps radicals originating from the scission of weak linkages or unzipping of the polymer chain and terminates the depolymerization at lower temperatures (<300 °C), accordingly. On the other hand, oxygen was found to practically not affect the thermal degradation of PMMA at a later stage (>300 °C), as the activation energies for random scission are reportedly very similar in both nitrogen and air (230 kJ mol^{-1} vs. 200 kJ mol^{-1}).[193]

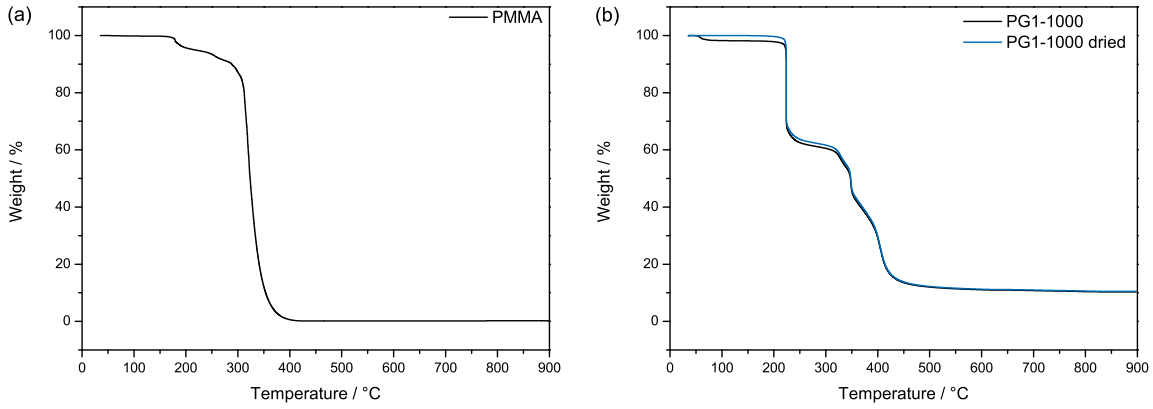

Figure 3-19: (**a**) Thermal degradation curve of radically polymerized poly(methyl methacrylate) with $M_n \approx 350$ kDa recorded in N_2; (**b**) Thermal degradation curves of radically polymerized (RAFT) dendronized polymer (**PG1-1000**) before (black) and after (blue) drying in HV at 60 °C for 48 h.

The thermal degradation curves obtained from thermogravimetric analysis of DPs comprising PMMA backbones feature a few noteworthy differences compared to the respective curves of pure PMMA. Figure 3-19(b) compares the TGA curves obtained from pristine and extensively dried DPs, as exemplified by "classic" **PG1-1000**. Whereas the TGA of the as-prepared material exhibits a weight loss of approximately 3% over the temperature range of 50 – 90 °C, the dried polymer virtually does not show any weight loss up to approximately 190 °C. In the former case, the weight loss can be ascribed to the presence of solvent traces (mostly 1,4-dioxane) that originate from the preceding freeze-drying process and are trapped inside the DPs. Therefore, all samples were dried in a vacuum drying oven at 60 °C and 1 mbar for at least 24 h prior to the TGA measurements in order to remove any solvents and to arrive at meaningful degradation curves. Furthermore, the onset of decomposition of such dried "classic" DPs is shifted to higher temperatures, i.e.

virtually no mass loss is observed at temperatures below 200 °C, which may be explained by the lack of noticeable amounts of head-to-head linkages and vinylidene chain ends in the samples. In fact, previous reports in the literature pointed out that the use of chain transfer agents in the polymerization process significantly reduces the number of these weak linkages and thereby stabilize radically polymerized PMMA, which would apply for the herein presented RAFT-derived DPs.[191] Viewed from a different angle, the initial scission fragments of DPs may not be volatile and, accordingly, they do not contribute to the mass loss of the sample until a later stage in the heating run. At temperatures above 200 °C, the "classic" DPs exhibit a noticeable and well-defined onset of mass loss, which can be ascribed to the thermolytic cleavage of the peripheral *tert*-butyloxycarbonyl (Boc) groups.[194] The usefulness of this feature for the characterization of DPs will be discussed in the following paragraphs (*vide infra*). Subsequently, degradation of "classic" DPs in the narrower sense is apparent at temperatures above 300 °C, which can be attributed to random scission processes in the polymeric backbone and the dendritic appendices yielding a black char upon removal of the sample pan from the thermobalance. Naturally, the presence of stable moieties such as benzene rings in the "classic" DPs leads to larger amounts of these carbonaceous residues in comparison with pure PMMA.

3.6.2 Thermogravimetric determination of DP structure perfection

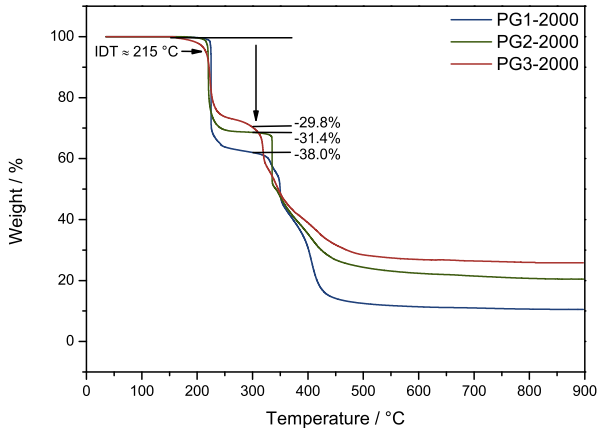

Figure 3-20: Thermal degradation curves of homologous "classic" **PG1 – 3** samples with a backbone chain length P_n of approximately 2000 repeating units. All measurements were performed at a heating rate of 20 °C min^{-1} in N_2.

The divergent approach to higher-generation dendritic macromolecules inevitably leads to an increasing amount of defects due to the large number of post-polymerization modification reactions involved (cf. Sections 1.1.3 and 1.2.2).[195] In this context, the tightly packed maximum generation (g_{max}) has been introduced as the theoretical packing limit,[57] be-

yond which the space available for the new generation or end group modification is not sufficient anymore to accommodate all the atoms required for complete conversion (so-called sterically induced stoichiometry).[196] Thereby, the reduced accessibility of the interior of DPs with increasing generation number not only renders dendronizations progressively difficult to accomplish, but ultimately also affects the labeling reaction between Sanger's reagent and any non-dendronized amine.

The thermogravimetric quantification of Boc groups, which have been reported to decompose quantitatively upon thermolysis,[194, 197] can be considered an attractive opportunity to cross-check the coverages determined by the labeling method, which aims at quantifying the unreacted amines. Previous studies in the literature have validated the thermogravimetric approach by using reference DPs with virtually perfect structures and reported an estimated error range for the quantification of Boc groups by TGA of ±3%.[198] Thereby, the theoretical mass loss α^0 (in %) caused by the thermolytic cleavage of Boc groups correlates with the number of Boc groups per ideal repeating unit (N_{Boc}), the molar mass per repeating unit ($M_{\mathrm{r.u.}}$), and the molar mass of a Boc group itself ($M_{\mathrm{Boc}} = 100.12\,\mathrm{g\,mol^{-1}}$) according to Equation 3-7:

$$\alpha^0 = \frac{N_{Boc} \cdot M_{Boc}}{M_{r.u.}} \cdot 100\% \tag{3-6}$$

$$= \frac{N_{Boc} \cdot 100.12}{M_{r.u.}} \cdot 100\% \tag{3-7}$$

In order to apply a unified evaluation procedure and obtain comparable results, the respective weights (in %) at 180 °C and 300 °C were used in the calculations. By choosing these temperature limits, the complete evaporation of any solvent traces and the quantitative thermolysis of the Boc groups prior to random scission setting in can be expected. Figure 3-20 exemplarily depicts the TGA curves obtained for the homologous series comprising of "classic" DPs with generation numbers $g = 1-3$ and a backbone chain length P_{n} of approximately 2000 repeating units, respectively (cf. Entry 5 in Table 3-2, Section 3.1.1; Entries 5, 11 in Table 3-3, Section 3.1.2). As apparent from the comparison of the degrees of DP structure perfection obtained by labeling and TGA (cf. Table 3-11.), the latter method underestimates the coverage of the investigated samples by 0.5 – 3.8%. Hence, the UV-labeling method is the more effective and reliable method for the determination of DP structure perfections, especially for DPs below g_{max}. Nevertheless, thermogravimetric analysis represents a reproducible, reliable and independent method for the characterization of DPs with regard to their structure perfection, especially for higher polymer generations where excessive steric crowding around the backbone may prevent the UV labeling reagent from reacting quantitatively with the defect sites.

Table 3-11: Comparison of the experimentally determined degrees of structure perfection (coverage) obtained by thermogravimetric analysis and UV-labeling.

						Coverage		
Entry	Polymer	$M_{\text{r.u.}}$, Da	N_{Boc}	α^0,[a] %	α,[b] %	TGA,[c] %	UV,[d] %	$\Delta_{\text{UV-TGA}}$, %
1	PG1-2000	522.63	2	38.2	38.0	99.5	100.0[e]	0.5
2	PG2-2000	1223.45	4	32.7	31.4	96.0	99.8	3.8
3	PG3-2000	2625.09	8	30.5	29.8	97.7	99.3	1.6

[a] Theoretical mass loss calculated based on Equation 3-7; [b] Mass loss directly measured by TGA in N_2 at a heating rate of 20 °C min^{-1}; [c] Based on $(\alpha/\alpha^0) \times 100\%$; [d] Determined by labeling with 1-Fluoro-2,4-dinitrofluorobenzene (Sanger's reagent); [e] Based on the assumption that the macromonomer approach yields structurally perfect DPs.

3.6.3 Thermal stability of UPy-functionalized DPs

In order to investigate the influence of UPy moieties on the thermal stability of DPs, thermogravimetric analyses were performed analogously to the "classic" DPs, i.e. all samples were heated from 30 °C to 900 °C at a rate of 20 °C min^{-1} in a flow of nitrogen in order to avoid thermal oxidation and to allow for a more direct correlation between chemical structure and thermal degradation. Image sections b) – d) of Figure 3-21 illustrate the recorded TGA curves for DPs with backbone chain lengths of $P_n \approx 40$ and generation numbers $g = 1-3$ containing 5, 25, and 50 mol% of UPy at their respective $g = 1$ levels (cf. Entries 2, 4, 6 in Table 3-6, Section 3.3.3.2; Entries 2 – 4, 6 – 8 in Table 3-8, Section 3.3.3.3). For comparison, the TGA curves of "classic" DPs (Entry 1 in Table 3-6 and Entries 1, 5 in Table 3-8) are depicted in Figure 3-21(a). The recorded TGA curves reveal that both the synthesized "classic" and UPy-functionalized DPs are thermally stable up to at least 200 °C. Beyond this temperature, both feature similar two-step degradation profiles with UPy-functionalized DPs undergoing somewhat faster degradation compared to the "classic" DPs. The initial degradation temperature (IDT), i.e. the temperature at 5% weight loss, shifts significantly towards lower temperatures from 223 °C (0 mol% UPy) to 209 °C (50 mol% UPy) with increasing degree of UPy-functionalization, consistently. At the same time, the influence of the generation number on the onset of thermal degradation appears to be negligible, i.e. higher-generation DPs feature virtually identical IDTs in comparison with their corresponding lower-generation homologues. The observed decrease in thermal stability with increasing degree of UPy-functionalization is in contrast to the general perception that, compared to a comparable unfunctionalized (pristine) material, the incorporation of hydrogen bonding motifs into polymers results in materials with enhanced thermal stability.[199, 200] Evidently, the presence of UPy moieties in conjunction with Boc-protected amines in the DPs at hand gives rise to this peculiar behavior, which may be explained by a UPy-induced alteration of the electron distribu-

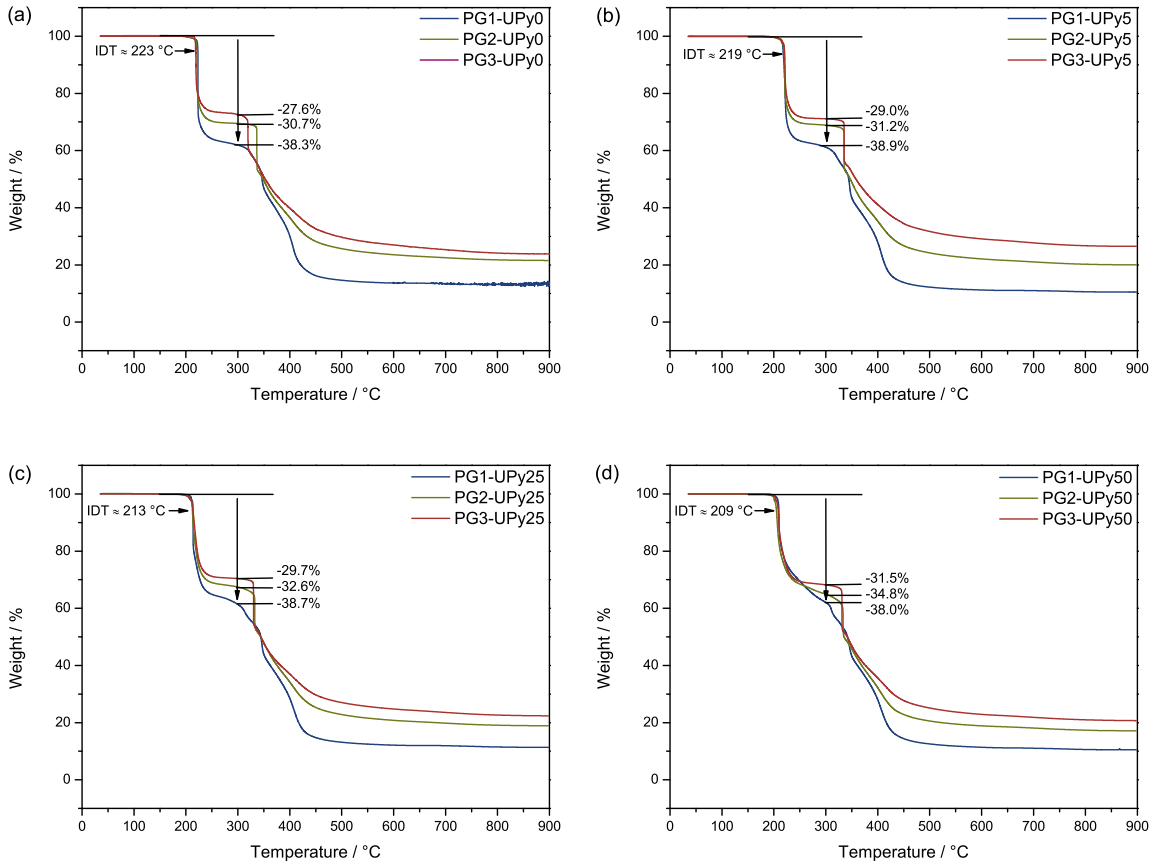

Figure 3-21: Thermal degradation curves of **PG1 – 3-UPy** samples comprising (**a**) 0 mol% UPy, (**b**) 5 mol% UPy, (**c**) 25 mol% UPy, (**d**) 50 mol% UPy at the $g = 1$-level. All measurements were performed at a heating rate of 20 °C min^{-1} in N_2.

tion in the Boc groups and a weakening of covalent bonds, respectively. More precisely, intramolecular hydrogen bonding between the etheral- and/or carbonyl oxygens of the Boc groups and the hydrogen-bearing donor atoms in the UPy moieties could lead to an increase in the partially positive charge of the tertiary carbon atom, which would ultimately lead to the heterolytic scission of the C – O bond in analogy to the well-known acid-catalyzed deprotection mechanism of Boc groups. Following the proposed mechanism delineated in Scheme 3-16, the observed independence of the IDT on the generation number could originate from back-folding of the dendritic branches towards the polymeric backbone and thus the UPy-moieties. Thereby, the liberation of gaseous scission products, i.e. isobutene and carbon dioxide, could result in the formation of cavities, which may constitute a driving force for the back-folding of Boc groups in an attempt to minimize density gradients inside the dendritic structure. The proposed mechanism is further supported by the broadening of the initial mass loss step with increasing UPy content, which is consistent with previous reports in the literature on the thermal degradation of UPy model complexes and related hydrogen bonded polymers.[201, 202] There,

the authors used a combination of TGA and gas chromatography-mass spectrometry (GC-MS) to elucidate the thermal degradation mechanism of the UPy model complex *N*-[(butylamino)carbonyl]-6-methylisocytosine, which was shown to proceed in distinct steps with the butane-1-isocyanate "tail" cleaving first above ≈225 °C, followed by the isocytosine "head" breaking down above ≈244 °C. In this regard, a similar compound was prepared to model the *n*-propyl "arms" of the branching units in the present DPs (cf. compound **29** on page 141 of the Experimental), which featured a comparable IDT of ≈222 °C (cf. Figure 8-26 on page 186 of the Appendix).

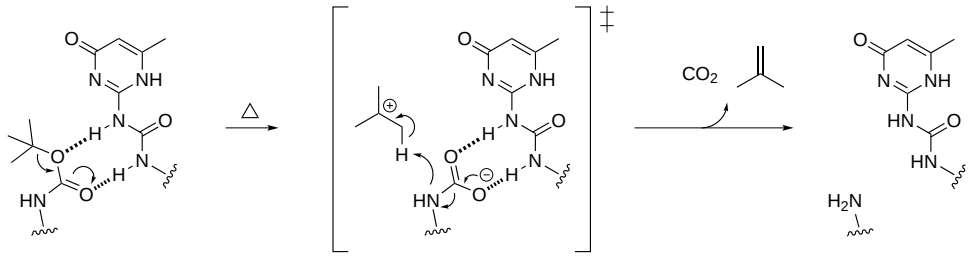

Scheme 3-16: Proposed mechanism for the 2-ureido-4[1*H*]-pyrimidinone (UPy)-facilitated thermolysis of *tert*-butyloxycarbonyl (Boc)-protected amines.

The higher thermal stability of UPy moieties compared to the Boc groups implies that the Boc groups cleave first, followed by the thermolysis of the UPy moieties over a somewhat broader temperature range. Hence, despite the fact that the initial degradation stage is characterized by a clear-cut mass loss spanning a temperature range of only ≈20 °C, the end of this process cannot be readily identified as the TGA curves do not completely level off before the next stage of the degradation begins, especially in the case of samples featuring higher degrees of UPy-functionalization or small Boc-to-UPy ratios (cf. Figures 3-21(c, d)). Hence, the temperature range between 180 °C and 300 °C was chosen to mark the starting and end points of the first degradation step (*vide supra*). In the case of the UPy-functionalized DP samples, the cumulative weight losses up to 300 °C are consistent with the combined thermolysis of the Boc and UPy groups. This was inferred from the respective theoretical mass losses α^0, which were calculated using Equation 3-10 in analogy to Equation 3-7 established for the thermolysis of "classic" DPs:

$$\alpha^0 = \frac{\frac{x \cdot 2^g \cdot M_{\mathrm{Boc}} + y \cdot 2^g/2 \cdot M_{\mathrm{Boc}} + y \cdot M_{\mathrm{UPy}}}{x+y}}{\frac{x \cdot M_{\mathrm{MG}g,\mathrm{Boc}} + y \cdot M_{\mathrm{MG}g,\mathrm{UPy}}}{x+y}} \cdot 100\% \tag{3-8}$$

$$= \frac{\frac{x \cdot 2^g + y \cdot 2^g/2}{x+y} \cdot M_{\mathrm{Boc}} + \frac{y}{x+y} \cdot M_{\mathrm{UPy}}}{\frac{x \cdot M_{\mathrm{MG}g,\mathrm{Boc}} + y \cdot M_{\mathrm{MG}g,\mathrm{UPy}}}{x+y}} \cdot 100\% \tag{3-9}$$

$$= \frac{N_{\mathrm{Boc}} \cdot M_{\mathrm{Boc}} + N_{\mathrm{UPy}} \cdot M_{\mathrm{UPy}}}{M_{\mathrm{r.u.}}} \cdot 100\% \tag{3-10}$$

Therein, the terms x and y denote the respective feed ratios of macromonomers **1c** and **4c** (cf. Table 3-6 on page 56), g denotes the generation number, M_{Boc} (100.12 g mol^{-1}) and M_{UPy} (125.13 g mol^{-1}) mark the molar mass loss caused by the scission of a respective moiety, and N_{Boc} and N_{UPy} denote the number of Boc and UPy groups per extended repeating unit. For each UPy-functionalized copolymer, the term $M_{\mathrm{r.u.}}$ indicates the average molar mass per repeating unit, which was calculated by dividing the theoretical molar masses of the **1c** and **4c**-derived macromonomers $M_{\mathrm{MG}g}$ (multiplied by their mole fractions, i.e. x and y) by the sum of both macromonomers per repeating unit ($x + y$). The thus calculated theoretical mass losses (α^0) for the individual samples are summarized in Table 3-12, together with the experimentally found weight losses between 180 °C and 300 °C, correspondingly. Finally, the char yields at 900 °C, i.e. the remaining mass after all organic material has been burned off, increase with the polymer generation for both "classic" and UPy-functionalized DP samples. This finding reflects the larger fraction of thermally stable aromatic moieties with increasing generation number.

Table 3-12: Comparison between the theoretically calculated and thermogravimetrically determined mass losses for homologous **PG1 − 3** with $P_{\mathrm{n}} \approx 40$ comprising 0, 5, 25, and 50 mol% UPy at their $g = 1$ levels.

Entry	Polymer	$M_{\mathrm{r.u.}}$,[a] Da	N_{Boc}	N_{UPy}	α^0,[b] %	α,[c] %	$\Delta_{\alpha^0\text{-}\alpha}$, %
1	PG1-UPy0	522.63	2.00	0.00	38.2	38.3	−0.1
2	PG1-UPy5	527.73	1.90	0.10	38.4	38.9	−0.5
3	PG1-UPy25	548.14	1.50	0.50	38.8	38.7	0.1
4	PG1-UPy50	573.64	1.00	1.00	39.2	38.0	1.2
5	PG2-UPy0	1223.45	4.00	0.00	32.7	30.7	2.0
6	PG2-UPy5	1193.51	3.80	0.10	32.9	31.2	1.7
7	PG2-UPy25	1073.75	3.00	0.50	33.8	32.6	1.2
8	PG2-UPy50	924.05	2.00	1.00	35.2	34.8	0.4
9	PG3-UPy0	2625.09	8.00	0.00	30.5	27.6	2.9
10	PG3-UPy5	2525.06	7.60	0.10	30.6	29.0	1.6
11	PG3-UPy25	2124.98	6.00	0.50	31.2	29.7	1.5
12	PG3-UPy50	1624.87	4.00	1.00	32.4	31.5	0.9

[a] Molar masses of the averaged copolymer repeating units; [b] Theoretical mass loss calculated based on Equation 3-10; [c] Mass loss directly measured by TGA in N_2 at a heating rate of 20 °C min^{-1}.

3.6.4 Thermogravimetric validation of PG1-UPy compositions

As discussed in Section 3.3.3.2, ^{1}H NMR spectroscopy was used to determine the composition of the prepared first-generation UPy-functionalized copolymers. Thereby, the theoretically calculated and experimentally determined copolymer compositions were found to be in accordance with the respective monomer feed ratios. Given the broad nature of polymer NMR signals and the concomitant uncertainty associated with the respective integrated peak areas, it was of obvious interest to investigate whether thermogravimetric analysis could be used to cross-check the results obtained from ^{1}H NMR spectroscopy.

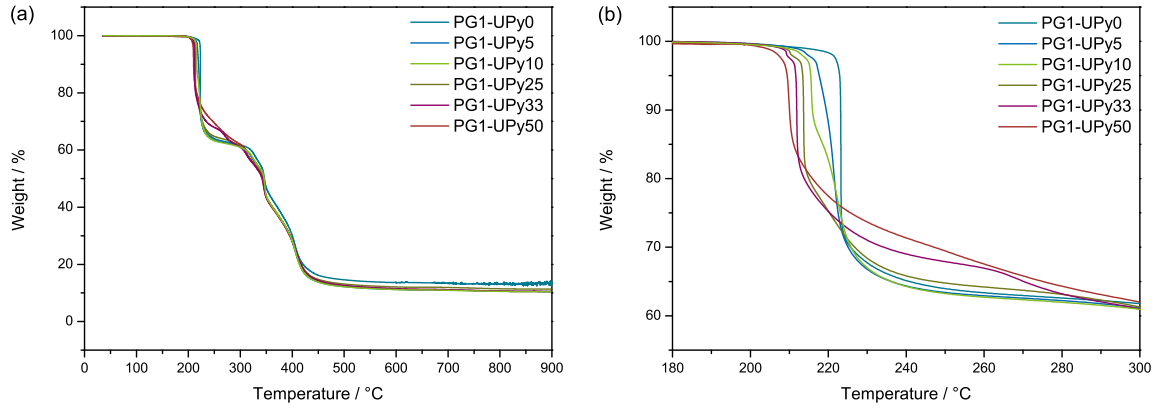

Figure 3-22: (**a**) Thermal degradation curves of **PG1-UPy** samples comprising 0, 5, 10, 25, 33, and 50 mol% UPy recorded at a heating rate of 20 °C in N_2; (**b**) Expanded image section to better visualize the shift of the initial degradation temperature as a function of UPy-functionalization.

Figure 3-22 illustrates the thermal degradation curves obtained for the first-generation dendronized copolymers comprising 0 – 50 mol% UPy in their side chains. As discussed earlier, the UPy-containing DPs underwent a two-step degradation process (*vide supra*), however, the larger set of **PG1-UPy** DPs demonstrates the shift of the IDT as a function of UPy-functionalization even further. The theoretically expected mass losses α^0 for the respective **PG1-UPy** copolymers were calculated using the previously discussed Equation 3-10. A numeric summary of the N- and $M_{\text{r.u.}}$-values used for the calculations of α^0 can be found in Table 3-13, along with the thermogravimetrically determined mass losses α. Evidently, the theoretically expected and experimentally determined combined mass loss of Boc and UPy groups in the copolymers agrees to within ±1% , with only the 50 mol% containing copolymer (Entry 6 in Table 3-13) featuring a somewhat larger deviation. However, since the theoretically calculated weight losses of the **PG1-UPy** copolymers are all very similar and within the reported TGA error range of ±3%, the measured α-values lack statistical significance. Despite the reproducibility and precision of replicate measurements, it follows that thermogravimetric analysis is not suitable for the validation of the copolymer compositions determined by ^{1}H NMR spectroscopy. This

is also due to the fact that the two thermally cleavable moieties at hand, i.e. Boc and UPy, feature no distinctive difference in their thermal stabilities and their combined thermolysis. Nevertheless, thermogravimetric analysis still constitutes a complementary method to the quantification of structure perfection *via* the Sanger labeling protocol.

Table 3-13: Comparison between the theoretically calculated and thermogravimetrically determined mass losses for **PG1-UPy** DPs.

Entry	Polymer	$M_{\text{r.u.}}$,[a] Da	N_{Boc}	N_{UPy}	α^0,[b] %	α,[c] %	$\Delta_{\alpha^0\text{-}\alpha}$, %
1	PG1-UPy0	522.63	2.00	0.00	38.2	38.3	−0.1
2	PG1-UPy5	527.73	1.90	0.10	38.4	38.9	−0.5
3	PG1-UPy10	532.83	1.80	0.20	38.5	39.0	−0.5
4	PG1-UPy25	548.14	1.50	0.50	38.8	38.7	0.1
5	PG1-UPy33	556.64	1.33	0.67	39.0	39.0	0.0
6	PG1-UPy50	573.64	1.00	1.00	39.2	38.0	1.2

[a] Molar masses of the averaged copolymer repeating units; [b] Theoretical mass loss calculated based on Equation 3-10; [c] Mass loss directly measured by TGA in N_2 at a heating rate of 20 °C min^{-1}.

3.6.5 Summary of Section 3.6

The preceding Section discussed the applicability of thermogravimetric analysis (TGA) to determine the degree of structure perfection and copolymer composition of the synthesized "classic" and UPy-functionalized DPs. Compared to poly(methyl methacrylate) (PMMA), the herein presented PMMA-based DPs feature a pronounced weight loss corresponding to the thermolytic cleavage of *tert*-butyloxycarbonyl (Boc) groups. It should be noted, however, that the detected onset of weight loss may not necessarily reflect the full structural integrity of DPs, as potential fragments originating from backbone scission at lower temperatures may simply not be volatile. Nevertheless, this does not hamper the use of TGA as a complementary method to labeling for the determination of the degree of DP structure perfection, as was exemplarily demonstrated for a homologous series of "classic" DPs with $P_n \approx 2000$ and $g = 1-3$. Thereby, it was shown that TGA underestimates the coverage by roughly 0.5 – 3.8% compared to the corresponding values obtained by UV-labeling of the same samples. In light of the relatively large error of the TGA method, which amounts to roughly ± 3%, this demonstrates the higher accuracy of the labeling method, especially for lower-generation DPs (below g_{max}). Moreover, the weight loss profile of the prepared ureidopyrimidinone (UPy)-functionalized DPs was investigated. Thereby, all samples were found to exhibit no mass loss to at least 200 °C, followed by a two-stage degradation profile similar to the "classic" DPs. The initial degradation

temperature (IDT), corresponding to the temperature at 5% weight loss, was found to decrease from 223 °C (0 mol% UPy) to 209 °C (50 mol% UPy) with increasing UPy-content, consistently. The experimentally determined weight losses in the temperature range encompassing the first degradation stage could be ascribed to the combined thermolysis of Boc and UPy moieties. Notably, within each homologous series, the IDT was found to be independent of the generation number and a UPy-bearing model compound exhibited comparable thermal stability to Boc. This resulted in the suggestion of a UPy-facilitated cleavage mechanism, according to which the UPy-induced alteration of electron density in the Boc groups leads to a weakened bond between the etheral oxygen and the tertiary carbon atom in the Boc group. Consequently, the heterolytic scission of the C – O bond is facilitated in analogy to the corresponding acid-catalyzed deprotection mechanism. The *g*-independence of the IDT within the studied samples was ascribed to intramolecular back-folding of the dendritic branches towards the UPy-moieties. However, the fact that Boc and UPy feature no distinctly different thermolysis stages renders TGA unsuitable for the validation of the composition of macromonomers **1c** and **4c** in the UPy-functionalized copolymers due to the large error of the method and the comparably small differences in theoretical weight loss between the samples, respectively.

3.7 Rheology of DPs

Rheology is the branch of science dealing with the flow and deformation of soft matter and plays an important role in many and diverse industrial applications, ranging from food and polymer processing to consumer products such as cosmetics. Therefore, a profound knowledge of the rheological properties of a system is important in process design, as it enables the prediction of a material's behavior as it passes through pumps, mixers, extruders, molds, etc. Moreover, from a quality control point of view, information on the rheological behavior of materials is also relevant, e.g. for controlling batch-to-batch consistency or for tuning the feel and texture of products, which - in many cases - contain polymers as additives.[203] Clearly, such industrial flows are complex, which brings the need to study the behavior of polymeric liquids in simple flows and well-defined conditions with the aim to transfer the knowledge gained therefrom to more complex flow patterns. In practice, oscillatory shear is the technique normally used to study the viscoelasticity of a molten polymer, where the sample is subjected to homogeneous deformations at a sinusoidally varying shear strain or shear stress. The typical frequency response of viscoelastic materials is a sinusoidal stress or strain wave with the same frequency but a phase lag between 0° and 90°, which can be decomposed into an elastic part (G'(ω)) and a viscous part (G"(ω)) to describe the viscoelastic behavior of a given material.

The linear viscoelastic properties of branched polymer melts have been extensively studied over the past few decades, both experimentally and by theoretical modelling. Several branched polymer structures have been considered, including star-shaped polymers,[204] polymer combs,[205] and dumbbell-shaped polymers.[206] In these systems, the dynamics are commonly described by a hierarchical relaxation process, characterized in that the outermost segments of the appendices relax first, while the internal segments near branching points relax at a later stage.[207] By comparison, the behavior of DPs in the melt has been less systematically investigated so far. Hence, the following sections aim to provide a qualitative insight into the rheological peculiarities of DPs with well-defined molecular structures, in which the backbone chain length, the generation number, the nature of the terminal end groups, as well as the position and concentration of strongly hydrogen bonding groups along the backbone have been systematically varied. Section 3.7.1 provides a discussion of the origin of the out-of-equilibrium state of pristine DP samples and the factors influencing the equilibration times determined in oscillatory time sweep tests of DPs. Thereafter, the linear viscoelasticity of DPs will be discussed in Section 3.7.2, particularly with respect to the structural parameters governing the rheology of DPs. In this context, the effects resulting from the tailored intermolecular interactions in the OEG-decorated and UPy-functionalized representatives will be emphasized compared to their "classic" counterparts. The rheological characterization presented in this chapter was accomplished in collaboration with the group of Prof. Dimitris Vlassopoulos (FORTH Heraklion, Crete, Greece), whereby the measurements presented herein were performed by Salvatore Costanzo at FORTH Heraklion and ETH Zurich.

3.7.1 Sample equilibration

The linear rheological properties of a material can only be studied if the system in question is in a steady state. In this context, the physical properties of glassy materials are usually time dependent owing to the thermodynamically out-of-equilibrium state they are trapped in. For amorphous polymers, the inherent effort of any material to attain equilibrium is reflected in macro- and/or microstructural rearrangements causing relaxation over time in a process that is commonly referred to in the literature as "physical aging".[208] Unsurprisingly, these conformational relaxations have direct implications for the rheological behavior of materials. In order to determine if a system has time-dependent rheological properties, oscillatory time sweep experiments can be performed at a fixed frequency and at fixed strain amplitude at the temperature of the measurement. By monitoring the storage- and loss moduli as a function of time, oscillatory time sweeps directly provide information on how the material's behavior changes with time. Depending on the sample tested, further information relating to polymer degradation or solvent evaporation can be retrieved from the measurement as well. However, in order to be able to accurately elucidate the relation between molecular structure and viscoelastic behavior, great care must be taken to ensure that the measurements are conducted at amplitudes where the obtained moduli are independent of the imposed stress or strain levels, i.e. in the so-called linear viscoelastic regime (cf. Section 3.7.2).[209] Put another way, the applied deformations have to be sufficiently small for the effect of two or more individual deformations to be equal to the sum of these deformations. To this end, it is necessary to determine the maximum strain for linear behavior over the frequency range of interest first, which is done by carrying out a strain sweep test. Thereby, the frequency and the strain amplitude of the test are fixed and the amplitude is incrementally increased, whereupon the transition from the linear to the nonlinear regime is characterized by the fact that the moduli are no longer strain independent.

Examples of oscillatory time sweep tests on homologous "classic" DPs comprising generation numbers $g = 2$ and 3 and a backbone chain length of approximately 2000 repeating units (Entries 5 and 11 in Table 3-3, Section 3.1.2) are illustrated in Figure 3-23. As the equilibration process advances, the values of both the elastic- (G') and the viscous (G") modulus increase and eventually level off, indicating that the material's structure has reached a steady state. From the curves plotted in Figure 3-23, it becomes immediately apparent that, in both cases, the time required for sample equilibration is relatively long, i.e. in the order of several hours. This is in contrast to conventional amorphous polymers, which simply relax after an imposed stress and do not age as there is no structure formation. Arguably, the significant difference in the equilibration times of both polymer types stems from distinct circumstances: Whereas the stress in conventional amorphous polymers originates predominantly from processing steps and frozen-in tension due to rapid cooling below the glass transition temperature, the non-equilibrium state of dendronized polymers can be attributed to their mode of synthesis involving a freeze-drying step. More

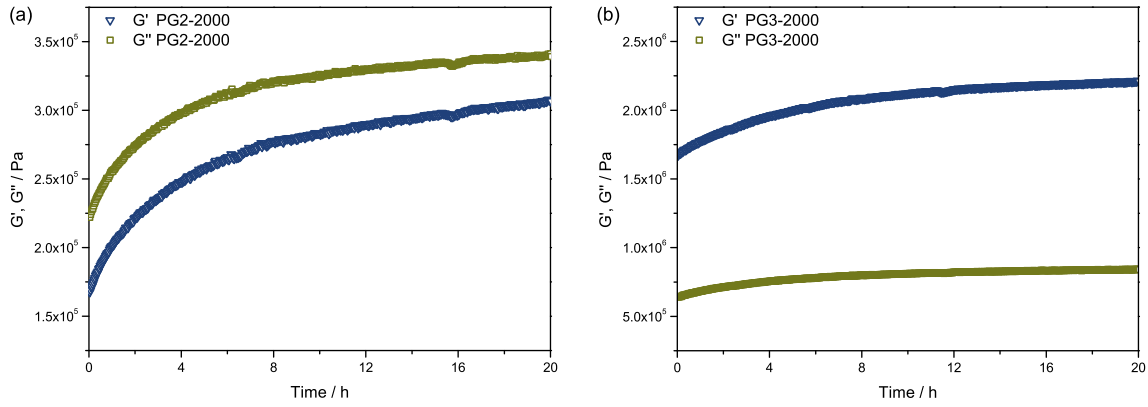

Figure 3-23: Shear moduli (G', G") as a function of time during the equilibration of "classic" **PG2-2000** (**a**) and **PG3-2000** (**b**) samples in the rheometer recorded at $T_{\mathrm{ref}} = T_{\mathrm{g}} + 30\,^{\circ}\mathrm{C}$.

precisely, the outcome of freeze-drying a dilute dendronized polymer solution is a foam, in which the individual chains have little interaction. It follows that these freeze-dried DP samples are far from equilibrium and undergo physical aging by interdigitation of the outermost layers of neighboring macromolecules. The driving force for this interpenetration process stems from the tendency of DPs to reduce local density gradients that arise from the distinct molecular structure of these polymers and their corresponding radial density profile, as supported by various simulations in the relevant literature (cf. Section 2).[61, 62] Hence, the long equilibration times observed can be linked to the weak interpenetration of the dendrons in the outermost layer, which is a complex and cooperative process involving multi-segmental local motions and rotations. Since equilibration involves spatial rearrangements at large length scales, the time required for complete equilibration is in the order of 20 hours when performed at a temperature 30 °C above the glass transition temperature of the respective DPs, as evidenced by the data shown in Figure 3-23. The outcome of this interpenetration process is a homogeneous melt, in which the average density is virtually constant.

In the case of "classic" DPs, the capability of the NHBoc groups to undergo intra- and intermolecular hydrogen bonding interactions represents an additional factor influencing the dynamics of DPs. Previous theoretical studies revealed that the location of the NHBoc moieties accounting for hydrogen bonding experiences a shift towards the topological periphery with increasing dendron generation, consistently.[62] Although the depth of mutual interdigitation of neighboring macromolecules is not large but rather limited to the outermost layers, the occurrence of supramolecular interactions between NHBoc groups provides directionality to the process which, in turn, leads to effectively faster equilibration and higher elastic moduli. This may already be appreciated by comparing the equilibration curves depicted in Figure 3-23(a) and (b), illustrating that the elastic modulus (G') of the third-generation DP sample becomes larger than the viscous mod-

ulus (G”), indicating a more solid-like behavior of the system.[209] Again, this may be ascribed to the different number of topologically peripheral hydrogen bonding moieties per backbone repeating unit in these DPs (8 Boc in PG3 vs. 4 Boc in PG2) and the concomitantly enhanced supramolecular interactions present in the third-generation sample. Moreover, judging from the shape of recorded equilibration curves, the time required for complete equilibration of the third-generation sample is arguably somewhat shorter compared to the respective time obtained for its second-generation homologue, which is also in agreement with the proposed conformational locking function exerted by the NHBoc groups.

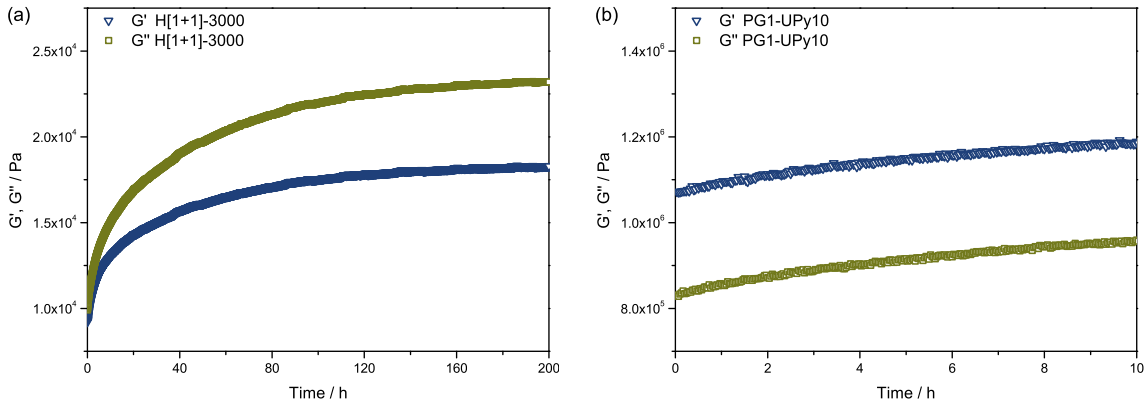

Figure 3-24: Shear moduli (G’, G”) as a function of time during the equilibration of a ”hybrid” **H[1+1]-3000** (**a**) and UPy-functionalized **PG1-UPy10** (**b**) sample in the rheometer recorded at $T_{ref} = T_g + 30\,°C$ (a) and $T_g + 38\,°C$ (b).

In this context, the influence of peripheral moieties on the equilibration dynamics becomes even more apparent in the case of the oligo(ethylene glycol)-decorated ”hybrid” DPs and the UPy-functionalized DPs, respectively. Figure 3-24(a) exemplarily illustrates the results of the performed oscillatory time sweep tests on the **H[1+1]-3000** sample (Entry 6 in Table 3-5, Section 3.2.3), whereas Figure 3-24(b) depicts the results obtained for the **PG1-UPy10** sample (Entry 3 in Table 3-7, Section 3.3.3.2). Compared to the ”classic” DPs, the time required to arrive at steady moduli is drastically prolonged in the hybridized samples, which can be explained by the shielding of intermolecular hydrogen bonding and π-π stacking interactions. In addition, the viscous modulus of the hybridized sample becomes larger than the elastic modulus, which is indicative of a more energy-dissipating behavior of the material.[209] On the other hand, the presence of UPy moieties in the side chains results in shorter equilibration times due to enhanced intermolecular hydrogen bonding interactions. The accelerated interdigitation dynamics become noticeable at comparatively low degrees of UPy-functionalization in the order of $5-10\,$mol% already. As evidenced by the data presented in Figure 3-24(b), under the chosen conditions, the sample exhibits a more pronounced energy-storing behavior and the elastic modulus is almost one order of magnitude higher compared to the one of the ”classic”, non-functionalized DPs

shown in Figure 3-23(a). This is noteworthy due to the comparatively large difference in the respective backbone chain lengths, i.e. approximately 40 vs. 2000 repeating units, which effectively rules out the possibility for entanglements in the case of the short-chained, UPy-functionalized sample. Hence, the values for the elastic moduli determined for the latter sample are indicative of the enhanced supramolecular interactions exerted by the UPy moieties. The combined results obtained from the oscillatory time sweep tests hint towards a mutual interpenetration process of neighboring macromolecules in the melt that is accelerated by intermolecular hydrogen bonding exerted by "sticky" sites, akin to a Velcro® fastening mode of action (*vide infra*).

3.7.2 Linear viscoelasticity

Since structural relaxations in polymers are typically accelerated as the temperature is increased, the so-called "time-temperature superposition" (TTS) principle can be applied to probe the linear behavior of polymeric systems over a significantly increased range of timescales and frequencies, respectively.[209] The essence of the concept is that changing the temperature of a measurement has the same effect on the data as shifting the data horizontally on the logarithmic time or frequency axis. In this context, horizontal shift factors are used to shift data taken at a certain temperature T along the x-axis in a way that they will equal data taken at the reference temperature T_{ref}. This way, temperature-independent "master curves" can be constructed. However, in order for TTS to hold true, it is crucial that all the relaxation phenomena feature the same temperature dependency and that increases in temperature only change the rate of relaxations while keeping the material's microstructure unaffected. Also, it should be noted that, while TTS is usually valid and frequently used for conventional polymeric systems, the applicability of TTS in the context of supramolecular systems is not straightforward as changes in temperature do not merely affect the thermal motion of the polymer chains but also interfere with supramolecular interactions.[210]

That being said, the measurements reported herein were performed on "aged" samples and at amplitudes where the response of the systems is linear, as discussed in Section 3.7.1. Figure 3-25 illustrates exemplary master curves of "classic" DPs that have been constructed by using the TTS principle and a reference temperature of 90 °C ($T_{\mathrm{g}} + 30$ °C). Figure 3-25(a) illustrates the master curves for a series of first-generation DPs with varied backbone chain lengths, which have been vertically shifted using the indicated shift factors to improve the legibility of the plots. For the sample comprising the lowest degree of polymerization ($P_{\mathrm{n}} \approx 50$), three different regimes can be identified in the G' and G" plots: A glassy state (G' > G") at high ω, a transition regime (G' ∼ G") at intermediate ω, and a dissipative regime (G' < G") at low ω. For the samples featuring longer backbone chain lengths ($P_{\mathrm{n}} \geq 1500$), a weak elastic "plateau" (G' > G") emerges at low ω, which becomes more apparent as the degree of polymerization increases, consistently. In this regard, the absence of a rubbery plateau at intermediate frequencies is in contrast

to conventional linear polymers of high molar mass and suggests that even the longest-chained DPs in this study remain unentangled. In fact, the large entanglement molar mass (M_e) is a consequence of steric crowding around the polymer backbone, which increases the persistence length and reduces the number of entanglements per backbone.[62] Thereby, the enhancement of the elastic plateau molduli can be attributed to improved backbone-to-backbone correlations with increasing degree of polymerization, as supported by recent SAXS studies.[180] Evidently, the improved chain alignment leads to an effective reinforcement of the plateau modulus via an enhanced number density of intermolecular bonds, e.g. by the topologically peripheral Boc groups. Hence, at fixed generation number, the master curves of "classic" DPs comprising varied degrees of polymerization show a marked rheological transition from weakly correlated, unentangled-like ($P_n \approx 50$) to strongly correlated, network-like ($P_n \approx 3000$).

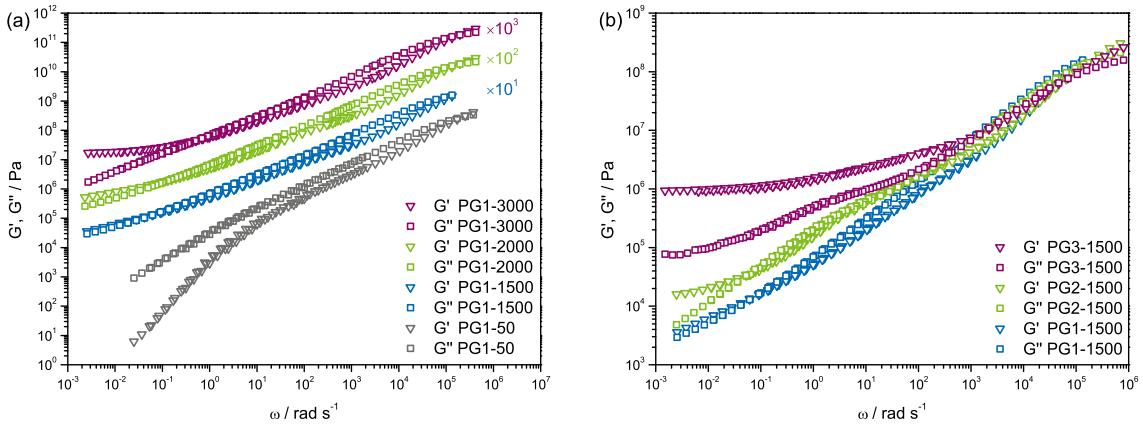

Figure 3-25: Dynamic master curves of G' (open triangles) and G" (open squares) of "classic" DPs as a function of angular frequency (ω) at a reference temperature of $T_{ref} = T_g + 30\,°C$ for (**a**) $g = 1$ and varied degrees of polymerization, and (**b**) $g = 1-3$ with $P_n \approx 1500$. For improved clarity, the master curves have been vertically shifted using the indicated shift factors.

At nearly constant degree of polymerization, the influence of the generation number on the viscoelastic properties of homologous "classic" DPs becomes apparent from the exemplary master curves presented in Figure 3-25(b) for samples with $P_n \approx 1500$. Increasing the generation number from $g = 1$ to $g = 3$ particularly affects the moduli in the intermediate frequency region of the viscoelastic spectrum, which describes the behavior of the repeatedly furcated side branches: Whereas the **PG1** sample shows characteristics of a viscous liquid (G" > G'), **PG2** features a more elastic behavior in the same frequency range (G' ∼ G") already. In general, both **PG1-1500** and **PG2-1500** are relatively flexible polymers, which may be compared to other branched systems, such as bottle brushes or wedge polymers. For these so-called super-soft elastomers, the onset of the elastic plateau is also shifted to lower ω, which reflects their large values of persistence length and M_e.[211] In contrast, the evolution of an elastic plateau featuring a plateau modulus

that is comparable to pure poly(methyl methacrylate) can be observed in the case of **PG3-1500**. Due to the very large values for the persistence length and M_e, the determined elasticity for **PG3-1500** should result exclusively from intermolecular interactions, which increase with generation. In addition, at sufficiently large degrees of polymerization (such as in the samples comprising $P_n \approx 1500$), the improved packing of individual macromolecules discussed in the previous paragraph promotes these interactions even further and enhances the values of the elastic moduli.

The results extracted from the measurements on the "classic" DPs hint towards an effective reinforcement by means of enhanced intermolecular interactions that increase with both the degree of polymerization and the generation number akin to a Velcro® fastening mechanism. Expectedly, the shielding effect exerted by the oligo(ethylene glycol) dendrons found in the "hybrid" DPs on the intermolecular hydrogen bonding and π-π stacking interactions yields a distinctly different viscoelastic behavior. The differences are mainly reflected in the low frequency regime, as highlighted by the master curves of **H[1+1]** samples featuring varied degrees of polymerization presented in Figure 3-26, exemplarily. In contrast to the previously described "classic" DPs, no elastic plateau can be identified, even at very long time scales. Furthermore, the values of the elastic moduli do not increase upon increasing the degree of polymerization beyond approximately 300 repeating units. Instead, the cross-over point of G' and G" is shifted towards much lower ω, whereafter the curves exhibit a parallelism of both moduli, which is indicative of very weakly interacting species and a more gel-like behavior, respectively. Thereby, the obtained results are in qualitative agreement with the significantly longer equilibration times determined for the "hybrid" DPs compared to the "classic" DPs in oscillatory time sweep experiments (cf. Section 3.7.1).

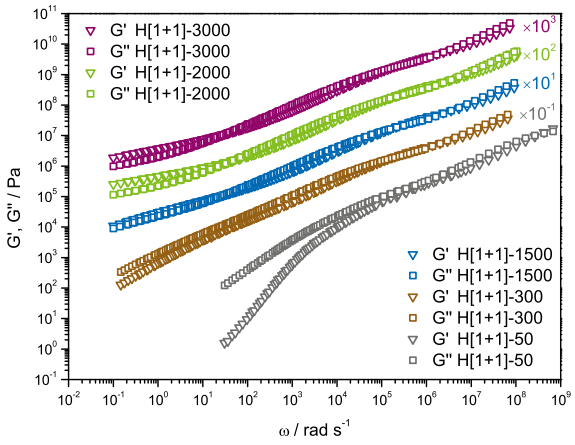

Figure 3-26: Dynamic master curves of G' (open triangles) and G" (open squares) for "hybrid" DPs with varied backbone chain lenghts $P_n \approx 50$, 300, 1500, 2000, and 3000 at a reference temperature of $T_{ref} = T_g + 30\,°C$. For improved clarity, the master curves have been vertically shifted using the indicated shfit factors.

Accordingly, in addition to the effects of P_n and g, the viscoelastic behavior of "classic" DPs can be further tuned by the presence of strongly hydrogen bonding UPy moieties acting as supramolecular "stickers". Figure 3-27(a) illustrates the master curves of short-chained, first-generation DPs ($P_n \approx 40$) as a function of UPy concentration. At relatively low degrees of UPy-functionalization, i.e. 5 mol% in **PG1-UPy5**), the master curves look similar to those of the unfunctionalized polymer **PG1-UPy0** with a comparable degree of polymerization. Accordingly, both samples exhibit a predominantly viscous response to the imposed deformation, as G" remains greater than G' over the whole range of explored frequencies. Also, both samples show a smooth transition from intermediate ω to terminal relaxation with slopes of 1 and 2 for G" and G', respectively. The observed liquid-like behavior is expected for these short-chained samples with relatively low molar masses below the entanglement threshold. As the concentration of UPy moieties is increased to 10 mol% in **PG1-UPy10**, the onset of an elastic plateau of G' at intermediate ω is clearly observable before terminal flow is approached. A further increase of the UPy content to 25% yields an elastic plateau for **PG1-UPy25**, whereby the plateau modulus is enhanced almost tenfold compared to **PG1-UPy10**. The cross-over frequency is consistently shifted towards lower frequencies with increasing UPy content in the copolymers. Moreover, the slope of G' in the terminal regime becomes smaller than 2, which is indicative of the formation of a cross-linked supramolecular network.

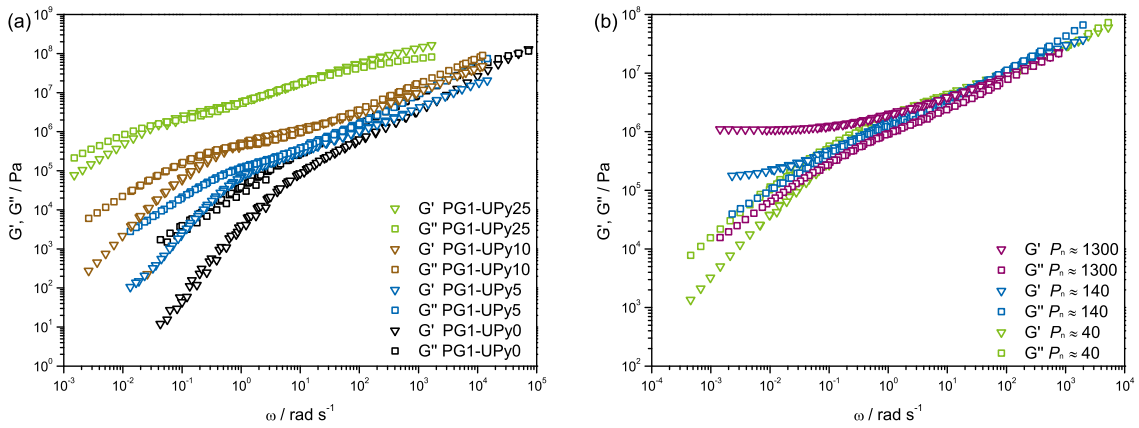

Figure 3-27: Dynamic master curves of G' (open triangles) and G" (open squares) for "classic" DPs comprising (**a**) 0 – 25 mol% UPy at the $g = 1$ level and (**b**) different backbone chain lengths but a constant UPy-loading of 25 mol% at a reference temperature of $T_{ref} = T_g + 38\,°C$.

In order to investigate the influence of UPy moieties on the dynamics of DPs with varied backbone chain lengths, further experiments were performed using first-generation "classic" DPs containing 25 mol% UPy in their side chains and with degrees of polymerization ranging from $P_n \approx 40$ to 1300. From the respective master curves depicted in Figure 3-27(b), a shift from viscous behavior to a more solid-like behavior can be noted when the degree of polymerization is increased from $P_n \approx 40$ to 140, as evidenced by the evolu-

tion of an elastic plateau at low ω, i.e. the fact that the elastic modulus becomes larger than the viscous modulus (G' > G") and levels off. Subsequently, the elastic plateau modulus increases by one decade upon further increase of the degree of polymerization from $P_n \approx 140$ to 1300. Evidently, the presence of UPy moieties enhances the previously described backbone-to-backbone correlation, which leads to even stronger intermolecular interactions. Naturally, this effect is increasingly reduced in the case of higher-generation DPs as the UPy moieties are still located at the $g = 1$ level and become progressively more immersed in the dendritic structure. As apparent from the master curves of homologous DPs comprising 25 mol% UPy depicted in Figure 3-28, the difference between G' and G" at low ω becomes smaller with increasing dendron generation and, eventually, the master curves become similar to those obtained using the unfunctionalized "classic" DP samples of similar backbone chain lengths. This result demonstrates the fine range in which mutual interdigitation of neighboring molecules can take place due to the topological restrains imposed by the dense interior of DPs. Depending on the concentration of UPy moieties blocking one of the two arms at the $g = 1$ level for further dendritic growth reactions and the concomitant differences in the overall accessibility of the interior of these DPs, the results show that already one dendron generation can suffice to shield the underlying generation from intermolecular interactions. This finding is also substantiated by the combined results obtained from DLS and ^{1}H NMR spectroscopy, which revealed that the formed SCPNs uncoil because formation of intramolecular UPy dimers becomes more hindered with increasing dendron generation (cf. Section 3.4 and Figure 8-25 on page 185 of the Appendix).

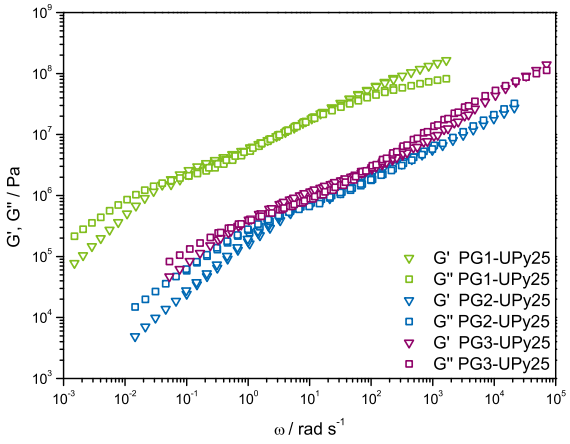

Figure 3-28: Dynamic master curves of G' (open triangles) and G" (open squares) for UPy-functionalized DPs with $P_n \approx 40$ and $g = 1-3$ and 25 mol% UPy at the $g = 1$ level at a reference temperature of $T_{ref} = T_g + 35\,°C$.

3.7.3 Summary of Section 3.7

The equilibration kinetics and linear viscoelasticity of structurally well-defined dendronized polymers were investigated by small amplitude oscillatory shear measurements and master curves were constructed by using the time-temperature superposition principle. In contrast to conventional polymers, DPs were found to exhibit very long equilibration times in the order of several hours to weeks, which can be ascribed to the out-of-equilibrium state of freeze-dried DPs. More precisely, DPs undergo physical aging by interdigitation of the outermost layers of neighboring molecules in order to reduce local density gradients. Compared to the "classic" DPs, the equilibration kinetics are significantly slowed in the case of the "hybrid" DPs, but are accelerated upon functionalization with strongly hydrogen bonding UPy-moieties. The obtained results can be rationalized by using the example of a Velcro® fastening mode of action: On the one hand, the presence of UPy moieties acting as strong supramolecular "stickers" along the polymer backbone reduces the relevant length scale for cooperative dendron rearrangements to the distance between two adjacent supramolecular cross-links. On the other hand, the lack of topologically peripheral moieties capable of undergoing intermolecular interactions in the case of the "hybrid" DPs extends this length scale to the entire backbone. Rheological measurements on aged DPs revealed a linear viscoelastic response in the melt that is predominantly determined by intermolecular interactions, whose extent in the frequency scale and actual value depends on both P_n and g. More specifically, interdigitation of DPs enhances molecular friction, which is directly related to the contact area of DPs that increases with g and P_n due to improved backbone-to-backbone correlations, consistently. The influence of intermolecular interactions on the viscoelastic response of DPs is further indicated by the measurements performed on the oligo(ethylene glycol)-decorated "hybrid" DPs, which exhibit a gel-like behavior for $P_n > 300$. This is indicative of significantly reduced supramolecular interactions, i.e. molecular friction, in these polymers. In contrast, the presence of strongly hydrogen bonding UPy moieties resulted in the evolution of rubbery plateau regions that broaden with increasing UPy content, consistently. This is indicative for the formation of a supramolecular network composed of self-complementary UPy cross-links. The elastic plateau modulus can be tailored by varying the concentration of topologically peripheral UPy groups, P_n, and g. Furnishing these UPy-functionalized DPs with additional generations resulted in master curves that became virtually indistinguishable from their unfunctionalized "classic" counterparts as of the third-generation. This clearly demonstrates the depth to which mutual interdigitation of neighboring molecules can take place due to the steric restrains imposed by the densely packed interior of DPs. All in all, owing to the controlled mode of synthesis, the well-defined molecular structure of DPs offers a unique handle to tailor the rheological properties of these polymers in a wide range.

4 Conclusion and outlook

The need for well-defined materials with controlled chemical structures is ever increasing in the area of nanotechnology. In this regard, dendronized polymers (DPs), the feature sizes of which range in the nano- to micrometer length scale and whose physical dimensions as well as diverse chemical functional groups can be controlled with nanometer precision, represent a versatile class of materials that is of particular interest.

In this work, various homologous series of DPs have been synthesized up to the third generation and modifications were introduced to suppress or enhance intermolecular hydrogen bonding interactions. In combination with the range of prepared backbone chain lengths, it was possible to pinpoint the effects exerted by the generation, the degree of polymerization, and supramolecular bonding interactions on the thermomechanical properties of DPs. In this regard, it can be concluded that the dynamics of DPs are strongly influenced by the dynamics of the dendrons: Due to the steric hindrance imparted by large dendrons and the fact that the dendrons are connected to every repeating unit of an underlying polymer backbone, the translational and rotational mobility of the dendrons is strongly constrained. Concomitantly, the mobility of the backbone segments is also restricted, since for a backbone segment to move, the dendrons must move as well. These constraints on the dynamics are less apparent when g and/or P_n are small or when the cohesive energy between the dendrons is low. However, they become obvious when the strength of intermolecular bonding interactions is enhanced. On the one hand, this was demonstrated by the synthesized "hybrid" DPs and their highly flexible chemical structures composed of peripheral oligo(ethylene glycol)-based dendrons. On the other hand, the presence of supramolecular binding motifs that are capable of undergoing strong inter and intramolecular secondary interactions can significantly reduce the mobility of the dendrons, as exemplified by the prepared UPy-functionalized DPs. The physical origins described above manifested themselves in the form of a wide range of glass transition temperatures. Here, the influence of intermolecular hydrogen bonding became also apparent from the rheological experiments that revealed a smooth crossover from a liquid-like behavior of flexible chains to a rubbery behavior of supramolecular networks as the degree of UPy-functionalization in the side chains increases. The matrix of prepared DPs also provided new experimental insights into the accessibility of the dendritic interior and the depth of intermolecular interdigitation.

In future research, the herein presented rheological measurements of dendronized polymers in the bulk phase could be complemented by the characterization of ultrathin dendronized polymer films and their organization at surfaces and interfaces. In this context, one of the most commonly used methods for the preparation and investigation of molecularly thin films confined to two dimensions is the Langmuir technique, which renders the assembly of building blocks at a liquid-gas interface under well controlled conditions and provides

opportunities to exercise molecular level control over the structure of the formed films. Subsequently, Langmuir-Blodgett film transfer allows for the immobilization of these films on solid substrates. Several characterization methods, such as atomic force microscopy and Brewster angle microscopy, can be integrated with the Langmuir technique, thus, adding to its value. Although, originally, the Langmuir and Langmuir-Blodgett technique were designed to study phase transitions in small amphiphilic molecules, they have soon become highly useful tools to form ordered films and investigate the equilibrium and dynamic behaviors of all types of materials, including many types of synthetic and biopolymers. The two dimensional confinement in Langmuir polymer films offers a particular opportunity to uncouple the observed relaxation dynamics from the possible effects of entanglements, as opposed to measurements of their three dimensional analogues, since the monolayers are prepared by spreading a dilute solution, in which each chain is isolated.

On a final note, synthetic chemists will have to further improve the reaction conditions and procedures in order to render the overall synthesis of DPs less tedious and more cost-efficient. While a fully-automated procedure for the synthesis of high-generation DPs may remain elusive or be a far-end goal at least, the herein presented use of photocleavable protecting groups can be seen as a first step towards a streamlined dendronization procedure and an overall "greener" process. For instance, future methodological studies could be directed towards the development of an integrated process, in which DPs protected with photolytically cleavable protecting groups are irradiated for a predetermined amount of time, followed by the addition of dendronization agents in the dark and isolation of the desired product by precipitation prior to subsequent dendronizations. This way, no acids would be required for the Boc deprotection reaction, quenching of excess acid and freeze-drying of the deprotected species could be omitted, and, perhaps most importantly, solubility issues resulting from incautiously taking DPs to dryness could be avoided due to the fact that the whole process takes place in solution. In this context, the ability to deprotect a fraction of DP functional groups selectively and quantitatively would also enable a higher degree of control over post-polymerization modifications and allow for the creation of more complex and multi-functional DP structures.

In conclusion, the field of dendronized polymers is a multidisciplinary topic that continues to attract attention from the research community. Even if they may never find their way into "real world" applications, DPs represent a class of complex materials and valuable tools to investigate the potential of well-defined, nanoscopic molecular objects that are not accessible otherwise and, hence, they can shed light on possible applications that are yet to be discovered.

5 Experimental

5.1 Materials

Unless noted otherwise, all reactions were carried out in dried Schlenk glassware, in dried solvents and in an inert nitrogen atmosphere. For reactions, the used solvents were of analytical grade and obtained from a SP-105 solvent purification system (LC Technology Solutions Inc., USA). Chromatography solvents were purchased as technical grade and distilled once prior to use. Ozone was generated by a multi purpose ozone generator MP-8000 (A2Z Ozone, USA). Methacryloyl chloride (MAC) was purchased from Sigma-Aldrich (97%) and freshly distilled before use. Azobis(isobutyronitrile) (AIBN) was purchased from Fluka-Chemie AG (>98%) and recrystallized from methanol.

All other chemicals were commercially obtained as reagent grade and used without further purification. In alphabetical order: Acetic anhydride (Sigma-Aldrich, ≥99%), 2-amino-4-hydroxy-6-methylpyrimidine (Acros Organics, 99%), bromoacetic acid (MBA) (ABCR, 98%), 1,1'-carbonyldiimidazole (Acros Organics, 97%), chloroacetic acid (Acros Organics, >99%), 3-chloro-2-chloromethyl-1-propene (MDC) (TCI, >98%), 1,3-dichloropropan-2-ol (ABCR, 98%), 1,3-dichloropropan-2-one (ABCR, 96%), 3,4-dimethoxyacetophenone (Acros Organics, 98%), 4-dimethylaminopyridine (DMAP) (Acros Organics, 99%), N,N'-disuccinimidyl carbonate (Fluorochem, 99%), (±)-epichlorohydrine (Fluka, ≥99%), 1-fluoro-2,4-dinitrobenzene (Sigma-Aldrich, ≥99%), hydrochloric acid (HCl)(Sigma-Aldrich, ≥37%), N-hydroxysuccinimide (NHS) (ABCR, 98%), lithium aluminiumhydride (Acros Organics, 2.4 M in THF), 2-methoxyethanol (EGME) (Sigma-Aldrich, ≥99%), methyl ester **1a** (Synwit Technology Co., >95%), nitric acid (Sigma-Aldrich, ≥65%), 2-phenyl-2-propyl benzodithioate (CDB) (Sigma-Aldrich, 99%), propylamine (Acros Organics, >99%), sodium borohydride (Merck, for synthesis), sodium hydride (Acros Organics, 60% dispersion in mineral oil), sodium hydroxide (NaOH) (Fischer Chemical, analytical grade), succinimidyl ester **1d** (Synwit Technology Co., >95%), sulfuric acid (Fisher Chemical, >95%), thionyl chloride (Acros Organics, >99%), trifluoroacetic acid (Sigma-Aldrich, ≥99%), triethylamine (Sigma-Aldrich, >99%).

TLC analyses were performed on pre-coated aluminum sheets (silica gel 60G/UV254, 0.20 mm) from Macherey-Nagel. UV-light (254 nm) was used for detection. Column chromatography was conducted on silica gel 60 Å from Fluka (230-400 mesh particle size) as the stationary phase.

5.2 Instrumentation and measurements

Dynamic light scattering

Dynamic light scattering (DLS) measurements were performed on a Nano ZS (Malvern Instruments, UK) equipped with a laser with a wavelength of 633 nm and a scattering angle of 173° at a software-regulated temperature of 22 °C. Samples were prepared by filtering solutions through a 0.45 µm PTFE syringe filter (Macherey-Nagel, Germany) in disposable cuvettes (VWR International, USA) with reduced volume and a path length of 1 cm.

Differential scanning calorimetry

Differential scanning calorimetry (DSC) measurements were conducted on a DSC Q1000 (TA Instruments, USA) over a temperature range from −90 °C to 250 °C in a nitrogen atmosphere. Approximately 4 – 25 mg of dried sample was weighed into an aluminum DSC pan and covered with a punched cap. The samples were subjected to ≥2 heating/cooling cycles with a linear heating/cooling rate of 10 °C min^{-1}. The glass transition temperatures (T_g) were determined from the second heating runs and analyzed using the commercially available Universal Analysis software (TA Instruments, USA).

Elemental analysis

Elemental analyses (EA) were performed by the service for microelemental analysis (LOC, ETH Zurich) on a EA 240 (PerkinElmer, USA) after drying of the samples in high vacuum (HV) to constant weight.

Fourier transform infrared spectroscopy

Fourier transform infrared spectroscopy (FTIR) was performed using an ALPHA FTIR spectrometer (Bruker, USA). The spectra were measured in attenuated total reflection (ATR) mode using a Ge crystal plate and the commercially available Opus software (Bruker, USA).

Gel permeation chromatography

Gel permeation chromatography (GPC) using DMF containing LiBr ($c = 1$ g L^{-1}) as the eluent was performed on a VISCOTEK GPCmax VE-2001 instrument (Malvern, UK)

equipped with D5000 columns (300 × 8.0 mm), refractive index (RI), viscometry (differential pressure) and light scattering (LS; 15° and 90° angles) detectors. Column oven and detector temperatures were regulated to 45 °C. All samples were filtered through 0.45 µm PTFE syringe filters (Macherey-Nagel, Germany) prior to injection and the flow rate was 1 mL min^{-1}. Poly(methyl methacrylate) standards with peak molecular weights (M_p) of 0.10, 0.212, 0.66, 0.981 and 2.73 MDa (Polymer Laboratories Ltd., UK) were used for calibration. Experimental molar masses (M_n, M_w) and polydispersity values (PDI) of the synthesized polymers were determined by light scattering using the commercially available OmniSEC software (Malvern, UK).

GPC using chloroform containing 0.1% toluene as the eluent was performed on a VISCOTEK GPCmax VE-2001 instrument (Malvern, UK) equipped with two columns (1 × PLGel Mix-B and 1 × PLGel Mix-C, 7.5 × 300 mm each), a separate VISCOTEK 2500 ultraviolet detector (UV, $\lambda = 254$ nm), and a VISCOTEK detector module (302 TDA) containing refractive index (RI), viscometry (differential pressure), and light scattering (LS; 15° and 90° angles) detectors. Column oven and detector temperatures were regulated to 35 °C. All samples were filtered through 0.45 µm PTFE syringe filters (Macherey-Nagel, Germany) prior to injection and the flow rate was 1 mL min^{-1}. Polystyrene standards with peak molecular weights (M_p) of 1.48, 2.97, 5.03, 10.68, 19.75, 52.22, 96.00 kDa and 0.184, 0.450, 0.609, 1.373, 2.650, 3.993 MDa (Polymer Laboratories Ltd., UK; PSS Polymer, Germany; Waters, USA) were used for calibration. Experimental molar masses (M_n, M_w) and polydispersity values (PDI) of the synthesized polymers were determined by light scattering using the commercially available OmniSEC software (Malvern, UK).

Mass spectrometry

Mass spectrometry (MS) was performed by the mass spectrometry service lab (LOC, ETH Zurich) on a maXis (Bruker, USA) (ESI-Qq-TOF-MS; solvent, CH_2Cl_2/MeOH; ion polarity, positive; set capillary, 4500.0 V) and a solariX 94 (Bruker, USA) (ESI/MALDI-FTICR-MS; matrix, THA; solvent, CH_2Cl_2/MeOH); ion polarity, positive; set capillary, 4500.0 V).

Nuclear magnetic resonance spectroscopy

^{1}H and ^{13}C nuclear magnetic resonance (NMR) spectra were recorded on an AV 300 spectrometer (Bruker, USA) (^{1}H, 300 MHz; ^{13}C, 75 MHz) at room temperature. Polymer spectra were recorded at 340 K to improve NMR resolution. Chemical shifts are reported as δ values (ppm) with residual H in the deuterated solvents serving as internal standards ($CDCl_3$: 7.26 ppm for ^{1}H and 77.0 ppm for ^{13}C; [D6]DMSO: 2.50 ppm for ^{1}H and 40.0 ppm for ^{13}C). ^{1}H multiplicities are designated by the following abbreviations: s = singlet, d = doublet, t = triplet, m = multiplet, br = broad.

Photochemical reactions

Photolysis reactions (irradiation experiments) were performed using a LED (Omicron, Germany) with an emission maximum (λ_{max}) centered around 365 nm and a nominal power output (P) of 250 mW that was controlled via Omicron's LED Controller software (v 1.3). In addition, a RMR-600 photoreactor (Rayonet, USA) equipped with 8 light bulbs (λ_{max} = 350 nm, no filter, P = 8 W each) and a cooling fan to lower the temperature inside the reactor to ≈ 28 °C was used to investigate the influence of flux on the speed of the photolysis reaction. In a standard protocol, a solution of the respective sample (preferably in a spectrophotometer-compatible quartz cuvette) was positioned at a distance of ≈ 10 cm from the light source. Both timekeeping and irradiation were started simultaneously. After each irradiation run, the reaction vessel was carefully wrapped in aluminium foil to prevent further ambient light-induced photolysis and transferred to the UV-Vis spectrophotometer (for instrument details cf. "Ultraviolet-visible spectroscopy" below). The reaction was carefully mixed prior to each UV-Vis measurement by careful turning of the reaction vessel. Subsequently, the reaction vessel was re-wrapped in aluminium foil and transferred to the respective light source (LED or Photoreactor) for a subsequent irradiation run.

Rheology

Rheological experiments were performed by Salvatore Costanzo at FORTH Heraklion (Crete, Greece) and ETH Zurich. Discoid DP specimens with diameters of 4–8 mm were obtained by compression molding *in vacuo* at a temperature of 5 °C above T_g of the respective polymer sample and a force of 0.1 ton. Linear rheological tests were performed with Physica MCR-502 and Physica MCR-702 rheometers (Anton Paar, Austria) using parallel plate geometries (stainless steel) with diameters of 4 and 8 mm. The rheometers were equipped with an electric hood (MCR-502) and a hybrid temperature control (CTD180 Peltier and convection oven, Anton Paar, MCR-702) to control the temperature. The measurements were performed in an inert atmosphere (N_2) to prevent sample degradation. With both rheometers, the temperature calibration was checked using an external thermocouple (type K) and small horizontal shifts were applied to the master curves in order to account for the small differences identified between the used machines.

Thermogravimetric analysis

Thermogravimetric analyses (TGA) were performed on a TGA Q500 (TA Instruments, USA). In the standard protocol, TGA experiments were conducted in an inert atmosphere and nitrogen was used to flush the furnace (60 ml min^{-1} sample purge flow). A heating rate of 20 °C min^{-1} was used in all experiments as a reasonable compromise on the comparability of the obtained results, sample throughput, and the effects caused by mass transport

processes of degradation products through the samples on the experimental results. The platinum pan used to hold the samples (diameter $\approx 10\,\mathrm{mm}$) was thoroughly cleaned and pre-baked prior to a tare run with the empty pan. Thereafter, approximately $4-7\,\mathrm{mg}$ of finely powdered sample was spread thinly over the bottom of the pan. The pan was loaded in the center of the furnace and placed under the thermocouple, the readout of which was used to control the temperature of the furnace. Experiments were conducted over a temperature range from $30-900\,^{\circ}\mathrm{C}$. The weight of the sample and its temperature were simultaneously recorded by TA Instruments' software, which was also used for evaluation.

Ultraviolet-visible spectroscopy

Ultraviolet-visible (UV-Vis) spectroscopy was performed on a J670 spectrophotometer (JASCO, USA) equipped with a thermally regulated cell. Measurements were carried out using quartz cuvettes with path lengths of $1\,\mathrm{cm}$.

5.3 Synthesis

5.3.1 General procedure A for free-radical polymerization

General procedure A: The required amounts of macromonomers **1c** and **4c** were placed in a Schlenk tube equipped with a magnetic stir bar under a N_2 atmosphere, followed by addition of azo*bis*(isobutyronitrile) (AIBN, 0.01 – 0.5M in DMF). The reaction was diluted with DMF to arrive at a final concentration of 0.25-1.00 g ml^{-1}. After homogenization and thorough degassing by several freeze-pump-thaw cycles, the polymerization mixture was placed in an oil bath that had been preheated to 65 °C, and the reaction was stirred at this temperature under N_2 for a predetermined amount of time. The progress of the polymerization could be macroscopically assessed by the mixture's increasing viscosity, which ultimately led to a merely oscillating or stalled stirring bar.

Workup:

"Classic" DPs: The reaction was quenched by rapid cooling with liquid nitrogen and addition of a small amount of CH_2Cl_2 to dilute the mixture. Purification by column filtration through a short pad of silica gel using CH_2Cl_2 as the eluent, followed by freeze-drying of the oily residue from 1,4-dioxane (20 ml) afforded the respective first-generation "classic" DP **PG1** as a colorless foam.

UPy-functionalized DPs: The reaction was quenched by rapid cooling with liquid nitrogen and addition of DMF (≈ 5 ml) to dilute the mixture. The polymer was obtained by repeated precipitation into cold MeOH. After decanting the supernatant, freeze-drying of the gummy residue from a mixture of 1,4-dioxane and water (v/v = 10/1) afforded **PG1-UPy$_{\mathbf{long}}$** as a colorless foam.

5.3.2 General procedure B for RAFT polymerization

General procedure B: The required amounts of macromonomers **1c** and **4c** were placed in a Schlenk tube equipped with a magnetic stir bar under a N_2 atmosphere, followed by addition of azo*bis*(isobutyronitrile) (AIBN, 0.01 – 0.5M in DMF) and cumyl dithiobenzoate (CDB, 0.01 – 0.5M in DMF). Unless noted otherwise, the reactions were diluted with DMF to arrive at a final concentration of 1.0 g ml^{-1}. After homogenization and thorough degassing by several freeze-pump-thaw cycles, the polymerization mixture was placed in an oil bath that had been preheated to 65 °C, and the reaction was stirred at this temperature under N_2 for a predetermined amount of time. The progress of the polymerization could be macroscopically assessed by both the increasing viscosity and attenuation of the mixture's color.

Workup:

"Classic" DPs: The reaction was quenched by rapid cooling with liquid nitrogen and addition of a small amount of CH_2Cl_2 to dilute the mixture. Purification by column filtration through a short pad of silica gel using CH_2Cl_2 as the eluent and freeze-drying of the oily residue from 1,4-dioxane afforded the respective first-generation "classic" DP **PG1** as a pink foam.

UPy-functionalized DPs: The reaction was quenched by rapid cooling with liquid nitrogen and addition of DMF to dissolve the mixture. The polymer was obtained by repeated precipitation into cold MeOH. After decanting the supernatant, freeze-drying of the gummy residue from a mixture of 1,4-dioxane and water (v/v = 10/1) afforded **PG1-UPy** as a pink foam.

5.3.3 General procedure C for NHBoc deprotection

PG*g* **de**PG***g***

General procedure C: TFA (20 equiv per amine) was slowly added to the polymer **PG*g*** and methanol (5 droplets, for better solubility) at −10 °C. The resulting suspension was allowed to warm to room temperature overnight, whereupon the reaction gradually became a solution. Excess TFA was removed from the resulting solution by repeated addition of methanol and evaporation to dryness. Addition of methanol and evaporation of the volatiles was repeated 5 times. The solid residue was taken up in water and freeze-dried to yield polymer ***de*PG*g*** as a beige foam.

5.3.4 General procedure D for amide bond formation (dendronization)

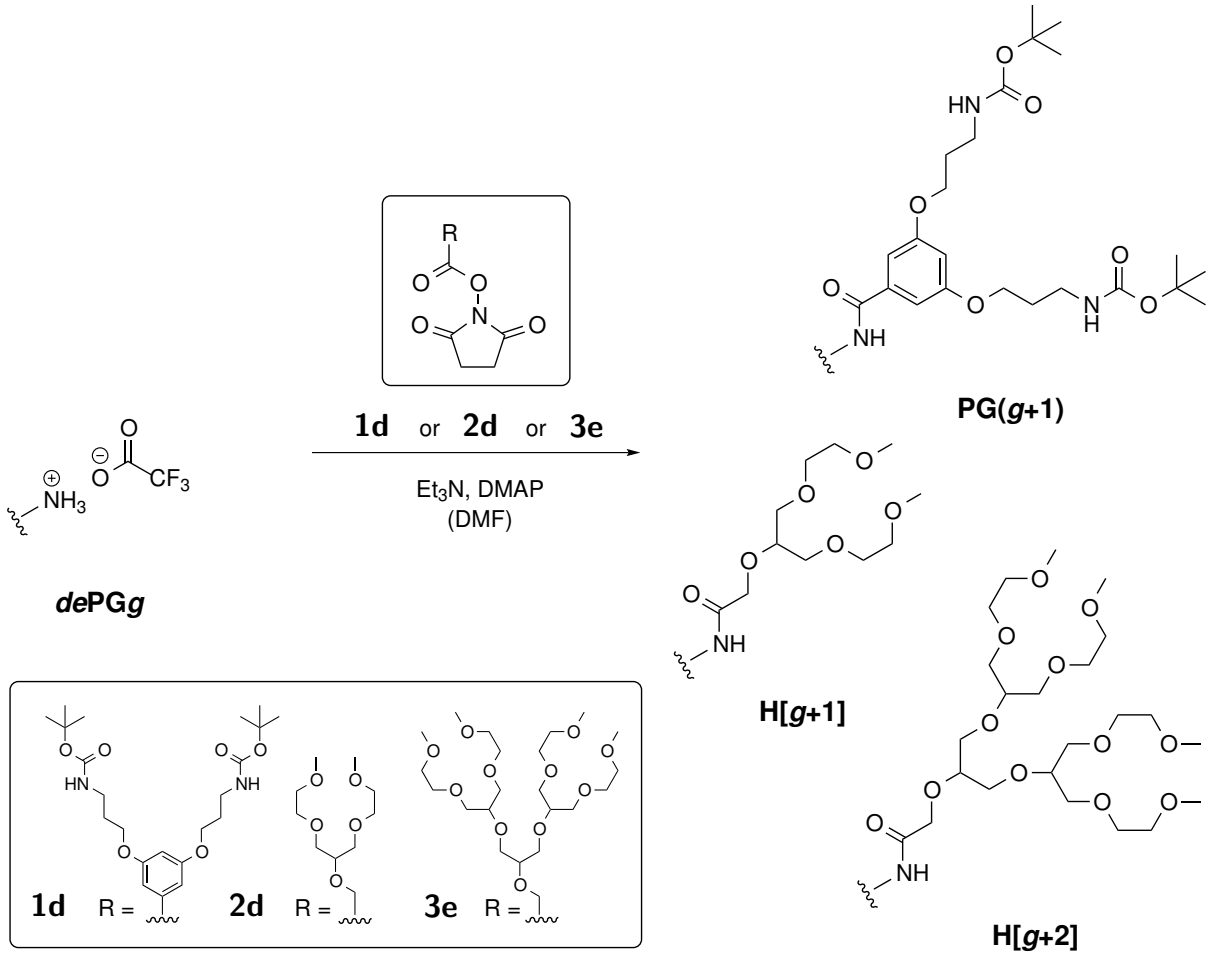

General procedure D: Deprotected polymer *de*PG*g* (1.0 equiv), DMAP (0.3 equiv per amine), and Et_3N (2.0 equiv per amine) were dissolved in DMF (and DMSO) ($c_{polymer} \approx 0.5\,mmol\,ml^{-1}$). The mixture was cooled to −10 °C using an ice/salt cooling bath. Succinimidyl ester ("classic" DPs: **1d**; "hybrid" **H[1+1]**: **2d**; "hybrid" **H[1+2]**: **3e**) (3.0 equiv per amine) was added in the cold and the mixture was subsequently allowed to reach room temperature. Two further additions of the respective activated ester (1.0 equiv per amine each) were performed over the course of 5 d. The mixture was stirred for a predetermined amount of time before the polymer was precipitated from $CHCl_3$ into cold Et_2O thrice. The precipitate was re-dissolved in CH_2Cl_2 and precipitated into ice-cooled Et_2O twice. The precipitate was subjected to column filtration through a short pad of silica gel using CH_2Cl_2 as the eluent. After evaporation of the solvent, freeze-drying of the residue from 1,4-dioxane gave **PG(*g*+1)** as a colorless foam or "hybrid" **H[*g*+1]** / **H[*g*+2]** as a sticky solids, respectively.

5.3.5 General procedure E for Sanger labeling

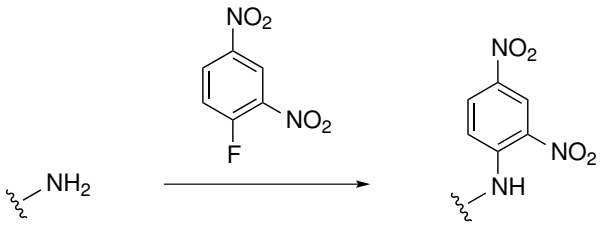

PG*g* **PG*g*-labeled**

Sample preparation

The UV-labeled polymers were prepared according to a previously reported procedure:[42] **PG*g+1*** was dissolved in 1,1,2,2-tetrachloroethane to give a concentration of ≈0.02 M. 0.1 M aqueous $NaHCO_3$ solution (0.7 equiv per amine) and Sanger's reagent (0.2 equiv per amine) dissolved in 1,1,2,2-tetrachloroethane were added and the reaction mixture was heated to 65 °C for 3 h with stirring. After cooling to room temperature, the reaction mixture was diluted with CH_2Cl_2 and successively washed with saturated aqueous Na_2CO_3 solution, water, and brine. After concentration of the organic layer *in vacuo*, the residue was dissolved in a minimum amount of CH_2Cl_2 and precipitated into ice cold Et_2O. Precipitation from CH_2Cl_2 into Et_2O was repeated twice. After freeze-drying from 1,4-dioxane, 2,4-dinitroaniline-labeled **PG(*g*+1)** was obtained as a slightly yellow foam.

Quantification of the dendronization reaction (coverage)

The labeled polymer was dissolved in 1,1,2,2-tetrachloroethane to give a concentrations of $\approx 2.641 \cdot 10^{-4}$M. The extinction coefficient of 2,4-dinitroaniline moiety ($\epsilon_{357\,nm} = 1.64 \cdot 10^4\,\mathrm{L\,mol^{-1}\,cm^{-1}}$) was taken from a previous report.[42] On the assumption that all the unreacted amino groups after the dendronization reaction were labeled by treatment with Sanger's reagent, the concentration of the dinitroanilino moieties, which is also considered as the concentration of unconverted terminal amino groups, was calculated according to the Lambert-Beer law (Equation 5-1):

$$c = \frac{A}{\epsilon \cdot l} \tag{5-1}$$

In Equation 5-1, l denotes the path length of the used UV cuvettes (1.0 cm) and A denotes the absorbance at 357 nm. Therefrom, the degree of structure perfection (X) for the conversion from ***de*PG*g*** to **PG*g+1*** was calculated according to Equation 5-2:

$$X = 1 - \frac{c}{c_0} \cdot 100\% \quad (5\text{-}2)$$

In Equation 5-2, c denotes the spectrophotometrically determined concentration of 2,4-dinitroanilino moieties in **PG*g+1*** and c_0 denotes the concentration of total termini in the starting material ***de*PG*g*** which, e.g., for **PG3** is 2 times the molar concentration of ***de*PG2**.

The recorded UV-Vis spectra are provided in Figures 8-28, 8-29, and 8-30 in Section 8.5 of the Appendix. Table 5-1 contains a numeric summary of the input values used to calculate the degrees of structure perfection.

Table 5-1: Numeric summary of the input values used in the calculations of DP structure perfection.

Entry	Polymer	c,[a] mol L^{-1}	c_0, mol L^{-1}	A,[b] a.u.	X,[c] %
1	PG2-2000	$5.9756 \cdot 10^{-7}$	$4.3276 \cdot 10^{-4}$	0.00980	99.8
2	PG2-3000	$3.8292 \cdot 10^{-7}$	$6.6002 \cdot 10^{-4}$	0.00628	99.9
3	PG3-2000	$5.8159 \cdot 10^{-6}$	$8.6559 \cdot 10^{-4}$	0.09538	99.3
4	PG3-3000	$6.4256 \cdot 10^{-7}$	$9.1426 \cdot 10^{-4}$	0.01053	99.9
5	H[1+2]-50	$2.8191 \cdot 10^{-6}$	$3.1571 \cdot 10^{-4}$	0.04623	99.1
6	H[1+2]1000	$8.4817 \cdot 10^{-6}$	$8.4450 \cdot 10^{-4}$	0.13910	99.0
7	PG2-UPy0	$5.4646 \cdot 10^{-6}$	$2.7404 \cdot 10^{-3}$	0.08962	99.8
8	PG2-UPy5	$3.3513 \cdot 10^{-6}$	$1.6453 \cdot 10^{-3}$	0.05496	99.8
9	PG2-UPy25	$1.2762 \cdot 10^{-6}$	$3.9615 \cdot 10^{-4}$	0.02093	99.7
10	PG2-UPy50	$5.1763 \cdot 10^{-6}$	$5.8363 \cdot 10^{-4}$	0.08489	99.1
11	PG3-UPy0	$2.4311 \cdot 10^{-6}$	$1.4701 \cdot 10^{-3}$	0.03987	99.8
12	PG3-UPy5	$8.3353 \cdot 10^{-7}$	$7.2595 \cdot 10^{-4}$	0.01367	99.9
13	PG3-UPy25	$6.2690 \cdot 10^{-6}$	$8.2672 \cdot 10^{-4}$	0.10281	99.2
14	PG3-UPy50	$6.7270 \cdot 10^{-6}$	$7.3968 \cdot 10^{-6}$	0.11032	99.1

[a] Calculated according to Equation 5-1; [b] Absorbance value taken at a wavelength of 357 nm; [c] Calculated according to Equation 5-2.

5.3.6 Compounds of Section 3.1 ("classic" DPs)

Synthesis of compound 1b

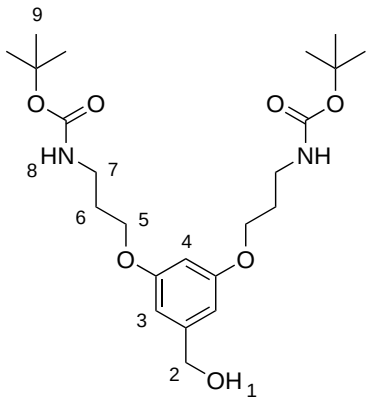

1b

Methyl ester **1a** (1.00 equiv, 30.0 g, 62.3 mmol) was dissolved in THF (400 ml) and the mixture was cooled to −20 °C. A 2.4 M solution of $LiAlH_4$ in THF (2.05 equiv, 53.0 ml, 127 mmol) was diluted with THF (120 ml) and added dropwise over 4 h, after which TLC (EtOAc/hexane 1:2) confirmed the consumption of the starting material. The reaction was quenched by the sequential addition of water (4.82 ml), 15% aqueous NaOH solution (4.82 ml) and water (14.5 ml), followed by continued stirring at room temperature overnight. After filtration, CH_2Cl_2 (300 ml) was added and the solution was washed once with saturated aqueous $NaHCO_3$ solution (100 ml) and once with saturated aqueous NaCl solution (100 ml). After evaporation of the solvents, the oily residue was dissolved in a minimum amount of EtOAc and precipitated into hexane. The precipitate was collected by filtration and dried *in vacuo* to yield the title compound **1b** (25.7 g, 86%) as a colorless solid.

R_f (hexane/EtOAc 1:1) = 0.30

^{1}H NMR (300 MHz, $CDCl_3$) δ = 6.51 (d, J = 2.1 Hz, 2H, H-3), 6.35 (t, J = 2.1 Hz, 1H, H-4), 4.77 (s, 2H, H-8), 4.61 (s, 2H, H-2), 3.99 (t, J = 6.0 Hz, 4H, H-5), 3.30 (q, J = 5.9 Hz, 4H, H-7), 2.05 – 1.85 (m, 5H, H-1, H-6), 1.43 (s, 18H, H-9)

^{13}C NMR (76 MHz, $CDCl_3$) δ = 160.1, 156.0, 143.5, 105.3, 100.6, 79.2, 65.8, 65.2, 38.0, 29.5, 28.4.

MS (MALDI-FTICR, 3-HPA Matrix): calcd for $C_{23}H_{38}N_2NaO_7$ ($[M+Na]^+$) 477.2577; found 477.2571

Synthesis of compound 1c

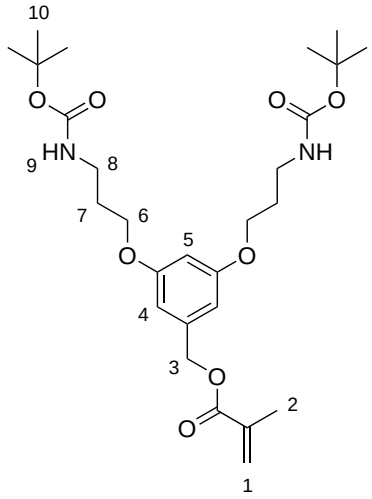

1c

Benzyl alcohol **1b** (1.00 equiv, 24.0 g, 52.9 mmol) was added to CH_2Cl_2 (270 ml), Et_3N (3.01 equiv, 22.2 ml, 159 mmol) and DMAP (0.03 equiv, 219 mg, 1.79 mmol). After cooling of the mixture to −10 °C, a solution of MAC (1.50 equiv, 7.63 ml, 79.4 mmol) in CH_2Cl_2 (50 ml) was added dropwise. After stirring for 2.5 h in cold, the reaction was quenched and washed with saturated aqueous $NaHCO_3$ solution (2 × 200 ml) and saturated aqueous NaCl solution (100 ml).The organic layer was dried over $MgSO_4$, filtered and the solvent was removed *in vacuo*. Purification of the thus obtained, yellowish oil by column chromatography (gradient hexane/EtOAc 3:1 to 1:1) yielded the title compound **1c** (26.0 g, 94%) as a white solid.

R_f (hexane/EtOAc 2:1) = 0.42

^{1}H NMR (300 MHz, $CDCl_3$) δ = 6.50 (d, J = 2.2 Hz, 2H, H-4), 6.39 (t, J = 2.2 Hz, 1H, H-5), 6.16 (dq, J = 1.8, 1.0 Hz, 1H, H-1), 5.59 (dq, J = 1.8, 1.0 Hz, 1H, H-1), 5.10 (s, 2H, H-3), 4.74 (s, 2H, H-9), 3.99 (t, J = 6.0 Hz, 4H, H-6), 3.31 (q, J = 6.2 Hz, 4H, H-8), 2.03- 1.89 (m, 7H, H-7), 1.44 (s, 18H, H-10)

^{13}C NMR (76 MHz, $CDCl_3$) δ = 167.1, 160.0, 156.0, 138.4, 136.1, 125.9, 106.4, 100.9, 79.2, 66.2, 65.8, 37.9, 29.5, 28.4, 18.3

MS (ESI-FTICR): calcd for $C_{27}H_{43}N_2O_8$ ($[M+H]^+$) 523.3014; found 523.3015

Elemental analysis calcd (%) for $C_{27}H_{42}N_2O_8$: C 62.05, H 8.10, N 5.36, O 24.49; found: C 61.92, H 8.17, N 5.24, O 24.37

Synthesis of first-generation "classic" dendronized polymers (PG1)

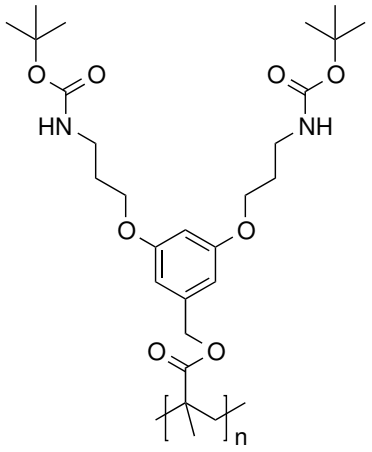

PG1

Synthesis of **PG1-50**: *Following general procedure B*, **1c** (3.01 g, 5.76 mmol), AIBN (0.1M in DMF, 1.15 ml), and CDB (0.1M in DMF, 1.15 ml) were dissolved in DMF (0.90 ml) and polymerized for 23 h. The final product (2.10 g, 70%) was obtained as a fluffy, pink foam.

Synthesis of **PG1-300**: *Following general procedure B*, **1c** (3.01 g, 5.77 mmol), AIBN (0.02M in DMF, 1.15 ml), and CDB (0.02M in DMF, 1.15 ml) were dissolved in DMF (0.70 ml) and polymerized for 18 h. The final product (2.02 g, 67%) was obtained as a fluffy, pink foam.

Synthesis of **PG1-1000**: *Following general procedure A*, **1c** (2.00 g, 3.83 mmol) and AIBN (0.1M in DMF, 76.5 μl) were dissolved in DMF (1.92 ml) and polymerized for 13 h. The final product (1.61 g, 81%) was obtained as a fluffy, colorless foam.

Synthesis of **PG1-1500**: *Following general procedure A*, **1c** (2.00 g, 3.83 mmol) and AIBN (0.1M in DMF, 76.5 μl) were dissolved in DMF (1.92 ml) and polymerized for 14 h. The final product (1.24 g, 62%) was obtained as a fluffy, colorless foam.

Synthesis of **PG1-2000**: *Following general procedure A*, **1c** (2.00 g, 3.83 mmol) and AIBN (0.1M in DMF, 76.5 μl) were dissolved in DMF (1.92 ml) and polymerized for 16 h. The final product (1.39 g, 73%) was obtained as a fluffy, colorless foam.

Synthesis of **PG1-3000**: *Following general procedure A*, **1c** (2.00 g, 3.83 mmol) and AIBN (0.1M in DMF, 38.3 μl) were dissolved in DMF (1.96 ml) and polymerized for 14 h. The final product (1.36 g, 68%) was obtained as a fluffy, colorless foam.

Synthesis of second-generation "classic" dendronized polymers (PG2)

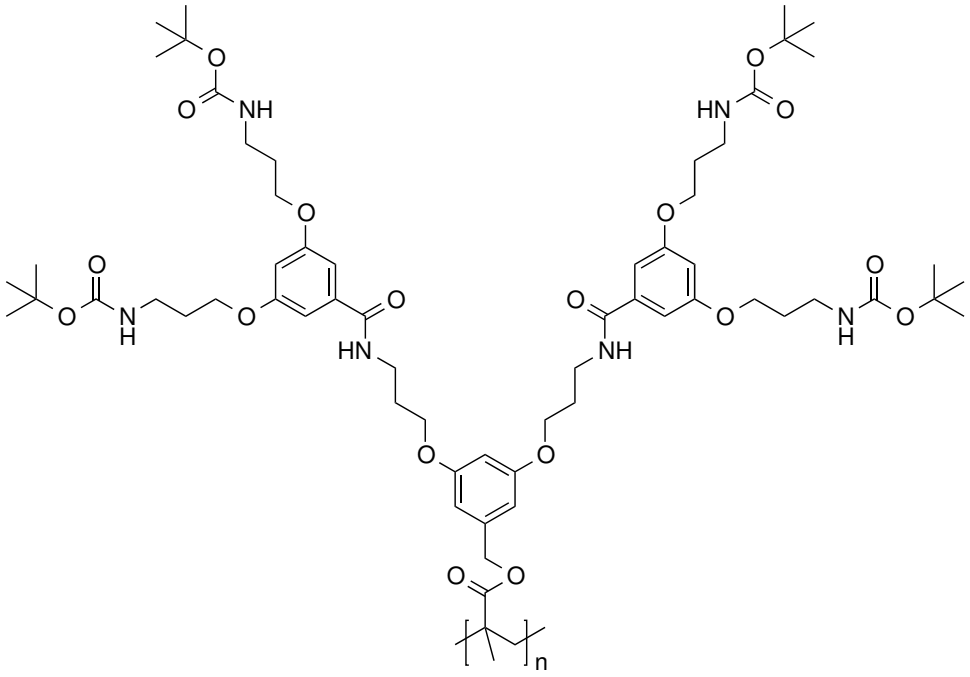

PG2

Synthesis of **PG2-50**: *Following general procedure C*, **PG1-50** (0.63 g, 1.13 mmol) was mixed with TFA (6.50 ml). *Following general procedure D*, ***de*PG1-50** (0.66 g, 1.12 mmol), DMAP (80 mg) and Et_3N (0.63 ml) were dissolved in DMF (12.2 ml), followed by batch-wise addition of **1d** (6.40 g, 11.3 mmol). After 16 d, the final product (0.99 g, 72%) was obtained as a colorless foam.

Synthesis of **PG2-300**: *Following general procedure C*, **PG1-300** (0.49 g, 0.93 mmol) was mixed with TFA (5.00 ml). *Following general procedure D*, ***de*PG1-300** (0.51 g, 0.93 mmol), DMAP (68 mg) and Et_3N (1.04 ml) were dissolved in DMF (9.70 ml), followed by batch-wise addition of **1d** (5.26 g, 9.31 mmol). After 7 d, the final product (0.80 g, 71%) was obtained as a colorless foam.

Synthesis of **PG2-1000**: *Following general procedure C*, **PG1-1000** (0.44 g, 0.84 mmol) was mixed with TFA (4.50 ml). *Following general procedure D*, ***de*PG1-1000** (0.50 g, 0.90 mmol), DMAP (61 mg) and Et_3N (0.70 ml) were dissolved in DMF (8.50 ml), followed by batch-wise addition of **1d** (4.74 g, 8.38 mmol). After 10 d, the final product (0.80 g, 79%) was obtained as a colorless foam.

Synthesis of **PG2-1500**: *Following general procedure C*, **PG1-1500** (0.51 g, 0.99 mmol) was mixed with TFA (4.00 ml). *Following general procedure D*, ***de*PG1-1500** (0.54 g, 0.99 mmol), DMAP (73 mg) and Et_3N (0.55 ml) were dissolved in DMF (12.4 ml), followed by batch-wise addition of **1d** (5.60 g, 9.90 mmol). After 7 d, the final product (0.93 g, 76%) was obtained as a colorless foam.

Synthesis of **PG2-2000**: *Following general procedure C*, **PG1-2000** (0.53 g, 1.00 mmol) was mixed with TFA (5.40 ml). *Following general procedure D*, ***de*PG1-2000** (0.60 g, 1.00 mmol), DMAP (74 mg) and Et_3N (0.56 ml) were dissolved in DMF (12.5 ml), followed by batch-wise addition of **1d** (5.68 g, 10.0 mmol). After 8 d, the final product (0.78 g, 64%) was obtained as a colorless foam.

Synthesis of **PG2-3000**: *Following general procedure C*, **PG1-3000** (0.48 g, 0.92 mmol) was mixed with TFA (5.70 ml). *Following general procedure D*, ***de*PG1-3000** (0.51 g, 0.93 mmol), DMAP (68 mg) and Et_3N (0.52 ml) were dissolved in DMF (11.0 ml), followed by batch-wise addition of **1d** (5.25 g, 9.28 mmol). After 9 d, the final product (0.93 g, 82%) was obtained as a colorless foam.

Synthesis of third-generation "classic" dendronized polymers (PG3)

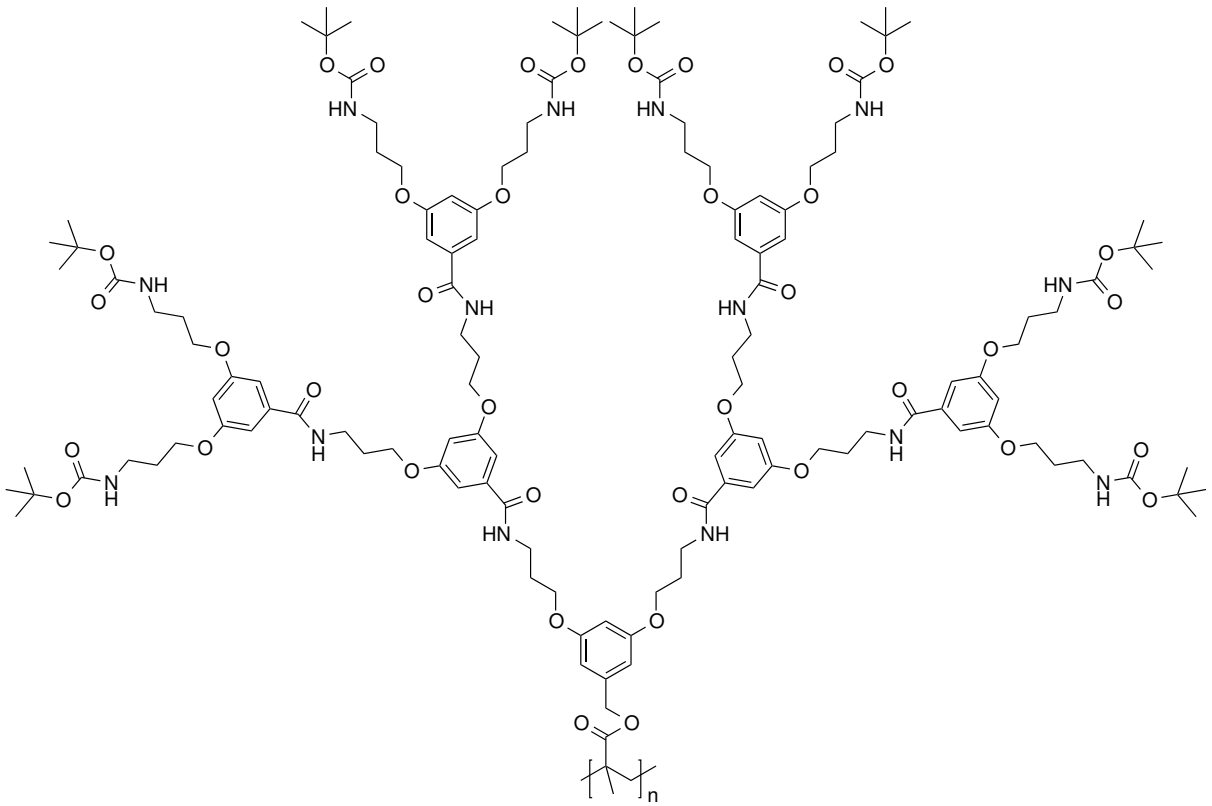

PG3

Synthesis of **PG3-50**: *Following general procedure C*, **PG2-50** (0.31 g, 0.26 mmol) was mixed with TFA (6.60 ml). *Following general procedure D*, ***de*PG2-50** (0.27 g, 0.21 mmol), DMAP (38 mg) and Et_3N (0.29 ml) were dissolved in DMF (6.20 ml), followed by batch-wise addition of **1d** (2.93 g, 5.18 mmol). After 8 d, the final product (0.55 g, 81%) was obtained as a colorless foam.

Synthesis of **PG3-300**: *Following general procedure C*, **PG2-300** (0.26 g, 0.21 mmol) was mixed with TFA (6.00 ml). *Following general procedure D*, ***de*PG2-300** (0.28 g, 0.51 mmol), DMAP (40 mg) and Et_3N (0.56 ml) were dissolved in DMF (7.00 ml), followed by batch-wise addition of **1d** (5.62 g, 9.94 mmol). After 16 d, the final product (0.35 g, 63%) was obtained as a colorless foam.

Synthesis of **PG3-1000**: *Following general procedure C*, **PG2-1000** (0.25 g, 0.20 mmol) was mixed with TFA (5.60 ml). *Following general procedure D*, ***de*PG2-1000** (0.27 g, 0.21 mmol), DMAP (63 mg) and Et_3N (0.24 ml) were dissolved in DMF (4.20 ml), followed by batch-wise addition of **1d** (2.36 g, 4.18 mmol). After 47 d, the final product (0.23 g, 45%) was obtained as a colorless foam.

Synthesis of **PG3-1500**: *Following general procedure C*, **PG2-1500** (0.25 g, 0.20 mmol) was mixed with TFA (5.60 ml). *Following general procedure D*, ***de*PG2-1500** (0.25 g, 0.19 mmol), DMAP (30 mg) and Et_3N (0.23 ml) were dissolved in DMF (4.30 ml), followed by batch-wise addition of **1d** (2.35 g, 4.16 mmol). After 20 d, the final product (0.35 g, 64%) was obtained as a colorless foam.

Synthesis of **PG3-2000**: *Following general procedure C*, **PG2-2000** (0.22 g, 0.18 mmol) was mixed with TFA (5.00 ml). *Following general procedure D*, ***de*PG2-2000** (0.23 g, 0.18 mmol), DMAP (27 mg) and Et_3N (0.21 ml) were dissolved in DMF (3.70 ml), followed by batch-wise addition of **1d** (2.07 g, 3.67 mmol). After 48 d, the final product (0.31 g, 65%) was obtained as a colorless foam.

Synthesis of **PG3-3000**: *Following general procedure C*, **PG2-3000** (0.22 g, 0.18 mmol) was mixed with TFA (5.00 ml). *Following general procedure D*, ***de*PG2-3000** (0.22 g, 0.18 mmol), DMAP (27 mg) and Et_3N (0.20 ml) were dissolved in DMF (6.00 ml), followed by batch-wise addition of **1d** (2.06 g, 3.65 mmol). After 22 d, the final product (0.35 g, 73%) was obtained as a colorless foam.

5.3.7 Compounds of Section 3.2 ("hybrid" DPs)

Synthesis of compound 2a

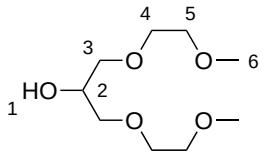

2a

Epichlorohydrine (79 ml, 1.0 mol) and 2-methoxyethanol (315 ml, 4.0 mol) were mixed in a 3-necked flask equipped with a stirrer, a dropping funnel and a reflux condenser and the mixture was warmed to 50 °C. 50% aqueous NaOH solution (31 ml, 1.0 mol) was added dropwise to the stirred reaction mixture over 90 min, followed by stirring at 80 °C overnight. After cooling to room temperature, the reaction mixture was filtered, neutralized with concentrated aqueous HCl, extracted with CH_2Cl_2 (5×150 ml) and the volatiles were removed using a rotary evaporator (60 °C, 4 mbar). The residue was purified by vacuum distillation using a suitable Vigreux column ($l \approx 30$ cm). The title compound **2a** (128 g, 61%) was collected at 118 °C and a pressure of $1.4 \cdot 10^{-1}$ mbar as a colorless oil.

R_f (hexane/EtOAc 1:1, 10% MeOH) = 0.31

^{1}H NMR (300 MHz, $CDCl_3$) δ = 3.99 (m, 1H, H-2), 3.66 – 3.63 (m, 4H, H-3), 3.59 – 3.46 (m, 8H, H-4, H-5), 3.36 (s, 6H, H-6), 2.86 (s, 1H, H-1)

^{13}C NMR (76 MHz, $CDCl_3$) δ = 72.5, 71.9, 70.7, 69.4, 59.0

MS (MALDI-TOF, 3-HPA): m/z $[M+Na]^+$ calcd for $C_9H_{20}O_5Na$: 231.1203, found: 231.1203

Elemental analysis calcd (%) for $C_9H_{20}O_5$: C 51.91, H 9.68, O 38.41, found: C 51.04, H 9.93, O 39.15

Synthesis of compound 2b

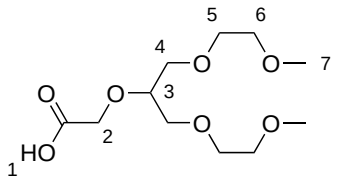

2b

A solution of **2a** (1.0 equiv, 20.0 g, 96.0 mmol) and KI (5 mol%) in dry THF (90 ml) was cooled to 0 °C under N_2 atmosphere before NaH (5.0 equiv, 19.2 g, 480 mmol) was added to the flask in portions. After stirring for 30 min, the cooling bath was removed and the mixture was allowed to warm to room temperature. After the evolution of gas had ceased, a solution of *mono*-bromoacetic acid (1.5 equiv, 20.0 g, 144 mmol) in dry THF (20 ml) was added dropwise. The reaction was stirred at room temperature for 4 h followed by stirring under reflux overnight. After cooling to 0 °C, residual NaH was quenched by addition of H_2O (100 ml). The thus obtained orange solution was washed with Et_2O (2×100 ml) to remove the mineral oil, acidified with conc. aqueous HCl (pH = 1) and extracted with CH_2Cl_2 (3×100 ml). To remove excess *mono*-bromoacetic acid, the combined organic layers were washed with H_2O (100 ml) and saturated aqueous NaCl solution. Drying over $MgSO_4$, filtration and evaporation of the solvent gave the title compound **2b** (22.2 g, 87%) as a light brown oil.

^{1}H NMR (300 MHz, $CDCl_3$) δ = 10.17 (s, 1H, H-1), 4.18 (s, 2H, H-2), 3.74 — 3.60 (m, 1H, H-3), 3.60 -– 3.38 (m, 12H, H-4, H-5, H-6), 3.27 (s, 6H, H-7)

^{13}C NMR (76 MHz, $CDCl_3$) δ = 172.2, 80.1, 71.6, 71.1, 70.9, 68.7, 58.9

MS (MALDI-TOF, 3-HPA): m/z $[M+Na]^+$ calcd for $C_{11}H_{22}NaO_7$: 289.1258, found: 289.1257

Synthesis of compound 2c

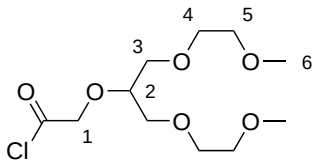

2c

Thionyl chloride (2.5 equiv, 14.3 ml, 196 mmol) was added to a solution of **2b** (1.0 equiv, 20.9 g, 78.4 mmol) in dry CH_2Cl_2 (50 ml) and DMF (0.1 equiv, 0.61 ml, 7.84 mmol) at room temperature under N_2. After stirring the solution overnight, the volatiles were removed *in vacuo* at the Schlenk line. Acyl chloride **2c** was obtained by vacuum distillation at 142 °C under an absolute pressure of $6.0 \cdot 10^{-1}$ mbar as a light yellow liquid (16.1 g, 72%).

^{1}H NMR (300 MHz, $CDCl_3$) δ = 4.63 (s, 2H, H-1), 3.88 -- 3.77 (m, 1H, H-2), 3.61 — 3.43 (m, 12H, H-3, H-4, H-5), 3.32 (s, 6H, H-6)

^{13}C NMR (76 MHz, $CDCl_3$) δ = 172.2, 79.2, 76.1, 71.9, 71.6, 70.6, 58.9

Synthesis of compound 2d

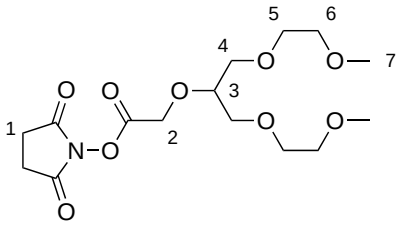

2d

Et_3N (1.0 equiv, 7.9 ml, 56.5 mmol) and N-hydroxysuccinimide (1.0 equiv, 6.5 g, 56.5 mmol) were dissolved in dry CH_2Cl_2 (60 ml) under N_2 and the colorless solution was cooled to −10 °C in an ice/salt cooling bath. Freshly distilled acyl chloride **2c** (1.0 equiv, 16.1 g, 56.5 mmol) was diluted with dry CH_2Cl_2 (10 ml) and added dropwise to the cooled solution. After stirring for 12 h, dry Et_2O (70 ml) was added and the reaction was filtered with a Schlenk-frit. The solvents were removed *in vacuo* and the oily residue was taken up in CH_2Cl_2 and washed once with saturated aqueous $NaHCO_3$ (70 ml) and H_2O (70 ml). The organic layer was then dried over $MgSO_4$, filtered and the volatiles were removed *in vacuo* to yield the title compound **2d** (18.3 g, 89%) as a pale yellow oil.

^{1}H NMR (300 MHz, $CDCl_3$) δ = 4.62 (s, 2H, H-2), 3.81 (m, 1H, H-3), 3.64—3.37 (m, 12H, H-4, H-5, H-6), 3.30 (s, 6H, H-7), 2.77 (s, 4H, H-1)

^{13}C NMR (76 MHz, $CDCl_3$) δ = 168.7, 166.3, 79.0, 71.6, 70.6, 65.9, 58.8, 25.4

MS (ESI-FTICR, Na-PFHA Calibration): m/z $[M+H]^+$ calcd for $C_{15}H_{26}O_9$ 364.1602; found 364.1601

Synthesis of compound 2f

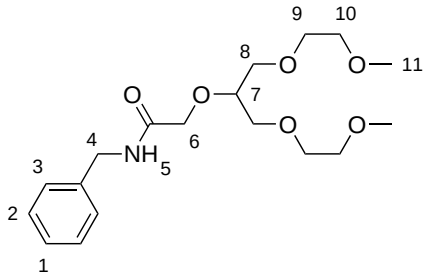

2f

Compound **2d** (1.0 equiv, 341 mg, 937 μmol) and Et_3N (1.0 equiv, 130 μl, 937 μmol) were dissolved in 1,4-dioxane (4.87 ml). To the resulting colorless solution, benzylamine **7** (2.0 equiv, 205 μl, 1.88 mmol) was quickly added under vigorous stirring at room temperature. After completion of the addition, the reaction immediately formed a white precipitate, whereupon the reaction solidified and the mixture was left to stand for 5 min. H_2O (5 ml) was added to dissolve the precipitate, followed by extraction of the solution with CH_2Cl_2 (3×20 ml). The combined organic layers were washed successively with 1M NaOH (50 ml) and 1M HCl (50 ml) aqueous solutions, dried over $MgSO_4$, filtered and concentrated *in vacuo* to yield the title compound **2f** (330 mg, 99%) as a yellowish oil.

R_f (hexane/EtOAc 1:1, 5% MeOH) = 0.46

^{1}H NMR (300 MHz, DMSO-d6) δ = 8.24 (t, J = 6.1 Hz, 1H, H-5), 7.36-–7.19 (m, 5H, H-1, H-2, H-3), 4.34 (d, J = 6.2 Hz, 2H, H-4), 4.07 (s, 2H, H-6), 3.68-–3.60 (m, 1H, H-7), 3.57-–3.43 (m, 8H, H-8, H-9), 3.41-–3.35 (m, 4H, H-10), 3.19 (s, 6H, H-11)

^{13}C NMR (76 MHz, DMSO-d6) δ = 170.2, 139.8, 128.7, 127.5, 127.2, 79.0, 71.6, 70.9, 70.4, 69.3, 58.5, 42.1

MS (MALDI-FTICR, 3-HPA Matrix): m/z $[M+Na]^+$ calcd for $C_{18}H_{29}NNaO_6$: 378.1887; found 378.1887

Synthesis of compound 3a

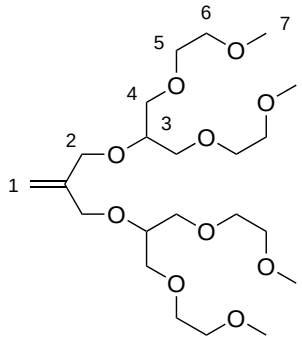

3a

NaH (12.7 g, 317 mmol), KI (1.8 g, 10.6 mmol) and 3-chloro-2-chloromethyl-1-propene (MDC), 12.2 ml, 106 mmol) were suspended in THF (150 ml) and the mixture was cooled to −10 °C. Alcohol **2a** (110 g, 528 mmol) was dissolved in THF (150 ml) and added dropwise in the cold over the course of 1 h. The mixture was slowly warmed to room temperature and then stirred at 65 °C for 4 d. After cooling to room temperature, the reaction was quenched with H_2O (300 ml) and extracted with CH_2Cl_2 (3×300 ml). The combined organic layers were dried over $MgSO_4$, filtered and concentrated *in vacuo*. Excess alcohol **2a** was distilled off (35.8 g, 172 mmol, 54% recovered). The residue was purified by column chromatography on silica gel (gradient hexane/EtOAc 3:1, 5% MeOH to 1:1, 5% MeOH) to yield the title compound **3a** (33.1 g, 67%) as a pale yellow oil.

R_f (hexane/EtOAc 2:1, 5% MeOH) = 0.49

^{1}H NMR (300 MHz, $CDCl_3$) δ = 5.17 (s, 2H, H-1), 4.14 (s, 4H, H-2), 3.69 – 3.50 (m, 26H, H-3, H-4, H-5, H-6), 3.36 (s, 12H, H-7)

^{13}C NMR (76 MHz, $CDCl_3$) δ = 143.3, 113.9, 77.1, 71.9, 71.2, 70.8, 59.0

MS (ESI-FTICR, Na-PFHA Calibration): m/z $[M+NH_4]^+$ calcd for $C_{22}H_{48}NO_{10}$: 486.3273, found: 486.3271

Synthesis of compound 3b

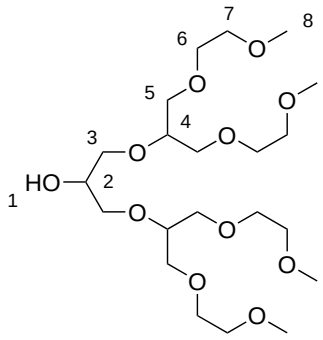

3b

Unsaturated compound **3a** (1.0 equiv, 25.6 g, 54.6 mmol) was dissolved in a solvent mixture of dry CH_2Cl_2 (280 ml) and dry MeOH (40 ml) and cooled to −78 °C. O_3 was bubbled through the solution with good stirring until the appearance of a light blue color. Ozonolysis was stopped and excess O_3 was removed from the reaction by purging with N_2 until the solution turned colorless. $NaBH_4$ (1.5 equiv, 3.11 g, 81.9 mmol) was added at −78 °C and the mixture was then allowed to slowly warm to room temperature with stirring overnight. After quenching with saturated aqueous NH_4Cl solution (8 ml) and extraction with CH_2Cl_2 (4×150 ml), the combined organic layers were dried over $MgSO_4$, filtered and concentrated *in vacuo*. Column chromatography on silica gel gave the title compound **3b** (25.8 g, 99%) as a colorless oil.

R_f (hexane/EtOAc 1:1, 10% MeOH) = 0.32

^{1}H NMR (300 MHz, $CDCl_3$) δ = 3.92 – 3.83 (m, 1H, H-1), 3.70 – 3.45 (m, 31H, H-2, H-3, H-4, H-5, H-6, H-7), 3.33 (s, 12H, H-8)

^{13}C NMR (76 MHz, $CDCl_3$) δ = 78.6, 72.0, 71.8, 71.8, 71.4, 71.3, 70.7, 70.6, 69.6, 58.9

MS (ESI-FTICR, Na-PFHA Calibration): m/z $[M+H]^+$ calcd for $C_{21}H_{45}O_{11}$: 473.2956, found 473.2956

Synthesis of compound 3c

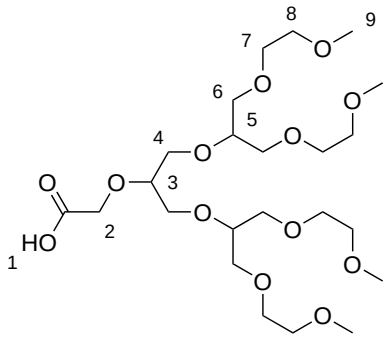

3c

A solution of **3b** (1.0 equiv, 30.0 g, 63.4 mmol) and KI (5 mol%, 0.79 g, 4.76 mmol) in dry THF (120 ml) was cooled to 0 °C under N_2 before NaH (5.0 equiv, 12.7 g, 317 mmol) was added to the flask in portions. After stirring for 60 min, the cooling bath was removed and the mixture was allowed to warm to room temperature. After the evolution of gas ceased, a solution of *mono*-bromoacetic acid (1.5 equiv, 13.2 g, 95.1 mmol) in dry THF (40 ml) was added dropwise. The reaction was stirred at room temperature for 8 h followed by stirring under reflux overnight. After cooling to 0 °C, residual NaH was quenched by addition of H_2O (100 ml). The thus obtained orange solution was washed with Et_2O (2×100 ml) to remove the mineral oil, acidified with conc. aqueous HCl (pH = 1) and extracted with CH_2Cl_2 (3×100 ml). To remove excess *mono*-bromoacetic acid, the combined organic layers were washed with H_2O (100 ml) and saturated aqueous NaCl solution (100 ml). Drying over $MgSO_4$, filtration and evaporation of the solvent gave the desired product **3c** (31.8 g, 93%) as a light brow oil.

^{1}H NMR (300 MHz, $CDCl_3$) δ = 9.70 (s, 1H, H-1), 4.25 (s, 2H, H-2), 3.75 -– 3.42 (m, 31H, H-3, H-4, H-5, H-6, H-7, H-8), 3.34 (s, 12H, H-9)

^{13}C NMR (76 MHz, $CDCl_3$) δ = 172.4, 80.7, 78.9, 71.8, 71.8, 71.2, 71.1, 70.6, 70.6, 70.5, 68.8, 58.9

MS (ESI-FTICR, Na-PFHA Calibration): m/z $[M+2Na]^+$ calcd for $C_{23}H_{45}Na_2O_{13}$: 575.2650, found: 575.2650

Synthesis of compound 3e

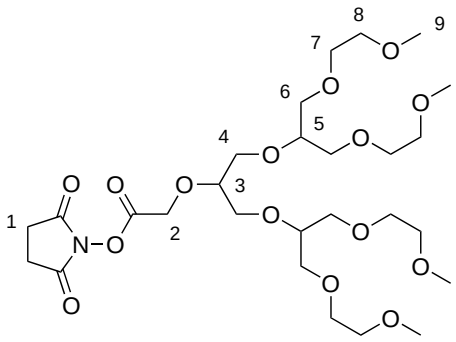

3e

Compound **3c** (1.0 equiv, 33.0 g, 62.2 mmol) and DMF (0.1 equiv, 0.5 ml, 6.2 mmol) were dissolved in CH_2Cl_2 (40 ml). Thionyl chloride (2.5 equiv, 11.4 ml, 155.7 mmol) was added dropwise at room temperature and the reaction was stirred in an atmosphere of N_2 overnight. Evaporation of the volatiles *in vacuo* gave the corresponding acyl chloride **3d**, which was used in the next step without further purification, in quantitative yield.

N-hydroxysuccinimide (1.0 equiv, 6.8 g, 59.3 mmol) and Et_3N (1.0 equiv, 8.6 ml, 62.2 mmol) were dissolved in CH_2Cl_2 and the colorless solution was cooled to −14 °C with an ice/salt cooling bath. The freshly prepared acyl chloride was dissolved in CH_2Cl_2 (10 ml,) and added dropwise to the reaction mixture via a syringe. The syringe was rinsed with CH_2Cl_2 (10 ml) and the reaction was allowed to warm to room temperature in an atmosphere of N_2 overnight. Et_2O (70 ml) was added and stirring was continued for 1 h, before the reaction was filtered with a Schlenk-frit. The solvents were removed *in vacuo* and the oily residue was subsequently taken up in CH_2Cl_2 (100 ml) and washed with saturated aqueous $NaHCO_3$ solution (100 ml) and H_2O (100 ml). The organic layer was dried over $MgSO_4$, filtered and concentrated *in vacuo* to yield the title compound **3e** (32.8 g, 84%) as a brownish oil.

^{1}H NMR (300 MHz, $CDCl_3$) δ = 4.73 (s, 2H, H-2), 3.85 – 3.47 (m, 31H, H-3, H-4, H-5, H-6, H-7, H8) 3.36 (s, 12H, H-9), 2.83 (s, 4H, H-1)

^{13}C NMR (76 MHz, $CDCl_3$) δ = 168.7, 166.5, 79.5, 78.7, 77.4, 77.0, 76.6, 71.8, 71.2, 71.0, 70.7, 65.9, 59.0, 25.5

MS (ESI-FTICR, Na-PFHA Calibration): m/z $[M+Na]^+$ calcd for $C_{27}H_{49}NNaO_{15}$ 650.2994; found 650.2994

Synthesis of compound 3g

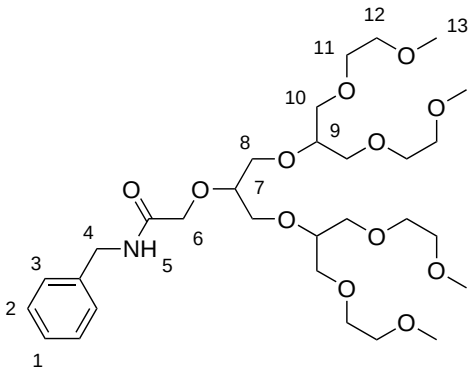

3g

Compound **3e** (1.0 equiv, 353 mg, 562 μmol) and Et_3N (1.0 equiv, 79 μl, 562 μmol) were dissolved in 1,4-dioxane (4.84 ml). To the resulting solution, benzylamine **7** (2.0 equiv, 123 μl, 1.12 mmol) was quickly added under vigorous stirring at room temperature. After completion of the addition, the reaction immediately solidified due to the formation of a white precipitate, whereupon the reaction was left to stand for 5 min. H_2O (5 ml) was added to dissolve the precipitate, followed by extraction of the solution with CH_2Cl_2 (3×20 ml). The combined organic layers were washed successively with 1M NaOH (50 ml) and 1M HCl (50 ml) aqueous solutions, dried over $MgSO_4$, filtered and concentrated *in vacuo* to yield the title compound **3g** (310 mg, 89%) as a brownish oil.

R_f (hexane/EtOAc 1:1, 5% MeOH) = 0.35

^{1}H NMR (300 MHz, DMSO-d6) δ = 8.22 (t, J = 6.3 Hz, 1H, H-5), 7.36 -– 7.19 (m, 5H, H-1, H-2, H-3), 4.35 (d, J = 6.2 Hz, 2H, H-4), 4.07 (s, 2H, H-6), 3.73 -– 3.30 (m, 31H, H-7, H-8, H-9, H-10, H-11, H-12), 3.23 (s, 12H, H-13)

^{13}C NMR (76 MHz, DMSO-d6) δ = 170.3, 139.9, 128.7, 127.5, 127.2, 79.4, 78.4, 71.7, 70.9, 70.7, 70.4, 70.4, 70.0, 69.3, 58.5, 41.9

MS (ESI-FTICR, DCTB Matrix): m/z $[M+Na]^+$ calcd for $C_{30}H_{53}NNaO_{12}$: 642.3460, found: 642.3459

Synthesis of H[1+1] "hybrid" DPs

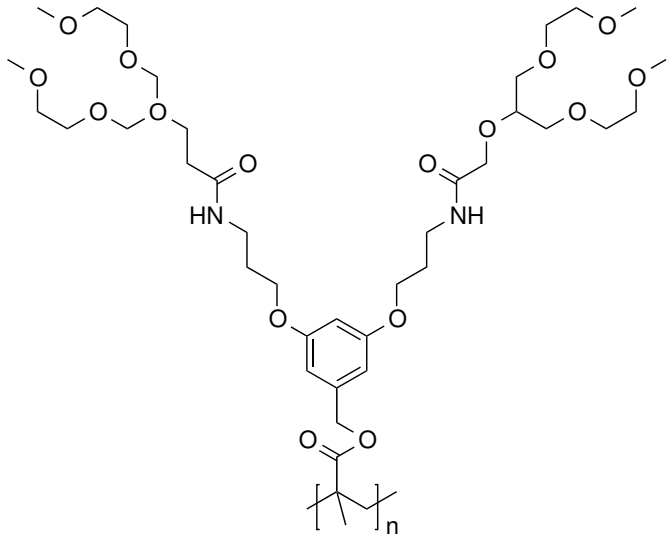

H[1+1]

Synthesis of **H[1+1]-50**: *Following general procedure C*, **PG1-50** (0.55 g, 1.05 mmol) was mixed with TFA (7.86 ml). *Following general procedure D*, ***de*PG1-50** (0.63 g, 1.14 mmol), DMAP (26 mg) and Et_3N (0.44 ml) were dissolved in DMF (3.40 ml), followed by batch-wise addition of **2d** (2.29 g, 6.31 mmol). After 9 d, the final product (0.38 g, 85%) was obtained as a yellowish sticky solid.

Synthesis of **H[1+1]-300**: *Following general procedure C*, **PG1-300** (0.52 g, 1.00 mmol) was mixed with TFA (5.90 ml). *Following general procedure D*, ***de*PG1-300** (0.55 g, 1.00 mmol), DMAP (74 mg) and Et_3N (0.84 ml) were dissolved in DMF (10.5 ml), followed by batch-wise addition of **2d** (2.19 g, 6.02 mmol). After 8 d, the final product (0.54 g, 66%) was obtained as a yellowish sticky solid.

Synthesis of **H[1+1]-1000**: *Following general procedure C*, **PG1-1000** (0.55 g, 1.06 mmol) was mixed with TFA (5.80 ml). *Following general procedure D*, ***de*PG1-1000** (0.58 g, 1.06 mmol), DMAP (78 mg) and Et_3N (0.88 ml) were dissolved in DMF (16.0 ml), followed by batch-wise addition of **2d** (2.31 g, 6.35 mmol). After 12 d, the final product (0.55 g, 62%) was obtained as a yellowish sticky solid.

Synthesis of **H[1+1]-1500**: *Following general procedure C*, **PG1-1500** (0.50 g, 0.97 mmol) was mixed with TFA (5.22 ml). *Following general procedure D*, ***de*PG1-1500** (0.53 g, 0.97 mmol), DMAP (71 mg) and Et_3N (0.81 ml) were dissolved in DMF (12.6 ml), followed by batch-wise addition of **2d** (3.53 g, 9.72 mmol). After 8 d, the final product (0.62 g, 78%) was obtained as a yellowish sticky solid.

Synthesis of **H[1+1]-2000**: *Following general procedure C*, **PG1-2000** (0.75 g, 1.43 mmol) was mixed with TFA (10.7 ml). *Following general procedure D*, ***de*PG1-2000** (0.79 g, 1.43 mmol), DMAP (105 mg) and Et_3N (1.19 ml) were dissolved in DMF (12.5 ml), followed by batch-wise addition of **2d** (5.20 g, 14.3 mmol). After 14 d, the final product (0.78 g, 67%) was obtained as a yellowish sticky solid.

Synthesis of **H[1+1]-3000**: *Following general procedure C*, **PG1-3000** (0.48 g, 0.87 mmol) was mixed with TFA (5.40 ml). *Following general procedure D*, ***de*PG1-3000** (0.48 g, 0.87 mmol), DMAP (64 mg) and Et_3N (0.73 ml) were dissolved in DMF (9.60 ml), followed by batch-wise addition of **2d** (1.90 g, 5.24 mmol). After 9 d, the final product (0.63 g, 89%) was obtained as a yellowish sticky solid.

Synthesis of H[1+2] "hybrid" DPs

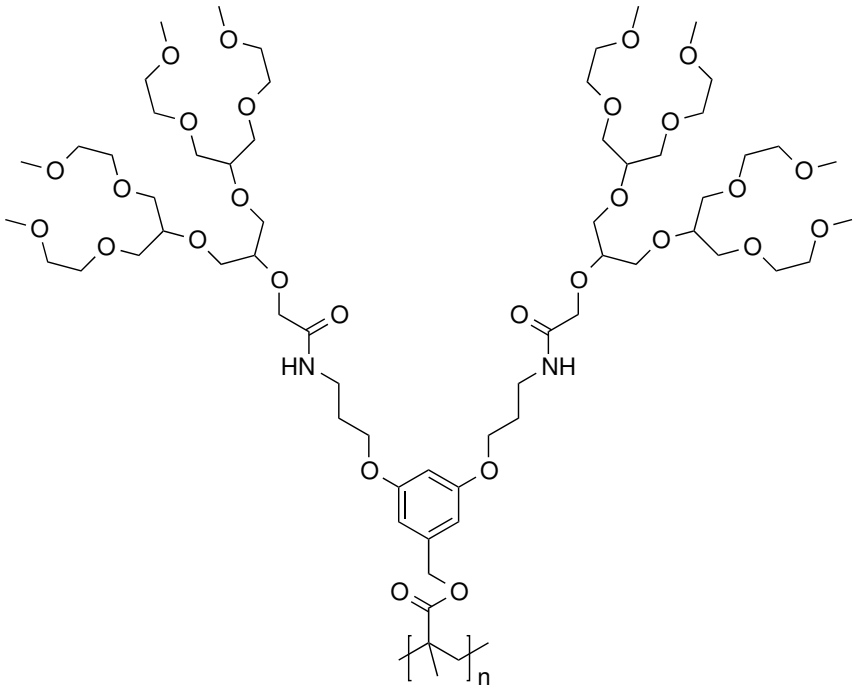

H[1+2]

Synthesis of **H[1+2]-50**: *Following general procedure C*, **PG1-50** (0.36 g, 0.67 mmol) was mixed with TFA (3.80 ml). *Following general procedure D*, ***de*PG1-50** (0.38 g, 0.67 mmol), DMAP (51 mg) and Et_3N (0.77 ml) were dissolved in DMF (7.20 ml), followed by batch-wise addition of **3e** (3.46 g, 5.52 mmol). After 8 d, the final product (0.71 g, 77%) was obtained as a brownish oil.

Synthesis of **H[1+2]-300**: *Following general procedure C*, **PG1-300** (0.24 g, 0.45 mmol) was mixed with TFA (5.20 ml). *Following general procedure D*, ***de*PG1-300** (0.26 g, 0.45 mmol), DMAP (34 mg) and Et_3N (0.51 ml) were dissolved in DMF (6.80 ml), followed by batch-wise addition of **3e** (2.30 g, 3.66 mmol). After 37 d, the final product (0.30 g, 49%) was obtained as a brownish oil.

Synthesis of **H[1+2]-1000**: *Following general procedure C*, **PG1-1000** (0.20 g, 0.38 mmol) was mixed with TFA (4.00 ml). *Following general procedure D*, ***de*PG1-1000** (0.21 g, 0.38 mmol), DMAP (28 mg) and Et_3N (0.42 ml) were dissolved in DMF (6.20 ml), followed by batch-wise addition of **3e** (1.88 g, 3.00 mmol). After 30 d, the final product (0.38 g, 74%) was obtained as a brownish oil.

Synthesis of **H[1+2]-1500**: *Following general procedure C*, **PG1-1500** (0.30 g, 0.58 mmol) was mixed with TFA (6.60 ml). *Following general procedure D*, ***de*PG1-1500** (0.32 g, 0.58 mmol), DMAP (49 mg) and Et_3N (0.74 ml) were dissolved in DMF (7.40 ml), followed by batch-wise addition of **3e** (3.35 g, 5.34 mmol). After 14 d, the final product (0.40 g, 50%) was obtained as a brownish oil.

Synthesis of **H[1+2]-2000**: *Following general procedure C*, **PG1-2000** (0.26 g, 0.50 mmol) was mixed with TFA (5.70 ml). *Following general procedure D*, ***de*PG1-2000** (0.28 g, 0.50 mmol), DMAP (39 mg) and Et_3N (0.59 ml) were dissolved in DMF (5.80 ml), followed by batch-wise addition of **3e** (2.64 g, 4.20 mmol). After 13 d, the final product (0.49 g, 72%) was obtained as a brownish oil.

Synthesis of **H[1+2]-3000**: *Following general procedure C*, **PG1-3000** (0.36 g, 0.69 mmol) was mixed with TFA (8.00 ml). *Following general procedure D*, ***de*PG1-3000** (0.38 g, 0.69 mmol), DMAP (51 mg) and Et_3N (0.78 ml) were dissolved in DMF (8.20 ml), followed by batch-wise addition of **3e** (3.50 g, 5.58 mmol). After 21 d, the final product (0.73 g, 79%) was obtained as a brownish oil.

Synthesis of H[2+1] "hybrid" DPs

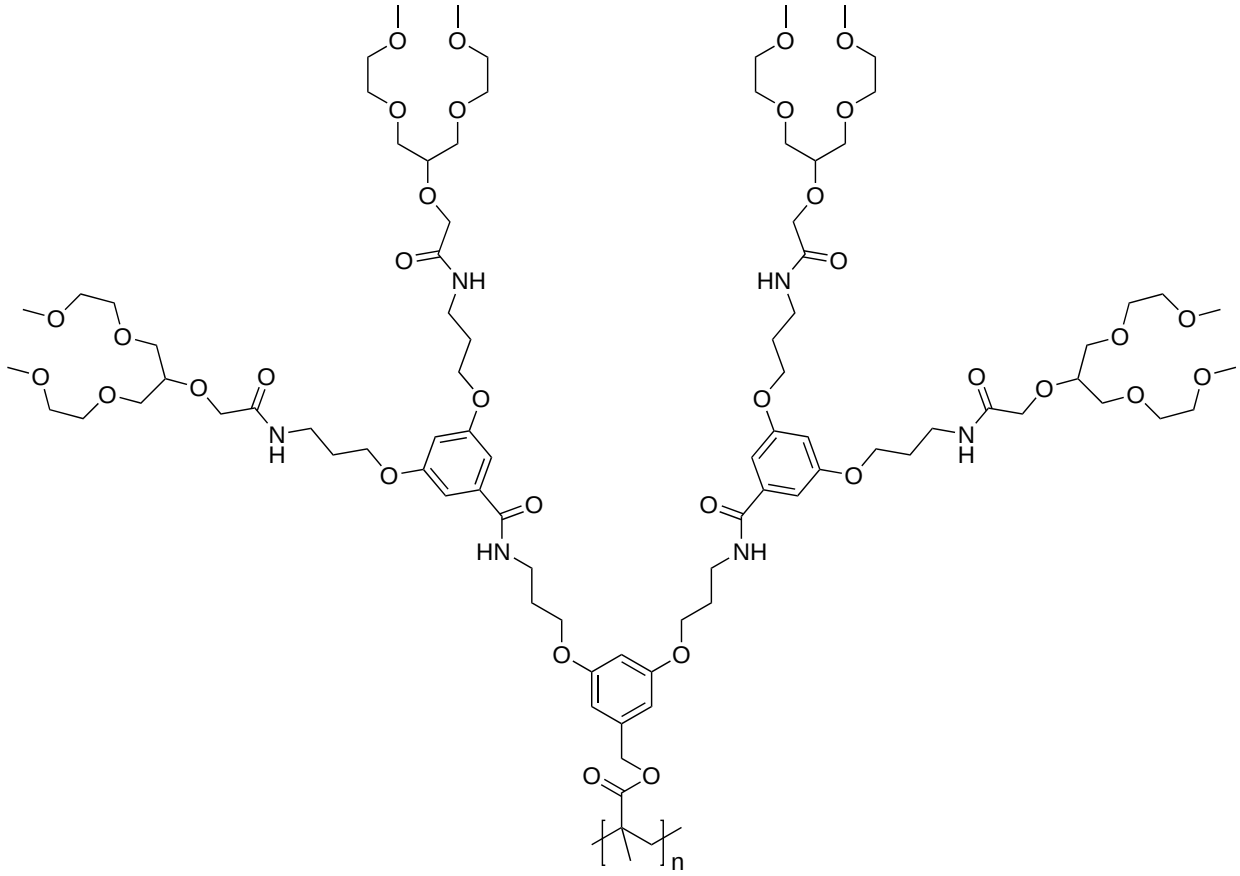

H[2+1]

Synthesis of **H[2+1]-50**: *Following general procedure C*, **PG2-50** (0.24 g, 0.19 mmol) was mixed with TFA (5.00 ml). *Following general procedure D*, ***de*PG2-50** (0.25 g, 0.19 mmol), DMAP (14 mg) and Et_3N (0.33 ml) were dissolved in DMF (7.00 ml), followed by batch-wise addition of **2d** (1.43 g, 3.94 mmol). After 18 d, the final product (0.30 g, 84%) was obtained as a brownish oil.

5.3.8 Compounds of Section 3.3 (MeNVOC- & UPy-functionalized DPs)

Synthesis of compound 19

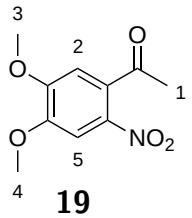

19

A solution of 4,5-dimethoxyacetophenone (1.0 equiv., 10.0 g, 55.49 mmol) in 17% HNO_3 (9.36 g) was added dropwise to a solution of sodium nitrite (0.04 equiv., 150 mg, 2.17 mmol) in concentrated HNO_3 (80 ml, 67%) at 0 °C. The reaction mixture was stirred for 30 min before quenching and washing with ice water (4×100 ml), $NaHCO_3$ (100 ml), and cold EtOH (300 ml). After filtration, the product was dried *in vacuo* to yield the title compound **19** (8.68 g, 69%) as a yellow solid.

R_f (hexane/EtOAc 2:1) = 0.37

^{1}H NMR (300 MHz, CDCl3) δ (ppm) = 7.62 (s, 1H, H-5), 6.76 (s, 1H, H-2), 3.98 (s, 6H, H-3, H-4), 2.50 (s, 3H, H-1)

^{13}C NMR (76 MHz, $CDCl_3$) δ (ppm) = 200.1, 154.1, 149.8, 138.7, 133.0, 108.8, 107.0, 56.8, 56.7, 30.5

MS (ESI-TOF): m/z $[M+H]^+$ calcd for $C_{10}H_{12}NO_5$: 226.0710, found: 226.0706

Synthesis of compound 20

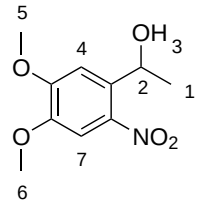

20

4,5-Dimethoxy-2-nitroacetophenone (**19**) (1.0 equiv., 8.0 g, 35.52 mmol) was dissolved in dry THF (85 ml) and dry MeOH (85 ml) and cooled to −15 °C. Sodium borohydride (1.06 equiv., 1.42 g, 37.65 mmol) was slowly added in six portions over the course of 1 h. The progress of the reduction was monitored by TLC (EtOAc/hexane 1:2). After 2 h, the reaction was quenched by addition of 2M HCl (25 ml) and extracted with CH_2Cl_2 (3×100 ml). The combined organic phases were dried over anhydrous $MgSO_4$ and filtered. The volatiles were removed *in vacuo* to yield the title compound **20** as a bright yellow solid (7.73 g, 96%).

R_f (hexane/EtOAc 2:1) = 0.34

^{1}H NMR (300 MHz, $CDCl_3$) δ (ppm) = 7.56 (s, 1H, H-7), 7.30 (s, 1H, H-4), 5.56 (q, J = 6.3 Hz, 1H, H-2), 3.99 (s, 3H, H-6), 3.94 (s, 3H, H-5), 2.33 (s, 1H, H-3), 1.55 (d, J = 6.3 Hz, 3H, H-1)

^{13}C NMR (76 MHz, $CDCl_3$) δ (ppm) = 153.9, 147.9, 139.8, 137.0, 108.6, 107.8, 65.9, 56.6, 56.5, 24.4

MS (ESI-FTICR, DCTB Matrix): m/z $[M+H]^+$ calcd for $C_{10}H_{13}NNaO_5$: 250.0691, found: 250.0686

Synthesis of compound 21

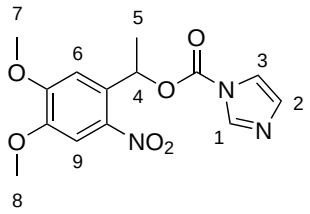

21

A solution of 1-(4,5-Dimethoxy-2-nitrophenyl)ethanol (**20**) (1.0 equiv., 7.73 g, 34.02 mmol) in dry CH_2Cl_2 (70 ml) was added to a solution of 1,1'-carbonyldiimidazole (2.5 equiv., 13.8 g, 85.11 mmol) in dry CH_2Cl_2 (170 ml). The reaction mixture was stirred overnight under an atmosphere of nitrogen. After TLC (EtOAc/hexane 1:1) confirmed the consumption of the starting material, the reaction mixture was washed with H_2O (3×150 ml). The aqueous phase was re-extracted with CH_2Cl_2 and the organic phases were combined, dried over $MgSO_4$ and filtered. The volatiles were removed *in vacuo* to yield the title compound **21** as a yellow solid (10.75 g, 98%).

R_f (hexane/EtOAc 1:1) = 0.22

^{1}H NMR (300 MHz, $CDCl_3$) δ (ppm) = 8.15 (s, 1H, H-1), 7.61 (s, 1H, H-9), 7.43 (t, J = 1.5 Hz, 1H, H-3), 7.08 (dd, J = 1.7, 0.9 Hz, 1H, H-2), 7.00 (s, 1H, H-6), 6.72 (q, J = 6.5 Hz, 1H, H-4), 3.94 (s, 6H, H-7, H-8), 1.81 (d, J = 6.5 Hz, 3H, H-5)

^{13}C NMR (76 MHz, $CDCl_3$) δ (ppm) = 153.9, 148.8, 147.7, 140.3, 137.0, 135.1, 131.1, 130.9, 117.2, 108.0, 107.7, 73.0, 56.6, 22.0

MS (ESI-FTICR, DCTB Matrix): m/z $[M+H]^+$ calcd for $C_{14}H_{15}N_3NaO_6$: 344.0853, found: 344.0853

Synthesis of compound 22

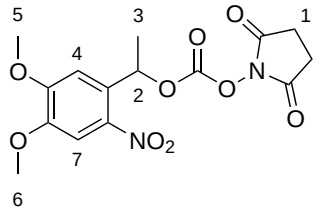

22

Alcohol **20** (1.0 equiv., 13.7 g, 60.2 mmol) was dissolved in anhydrous MeCN and Et_3N (2.0 equiv., 16.7 ml, 120.3 mmol). The resulting solution was cooled to 0 °C, followed by addition of N,N'-disuccinimidyl carbonate (1.2 equiv., 18.5 g, 72.2 mmol) and stirring of the mixture in an atmosphere of N_2 for 3 d. After evaporation of the volatiles *in vacuo*, the residue was dissolved in EtOAc (100 ml) and washed successively with 20 wt% citric acid aqueous solution (100 ml), saturated aqueous Na_2CO_3 solution (100 ml), and saturated aqueous NaCl solution (100 ml). The organic phase was dried over $MgSO_4$, filtered and concentrated *in vacuo*. The residue was recrystallized from a 1:1-mixture of *n*-hexane and chloroform to give the title compound **22** (16.0 g, 72%) as a bright yellow solid.

^{1}H NMR (300 MHz, $CDCl_3$) δ = 7.64 (s, 1H, H-7), 7.08 (s, 1H, H-4), 6.50 (q, J = 6.4 Hz, 1H, H-2), 4.06 (s, 3H, H-6), 3.95 (s, 3H, H-5), 2.80 (s, 4H, H-1), 1.76 (d, J = 6.4 Hz, 3H, H-3)

^{13}C NMR (76 MHz, $CDCl_3$) δ = 168.4, 154.3, 150.6, 148.4, 139.3, 131.2, 107.9, 107.2, 56.6, 56.4, 25.4, 21.9

MS (ESI-FTICR, DCTB Matrix): m/z $[M+Na]^+$ calcd for $C_{15}H_{16}N_2NaO_9$: 391.0752, found: 391.0747

Synthesis of compound 4a

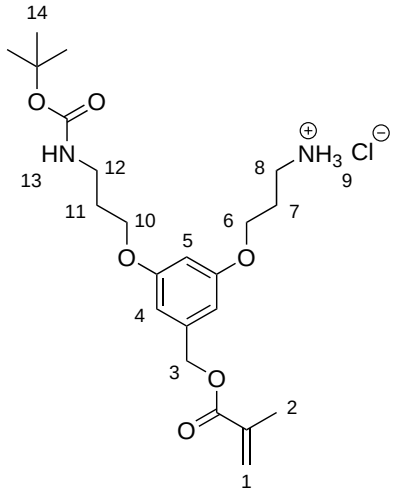

4a

A mixture of trifluoroacetic acid (2.6 equiv., 12.8 ml, 166.5 mmol) in CH_2Cl_2 (50 ml) was added dropwise to a vigorously stirred solution of **1c** (1.0 equiv., 33.9 g, 64.8 mmol) in CH_2Cl_2 (320 ml) cooled to −10 °C. The reaction mixture was allowed to reach room temperature and stirring was continued with daily monitoring of the deprotection progress by TLC ($CHCl_3$/MeOH/Et_3N 10:1:0.1). After 6 d, the reaction was quenched by addition of MeOH (200 ml), concentrated *in vacuo*, and the oily residue was purified by column chromatography (same solvent mixture as for TLC). The mono-deprotected species was dissolved in CH_2Cl_2, washed with 5% aqueous HCl (2 × 300 ml) and dried over anhydrous $MgSO_4$. The volatiles were removed *in vacuo* to yield the title compound **4a** as a pale yellow solid (17.1 g, 57%).

R_f ($CHCl_3$/MeOH/Et_3N 10:1:0.1) = 0.45

^{1}H NMR (300 MHz, DMSO–d6) δ (ppm) = 8.07 (br, 3H, H-9), 6.89 (t, J = 5.1 Hz, 1H, H-13), 6.53 (d, J = 2.1 Hz, 2H, H-4), 6.46 (t, J = 2.3 Hz, 1H, H-5), 6.12 – 6.03 (m, H-1), 5.76 – 5.67 (m, 1H, H-1), 5.09 (s, 2H, H-3), 4.04 (t, J = 6.1 Hz, 2H, H-6), 3.94 (t, J = 6.2 Hz, 2H, H-10), 3.06 (q, J = 6.5 Hz, 2H, H-12), 2.99 – 2.86 (m, 2H, H-8), 2.01 (p, J = 6.3 Hz, 2H, H-7), 1.91 (s, 3H, H-2), 1.80 (p, J = 6.4 Hz, 2H, H-11), 1.37 (s, 9H, H-14)

^{13}C NMR (76 MHz, DMSO–d6) δ (ppm) = 166.3, 159.8 159.5, 155.6, 138.4, 135.7, 126.1, 106.2, 106.2, 100.6, 77.5, 65.6, 65.4, 64.7, 36.9, 36.1, 29.2, 28.2, 26.8, 18.0

MS (MALDI-TOF): calcd for $C_{22}H_{35}N_2O_6$ ($[M+H]^+$) 423.2490; found 423.2490

Synthesis of compound 4b

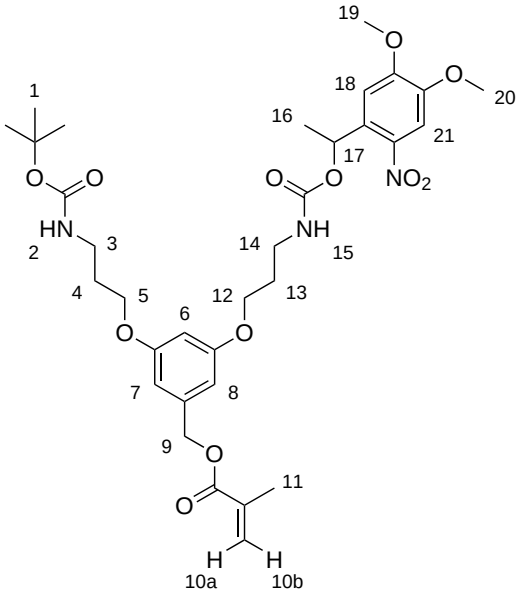

4b

Macromonomer **4a** (1.0 equiv., 9.4 g, 20.4 mmol) was dissolved in CH_2Cl_2 (50 ml) and Et_3N (1.1 equiv., 3.1 ml, 22.2 mmol), followed by dropwise addition of a solution of imidazolide **21** (1.1 equiv., 6.0 g, 22.2 mmol) in CH_2Cl_2 (25 ml) at 0 °C. The reaction mixture was stirred for 3 d. Purification by column chromatography (EtOAc/hexane 1:1) afforded the title compound **4b** (8.8 g, 70%) as a slightly yellow solid.

^{1}H NMR (300 MHz, $CDCl_3$) δ (ppm) = 7.56 (s, 1H, H-21), 6.99 (s, 1H, H-18), 6.49 (dt, J = 5.6, 1.5 Hz, 2H, H-7, H-8), 6.42 – 6.32 (m, 2H, H-6, H-17), 6.18 – 6.13 (m, 1H, H-10a), 5.59 (p, J = 1.6 Hz, 1H, H-10b), 5.11 (br, 1H, H-2), 5.09 (s, 1H, H-9), 4.75 (br, 1H, H-15), 3.98 (t, J = 6.0 Hz, 4H, H-5, H-12), 3.92 – 3.91 (2 × s, 6H, H-19, H-20), 3.31 (dq, J = 13.1, 6.7 Hz, 4H, H-3, H-14), 2.02 – 1.89 (m, 7H, H-4, H-11, H-13), 1.58 (d, J = 6.4 Hz, 3H, H-16), 1.42 (s, 9H, H-1)

^{13}C NMR (76 MHz, $CDCl_3$) δ (ppm) = 167.3, 160.2, 160.0, 156.1, 155.4, 153.7, 148.0, 139.9, 138.7, 136.3, 134.2, 126.1, 108.0, 107.9, 106.6, 101.1, 79.4, 69.0, 66.3, 65.9, 56.5, 38.7, 29.7, 29.4, 28.5, 22.4, 18.5

MS (MALDI-TOF): calcd for $C_{33}H_{45}N_3NaO_{12}$ ($[M+Na]^+$) 698.2901; found 698.2896.

Synthesis of first-generation MeNVOC-functionalized DPs (PG1-MeNVOC)

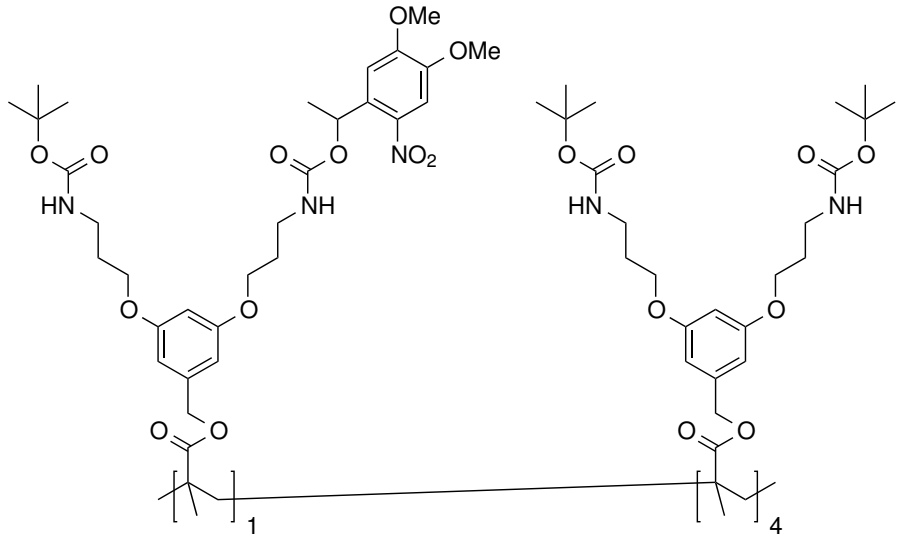

PG1-MeNVOC10

Synthesis of **PG1-MeNVOC10**. *Following general procedure B*, **1c** (1.55 g, 2.96 mmol), **4b** (0.50 g, 0.74 mmol), AIBN (0.82 ml), and CDB (0.82 ml) were dissolved in DMF (0.36 ml) and polymerized for 18 h. The final product (1.82 g, 89%) was obtained as a fluffy, slightly yellow foam.

Synthesis of compound 5

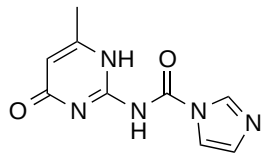

5

6-Methylisocytosine (1.0 equiv., 3.3 g, 26.7 mmol) and 1,1'-carbonyldiimidazole (1.3 equiv., 5.6 g, 34.6 mmol) were mixed in dry THF (25 ml) and the resulting white suspension was heated to 70 °C and stirred overnight. After cooling to room temperature, the reaction was filtered and the solid was washed three times with acetone. Drying *in vacuo* afforded the UPy-imidazolide **5** as a white solid (5.6 g, 97%). Note: Due to its extremely low solubility in most solvents, this compound is hard to characterize.

IR (ATR): ν (cm^{-1}) = 3174, 3073, 2594 (bs), 1699, 1647, 1594, 1507, 1472, 1376, 1336, 1315, 1271, 1219, 1189, 1162, 1092, 1062, 1018, 979, 909, 853, 795, 756, 643, 560, 490.

MS (MALDI-TOF): calcd for $C_9H_{10}N_5O_2$ ($[M+H]^+$) 220.0829; found 220.0829.

Elemental analysis calcd (%) for $C_9H_9N_5O_2$: C 49.31, H 4.14, N 31.95, O 14.60; found: C 49.21, H 4.09, N 32.18, O 14.49.

m.p.: 235-236 °C.

Synthesis of compound 29

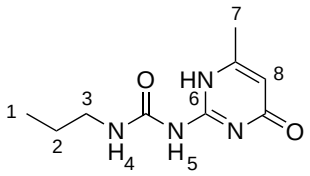

29

UPy-imidazolide **5** (1.0 equiv., 291 mg, 1.33 mmol) was suspended in $CHCl_3$ (3 ml), followed by addition of *n*-propylamine (1.1 equiv., 121 μl, 1.46 mmol). The resulting mixture was heated to 55 °C and stirred overnight. After cooling to room temperature, the reaction was diluted with $CHCl_3$ (20 ml) and washed successively with 1M HCl (30 ml) and saturated $NaHCO_3$ (30 ml) aqueous solutions. The organic layer was dried over $MgSO_4$, filtered, and concentrated *in vacuo* to give the title compound **29** (98 mg, 35%) as a white solid.

R_f ($CHCl_3$, 3% Methanol) = 0.47

^{1}H NMR (300 MHz, $CDCl_3$) δ = 13.10 (s, 1H, H-6), 11.79 (s, 1H, H-5), 10.11 (s, 1H, H-4), 5.76 (s, 1H, H-8), 3.16 (q, J = 6.6 Hz, 2H, H-3), 2.18 (s, 3H, H-7), 1.58 (h, J = 7.2 Hz, 2H, H-2), 0.90 (t, J = 7.4 Hz, 3H, H-1)

^{13}C NMR (76 MHz, $CDCl_3$) δ = 172.9, 156.5, 154.6, 148.1, 106.5, 41.7, 22.7, 18.8, 11.3

MS (ESI-FTICR, DCTB Matrix): m/z $[M+Na]^+$ calcd for $C_9H_{14}N_4NaO_2$: 233.1009, found: 233.1009

Synthesis of compound 4c

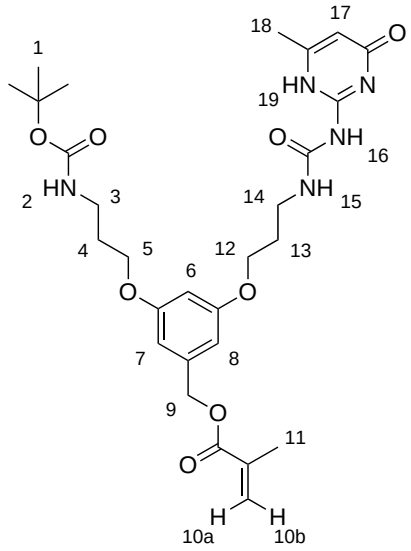

4c

A solution of **4a** (1.0 equiv., 3.1 g, 6.7 mmol) in DMF (21 ml) and Et_3N (1.5 equiv., 1.4 ml, 10.1 mmol) was added dropwise to a vigorously stirred suspension of **5** (1.2 equiv., 1.8 g, 8.1 mmol) in DMF (24 ml) and the mixture was stirred at room temperature overnight, whereupon the reaction mixture gradually clarified. The reaction was diluted with $CHCl_3$ (200 ml) and subsequently washed with 5% aqueous HCl (200 ml), saturated aqueous $NaHCO_3$ solution (200 ml), and saturated aqueous NaCl solution (100 ml). The organic phase was dried over $MgSO_4$, filtered and the solvent was removed *in vacuo* to yield the title compound **4c** as a beige solid (3.8 g, 99%).

R_f (hexane/EtOAc 2:1) = 0.20

^{1}H NMR (300 MHz, $CDCl_3$) δ (ppm) = 13.04 (br, 1H, H-19), 11.89 (br, 1H, H-16), 10.28 (s, 1H, H-15), 6.49 (dt, J = 9.8, 1.6 Hz, 2H, H-7, H-8), 6.40 (t, J = 2.3 Hz, 1H, H-6), 6.14 – 6.15 (m, 1H, H-10a), 5.78 (br, 1H, H-17), 5.58 (p, J = 1.5 Hz, 1H, H-10b), 5.08 (s, 2H, H-9), 4.77 (br, 1H, H-2), 3.99 (dt, J = 13.8, 6.0 Hz, 4H, H-5, H-12), 3.45 (q, J = 6.5 Hz, 2H, H-14), 3.30 (q, J = 6.5 Hz, 2H, H-3), 2.27 – 2.14 (m, 3H, H-18), 2.14 – 2.02 (m, 2H, H-13), 2.01 — 1.88 (m, 5H, H-4, H-11), 1.43 (s, 9H, H-1)

^{13}C NMR (76 MHz, $CDCl_3$) δ (ppm) = 172.9, 167.1, 160.3, 160.0, 156.6, 155.9, 148.2, 138.2, 136.1, 125.9, 106.7, 106.5, 106.3, 101.0, 66.2, 65.8, 65.6, 38.0, 37.1, 29.5, 29.1, 28.4, 18.9, 18.3

MS (MALDI-TOF): calcd for $C_{28}H_{40}N_5O_8$ ($[M+H]^+$) 574.2877; found 574.2872

Synthesis of first-generation UPy-functionalized DPs (PG1-UPy)

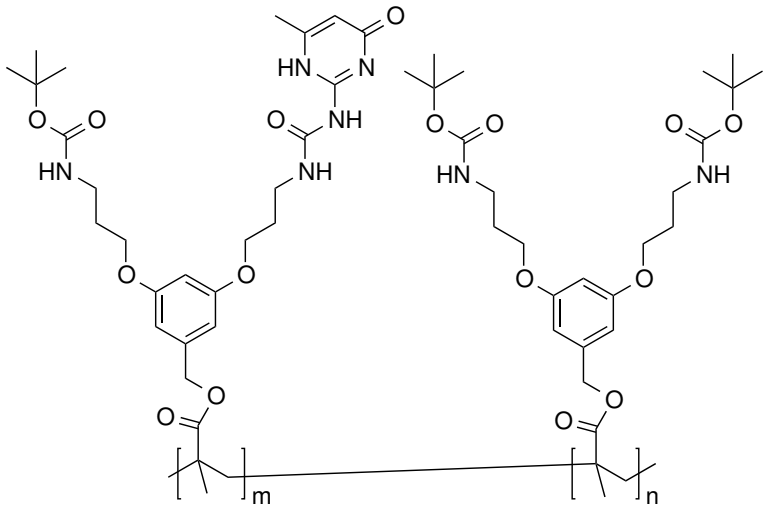

PG1-UPy

Synthesis of **PG1-UPy5**: *Following general procedure B*, **1c** (1.54 g, 2.95 mmol), **4c** (0.19 g, 0.33 mmol), AIBN (0.1M in DMF, 0.73 ml), and CDB (0.1M in DMF, 0.73 ml) were dissolved in DMF (0.27 ml) and polymerized for 19 h. The final product (1.53 g, 88%) was obtained as a fluffy, pink foam.

Synthesis of **PG1-UPy10**: *Following general procedure B*, **1c** (1.33 g, 2.55 mmol), **4c** (0.36 g, 0.64 mmol), AIBN (0.1M in DMF, 0.71 ml), and CDB (0.1M in DMF, 0.71 ml) were dissolved in DMF (0.28 ml) and polymerized for 19 h. The final product (1.39 g, 82%) was obtained as a fluffy, pink foam.

Synthesis of **PG1-UPy25**: *Following general procedure B*, **1c** (1.00 g, 1.93 mmol), **4c** (1.10 g, 1.93 mmol), AIBN (0.1M in DMF, 0.86 ml), and CDB (0.1M in DMF, 0.86 ml) were dissolved in DMF (0.40 ml) and polymerized for 18 h. The final product (1.68 g, 80%) was obtained as a dense, pink foam.

Synthesis of **PG1-UPy33**: *Following general procedure B*, **1c** (0.43 g, 0.82 mmol), **4c** (0.97 g, 1.64 mmol), AIBN (0.1M in DMF, 0.55 ml), and CDB (0.1M in DMF, 0.55 ml) were dissolved in DMF (0.30 ml) and polymerized for 16 h. The final product (1.30 g, 92%) was obtained as a dense, pink foam.

Synthesis of **PG1-UPy25a**: *Following general procedure A*, **1c** (0.24 g, 0.45 mmol), **4c** (0.26 g, 0.45 mmol) and AIBN (0.01M in DMF, 181.7 μl) were dissolved in DMF (1.81 ml; final concentration 0.25 g ml^{-1}) and polymerized for 19 h. The final product (0.48 g, 97%) was obtained as a fluffy, colorless foam.

Synthesis of **PG1-UPy25b**: *Following general procedure A*, **1c** (0.57 g, 1.09 mmol), **4c** (0.64 g, 1.09 mmol) and AIBN (0.1M in DMF, 43.6 μl) were dissolved in DMF (3.06 ml; final concentration 0.39 g ml^{-1}) and polymerized for 16 h. The final product (1.11 g, 91%) was obtained as a fluffy, colorless foam.

Synthesis of **PG1-UPy25c**: *Following general procedure A*, **1c** (0.38 g, 0.74 mmol), **4c** (0.42 g, 0.74 mmol) and AIBN (0.1M in DMF, 29.5 μl) were dissolved in DMF (1.15 ml; final concentration 0.50 g ml^{-1}) and polymerized for 19 h. The final product (0.79 g, 97%) was obtained as a fluffy, colorless foam.

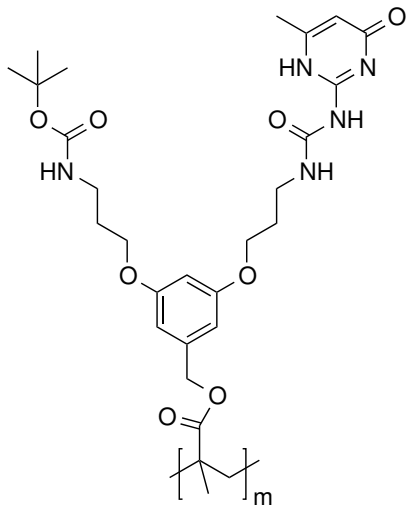

PG1-UPy50

Macromonomer **4c** (0.74 g, 1.29 mmol) was placed in a Schlenk tube equipped with a magnetic stir bar under N_2 atmosphere, followed by addition of 0.1M solutions of azobis(isobutyronitrile) (AIBN; 0.025 equiv., 0.32 ml) and cumyl dithiobenzoate (CDB; 0.025 equiv., 0.3 ml) in DMF. The reaction was diluted with DMF (0.10 ml) to arrive at a final concentration of 1.0 g ml^{-1}. After homogenization and thorough degassing by several freeze-pump-thaw cycles, the polymerization mixture was placed in an oil bath that had been preheated to 65 °C under N_2. The polymerization mixture solidified over the course of the reaction. After 14 h, the reaction was stopped by removing the flask from the oil bath and rapid cooling in liquid N_2. $CHCl_3$ (10 ml) was added to the flask, the polymer was suspended while heating to 60 °C, transferred into a glass frit (Por. 3) and hot filtered. Washing with hot $CHCl_3$ was repeated three times (3×20 ml). Drying *in vacuo* afforded **PG1-UPy50** (0.64 g, 87%) as a pink, granular solid.

Synthesis of second-generation UPy-functionalized DPs (PG2-UPy)

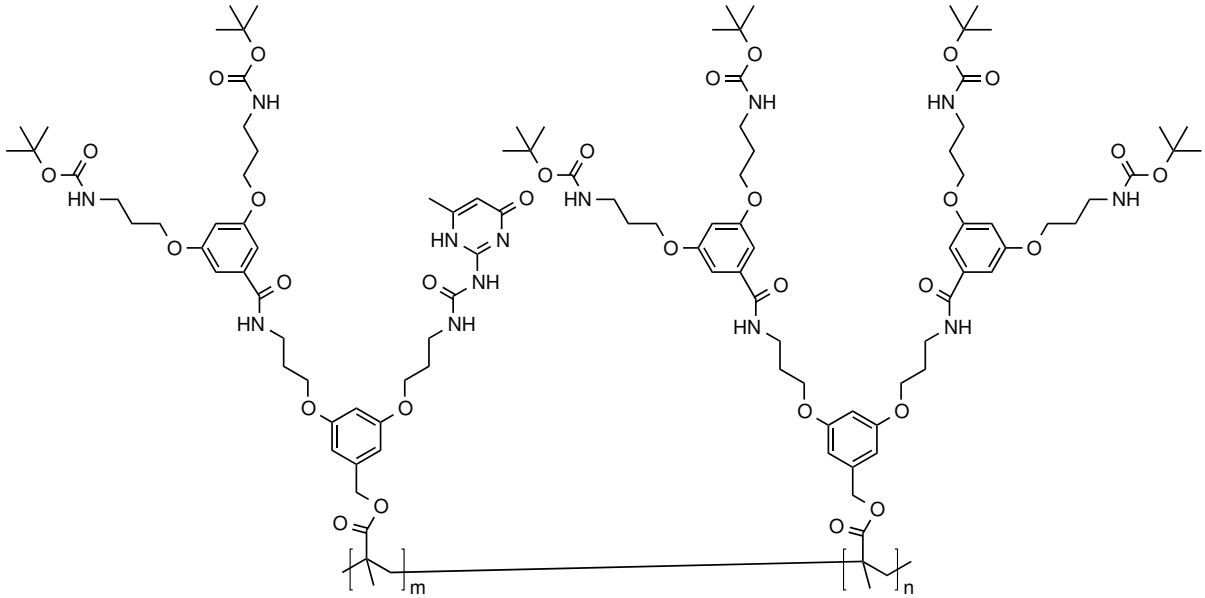

PG2-UPy

Synthesis of **PG2-UPy5**: *Following general procedure C*, **PG1-UPy5** (0.23 g, 0.43 mmol) was mixed with TFA (3.00 ml). *Following general procedure D*, ***de*PG1-UPy5** (0.24 g, 0.43 mmol), DMAP (32 mg) and Et_3N (0.25 ml) were dissolved in DMF/DMSO (4.00/0.50 ml), followed by batch-wise addition of **1d** (2.50 g, 4.36 mmol). After 7 d, the final product (0.30 g, 69%) was obtained as a colorless foam.

Synthesis of **PG2-UPy25**: *Following general procedure C*, **PG1-UPy25** (0.23 g, 0.41 mmol) was mixed with TFA (3.00 ml). *Following general procedure D*, ***de*PG1-UPy25** (0.24 g, 0.41 mmol), DMAP (30 mg) and Et_3N (0.23 ml) were dissolved in DMF/DMSO (4.00/0.50 ml), followed by batch-wise addition of **1d** (1.90 g, 3.36 mmol). After 7 d, the final product (0.30 g, 69%) was obtained as a colorless foam.

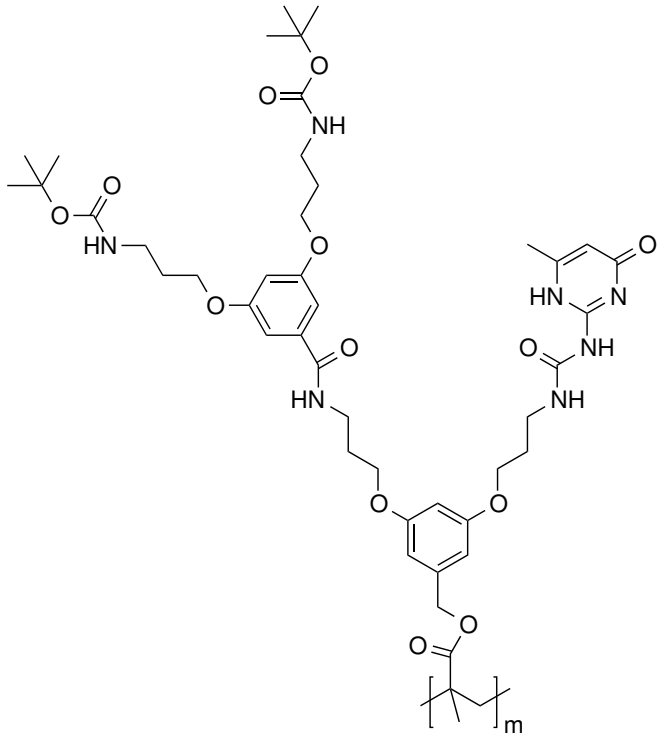

PG2-UPy50

Synthesis of **PG2-UPy50**: *Following general procedure C*, **PG1-UPy50** (0.16 g, 0.28 mmol) was mixed with TFA (2.00 ml). *Following general procedure D*, ***de*PG1-UPy50** (0.16 g, 0.28 mmol), DMAP (20 mg) and Et_3N (0.16 ml) were dissolved in DMF/DMSO (3.50/1.00 ml), followed by batch-wise addition of **1d** (1.30 g, 2.30 mmol). After 8 d, the final product (0.18 g, 70%) was obtained as a colorless foam.

Synthesis of third-generation UPy-functionalized DPs (PG3-UPy)

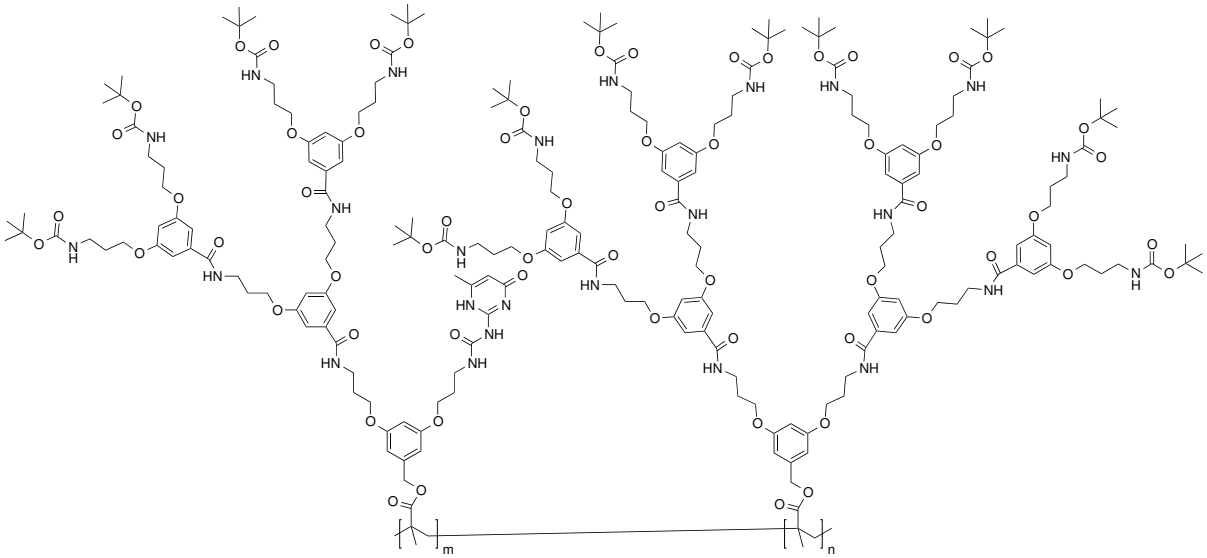

PG3-UPy

Synthesis of **PG3-UPy5**: *Following general procedure C*, **PG2-UPy5** (0.16 g, 0.28 mmol) was mixed with TFA (2.00 ml). *Following general procedure D*, ***de*PG2-UPy5** (0.16 g, 0.28 mmol), DMAP (20 mg) and Et_3N (0.16 ml) were dissolved in DMF/DMSO (3.50/1.00 ml), followed by batch-wise addition of **1d** (1.30 g, 2.30 mmol). After 8 d, the final product (0.18 g, 70%) was obtained as a colorless foam.

Synthesis of **PG3-UPy25**: *Following general procedure C*, **PG2-UPy25** (85 mg, 0.08 mmol) was mixed with TFA (4.00 ml). *Following general procedure D*, ***de*PG2-UPy25** (88 mg, 0.08 mmol), DMAP (6 mg) and Et_3N (0.14 ml) were dissolved in DMF/DMSO (3.00/0.60 ml), followed by batch-wise addition of **1d** (1.35 g, 2.38 mmol). After 8 d, the final product (0.18 g, 70%) was obtained as a colorless foam.

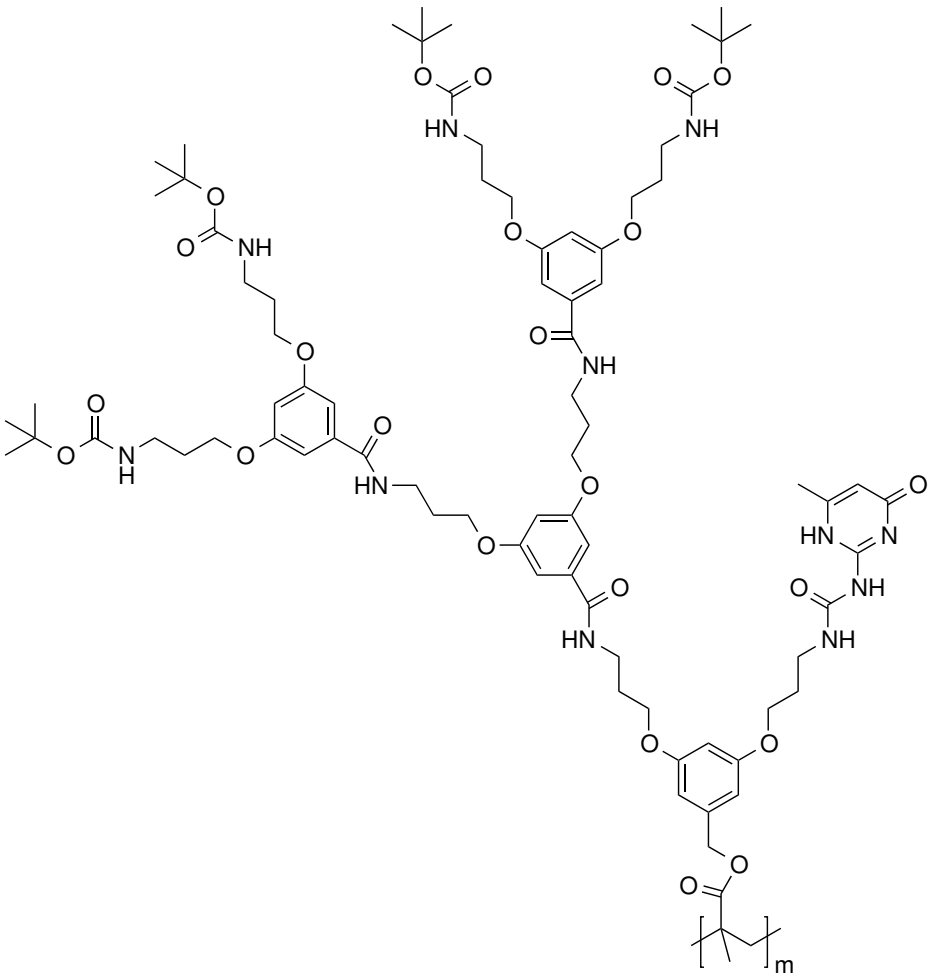

PG3-UPy50

Synthesis of **PG3-UPy50**: *Following general procedure C*, **PG2-UPy50** (79 mg, 0.08 mmol) was mixed with TFA (3.00 ml). *Following general procedure D*, ***de*PG2-UPy50** (81 mg, 0.08 mmol), DMAP (6 mg) and Et_3N (0.10 ml) were dissolved in DMF/DMSO (2.80/1.60 ml), followed by batch-wise addition of **1d** (0.78 g, 1.36 mmol). After 8 d, the final product (0.18 g, 70%) was obtained as a colorless foam.

6 References

[1] U. W. Gedde in *Polymer Physics*, Springer Netherlands, Dordrecht, **1999**, pp. 1–18.

[2] P. J. Flory, *Principles of Polymer Chemistry*, First Edit, Cornell University Press, Ithaca, **1953**.

[3] W. F. M. Daniel, J. Burdynska, M. Vatankhah-Varnoosfaderani, K. Matyjaszewski, J. Paturej, M. Rubinstein, A. V. Dobrynin, S. S. Sheiko, Solvent-Free, Supersoft and Superelastic Bottlebrush Melts and Networks, *Nature Materials* **2016**, *15*, 183–189.

[4] N. A. Platé, V. P. Shibaev, Comb-Like Polymers. Structure and Properties, *Journal of Polymer Science: Macromolecular Reviews* **1974**, *8*, 117–253.

[5] J. M. Ren, T. G. McKenzie, Q. Fu, E. H. H. Wong, J. Xu, Z. An, S. Shanmugam, T. P. Davis, C. Boyer, G. G. Qiao, Star Polymers, *Chemical Reviews* **2016**, *116*, 6743–6836.

[6] Y. Zheng, S. Li, Z. Weng, C. Gao, Hyperbranched Polymers: Advances from Synthesis to Applications, *Chemical Society Reviews* **2015**, *44*, 4091–4130.

[7] D. A. Tomalia, J. M. J. Fréchet, Discovery of Dendrimers and Dendritic polymers: A Brief Historical Perspective, *Journal of Polymer Science Part A: Polymer Chemistry* **2002**, *40*, 2719–2728.

[8] Y. Zhu, N. S. Hosmane, Advanced Developments in Cyclic Polymers: Synthesis, Applications, and Perspectives, *ChemistryOpen* **2015**, *4*, 408–417.

[9] W. H. Carothers, Studies on Polymerization and Ring Formation I. An Introduction to the General Theory of Condensation Polymers, *Journal of the American Chemical Society* **1929**, *51*, 2548–2559.

[10] W. H. Carothers, Polymerization, *Chemical Reviews* **1931**, *8*, 353–426.

[11] W. K. Czerwinski, Solvent Effects on Free-Radical Polymerization, 1. Solvent Effect on Initiation of Methyl Methacrylate and N-Vinyl-2-pyrrolidone, *Die Makromolekulare Chemie* **1991**, *192*, 1285–1296.

[12] D. H. Solomon, G. Moad, Initiation. The Reactions of Primary Radicals, *Makromolekulare Chemie. Macromolecular Symposia* **1987**, *10-11*, 109–125.

[13] A Ravve in *Principles of Polymer Chemistry*, Springer New York, New York, NY, **2012**, pp. 69–150.

[14] M. Szwarc, Living Polymers. Their Discovery, Characterization, and Properties, *Journal of Polymer Science Part A: Polymer Chemistry* **1998**, *36*, IX–XV.

[15] A. D. Jenkins, R. G. Jones, G. Moad, Terminology for Reversible-Deactivation Radical Polymerization Previously Called "Controlled" Radical or "Living" Radical Polymerization (IUPAC Recommendations 2010), *Pure and Applied Chemistry* **2010**, *82*, 483–491.

[16] C. J. Hawker, A. W. Bosman, E. Harth, New Polymer Synthesis by Nitroxide Mediated Living Radical Polymerizations, *Chemical Reviews* **2001**, *101*, 3661–3688.

[17] K. Matyjaszewski, J. Xia, Atom Transfer Radical Polymerization, *Chemical Reviews* **2001**, *101*, 2921–2990.

[18] G. Moad, E. Rizzardo, S. H. Thang, Radical Addition-Fragmentation Chemistry in Polymer Synthesis, *Polymer* **2008**, *49*, 1079–1131.

[19] G. F. Meijs, E. Rizzardo, Chain Transfer by an Addition-Fragmentation Mechanism. The use of α-Benzyloxystyrene for the Preparation of Low-Molecular-Weight Poly(methyl methacrylate) and Polystyrene, *Die Makromolekulare Chemie Rapid Communications* **1988**, *9*, 547–551.

[20] G. Moad, E. Rizzardo, S. H. Thang, Living Radical Polymerization by the RAFT Process - A Second Update, *Australian Journal of Chemistry* **2009**, *62*, 1402–1472.

[21] J. Chiefari, Y. K. Chong, F. Ercole, J. Krstina, J. Jeffery, T. P. T. Le, R. T. A. Mayadunne, G. F. Meijs, C. L. Moad, G. Moad, E. Rizzardo, S. H. Thang, Living Free-Radical Polymerization by Reversible Addition-Fragmentation Chain Transfer: The RAFT Process, *Macromolecules* **1998**, *31*, 5559–5562.

[22] J. Chiefari, R. T. A. Mayadunne, C. L. Moad, G. Moad, E. Rizzardo, A. Postma, S. H. Thang, Thiocarbonylthio Compounds (S=C(Z)S-R) in Free Radical Polymerization with Reversible Addition-Fragmentation Chain Transfer (RAFT Polymerization). Effect of the Activating Group Z, *Macromolecules* **2003**, *36*, 2273–2283.

[23] Y. K. Chong, T. P. T. Le, G. Moad, E. Rizzardo, S. H. Thang, A More Versatile Route to Block Copolymers and Other Polymers of Complex Architecture by Living Radical Polymerization: The RAFT Process, *Macromolecules* **1999**, *32*, 2071–2074.

[24] F. R. Mayo, F. M. Lewis, Copolymerization. I. A Basis for Comparing the Behavior of Monomers in Copolymerization; The Copolymerization of Styrene and Methyl Methacrylate, *Journal of the American Chemical Society* **1944**, *66*, 1594–1601.

[25] K. A. Günay, P. Theato, H.-A. Klok in *Functional Polymers by Post-Polymerization Modification*, Wiley-VCH Verlag GmbH & Co. KGaA, **2012**, pp. 1–44.

[26] W. A. Cunningham, Sulfur. III, *Journal of Chemical Education* **1935**, *12*, 120.

[27] R. E. Oesper, Christian Friedrich Schonbein. Part II. Experimental Labors, *Journal of Chemical Education* **1929**, *6*, 677.

[28] P. Rustemeyer, 1. History of CA and Evolution of the Markets, *Macromolecular Symposia* **2004**, *208*, 1–6.

[29] H. Staudinger, Soluble and Insoluble Rubber, *Rubber Chemistry and Technology* **1939**, *12*, 117–118.

[30] C. E. Hoyle, C. N. Bowman, Thiol-Ene Click Chemistry, *Angewandte Chemie International Edition* **2010**, *49*, 1540–1573.

[31] H.-G. Batz, G. Franzmann, H. Ringsdorf, Model Reactions for Synthesis of Pharmacologically Active Polymers by Way of Monomeric and Polymeric Reactive Esters, *Angewandte Chemie International Edition in English* **1972**, *11*, 1103–1104.

[32] P. Ferruti, A. Bettelli, A. Feré, High Polymers of Acrylic and Methacrylic Esters of N-Hydroxysuccinimide as Polyacrylamide and Polymethacrylamide Precursors, *Polymer* **1972**, *13*, 462–464.

[33] S. R. A. Devenish, J. B. Hill, J. W. Blunt, J. C. Morris, M. H. G. Munro, Dual Side-Reactions Limit the Utility of a Key Polymer Therapeutic Precursor, *Tetrahedron Letters* **2006**, *47*, 2875–2878.

[34] S. Y. Wong, D. Putnam, Overcoming Limiting Side Reactions Associated with an NHS-Activated Precursor of Polymethacrylamide-Based Polymers, *Bioconjugate Chemistry* **2007**, *18*, 970–982.

[35] W. Stocker, B. Karakaya, B. L. Schürmann, J. P. Rabe, A. D. Schlüter, Ordered Dendritic Nanorods with a Poly(p-phenylene) Backbone, *Journal of the American Chemical Society* **1998**, *120*, 7691–7695.

[36] I. Neubert, A. D. Schlüter, Dendronized Polystyrenes with Hydroxy and Amino Groups in the Periphery, *Macromolecules* **1998**, *31*, 9372–9378.

[37] L. Shu, A. Schäfer, A. D. Schlüter, Dendronized Polymers: Increasing of Dendron Generation by the Attach-to Approach, *Macromolecules* **2000**, *33*, 4321–4328.

[38] L. Shu, I. Göossl, J. P. Rabe, A. D. Schlüter, Quantitative Aspects of the Dendronization of Dendronized Linear Polystyrenes, *Macromolecular Chemistry and Physics* **2002**, *203*, 2540–2550.

[39] L. Shu, A. D. Schlüter, C. Ecker, N. Severin, J. P. Rabe, Extremely Long Dendronized Polymers: Synthesis, Quantification of Structure Perfection, Individualization, and SFM Manipulation, *Angewandte Chemie International Edition* **2001**, *40*, 4666–4669.

[40] A. Zhang, L. Shu, Z. Bo, A. D. Schlüter, Dendronized Polymers: Recent Progress in Synthesis, *Macromolecular Chemistry and Physics* **2003**, *204*, 328–339.

[41] A. Zhang, L. Okrasa, T. Pakula, A. D. Schlüter, Homologous Series of Dendronized Polymethacrylates with a Methyleneoxycarbonyl Spacer between the Backbone and Dendritic Side Chain: Synthesis, Characterization, and Some Bulk Properties, *Journal of the American Chemical Society* **2004**, *126*, 6658–6666.

[42] B. Zhang, R. Wepf, K. Fischer, M. Schmidt, S. Besse, P. Lindner, B. T. King, R. Sigel, P. Schurtenberger, Y. Talmon, Y. Ding, M. Kröger, A. Halperin, A. D. Schlüter, The Largest Synthetic Structure with Molecular Precision: Towards a Molecular Object, *Angewandte Chemie International Edition* **2011**, *50*, 737–740.

[43] A. Ammala, S. Bateman, K. Dean, E. Petinakis, P. Sangwan, S. Wong, Q. Yuan, L. Yu, C. Patrick, K. H. Leong, An Overview of Degradable and Biodegradable Polyolefins, *Progress in Polymer Science* **2011**, *36*, 1015–1049.

[44] F. D. Jochum, P. Theato, Temperature- and Light-Responsive Smart Polymer Materials, *Chemical Society Reviews* **2013**, *42*, 7468–7483.

[45] C. C. Lee, J. A. MacKay, J. M. J. Frechet, F. C. Szoka, Designing Dendrimers for Biological Applications, *Nature Biotechnology* **2005**, *23*, 1517–1526.

[46] J. N. H. Reek, S. Arévalo, R. van Heerbeek, P. C. J. Kamer, P. W.N. M. van Leeuwen, Dendrimers in Catalysis, *Advances in Catalysis* **2006**, *Volume 49*, (Eds.: C. G. Bruce, K. Helmut), 71–151.

[47] D. Astruc, C. Ornelas, J. Ruiz, Metallocenyl Dendrimers and their Applications in Molecular Electronics, Sensing, and Catalysis, *Accounts of Chemical Research* **2008**, *41*, 841–856.

[48] P. M. Kirchhoff, D. A. Tomalia, US4694064 Rod-Shaped Dendrimer, **1987**.

[49] W. Stocker, B. L. Schürmann, J. P. Rabe, S. Förster, P. Lindner, I. Neubert, A. D. Schlüter, A Dendritic Nanocylinder: Shape Control Through Implementation of Steric Strain, *Advanced Materials* **1998**, *10*, 793–797.

[50] Y. Guo, J. D. van Beek, B. Zhang, M. Colussi, P. Walde, A. Zhang, M. Kröger, A. Halperin, A Dieter Schlüter, Tuning Polymer Thickness: Synthesis and Scaling Theory of Homologous Series of Dendronized Polymers, *Journal of the American Chemical Society* **2009**, *131*, 11841–11854.

[51] M. Wintermantel, M. Gerle, K. Fischer, M. Schmidt, I. Wataoka, H. Urakawa, K. Kajiwara, Y. Tsukahara, Molecular Bottlebrushes, *Macromolecules* **1996**, *29*, 978–983.

[52] O. Kratky, G. Porod, Röntgenuntersuchung gelöster Fadenmoleküle, *Recueil des Travaux Chimiques des Pays-Bas* **1949**, *68*, 1106–1122.

[53] A. D. Schlüter, J. P. Rabe, Dendronized Polymers: Synthesis, Characterization, Assembly at Interfaces, and Manipulation, *Angewandte Chemie International Edition* **2000**, *39*, 864–883.

[54] A. D. Schlüter, A. Halperin, M. Kröger, D. Vlassopoulos, G. Wegner, B. Zhang, Dendronized Polymers: Molecular Objects between Conventional Linear Polymers and Colloidal Particles, *ACS Macro Letters* **2014**, 991–998.

[55] O. Bertran, B. Zhang, A. D. Schlüter, A. Halperin, M. Kroger, C. Aleman, Computer Simulation of Dendronized Polymers: Organization and Characterization at the Atomistic Level, *RSC Advances* **2013**, *3*, 126–140.

[56] H. Frauenrath, Dendronized Polymers - Building a New Bridge from Molecules to Nanoscopic Objects, *Progress in Polymer Science* **2005**, *30*, 325–384.

[57] B. Zhang, H. Yu, A. D. Schlüter, A. Halperin, M. Kröger, Synthetic Regimes due to Packing Constraints in Dendritic Molecules Confirmed by Labelling Experiments, *Nature Communications* **2013**, *4*, 1–9.

[58] V. Percec, C. H. Ahn, G Ungar, D. J. P. Yeardley, M. Moller, S. S. Sheiko, Controlling Polymer Shape Through the Self-Assembly of Dendritic Side-Groups, *Nature* **1998**, *391*, 161–164.

[59] S. Förster, I. Neubert, A. D. Schlüter, P. Lindner, How Dendrons Stiffen Polymer Chains: A SANS Study, *Macromolecules* **1999**, *32*, 4043–4049.

[60] S. Jahromi, J. H. M. Palmen, P. A. M. Steeman, Rheology of Side Chain Dendritic Polymers, *Macromolecules* **2000**, *33*, 577–581.

[61] E. Cordova-Mateo, O. Bertran, B. Zhang, D. Vlassopoulos, R. Pasquino, A. D. Schlüter, M. Kröger, C. Aleman, Interactions in Dendronized Polymers: Intramolecular Dominates Intermolecular, *Soft Matter* **2014**, *10*, 1032–1044.

[62] R. Pasquino, B. Zhang, R. Sigel, H. Yu, M. Ottiger, O. Bertran, C. Aleman, A. D. Schlüter, D. Vlassopoulos, Linear Viscoelastic Response of Dendronized Polymers, *Macromolecules* **2012**, *45*, 8813–8823.

[63] T.-L. Ho, M. Fieser, L. Fieser, L. F. Fieser, M. Fieser, T.-L. Ho in *Fieser and Fieser's Reagents for Organic Synthesis*, John Wiley & Sons, Inc., **2006**.

[64] A. Zhang, L. Wei, A. D. Schlüter, Narrowly Distributed Dendronized Polymethacrylates by Reversible Addition-Fragmentation Chain Transfer (RAFT) Polymerization, *Macromolecular Rapid Communications* **2004**, *25*, 799–803.

[65] T. Otsu, M. Yoshida, Role of Initiator-Transfer Agent-Terminator (Iniferter) in Radical Polymerizations: Polymer Design by Organic Disulfides as Iniferters, *Die Makromolekulare Chemie Rapid Communications* **1982**, *3*, 127–132.

[66] G. Moad, E. Rizzardo, D. H. Solomon, S. R. Johns, R. I. Willing, Application of 13C-Labelled Initiators and 13C NMR to the Study of the Kinetics and Efficiency of Initiation of Styrene Polymerization, *Die Makromolekulare Chemie Rapid Communications* **1984**, *5*, 793–798.

[67] G. Moad in *Controlled Radical Polymerization: Mechanisms*, ACS Symposium Series, American Chemical Society, **2015**, pp. 12–211.

[68] M. R. Hill, R. N. Carmean, B. S. Sumerlin, Expanding the Scope of RAFT Polymerization: Recent Advances and New Horizons, *Macromolecules* **2015**, *48*, 5459–5469.

[69] M. Yoshida, Z. M. Fresco, S. Ohnishi, J. M. J. Fréchet, Efficient Divergent Synthesis of Dendronized Polymers with Extremely High Molecular Weight: Structural Characterization by SEC-MALLS and SFM and Novel Organic Gelation Behavior, *Macromolecules* **2005**, *38*, 334–344.

[70] E. Kasëmi, W. Zhuang, J. P. Rabe, K. Fischer, M. Schmidt, M. Colussi, H. Keul, D. Yi, H. Cölfen, A. D. Schlüter, Synthesis of an Anionically Chargeable, High-Molar-Mass, Second-Generation Dendronized Polymer and the Observation of Branching by Scanning Force Microscopy, *Journal of the American Chemical Society* **2006**, *128*, 5091–5099.

[71] A. Zhang, B. Zhang, E. Wächtersbach, M. Schmidt, A. D. Schlüter, Efficient Synthesis of High Molar Mass, First- to Fourth-Generation Distributed Dendronized Polymers by the Macromonomer Approach, *Chemistry – A European Journal* **2003**, *9*, 6083–6092.

[72] Y. Chujo, H. Matsuki, S. Kure, T. Saegusa, T. Yazawa, Control of Pore Size of Porous Silica by Means of Pyrolysis of an Organic-Inorganic Polymer Hybrid, *Journal of the Chemical Society Chemical Communications* **1994**, 635–636.

[73] J. Iyer, K. Fleming, P. T. Hammond, Synthesis and Solution Properties of New Linear-Dendritic Diblock Copolymers, *Macromolecules* **1998**, *31*, 8757–8765.

[74] J. L. Mynar, T.-L. Choi, M. Yoshida, V. Kim, C. J. Hawker, J. M. J. Frechet, Doubly-Dendronized Linear Polymers, *Chemical Communications* **2005**, 5169–5171.

[75] K. L. Wooley, C. J. Hawker, J. M. J. Frechet, Hyperbranched Macromolecules via a Novel Double-Stage Convergent Growth Approach, *Journal of the American Chemical Society* **1991**, *113*, 4252–4261.

[76] Z.-B. Zhang, Y.-H. Teng, W. Freas, D. K. Mohanty, Unimolecular Amphiphilic Nanocontainers Based on Dendronized Linear Polymers, *Macromolecular Rapid Communications* **2006**, *27*, 626–630.

[77] B. Zhang, A. Schlüter, Non-Charged, Water Soluble Dendronized Polymers, *New Journal of Chemistry* **2012**, *36*, 414–418.

[78] W. Li, X. Zhang, X. Zhao, X. Zhang, A. Zhang, Doubly Dendronized Chiral Polymers Showing Thermoresponsive Properties, *Journal of Polymer Science Part A: Polymer Chemistry* **2013**, *51*, 5143–5152.

[79] K. H. Khayat, Viscosity-Enhancing Admixtures for Cement-Based Materials - An Overview, *Cement and Concrete Composites* **1998**, *20*, 171–188.

[80] A. Nussinovitch, *Water-Soluble Polymer Applications in Foods*, Blackwell Science Ltd, **2003**.

[81] J. Kopeček, Polymer-Drug Conjugates: Origins, Progress to Date and Future Directions, *Advanced Drug Delivery Reviews* **2013**, *65*, 49–59.

[82] W. Li, A. Zhang in *Encyclopedia of Polymer Science and Technology*, John Wiley & Sons, Inc., **2002**.

[83] S. Müller, A. D. Schlüter, Synthesis of Water-Soluble, Multiple Functionalizable Dendrons for the Conversion of Large Dendrimers or Other Molecular Objects into Potential Drug Carriers, *Chemistry – A European Journal* **2005**, *11*, 5589–5610.

[84] W. Li, A. Zhang, K. Feldman, P. Walde, A. D. Schlüter, Thermoresponsive Dendronized Polymers, *Macromolecules* **2008**, *41*, 3659–3667.

[85] M. J. N. Junk, W. Li, A. D. Schlüter, G. Wegner, H. W. Spiess, A. Zhang, D. Hinderberger, EPR Spectroscopic Characterization of Local Nanoscopic Heterogeneities during the Thermal Collapse of Thermoresponsive Dendronized Polymers, *Angewandte Chemie International Edition* **2010**, *49*, 5683–5687.

[86] J. Roeser, F. Moingeon, B. Heinrich, P. Masson, F. Arnaud-Neu, M. Rawiso, S. Méry, Dendronized Polymers with Peripheral Oligo(ethylene oxide) Chains: Thermoresponsive Behavior and Shape Anisotropy in Solution, *Macromolecules* **2011**, *44*, 8925–8935.

[87] J. Mei, Z. Bao, Side Chain Engineering in Solution-Processable Conjugated Polymers, *Chemistry of Materials* **2013**, *26*, 604–615.

[88] H. Nemoto, J. G. Wilson, H. Nakamura, Y. Yamamoto, Polyols of a Cascade Type as a Water-Solubilizing Element of Carborane Derivatives for Boron Neutron Capture Therapy, *The Journal of Organic Chemistry* **1992**, *57*, 435.

[89] H. Nemoto, M. Kamiya, Y. Minami, T. Araki, T. Kawamura, Synthesis of Branched Heptaglycerol Bearing Eight Hydroxyl Groups with Four Cyclic Protecting Groups, EN, *Synlett* **2007**, *2007*, 2091–2095.

[90] H. Nemoto, T. Araki, M. Kamiya, T. Kawamura, T. Hino, A Quantitative Investigation of the Water-Solubilizing Properties of Branched Oligoglycerols, *European Journal of Organic Chemistry* **2007**, *2007*, 3003–3011.

[91] H. Nemoto, M. Kamiya, A. Nakamoto, A. Katagiri, K. Yoshitomi, T. Kawamura, H. Hattori, An Efficient and Practical Method for the Preparation of a Branched Oligoglycerol with Acetonide Protection Groups, *Chemistry Letters* **2010**, *39*, 856–857.

[92] H. Nemoto, A. Katagiri, M. Kamiya, T. Kawamura, T. Matsushita, K. Matsumura, T. Itou, H. Hattori, M. Tamaki, K. Ishizawa, L. Miyamoto, S. Abe, K. Tsuchiya, Synthesis of Paclitaxel-BGL Conjugates, *Bioorganic & Medicinal Chemistry* **2012**, *20*, 5559–5567.

[93] S. Cassel, C. Debaig, T. Benvegnu, P. Chaimbault, M. Lafosse, D. Plusquellec, P. Rollin, Original Synthesis of Linear, Branched and Cyclic Oligoglycerol Standards, *European Journal of Organic Chemistry* **2001**, *2001*, 875–896.

[94] M. Calderón, M. A. Quadir, S. K. Sharma, R. Haag, Dendritic Polyglycerols for Biomedical Applications, *Advanced Materials* **2010**, *22*, 190–218.

[95] B. S. Murray, A. W. Jackson, C. S. Mahon, D. A. Fulton, Reactive Thermoresponsive Copolymer Scaffolds, *Chemical Communications* **2010**, *46*, 8651–8653.

[96] M. A. Ward, T. K. Georgiou, Thermoresponsive Terpolymers Based on Methacrylate Monomers: Effect of Architecture and Composition, *Journal of Polymer Science Part A: Polymer Chemistry* **2010**, *48*, 775–783.

[97] Y.-Z. You, C.-Y. Hong, C.-Y. Pan, P.-H. Wang, Synthesis of a Dendritic Core-Shell Nanostructure with a Temperature-Sensitive Shell, *Advanced Materials* **2004**, *16*, 1953–1957.

[98] T. Martinu, W. P. Dailey, Facile One-Pot Preparation of 3-Chloro-2-(chloromethyl) propene and an ab Initio Study of the Deamination Reaction of Nitrosoaziridine, *The Journal of Organic Chemistry* **2000**, *65*, 6784–6786.

[99] X. Sun, J.-P. Lindner, B. Bruchmann, A. D. Schlüter, Synthesis of Neutral, Water-Soluble Oligo-Ethylene Glycol-Containing Dendronized Homo- and Copolymers of Generations 1, 1.5, 2, and 3, *Macromolecules* **2014**, *47*, 7337–7346.

[100] W. Zhuang, E. Kasëmi, Y. Ding, M. Kröger, A. D. Schlüter, J. P. Rabe, Self-Folding of Charged Single Dendronized Polymers, *Advanced Materials* **2008**, *20*, 3204–3210.

[101] Y. Ding, H. C. Öttinger, A. D. Schlüter, M. Kröger, From Atomistic Simulation to the Dynamics, Structure and Helical Network Formation of Dendronized Polymers: The Janus Chain Model, *The Journal of Chemical Physics* **2007**, *127*.

[102] M. Kroger, O. Peleg, Y. Ding, Y. Rabin, Formation of Double Helical and Filamentous Structures in Models of Physical and Chemical Gels, *Soft Matter* **2008**, *4*, 18–28.

[103] H. Yu, A. D. Schlüter, B. Zhang, Synthesis of Dendronized Polymers by a n + 2 Approach, *Macromolecules* **2012**, *45*, 8555–8560.

[104] L. Brunsveld, B. J. B. Folmer, E. W. Meijer, R. P. Sijbesma, Supramolecular Polymers, *Chemical Reviews* **2001**, *101*, 4071–4098.

[105] C. Tang, E. M. Lennon, G. H. Fredrickson, E. J. Kramer, C. J. Hawker, Evolution of Block Copolymer Lithography to Highly Ordered Square Arrays, *Science* **2008**, *322*, 429–432.

[106] H. Zeng, X. Yang, A. L. Brown, S. Martinovic, R. D. Smith, B. Gong, An Extremely Stable, Self-Complementary Hydrogen-Bonded Duplex, *Chemical Communications* **2003**, 1556–1557.

[107] R. P. Sijbesma, F. H. Beijer, L. Brunsveld, B. J. B. Folmer, J. H.K. K. Hirschberg, R. F. M. Lange, J. K. L. Lowe, E. W. Meijer, Reversible Polymers Formed from Self-Complementary Monomers Using Quadruple Hydrogen Bonding, *Science* **1997**, *278*, 1601–1604.

[108] B. J. B. Folmer, R. P. Sijbesma, R. M. Versteegen, J. A. J. van der Rijt, E. W. Meijer, Supramolecular Polymer Materials: Chain Extension of Telechelic Polymers Using a Reactive Hydrogen-Bonding Synthon, *Advanced Materials* **2000**, *12*, 874–878.

[109] D. J. M. van Beek, A. J. H. Spiering, G. W. M. Peters, K. te Nijenhuis, R. P. Sijbesma, Unidirectional Dimerization and Stacking of Ureidopyrimidinone End Groups in Polycaprolactone Supramolecular Polymers, *Macromolecules* **2007**, *40*, 8464–8475.

[110] N. E. Botterhuis, D. J. M. van Beek, G. M. L. van Gemert, A. W. Bosman, R. P. Sijbesma, Self-Assembly and Morphology of Polydimethylsiloxane Supramolecular Thermoplastic Elastomers, *Journal of Polymer Science Part A: Polymer Chemistry* **2008**, *46*, 3877–3885.

[111] S. H. M. Söntjens, R. P. Sijbesma, M. H. P. van Genderen, E. W. Meijer, Stability and Lifetime of Quadruply Hydrogen Bonded 2-Ureido-4[1H]-pyrimidinone Dimers, *Journal of the American Chemical Society* **2000**, *122*, 7487–7493.

[112] T. F. A. de Greef, M. M. L. Nieuwenhuizen, R. P. Sijbesma, E. W. Meijer, Competitive Intramolecular Hydrogen Bonding in Oligo(ethylene oxide) Substituted Quadruple Hydrogen Bonded Systems, *The Journal of Organic Chemistry* **2010**, *75*, 598–610.

[113] M. G. McKee, C. L. Elkins, T. Park, T. E. Long, Influence of Random Branching on Multiple Hydrogen Bonding in Poly(alkyl methacrylate)s, *Macromolecules* **2005**, *38*, 6015–6023.

[114] K. E. Feldman, M. J. Kade, E. W. Meijer, C. J. Hawker, E. J. Kramer, Model Transient Networks from Strongly Hydrogen-Bonded Polymers, *Macromolecules* **2009**, *42*, 9072–9081.

[115] K. Yamauchi, J. R. Lizotte, T. E. Long, Thermoreversible Poly(alkyl acrylates) Consisting of Self-Complementary Multiple Hydrogen Bonding, *Macromolecules* **2003**, *36*, 1083–1088.

[116] C. L. Elkins, T. Park, M. G. McKee, T. E. Long, Synthesis and Characterization of Poly(2-Ethylhexyl Methacrylate) Copolymers Containing Pendant, Self-Complementary Multiple-Hydrogen-Bonding Sites, *Journal of Polymer Science Part A: Polymer Chemistry* **2005**, *43*, 4618–4631.

[117] R. Klopsch, S. Koch, A. D. Schlüter, Amino-Functionalized, Second-Generation Dendritic Building Blocks, *European Journal of Organic Chemistry* **1998**, *1998*, 1275–1283.

[118] M. B. Steffensen, E. E. Simanek, Synthesis and Manipulation of Orthogonally Protected Dendrimers: Building Blocks for Library Synthesis, *Angewandte Chemie International Edition* **2004**, *43*, 5178–5180.

[119] R. Al-Hellani, A. D. Schlüter, A Series of First- and Second-Generation Dendronized Polymers with Orthogonally Protected Amine Groups in the Periphery, *Macromolecules* **2006**, *39*, 8943–8951.

[120] R. Al-Hellani, A. D. Schlüter, On the Synthesis and Selective Deprotection of Low-Generation Dendrons with Orthogonally Protected Peripheral Amine Groups and a Possible Impact of the Deprotection Conditions on the Stability of Dendronized Polymers' Skeletons, *Helvetica Chimica Acta* **2006**, *89*, 2745–2763.

[121] K. D. Stigers, M. R. Koutroulis, D. M. Chung, J. S. Nowick, Fmoc Star: A More Soluble Analogue of the 9-Fluorenylmethoxycarbonyl Protecting Group, *The Journal of Organic Chemistry* **2000**, *65*, 3858–3860.

[122] R. Chinchilla, D. J. Dodsworth, C. Nájera, J. M. Soriano, 2,7-Di-tert-butyl-Fmoc-P-OSu: A New Polymer-Supported Reagent for the Protection of the Amino Group, *Bioorganic & Medicinal Chemistry Letters* **2002**, *12*, 1817–1820.

[123] P. G. M. Wuts, T. W. Greene in *Greene's Protective Groups in Organic Synthesis*, John Wiley & Sons, Inc., **2006**, pp. 696–926.

[124] R. Al-Hellani, J. Barner, J. P. Rabe, A. D. Schlüter, Covalent Connection of Individualized, Neutral, Dendronized Polymers on a Solid Substrate Using a Scanning Force Microscope, *Chemistry – A European Journal* **2006**, *12*, 6542–6551.

[125] P. J. Kocienski, *Protecting Groups*, *Vol. 337*, 3rd, Thieme Verlag, New York, **1995**, p. 202.

[126] J. S. Nowick, P. Ballester, F. Ebmeyer, J. Rebek, Convergent Functional Groups. 9. Complexation in New Molecular Clefts, *Journal of the American Chemical Society* **1990**, *112*, 8902–8906.

[127] J. M. Chong, G. Lajoie, M. W. Tjepkema, An Expedient Preparation of 9-Fluorenylmethanol, EN, *Synthesis* **1992**, *1992*, 819–820.

[128] C. G. Bochet, Photolabile Protecting Groups and Linkers, *Journal of the Chemical Society Perkin Transactions 1* **2002**, 125–142.

[129] J. H. Clark, Green Chemistry: Challenges and Opportunities, *Green Chemistry* **1999**, *1*, 1–8.

[130] V. Hagen, B. Dekowski, N. Kotzur, R. Lechler, B. Wiesner, B. Briand, M. Beyermann, {7-[Bis(carboxymethyl)amino]coumarin-4-yl}methoxycarbonyl Derivatives

for Photorelease of Carboxylic Acids, Alcohols/Phenols, Thioalcohols/Thiophenols, and Amines, *Chemistry – A European Journal* **2008**, *14*, 1621–1627.

[131] J.-M. Kim, T.-E. Chang, R. H. Park, D. J. Kim, D. K. Han, K.-D. Ahn, Generation of Patterned Color Images in Polymer Film with Photogenerated Base, *Chemistry Letters* **2000**, *29*, 712–713.

[132] C. G. Bochet, Wavelength-Selective Cleavage of Photolabile Protecting Groups, *Tetrahedron Letters* **2000**, *41*, 6341–6346.

[133] C. G. Bochet, Orthogonal Photolysis of Protecting Groups, *Angewandte Chemie International Edition* **2001**, *40*, 2071–2073.

[134] J. F. Cameron, C. G. Willson, J. M. J. Frechet, New Photolabile Amino Protecting Groups: Photogeneration of Amines from [(3[Prime or Minute],5[Prime or Minute]-Dimethoxybenzoinyl)oxy]carbonyl Carbamates, *Journal of the Chemical Society Chemical Communications* **1995**, 923–924.

[135] J. F. Cameron, C. G. Willson, J. M. J. Fréchet, Photogeneration of Amines from α-Keto Carbamates: Photochemical Studies, *Journal of the American Chemical Society* **1996**, *118*, 12925–12937.

[136] G. Papageorgiou, J. E. T. Corrie, Synthesis and Properties of Carbamoyl Derivatives of Photolabile Benzoins, *Tetrahedron* **1997**, *53*, 3917–3932.

[137] A. Patchornik, B Amit, R. B. Woodward, Photosensitive Protecting Groups, *Journal of the American Chemical Society* **1970**, *92*, 6333–6335.

[138] J. F. Cameron, J. M. J. Frechet, Photogeneration of Organic Bases from o-Nitrobenzyl-Derived Carbamates, *Journal of the American Chemical Society* **1991**, *113*, 4303–4313.

[139] J. E. Beecher, J. F. Cameron, J. M. J. Frechet, Photogeneration of Polymeric Amines: Synthesis, Photocrosslinking and Photoimaging of Copolymers Containing Photoactive Carbamate Pendant Groups, *Journal of Materials Chemistry* **1992**, *2*, 811–816.

[140] G. Bucher, J. C. Scaiano, R Sinta, G Barclay, J Cameron, Laser Flash Photolysis of Carbamates Derived from 9-Fluorenone Oxime, *Journal of the American Chemical Society* **1995**, *117*, 3848–3855.

[141] B. Wang, A. Zheng, A Photo-Sensitive Protecting Group for Amines Based on Coumarin Chemistry, *Chemical & Pharmaceutical Bulletin* **1997**, *45*, 715–718.

[142] B. Schade, V. Hagen, R. Schmidt, R. Herbrich, E. Krause, T. Eckardt, J. Bendig, Deactivation Behavior and Excited-State Properties of (Coumarin-4-yl)methyl Derivatives. 1. Photocleavage of (7-Methoxycoumarin-4-yl)methyl-Caged Acids with Fluorescence Enhancement, *The Journal of Organic Chemistry* **1999**, *64*, 9109–9117.

[143] R. Schmidt, D. Geissler, V. Hagen, J. Bendig, Mechanism of Photocleavage of (Coumarin-4-yl)methyl Esters, *The Journal of Physical Chemistry A* **2007**, *111*, 5768–5774.

[144] R. S. Givens, M. Rubina, J. Wirz, Applications of p-Hydroxyphenacyl (pHP) and Coumarin-4-ylmethyl Photoremovable Protecting Groups, *Photochemical & Photobiological Sciences* **2012**, *11*, 472–488.

[145] A. P. Pelliccioli, J. Wirz, Photoremovable Protecting Groups: Reaction Mechanisms and Applications, *Photochemical & Photobiological Sciences* **2002**, *1*, 441–458.

[146] S. P. Fodor, J. L. Read, M. C. Pirrung, L Stryer, A. T. Lu, D Solas, Light-Directed, Spatially Addressable Parallel Chemical Synthesis, *Science* **1991**, *251*, 767–773.

[147] Q. Huang, T. Liu, C. Bao, Q. Lin, M. Ma, L. Zhu, Light and Reductive Dual Stimuli-Responsive PEI Nanoparticles: "AND" Logic Response and Controllable Release, *Journal of Materials Chemistry B* **2014**, *2*, 3333–3339.

[148] M. Naoki, Y. Satoshi, Y. Ayako, N. Tatsuo, EP1559715 (A1) N-{2-Chloro-4-[(6,7-dimethoxy-4- quinolyl)oxy]phenyl}-N'-(5-methyl-3-isoxazolyl)Urea Salt in Crystalline Form, **2005**.

[149] H. Sun, A. E. Kaifer, Unsymmetric Dendrimers Containing a Single Ureidopyrimidine Unit: Generation-Dependent Dimerization via Hydrogen Bonding, *Organic Letters* **2005**, *7*, 3845–3848.

[150] E. Reichmanis, B. C. Smith, R. Gooden, O-Nitrobenzyl Photochemistry: Solution vs. Solid-State Behavior, *Journal of Polymer Science: Polymer Chemistry Edition* **1985**, *23*, 1–8.

[151] M. E. Lee, E. Gungor, A. M. Armani, Photocleavage of Poly(methyl acrylate) with Centrally Located o-Nitrobenzyl Moiety: Influence of Environment on Kinetics, *Macromolecules* **2015**, *48*, 8746–8751.

[152] T. Nowicka-Jankowska, Some Properties of Isosbestic Points, *Journal of Inorganic and Nuclear Chemistry* **1971**, *33*, 2043–2050.

[153] A. D. Mcnaught, A Wilkinson, *IUPAC. Compendium of Chemical Terminology (the "Gold Book")*, 2nd Revise, Blackwell Scientific Publications, Oxford, **1997**.

[154] B. S. Berlett, R. L. Levine, E. R. Stadtman, Use of Isosbestic Point Wavelength Shifts to Estimate the Fraction of a Precursor That Is Converted to a Given Product, *Analytical Biochemistry* **2000**, *287*, 329–333.

[155] D. Klinger, K. Landfester, Photo-Sensitive PMMA Microgels: Light-Triggered Swelling and Degradation, *Soft Matter* **2011**, *7*, 1426–1440.

[156] C. Reichardt in *Solvents and Solvent Effects in Organic Chemistry*, Wiley-VCH Verlag GmbH & Co. KGaA, **2004**, pp. 329–388.

[157] C.-H. Wong, H.-F. Chow, S.-K. Hui, K.-H. Sze, Generation-Independent Dimerization Behavior of Quadruple Hydrogen-Bond-Containing Oligoether Dendrons, *Organic Letters* **2006**, *8*, 1811–1814.

[158] F. H. Beijer, R. P. Sijbesma, H. Kooijman, A. L. Spek, E. W. Meijer, Strong Dimerization of Ureidopyrimidones via Quadruple Hydrogen Bonding, *Journal of the American Chemical Society* **1998**, *120*, 6761–6769.

[159] M. V. Biyani, E. J. Foster, C. Weder, Light-Healable Supramolecular Nanocomposites Based on Modified Cellulose Nanocrystals, *ACS Macro Letters* **2013**, *2*, 236–240.

[160] J. R. McKee, J. Huokuna, L. Martikainen, M. Karesoja, A. Nykänen, E. Kontturi, H. Tenhu, J. Ruokolainen, O. Ikkala, Molecular Engineering of Fracture Energy Dissipating Sacrificial Bonds Into Cellulose Nanocrystal Nanocomposites, *Angewandte Chemie International Edition* **2014**, *53*, 5049–5053.

[161] M. Ouchi, N. Badi, J.-F. Lutz, M. Sawamoto, Single-Chain Technology Using Discrete Synthetic Macromolecules, *Nature Chemistry* **2011**, *3*, 917–924.

[162] O. Altintas, C. Barner-Kowollik, Single Chain Folding of Synthetic Polymers by Covalent and Non-Covalent Interactions: Current Status and Future Perspectives, *Macromolecular Rapid Communications* **2012**, *33*, 958–971.

[163] C. K. Lyon, A. Prasher, A. M. Hanlon, B. T. Tuten, C. A. Tooley, P. G. Frank, E. B. Berda, A Brief User's Guide to Single-Chain Nanoparticles, *Polymer Chemistry* **2015**, *6*, 181–197.

[164] M. Huo, N. Wang, T. Fang, M. Sun, Y. Wei, J. Yuan, Single-Chain Polymer Nanoparticles: Mimic the Proteins, *Polymer* **2015**, *66*, A11–A21.

[165] P. J. M. Stals, M. A. J. Gillissen, R. Nicolay, A. R. A. Palmans, E. W. Meijer, The Balance Between Intramolecular Hydrogen Bonding, Polymer Solubility and Rigidity in Single-Chain Polymeric Nanoparticles, *Polymer Chemistry* **2013**, *4*, 2584–2597.

[166] C.-C. Cheng, F.-C. Chang, H.-C. Yen, D.-J. Lee, C.-W. Chiu, Z. Xin, Supramolecular Assembly Mediates the Formation of Single-Chain Polymeric Nanoparticles, *ACS Macro Letters* **2015**, *4*, 1184–1188.

[167] C. Schick in *Polymer Science: A Comprehensive Reference*, Elsevier, Amsterdam, **2012**, pp. 793–823.

[168] E. S. Watson, M. J. O'Neill, J. Justin, N. Brenner, A Differential Scanning Calorimeter for Quantitative Differential Thermal Analysis, *Analytical Chemistry* **1964**, *36*, 1233–1238.

[169] M. J. Richardson, Thermal Analysis of Polymers Using Quantitative Differential Scanning Calorimetry, *Polymer Testing* **1984**, *4*, 101–115.

[170] Q. Zhu, J. Wu, C. Tu, Y. Shi, L. He, R. Wang, X. Zhu, D. Yan, Role of Branching Architecture on the Glass Transition of Hyperbranched Polyethers, *The Journal of Physical Chemistry B* **2009**, *113*, 5777–5780.

[171] A. Sunder, T. Bauer, R. Mülhaupt, H. Frey, Synthesis and Thermal Behavior of Esterified Aliphatic Hyperbranched Polyether Polyols, *Macromolecules* **2000**, *33*, 1330–1337.

[172] H. Liu, C.-E. Wilén, Preparation and Glass Transition Temperature of Hyperbranched Poly[allyl methyl maleate-co-N-propyl maleimide], *Journal of Applied Polymer Science* **2005**, *97*, 1941–1947.

[173] M. Kröger, Simple Models for Complex Nonequilibrium Fluids, *Physics Reports* **2004**, *390*, 453–551.

[174] H. Stutz, The Glass Temperature of Dendritic Polymers, *Journal of Polymer Science Part B: Polymer Physics* **1995**, *33*, 333–340.

[175] X. Luo, S. Xie, J. Liu, H. Hu, J. Jiang, W. Huang, H. Gao, D. Zhou, Z. Lu, D. Yan, The Relationship Between the Degree of Branching and Glass Transition Temperature of Branched Polyethylene: Experiment and Simulation, *Polymer Chemistry* **2014**, *5*, 1305–1312.

[176] T. G. Fox, P. J. Flory, Second-Order Transition Temperatures and Related Properties of Polystyrene. I. Influence of Molecular Weight, *Journal of Applied Physics* **1950**, *21*, 581–591.

[177] Y. H. Kim, O. W. Webster, Hyperbranched Polyphenylenes, *Macromolecules* **1992**, *25*, 5561–5572.

[178] K. L. Wooley, C. J. Hawker, J. M. Pochan, J. M. J. Frechet, Physical Properties of Dendritic Macromolecules: A Study of Glass Transition Temperature, *Macromolecules* **1993**, *26*, 1514–1519.

[179] H. Liu, C.-E. Wilén, Extension of the Chain-End, Free-Volume Theory for Predicting Glass Temperature as a Function of Conversion in Hyperbranched Polymers Obtained Through One-Pot Approaches, *Journal of Polymer Science Part B: Polymer Physics* **2004**, *42*, 1235–1242.

[180] S. Costanzo, L. F. Scherz, G. Floudas, M. Kröger, T. Schweizer, A. D. Schlüter, D. Vlassopoulos, Rheology and Packing of Dendronized Polymers, *Macromolecules* **2016**, *49*, 7054–7068.

[181] C. J. Hawker, P. J. Farrington, M. E. Mackay, K. L. Wooley, J. M. J. Frechet, Molecular Ball Bearings: The Unusual Melt Viscosity Behavior of Dendritic Macromolecules, *Journal of the American Chemical Society* **1995**, *117*, 4409–4410.

[182] A. Kumar, S Ramakrishnan, Structural Variants of Hyperbranched Polyesters, *Macromolecules* **1996**, *29*, 2524–2530.

[183] M. Wang, D. Gan, K. L. Wooley, Linear and Hyperbranched Poly(silyl ester)s: Synthesis via Cross-Dehydrocoupling-Based Polymerization, Hydrolytic Degradation Properties, and Morphological Analysis by Atomic Force Microscopy, *Macromolecules* **2001**, *34*, 3215–3223.

[184] C. L. Lewis, K. Stewart, M. Anthamatten, The Influence of Hydrogen Bonding Side-Groups on Viscoelastic Behavior of Linear and Network Polymers, *Macromolecules* **2014**, *47*, 729–740.

[185] E. Penzel, J. Rieger, H. A. Schneider, The Glass Transition Temperature of Random Copolymers: 1. Experimental Data and the Gordon-Taylor Equation, *Polymer* **1997**, *38*, 325–337.

[186] A. W. Coats, J. P. Redfern, Thermogravimetric Analysis. A Review, *Analyst* **1963**, *88*, 906–924.

[187] L. Reich, D. W. Levi, Dynamic Thermogravimetric. Analysis in Polymer Degradation, *Journal of Polymer Science: Macromolecular Reviews* **1967**, *1*, 173–275.

[188] E. Ihms, D. Brinkman, Thermogravimetric Analysis as a Polymer Identification Technique in Forensic Applications BT - Thermogravimetric Analysis as a Polymer

Identification Technique in Forensic Applications, *Journal of Forensic Sciences* **2004**, *49*, 1–6.

[189] C. Capone, L. Di Landro, F. Inzoli, M. Penco, L. Sartore, Thermal and Mechanical Degradation During Polymer Extrusion Processing, *Polymer Engineering & Science* **2007**, *47*, 1813–1819.

[190] R. Agnaou, M. Capelot, S. Tencé-Girault, F. Tournilhac, L. Leibler, Supramolecular Thermoplastic with 0.5 Pa s Melt Viscosity, *Journal of the American Chemical Society* **2014**, *136*, 11268–11271.

[191] T. Kashiwagi, A. Inaba, J. E. Brown, K. Hatada, T. Kitayama, E. Masuda, Effects of Weak Linkages on the Thermal and Oxidative Degradation of Poly(methyl Methacrylates), *Macromolecules* **1986**, *19*, 2160–2168.

[192] A. Meisters, G. Moad, E. Rizzardo, D. H. Solomon, Thermal Stability of Poly(methyl methacrylate), *Polymer Bulletin* **1988**, *20*, 499–503.

[193] J. D. Peterson, S. Vyazovkin, C. A. Wight, Kinetic Study of Stabilizing Effect of Oxygen on Thermal Degradation of Poly(methyl methacrylate), *The Journal of Physical Chemistry B* **1999**, *103*, 8087–8092.

[194] F. S. Gibson, S. C. Bergmeier, H. Rapoport, Selective Removal of an N-BOC Protecting Group in the Presence of a tert-Butyl Ester and Other Acid-Sensitive Groups, *The Journal of Organic Chemistry* **1994**, *59*, 3216–3218.

[195] U. Boas, J. B. Christensen, P. M. H. Heegaard, Dendrimers: Design, Synthesis and Chemical Properties, *Journal of Materials Chemistry* **2006**, *16*, 3785–3798.

[196] D. A. Tomalia, J. B. Christensen, U. Boas, *Dendrimers, Dendrons, and Dendritic Polymers: Discovery, Applications, and the Future*, Cambridge University Press, Cambridge, **2012**.

[197] V. H. Rawal, M. P. Cava, Thermolytic Removal of t-Butyloxycarbonyl (BOC) Protecting Group on Indoles and Pyrroles, *Tetrahedron Letters* **1985**, *26*, 6141–6142.

[198] H. Yu, A. D. Schlüter, B. Zhang, Synthesis of High Generation Dendronized Polymers and Quantification of their Structure Perfection, *Macromolecules* **2014**, *47*, 4127–4135.

[199] C. Heinzmann, U. Salz, N. Moszner, G. L. Fiore, C. Weder, Supramolecular Cross-Links in Poly(alkyl methacrylate) Copolymers and Their Impact on the Mechanical and Reversible Adhesive Properties, *ACS Applied Materials & Interfaces* **2015**, *7*, 13395–13404.

[200] C. Heinzmann, I. Lamparth, K. Rist, N. Moszner, G. L. Fiore, C. Weder, Supramolecular Polymer Networks Made by Solvent-Free Copolymerization of a Liquid 2-Ureido-4[1H]-pyrimidinone Methacrylamide, *Macromolecules* **2015**, *48*, 8128–8136.

[201] G. Armstrong, M. Buggy, Thermal Stability of a Ureidopyrimidinone Model Compound, *Materials Science and Engineering: C* **2001**, *18*, 45–49.

[202] G. Armstrong, M. Buggy, Thermal Stability of Some Self-Assembling Hydrogen-Bonded Polymers and Related Model Complexes, *Polymer International* **2002**, *51*, 1219–1224.

[203] P. Sunthar in *Rheology of Complex Fluids*, (Eds.: M. J. Krishnan, P. A. Deshpande, S. P. B. Kumar), Springer New York, New York, NY, **2010**, pp. 171–191.

[204] F. Snijkers, H. Y. Cho, A. Nese, K. Matyjaszewski, W. Pyckhout-Hintzen, D. Vlassopoulos, Effects of Core Microstructure on Structure and Dynamics of Star Polymer Melts: From Polymeric to Colloidal Response, *Macromolecules* **2014**, *47*, 5347–5356.

[205] K. M. Kirkwood, L. G. Leal, D. Vlassopoulos, P. Driva, N. Hadjichristidis, Stress Relaxation of Comb Polymers with Short Branches, *Macromolecules* **2009**, *42*, 9592–9608.

[206] E. van Ruymbeke, M. Kapnistos, D. Vlassopoulos, T. Huang, D. M. Knauss, Linear Melt Rheology of Pom-Pom Polystyrenes with Unentangled Branches, *Macromolecules* **2007**, *40*, 1713–1719.

[207] J. H. Lee, L. J. Fetters, L. A. Archer, Stress Relaxation of Branched Polymers, *Macromolecules* **2005**, *38*, 10763–10771.

[208] I. M. Hodge, Physical Aging in Polymer Glasses, *Science* **1995**, *267*, 1945 LP – 1947.

[209] J. M. Dealy, R. G. Larson in *Structure and Rheology of Molten Polymers*, Carl Hanser Verlag GmbH & Co. KG, **2006**, pp. 91–130.

[210] S. Seiffert, J. Sprakel, Physical Chemistry of Supramolecular Polymer Networks, *Chemical Society Reviews* **2012**, *41*, 909–930.

[211] T. Pakula, Y. Zhang, K. Matyjaszewski, H.-i. Lee, H. Boerner, S. Qin, G. C. Berry, Molecular Brushes as Super-Soft Elastomers, *Polymer* **2006**, *47*, 7198–7206.

7 Abbreviations and symbols

List of abbreviations

AIBN	Azo*bis*isobutyronitrile
BGL	Branched glycerol
Boc	*tert*-Butyloxycarbonyl
Cbz	Benzyloxycarbonyl
CDB	Cumyl dithiobenzoate
CDI	1,1'-Carbonyldiimidazole
CPDB	2-(2-cyanopropyl) dithiobenzoate
CRP	Controlled radical polymerization
CuAAC	Copper-catalyzed azide-alkyne cycloaddition
d	Doublet
DCTB	Trans-2-[3-(4-t-butylphenyl)-2-methyl-2-propenylidene]malononitrile
1,3-DCPol	1,3-Dichloropropanol
1,3-DCPone	1,3-Dichloropropanone
DLS	Dynamic light scattering
4-DMAP	4-(Dimethylamino)-pyridine, N,N-Dimethylpyridin-4-amine
DMF	N,N-Dimethylformamide
DMSO	Dimethylsulfoxide
DP	Dendronized polymer
DSC	Differential scanning calorimetry
EA	Elemental analysis
ECH	Epichlorohydine
EDTA	Ethylenediaminetetraacetic acid
EGME	Ethylene glycol monomethyl ether, 2-Methoxyethanol
ESI	Electrospray ionization
ETH	Eidgenössische Technische Hochschule
FORTH	Foundation for Research & Technology – Hellas
Fmoc	9-Fluorenyloxycarbonyl
Fmoc*	2,7-Di(*tert*-butyl)-9-fluorenyloxycarbonyl
FRP	Free radical polymerization
FTICR	Fourier transform ion cyclotron resonance
FTIR	Fourier transform infrared (spectroscopy)
GPC	Gel permeation chromatography
3-HPA	3-Hydroxypropionaldehyde
IDT	Initial degradation temperature

IR	Infrared
LAH	Lithium aluminium hydride
LED	Light emitting diode
LOC	Laboratory of Organic Chemistry (ETH Zurich)
LS	Light scattering
LVE	Linear viscoelasticity
m	Multiplet
MAC	Methacryloyl chloride
MALDI	Matrix-assisted laser desorption/ionization
MALLS	Multi-angle laser light scattering
MBA	*mono*-bromoacetic acid
MCA	*mono*-chloroacetic acid
MD	Molecular dynamics
MDC	Methallyl dichloride, 3-Chloro-2-chloromethyl-1-propene
MeNVOC	*alpha*-Methyl-Nitroveratryloxycarbonyl
MS	Mass spectrometry
MW	Molecular weight
MWD	Molecular weight distribution ($M_\mathrm{w}/M_\mathrm{n}$)
Na-PFHA	Sodium perfluorohexanoic acid
NHS	N-Hydroxysuccinimide
NMR	Nuclear magnetic resonance
NOESY	Nuclear Overhauser Effect Spectroscopy
NVOC	6-Nitroveratryloxycarbonyl, 4,5-Dimethoxy-2-nitrobenzyl chloroformate
OEG	Oligo(ethylene glycol)
PEPDTA	1-phenylethyl phenyldithioacetate
PPPDTA	2-phenylprop-2-yl phenyldithioacetate
PDI	Polydispersity index
PHS	Poly(*p*-hydroxystyrene)
PIB	Poly(isobutylene)
PMMA	Poly(methyl methacrylate)
PPM	Post polymerization modification
PTFE	Poly(tetrafluorethylene)
q	Quartet
RAFT	Reversible addition–fragmentation chain transfer
RALS	Right-angle light scattering
RI	Refractive index
RT	Room temperature (22 °C)
s	Singlet
SCPNs	Single-chain polymeric nanoparticles
SD	Standard deviation
SEC	Size-exclusion chromatography
SEC-LS	Size-exclusion chromatography with on-line light-scattering

t	Triplett
TCE	1,1,2,2-Tetrachloroethane
TFA	Trifluoroacetic acid
TGA	Thermogravimetric analysis
THF	Tetrahydrofuran
TLC	Thin layer chromatography
TOF	Time of flight
TTS	Time-temperature superposition
TU	Technical university
UPy	2-Ureido-4[1H]-pyrimidinone
UV	Ultraviolet
UV-Vis	Ultraviolet-visible
WAXS	Wide-angle X-ray scattering
WLC	Worm-like chain (model)

List of symbols

α	observed mass loss in TGA	%
α^0	theoretical mass loss in TGA	%
β	Conversion of unphotolyzed starting material	%
c	Concentration	M
C_p	Heat capacity	$\mathrm{J\,K^{-1}}$
δ	Chemical shift	ppm
Δ	Difference	%
$\Delta_{\alpha^0-\alpha}$		%
D_h	Hydrodynamic diameter	nm
g	Polymer generation number	-
g_max	Maximum g for which structure perfection can be achieved	-
G'	Elastic modulus	Pa
G''	Viscous modulus	Pa
h	Planck constant ($6.626070040{\cdot}10^{-34}$)	J s
H	Enthalpy	$\mathrm{J\,kg^{-1}}$
I_Boc	integrated peak area in ^{1}H NMR at around 1.4 ppm	-
$I_{\alpha\text{-Me, t}}$	integrated peak area of α-methyl protons in ^{1}H NMR after time of irradiation t	-
I_UPy	integrated peak area in ^{1}H NMR at around 5.7 ppm	-
J	Coupling constant	Hz
k	Reaction rate constant	-
K	Equilibrium constant	-
λ	Wavelength	nm
λ_max	Emission wavelength maximum	nm
$[M]$	Monomer concentration	$\mathrm{mol\,L^{-1}}$
M_Boc	Molar mass of Boc group (100.12)	$\mathrm{g\,mol^{-1}}$
M_e	Entanglement molar mass	$\mathrm{g\,mol^{-1}}$, kDa
$M_{\mathrm{MG}g}$	Theoretical molar mass of the macromonomers	$\mathrm{g\,mol^{-1}}$
M_n	Number average molar mass	$\mathrm{g\,mol^{-1}}$, kDa
M_P	Peak molar mass	$\mathrm{g\,mol^{-1}}$, kDa
$M_\mathrm{r.u.}$	Molar mass per repeating unit	$\mathrm{g\,mol^{-1}}$
M_UPy	Molar mass of UPy group (125.13)	$\mathrm{g\,mol^{-1}}$
M_w	Weight average molar mass	$\mathrm{g\,mol^{-1}}$, kDa
N_Boc	Number of Boc groups per repeating unit	-
N_UPy	Number of UPy groups per repeating unit	-
ν	Frequency	Hz
P	Power	W
P_n	Number average degree of polymerization	-
ρ	Density	$\mathrm{g\,cm^{-3}}$
r	Monomer reactivity ratio	-

R^2	Correlation coefficient	-
R_f	Retention factor	-
t	Irradiation time	h
T_g	Glass transition temperature	°C
T_{ref}	Reference temperature	°C
ω	Angular frequency	rad s^{-1}
x	Feed ratio of macromonomer	-
$\chi_{\mathbf{4c},\,exp}$	Experimental molar fraction of UPy	mol %
$\chi_{\mathbf{4c},\,th}$	Theoretic molar fraction of UPy	mol %
χ_{UPy}	Molar fraction of UPy	mol %
X	Structure perfection (coverage) from UV-labeling	%
y	Feed ratio of macromonomer	-

8 Appendix

8.1 Supplementary DSC data

Table 8-1: Summary of the experimentally determined T_g values of "classic" **PG1 – 3** from DSC measurements.

		PG1		**PG2**		**PG3**	
Entry	P_n	T_g, °C	SD[a], °C	T_g, °C	SD[a], °C	T_g, °C	SD[a], °C
1	50	37.7	1.8	62.3	1.5	68.4	1.3
2	300	46.8	0.7	65.1	0.4	68.3	0.8
3	1000	51.9	1.7	67.8	1.6	69.4	1.9
4	1500	53.3	0.4	66.8	0.8	69.3	0.6
5	2000	53.8	1.2	67.0	1.8	68.7	1.0
6	3000	52.9	1.5	67.1	1.1	69.1	1.3

[a]Standard deviation of 3 individual measurements.

Table 8-2: Summary of the experimentally determined T_g values of hybrid **H[1+1]** and **H[1+2]** from DSC measurements.

		H[1+1]		**H[1+2]**	
Entry	P_n	T_g, °C	SD[a], °C	T_g, °C	SD[a], °C
1	50	-28.1	1.0	-48.3	1.8
2	300	-21.5	0.9	-46.8	0.7
3	1000	-20.8	1.5	-47.7	1.6
4	1500	-21.7	0.7	-46.6	1.0
5	2000	-23.2	1.9	-47.7	1.6
6	3000	-22.9	2.0	-47.3	1.6

[a]Standard deviation of 3 individual measurements.

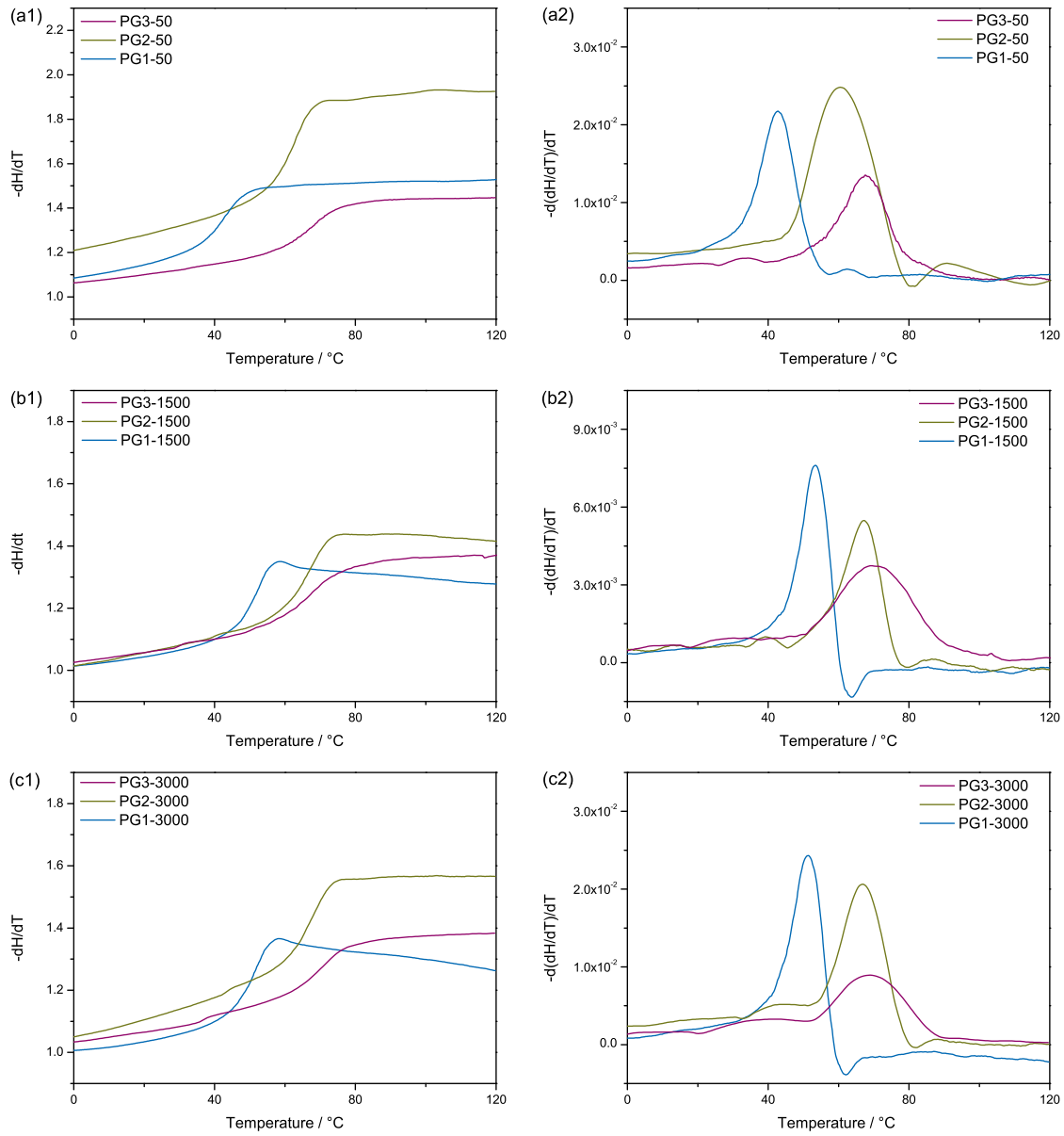

Figure 8-1: (**1**) Second heating DSC thermograms normalized by the sample weight and the initial heat flow at low temperature and (**2**) Differentiated DSC heat flow traces of "classic" **PG1 – 3** with (**a**) $P_n \approx 50$, (**b**) $P_n \approx 1500$, and (**c**) $P_n \approx 3000$. All measurements were performed from 0 – 120 °C at a heating rate of 10 °C min^{-1} in N_2.

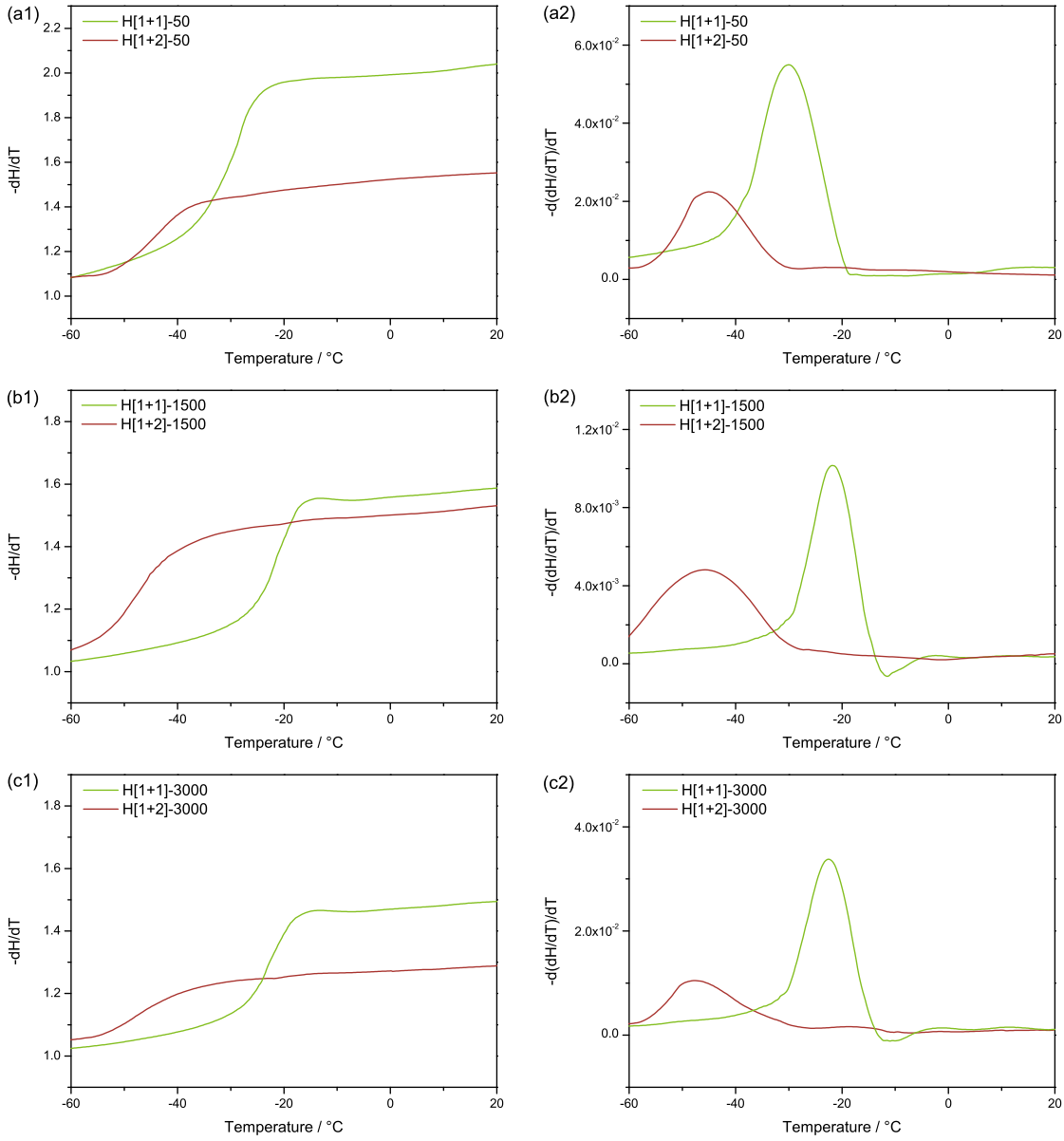

Figure 8-2: (**1**) Second heating DSC thermograms normalized by the sample weight and the initial heat flow at low temperature and (**2**) Differentiated DSC heat flow traces of "hybrid" **H[1+1]** and **H[1+2]** with (**a**) $P_n \approx 50$, (**b**) $P_n \approx 1500$, and (**c**) $P_n \approx 3000$. All measurements were performed from -60 – 20 °C at a heating rate of 10 °C min^{-1} in N_2.

Table 8-3: Summary of the experimentally determined T_g values of **PG1 – 3-UPy** with $P_n \approx 40$ from DSC measurements.

		PG1		**PG2**		**PG3**	
Entry	χ UPy, mol%	T_g, °C	SD[a], °C	T_g, °C	SD[a], °C	T_g, °C	SD[a], °C
1	0	37.7	±1.8	64.1	±0.7	69.4	±0.8
2	5	50.9	±2.9	67.5	±1.3	70.7	±0.5
3	10	53.6	±1.1	-	-	-	-
4	25	69.0	±0.8	74.5	±0.6	75.2	±0.7
5	33	94.4	±1.0	-	-	-	-
6	50	127.7	±1.7	92.4	±0.7	83.4	±0.7

[a]Standard deviation of 3 individual measurements.

Table 8-4: Summary of the experimentally determined T_g values of **PG1-UPy** containing 25 mol% UPy and different P_ns from DSC measurements.

			PG1	
Entry	Polymer	P_n	T_g, °C	SD[a], °C
1	PG1-UPy25a	130	80.0	±1.5
2	PG1-UPy25b	710	82.5	±1.1
3	PG1-UPy25c	1200	86.9	±0.5

[a]Standard deviation of 3 individual measurements.

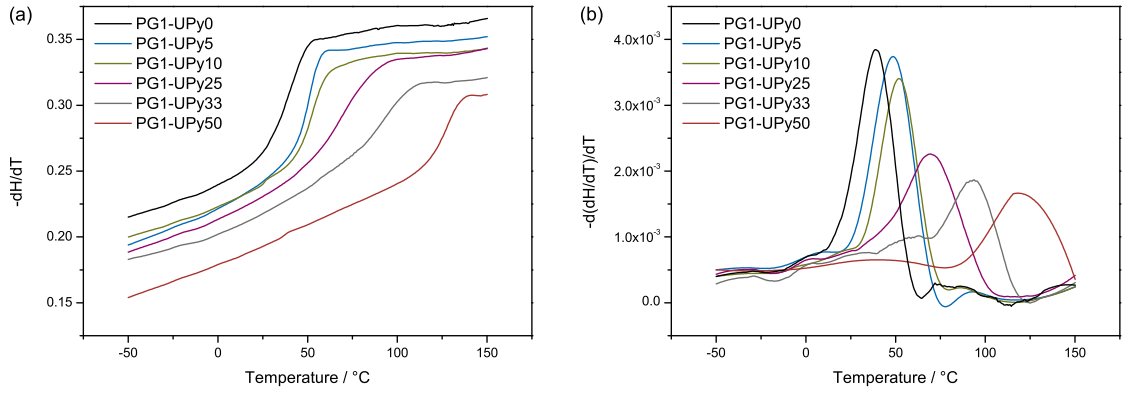

Figure 8-3: DSC measurements of the first-generation DPs containing 0 – 50 mol% UPy at the $g = 1$ level: (**a**) Second heating DSC thermograms normalized by the sample weight; (**b**) Differentiated DSC heat flow traces. All measurements were performed from −50 to 150 °C at a heating rate of 10 °C min^{-1} in N_2.

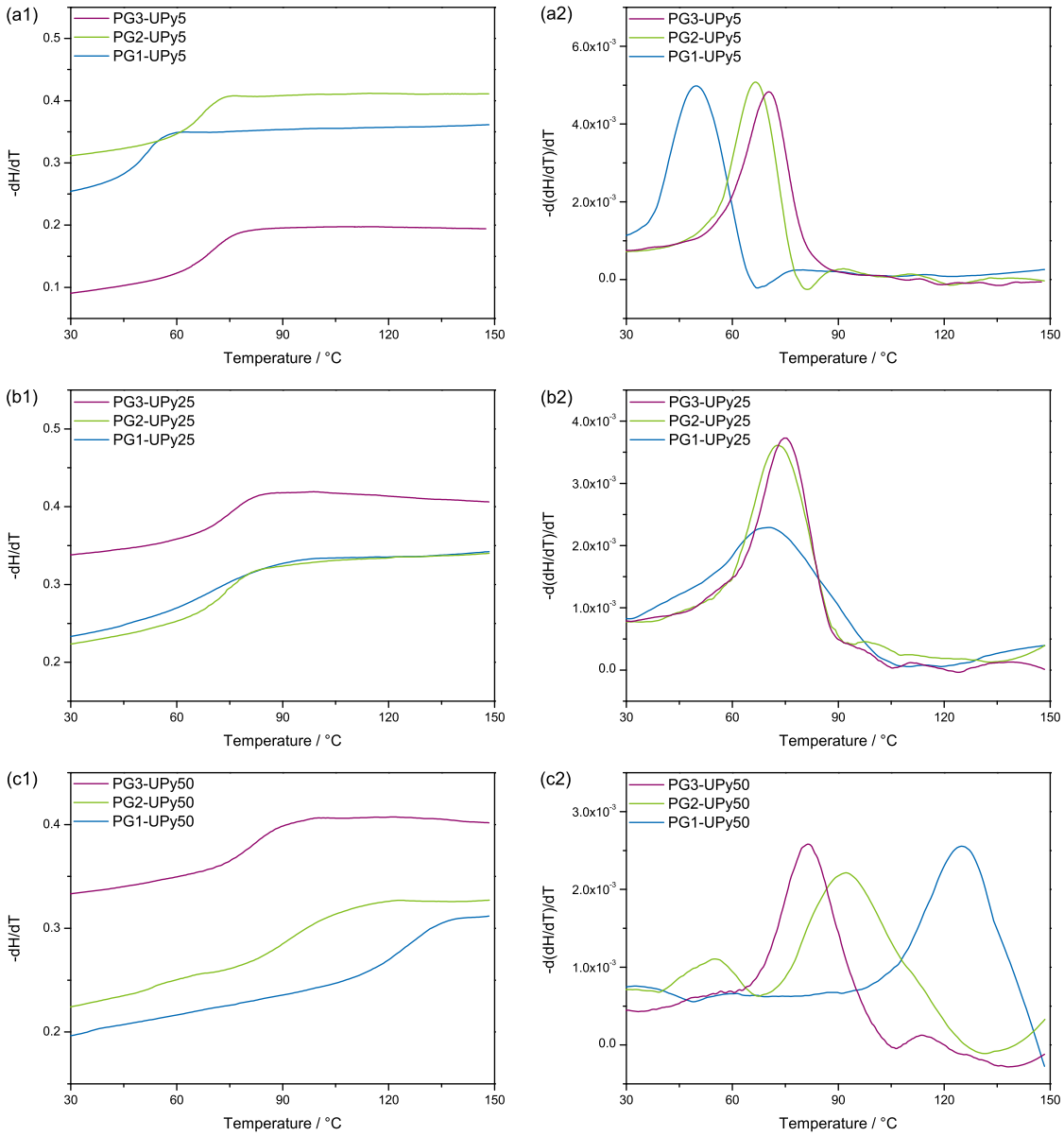

Figure 8-4: (**1**) Second heating DSC thermograms normalized by the sample weight and (**2**) Differentiated DSC heat flow traces of **PG*g*-UPy** with (**a**) 5 mol%, (**b**) 25 mol%, and (**c**) 50 mol% UPy at the $g = 1$ level. All measurements were performed from −30 to 150 °C at a heating rate of 10 °C min^{-1} in N_2.

8.2 Supplementary GPC traces

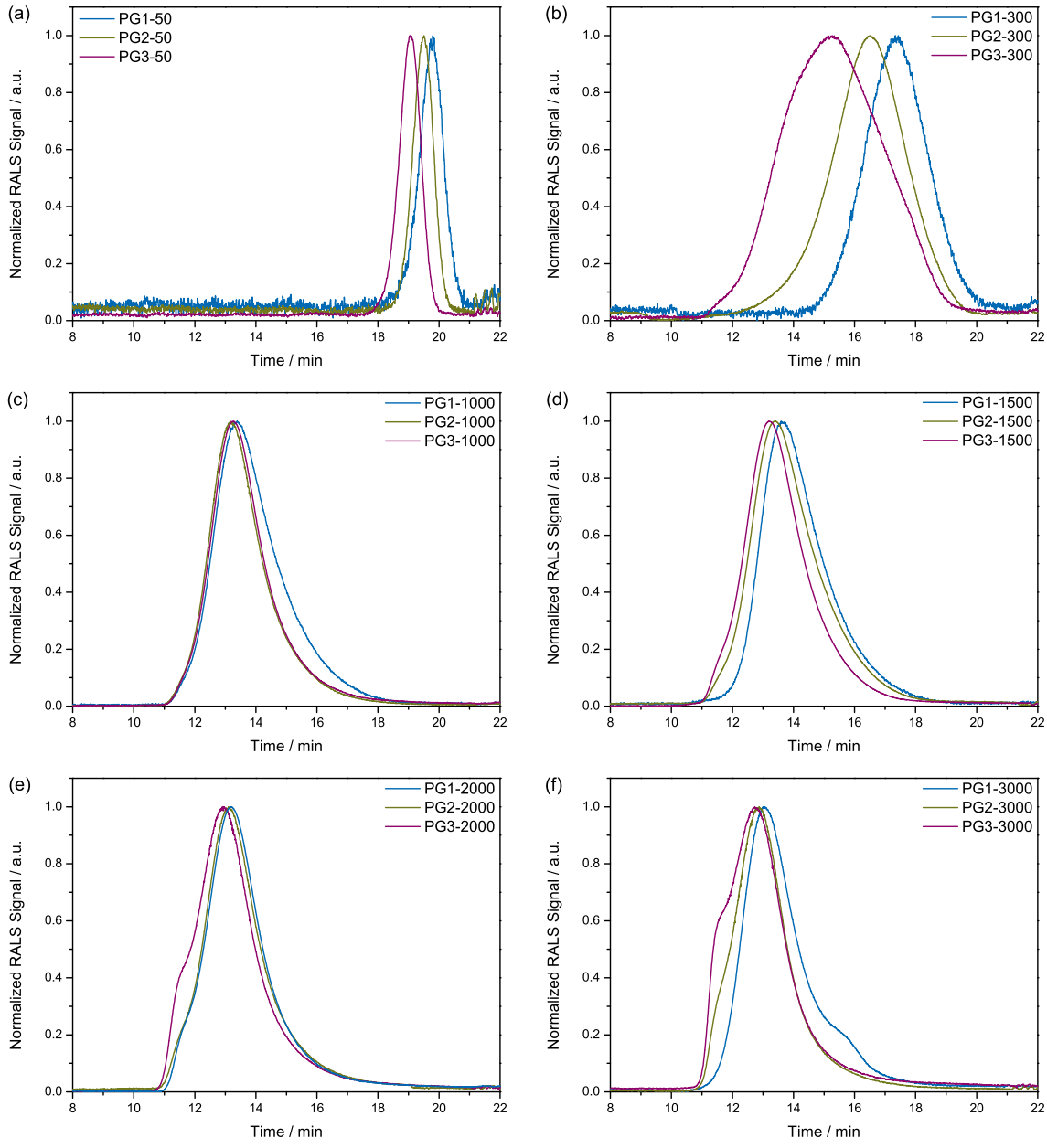

Figure 8-5: GPC elution traces of homologous "classic" **PG1 – 3** samples with (**a**) $P_n \approx 50$; (**b**) $P_n \approx 300$; (**c**) $P_n \approx 1000$; (**d**) $P_n \approx 1500$; (**e**) $P_n \approx 2000$; (**f**) $P_n \approx 3000$.

8.3 Supplementary NMR spectra

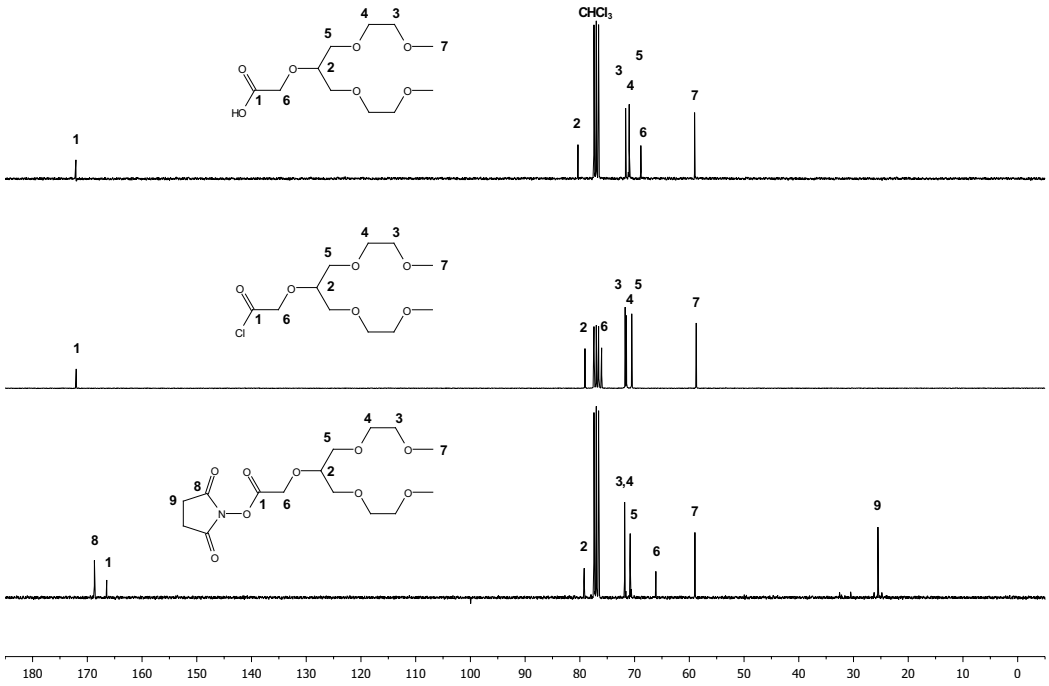

Figure 8-6: ^{13}C NMR spectra of compounds **2b** (top), **2c** (middle), and **2d** (bottom) recorded in $CDCl_3$ at 298 K.

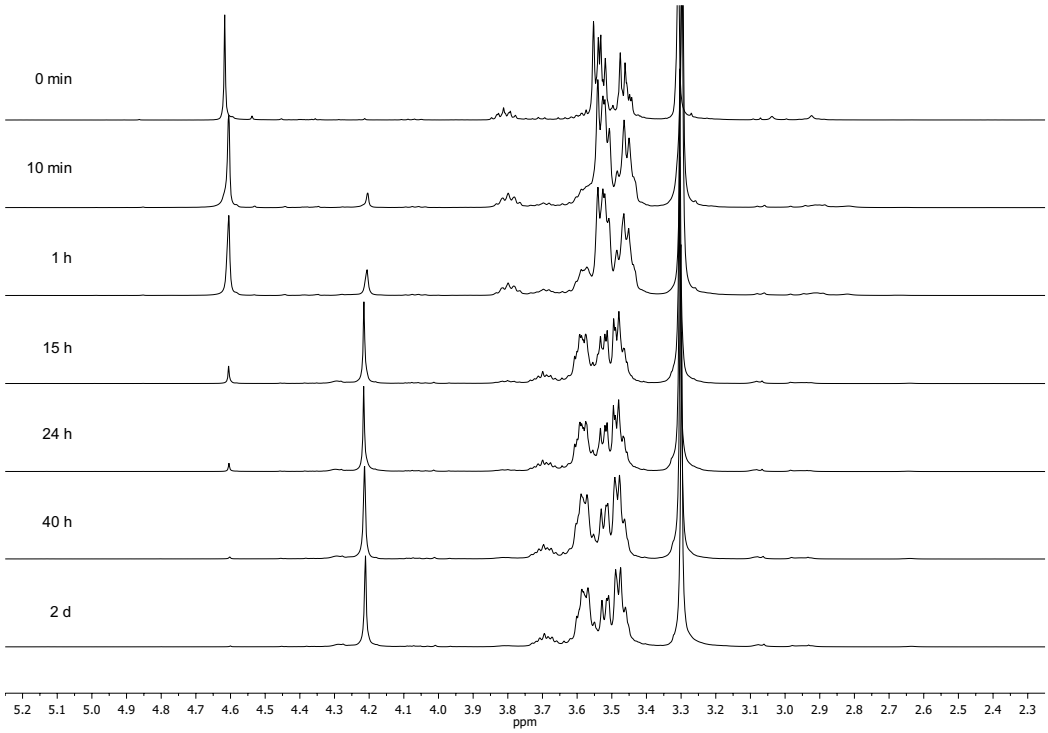

Figure 8-7: ^{1}H NMR spectra of compound **2c** recorded in $CDCl_3$ at 298 K after different exposure times to 10 vol% D_2O.

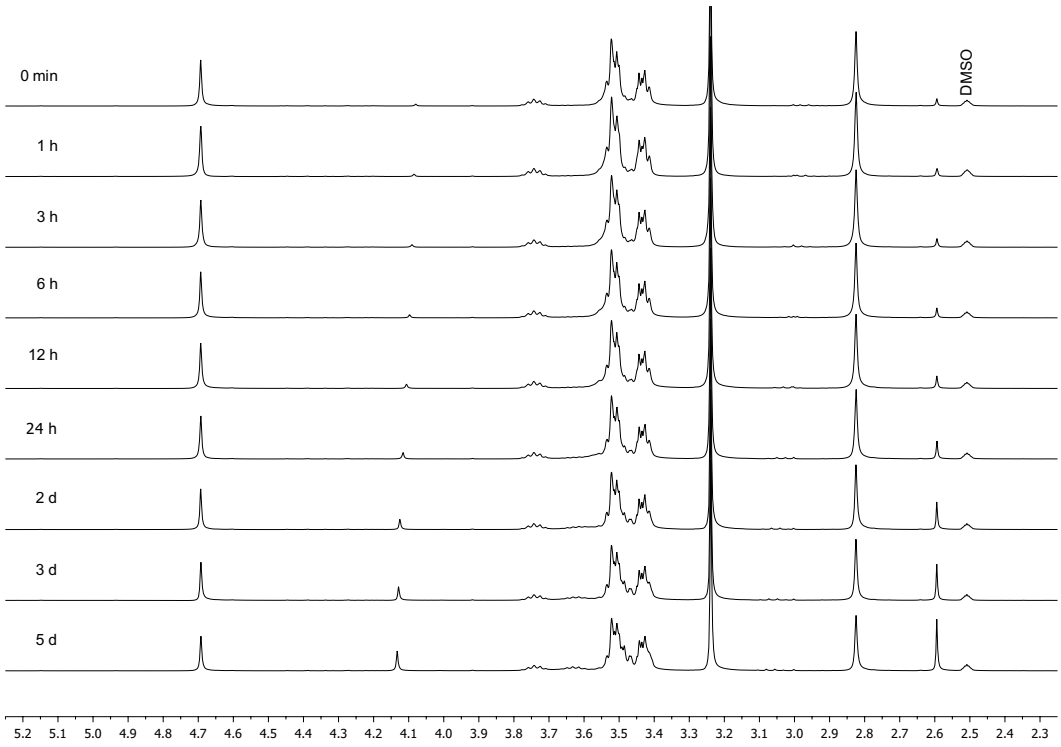

Figure 8-8: ^{1}H NMR spectrum of compound **2d** recorded in DMSO-d6 at 298 K after different exposure times to 10 vol% D_2O.

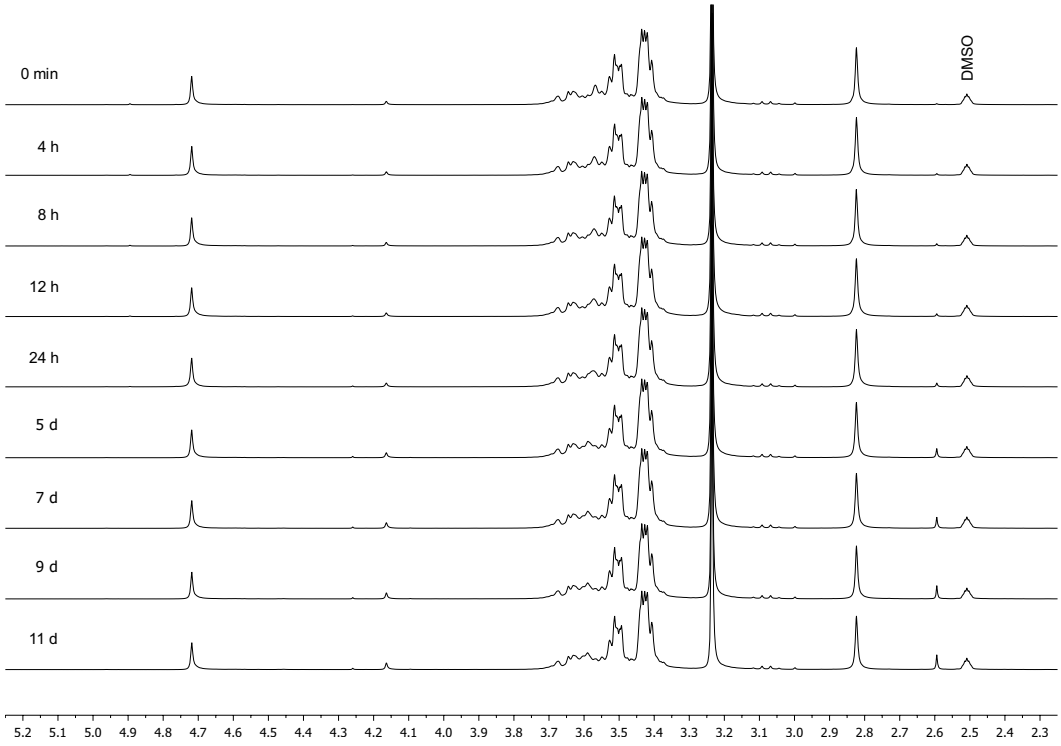

Figure 8-9: ^{1}H NMR spectrum of compound **3e** recorded in DMSO-d6 at 298 K after different exposure times to 10 vol% D_2O.

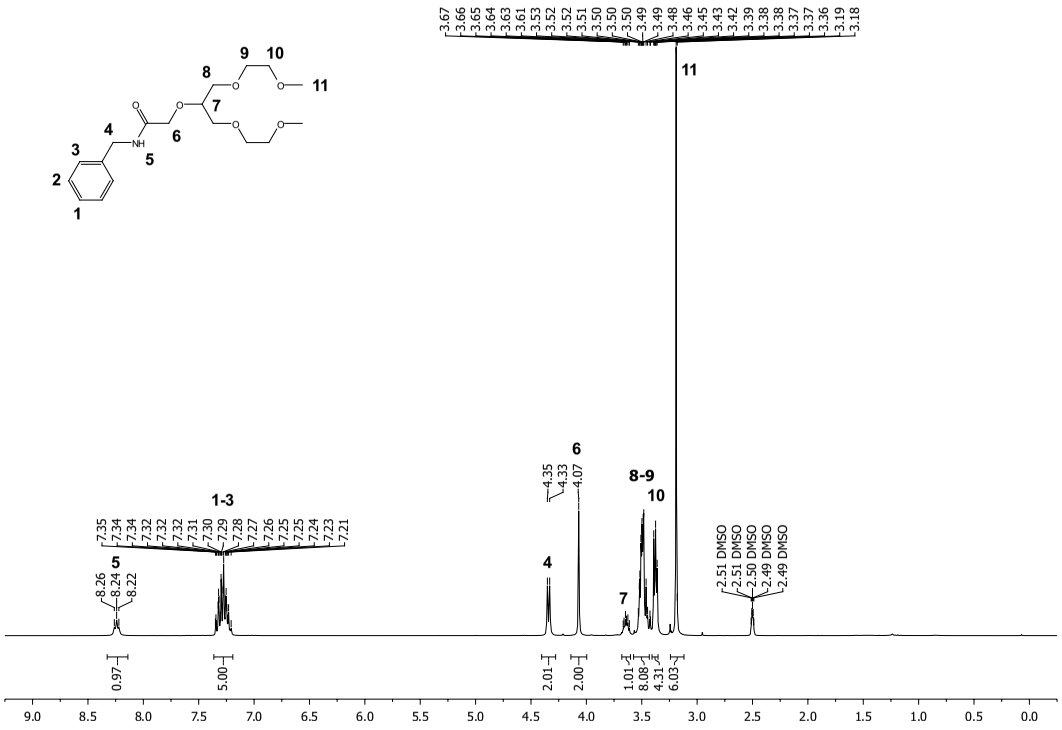

Figure 8-10: ^{1}H NMR spectrum of compound **2f** recorded in DMSO-d6 at 298 K.

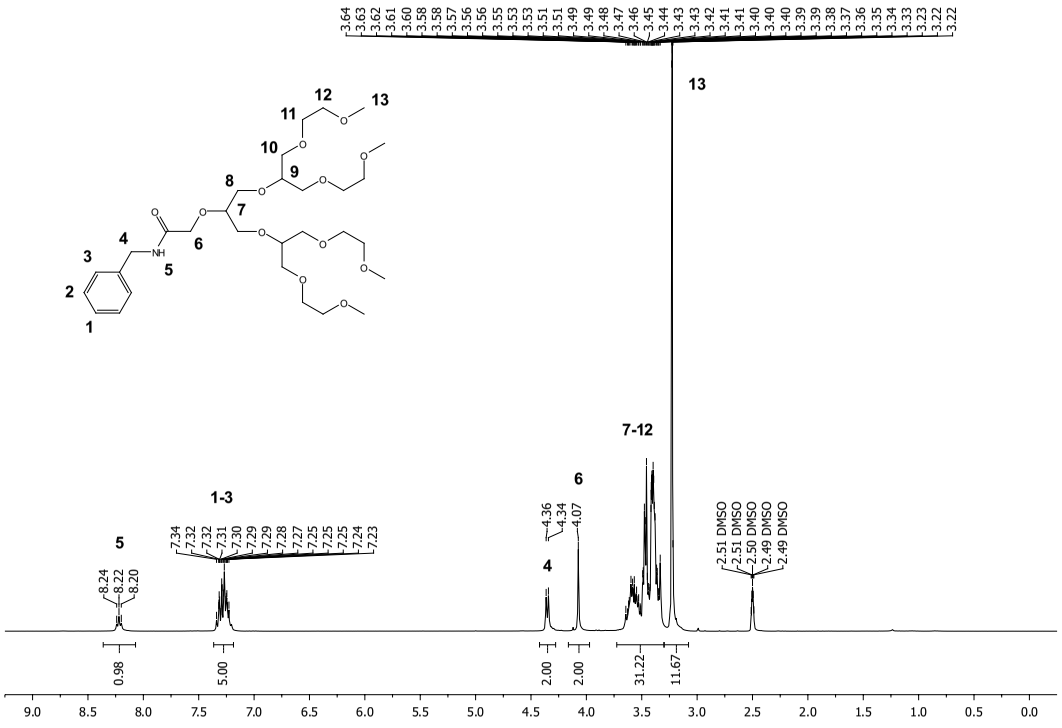

Figure 8-11: ^{1}H NMR spectrum of compound **3g** recorded in DMSO-d6 at 298 K.

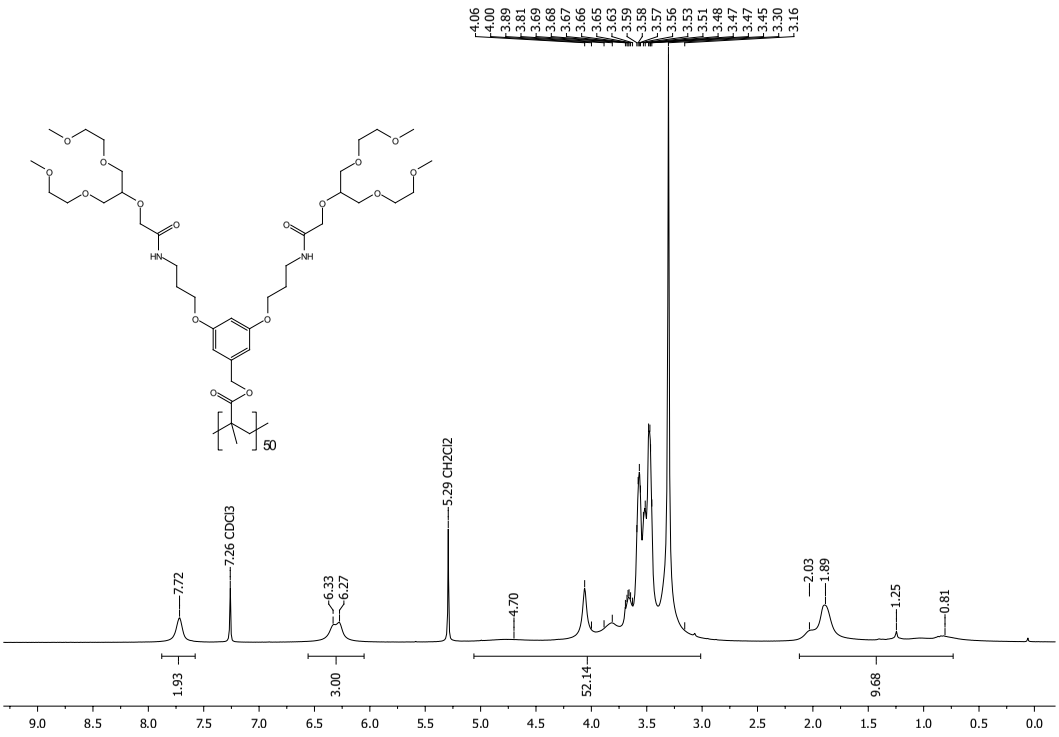

Figure 8-12: ^{1}H NMR spectrum of **H[1+1]** with $P_\mathrm{n} \approx 50$ recorded in $CDCl_3$ at 340 K.

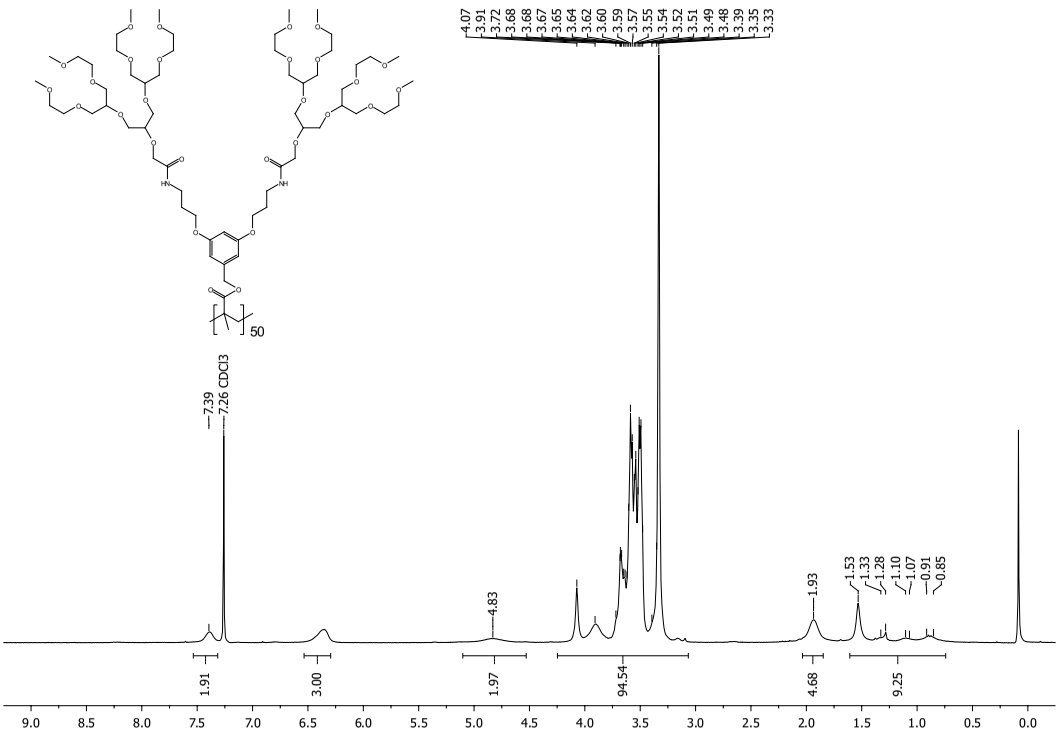

Figure 8-13: ^{1}H NMR spectrum of **H[1+2]** with $P_\mathrm{n} \approx 50$ recorded in $CDCl_3$ at 340 K.

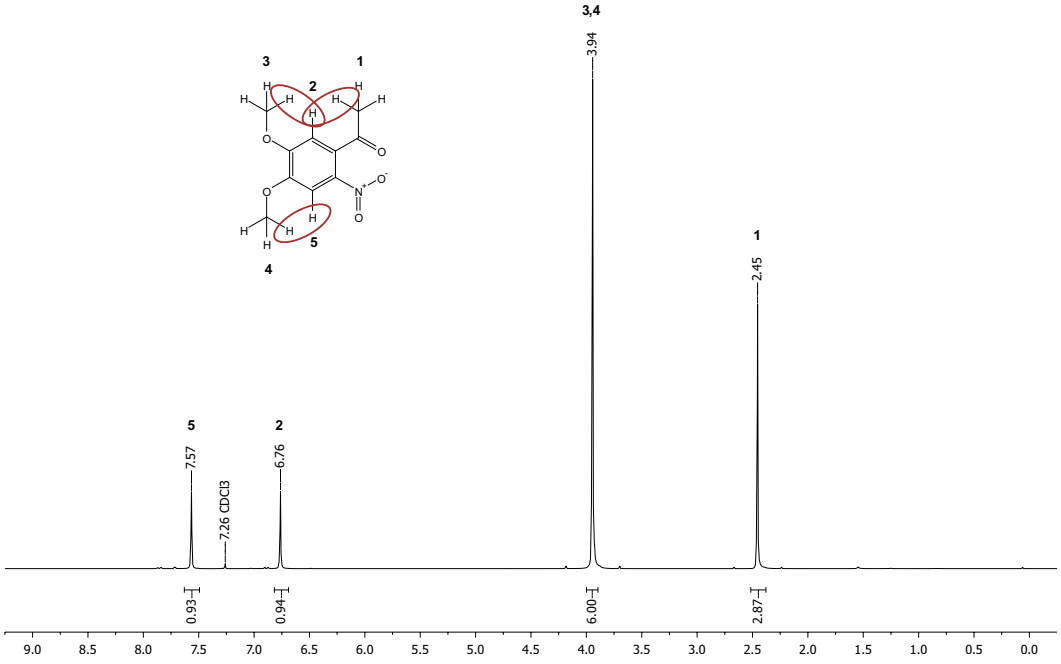

Figure 8-14: ^{1}H NMR spectrum of compound **19** recorded in $CDCl_3$ at 298 K. The ellipsoid markings are drawn to highlight the steric H – H-interactions as demonstrated in Figure 8-15.

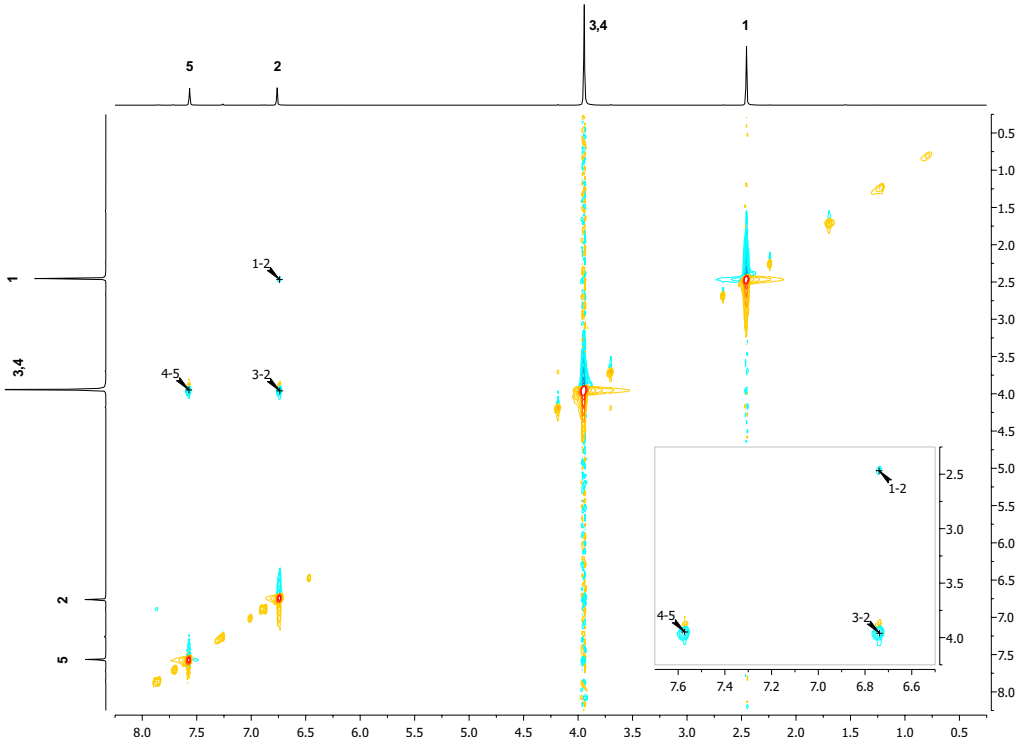

Figure 8-15: ^{1}H – ^{1}H NOESY NMR spectrum of compound **19** recorded in $CDCl_3$ at 298 K.

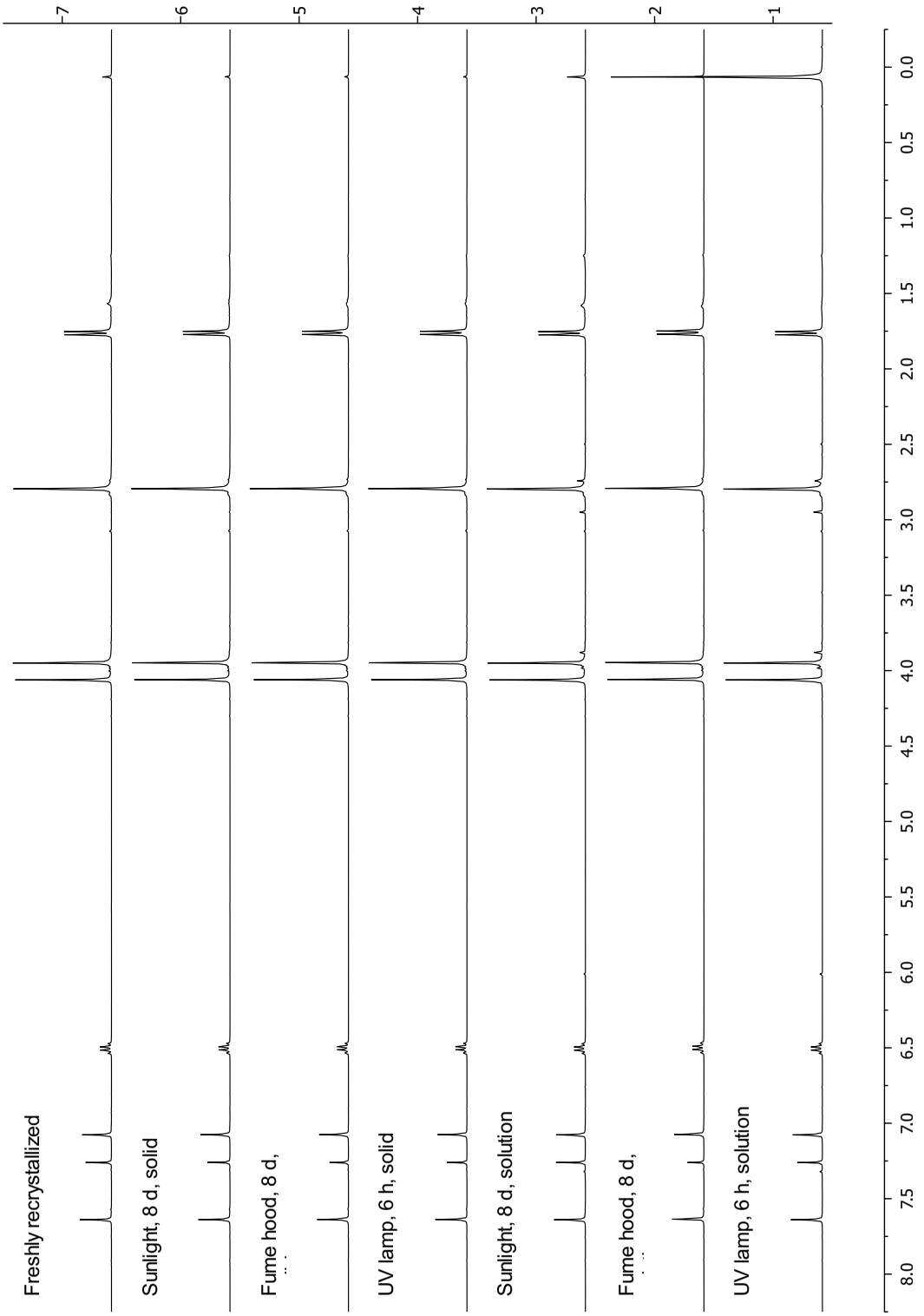

Figure 8-16: Compiled ^{1}H NMR spectra of compound **22** recorded in $CDCl_3$ at 298 K after exposure to various lighting conditions. The precise conditions are stated with the corresponding NMR spectra.

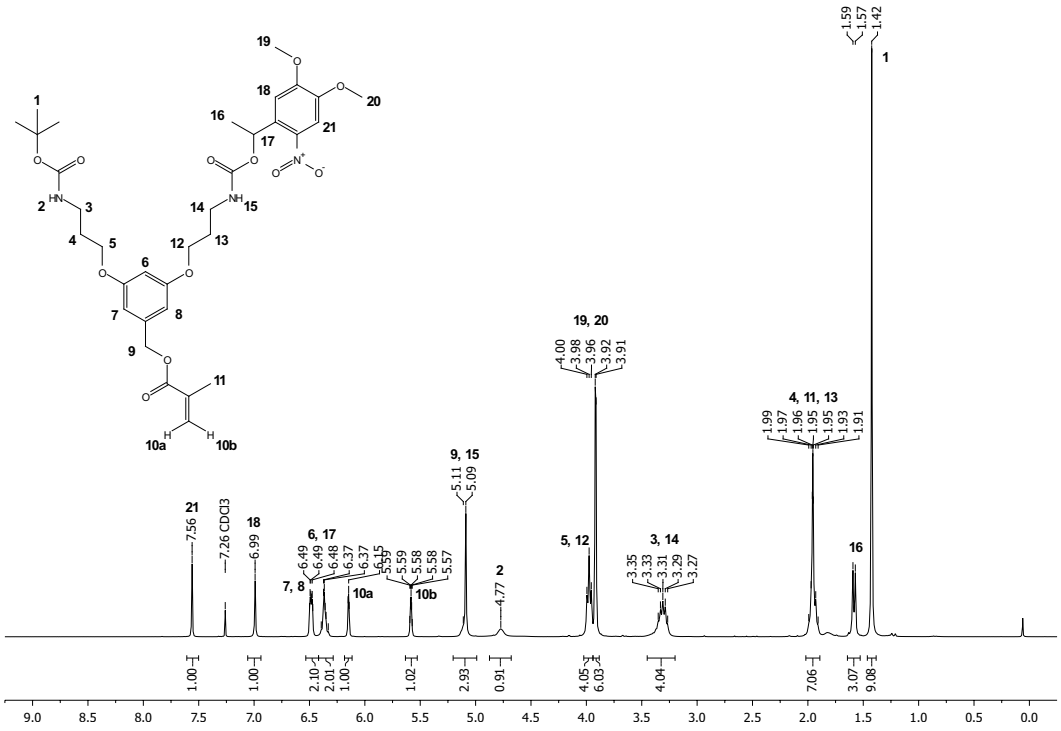

Figure 8-17: ^{1}H NMR spectrum of compound **4b** recorded in $CDCl_3$ at 298 K.

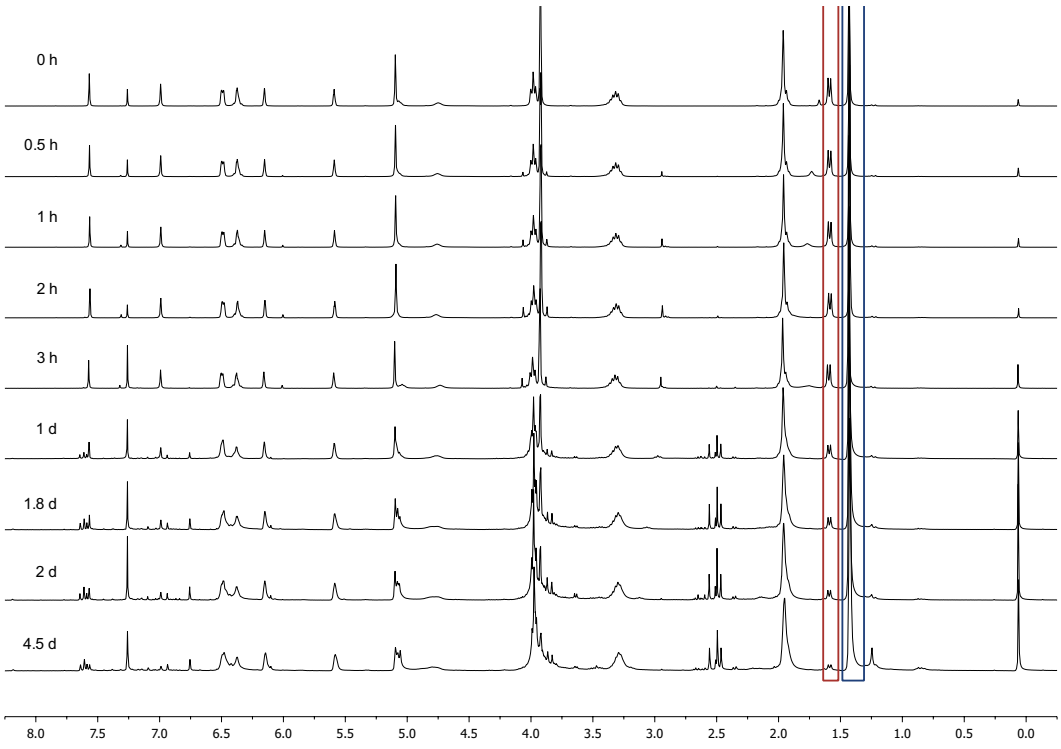

Figure 8-18: ^{1}H NMR spectra of compound **4b** recorded in $CDCl_3$ at 298K as a function of irradiation time ($\lambda_{max} = 365\,nm$, $P = 250\,mW$).

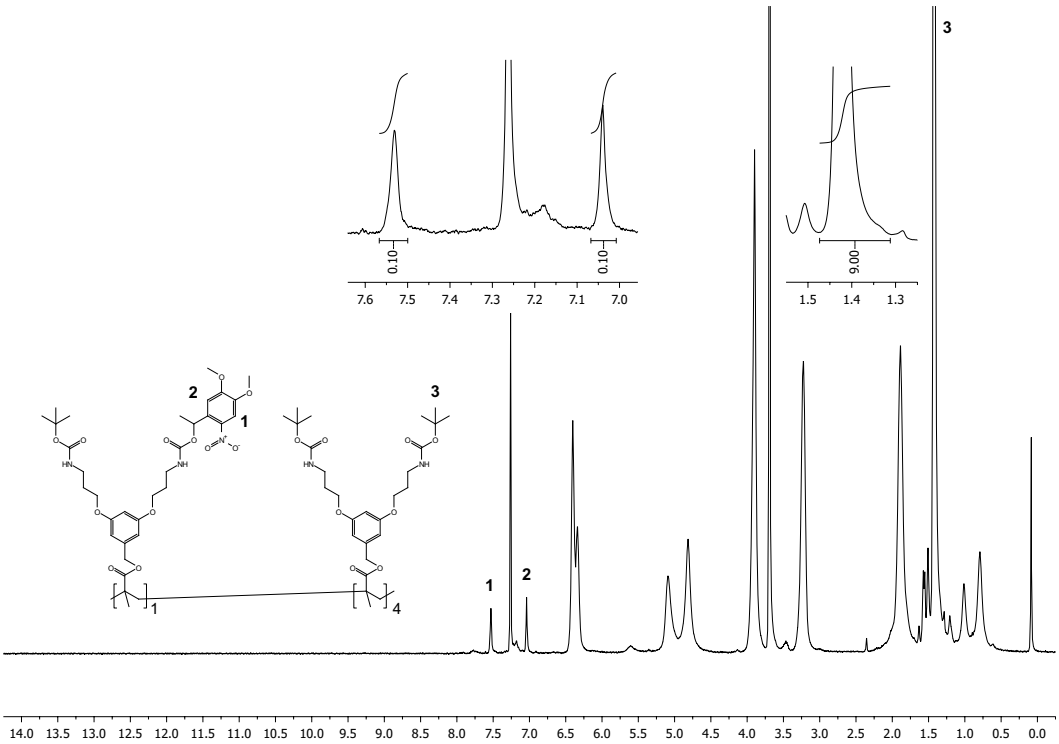

Figure 8-19: ^{1}H NMR spectrum of **PG1-MeNOVC10** recorded in $CDCl_3$ at 340K.

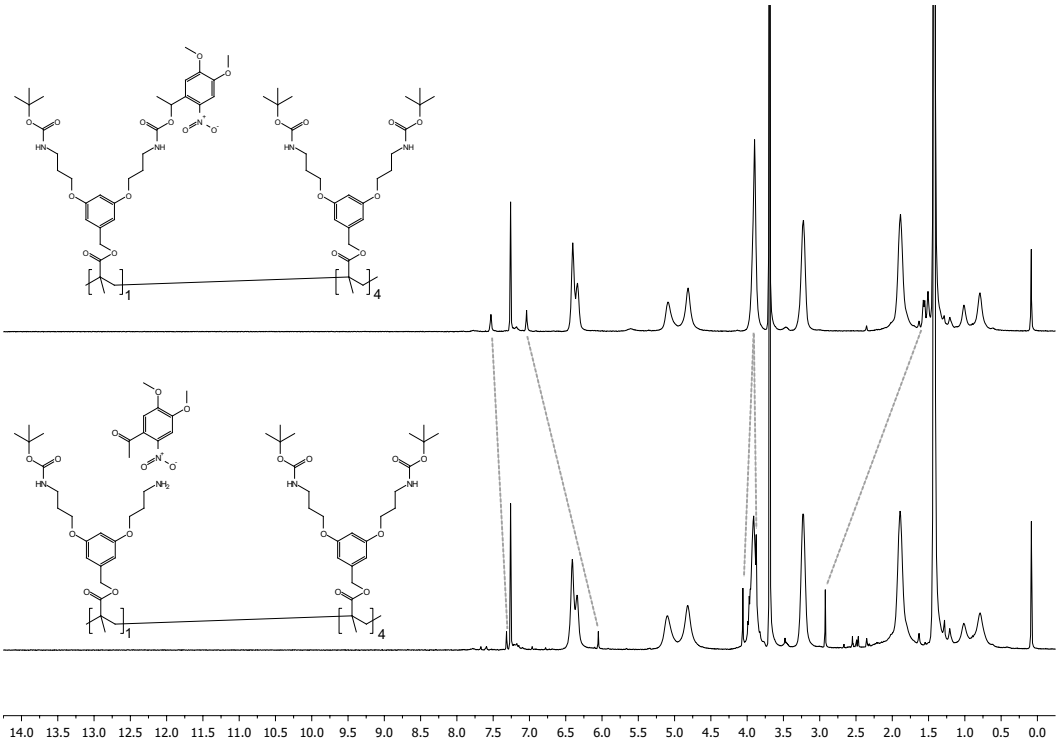

Figure 8-20: ^{1}H NMR spectra of **PG1-MeNVOC10** recorded in $CDCl_3$ at 340K. The spectra were recorded before (top) and after (bottom) irradiation at $\lambda_{max} = 365\,\text{nm}$, $P = 250\,\text{mW}$ for 2.5 d directly in the NMR tube.

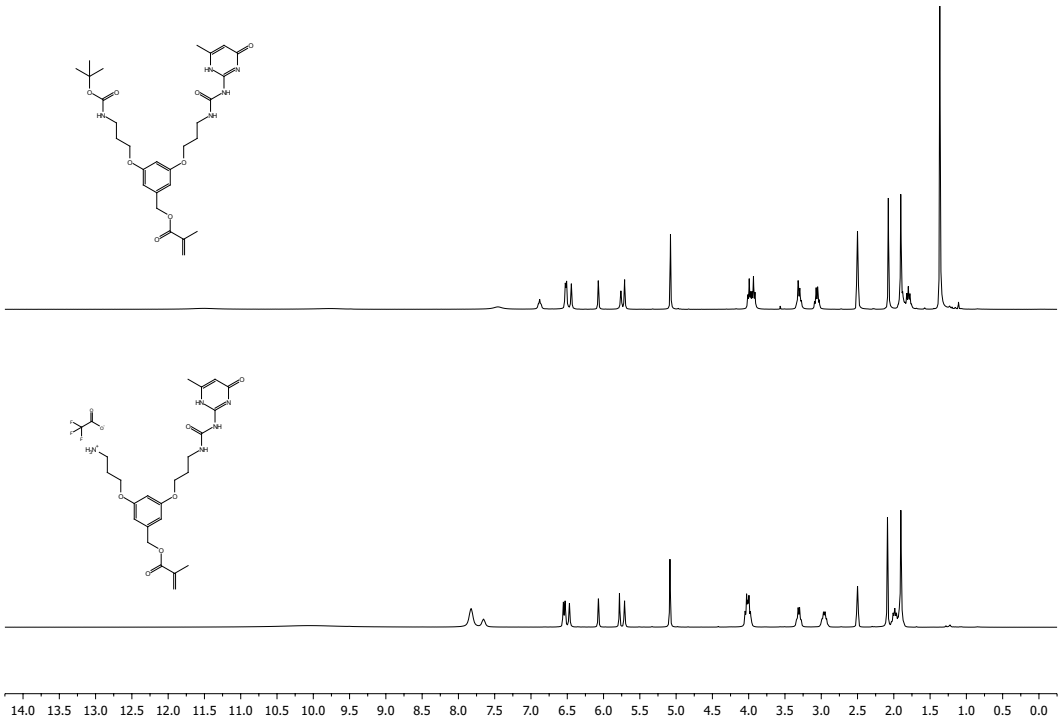

Figure 8-21: ^{1}H NMR spectra of compound **4c** recorded in DMSO-d6 at 298 K before (top) and after (bottom) deprotection of NHBoc with TFA.

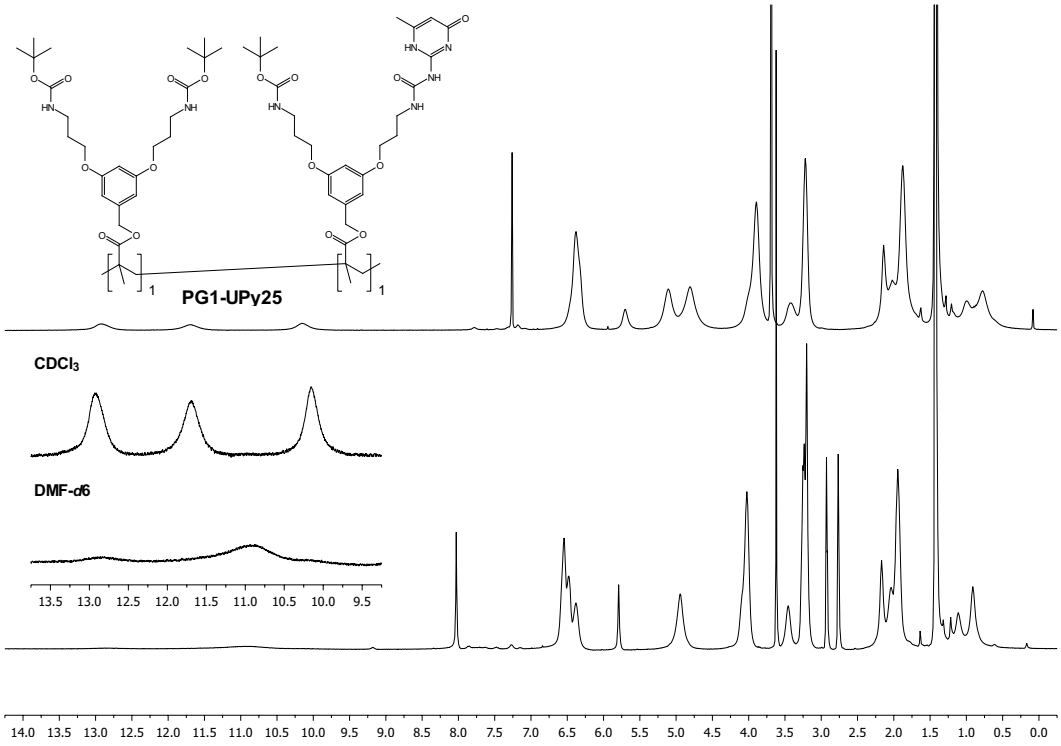

Figure 8-22: ^{1}H NMR spectra of **PG1-UPy25** recorded in $CDCl_3$ (top) and DMF-*d*6 (bottom) at 340 K.

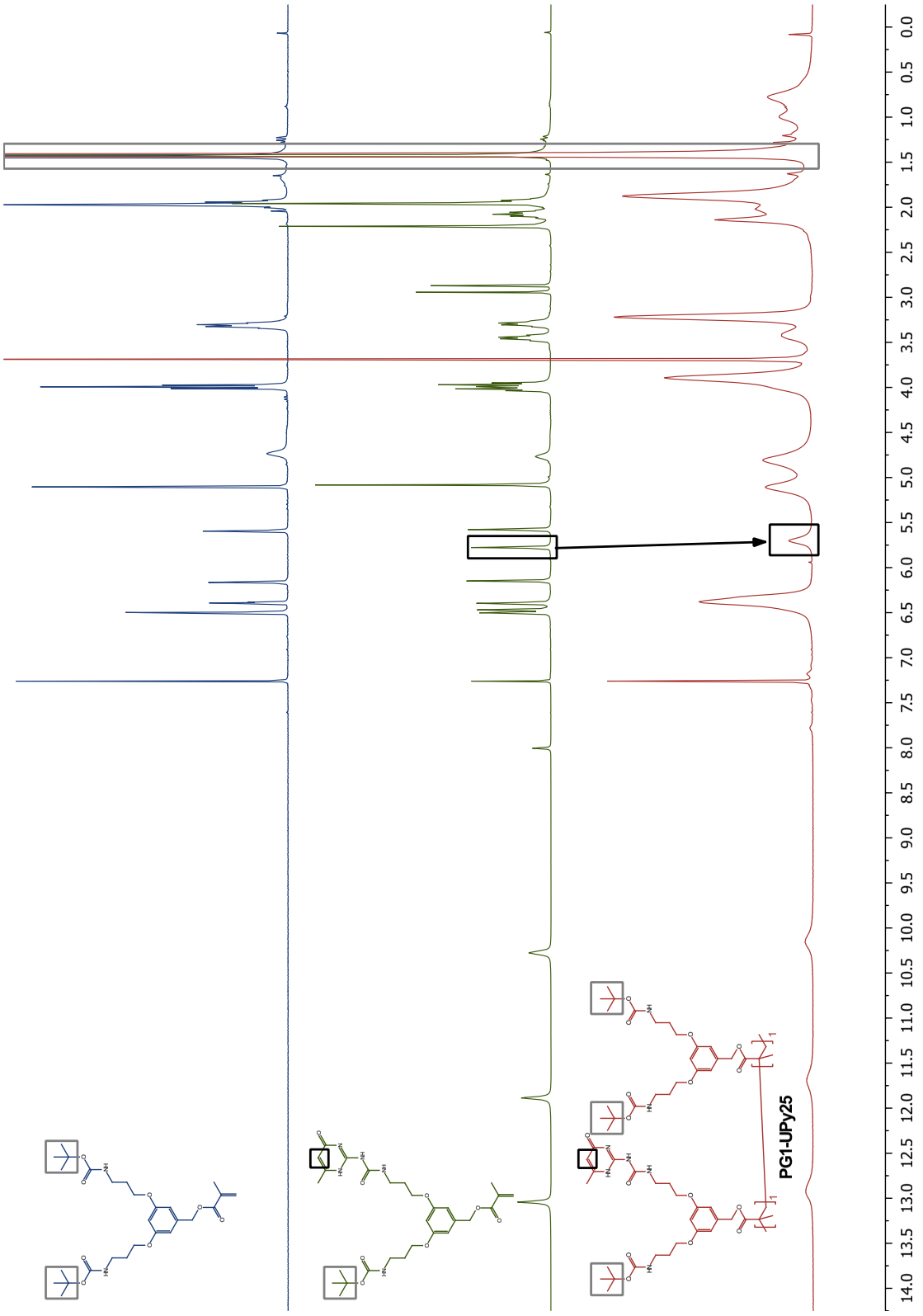

Figure 8-23: ^{1}H NMR spectra of compounds **1c** (top, blue), **4c** (middle, olive) and **PG1-UPy25** (bottom, red) recorded in $CDCl_3$ at 298 K. The framed peak areas at $\delta \approx 1.4$ and 5.7 ppm correspond to the allylic proton of UPy (black) and ^{tert}butyl of Boc (gray), respectively.

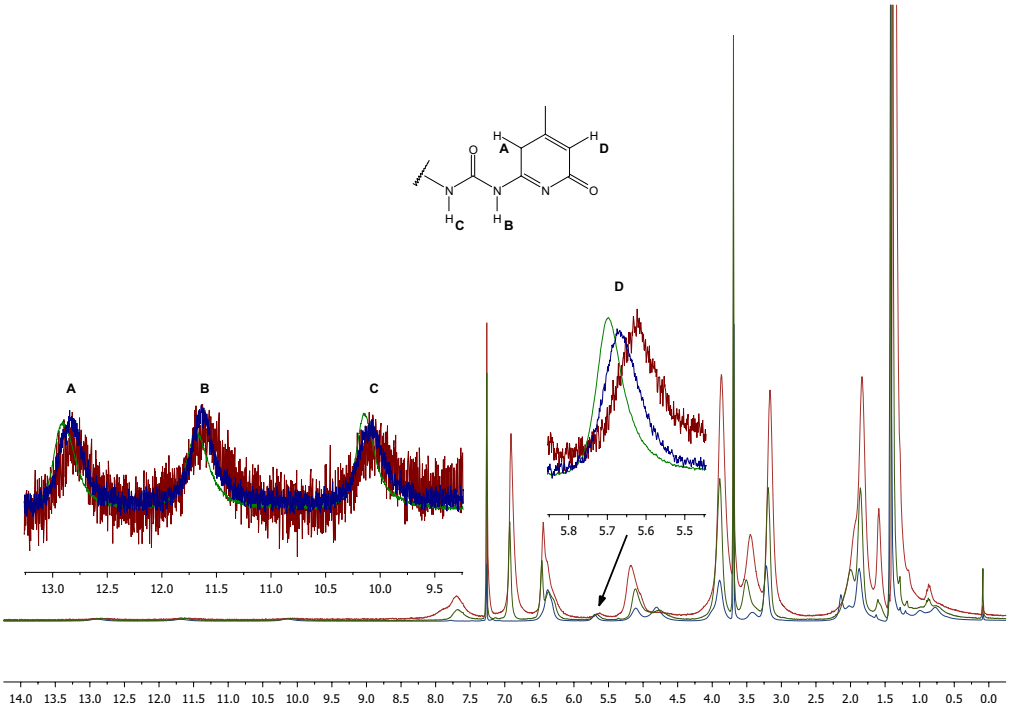

Figure 8-24: ^{1}H NMR spectra of **PG1-UPy25** (olive), **PG2-UPy25** (blue) and **PG3-UPy25** (red) recorded in $CDCl_3$ at 340 K. The magnified inset in the range of $\delta \approx 13.0 - 9.5$ ppm depicts the intensity of UPy signals A – C obtained by normalization of UPy signal D located in the range of $\delta \approx 5.8 – 5.5$ ppm.

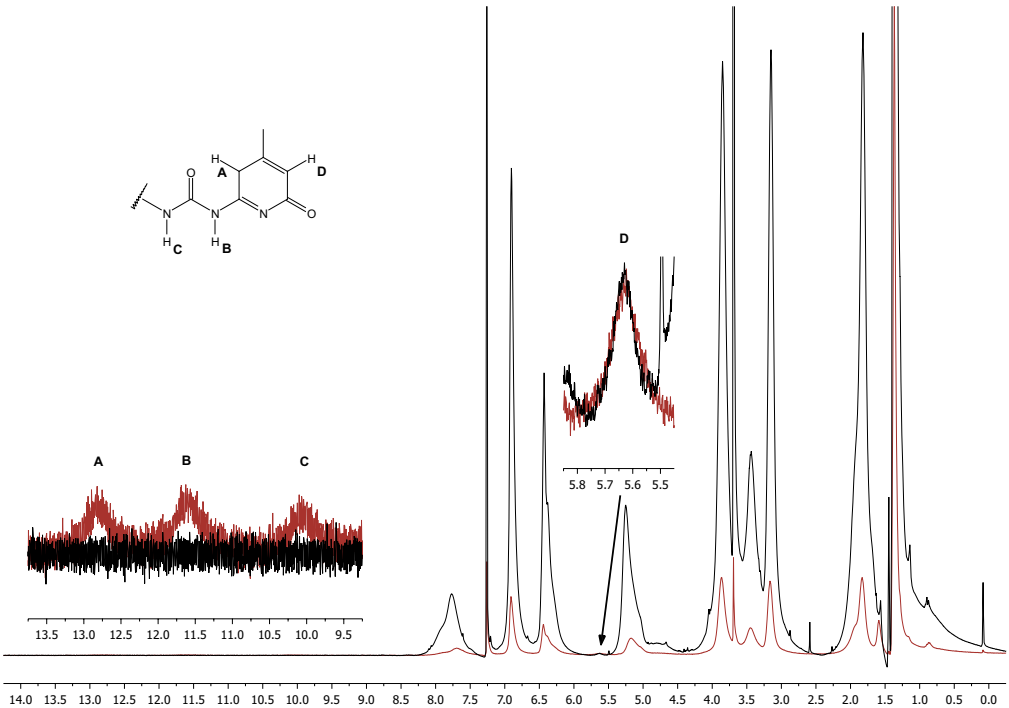

Figure 8-25: ^{1}H NMR spectra of **PG3-UPy5** (black) and **PG3-UPy25** (red) recorded in $CDCl_3$ at 340 K. The magnified inset in the range of $\delta \approx 13.2 - 9.3$ ppm depicts the intensity of UPy signals A – C obtained by normalization of UPy signal D located in the range of $\delta \approx 5.8 – 5.5$ ppm.

8.4 Supplementary TGA curves

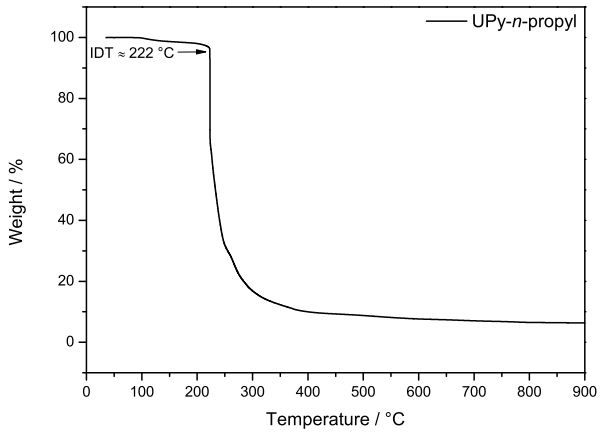

Figure 8-26: Thermal degradation curve of **29** recorded at a heating rate of 20 °C min^{-1} in N_2.

8.5 Supplementary UV-Vis spectra

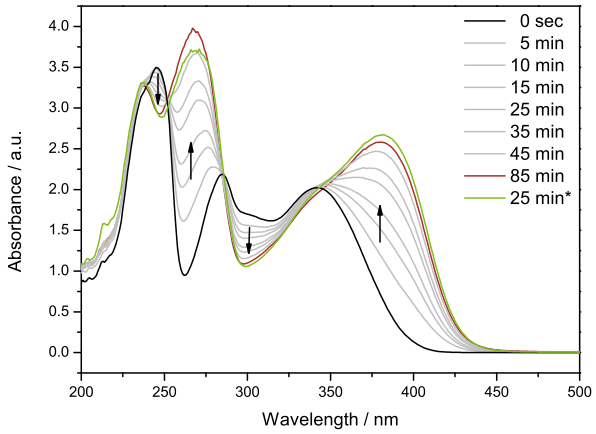

Figure 8-27: UV-Vis spectra of **4b** recorded in THF with and without (*) the addition of *bis*(pinacolato)diboron scavenger as a function of irradiation time at $\lambda_{max} = 365\,nm$.

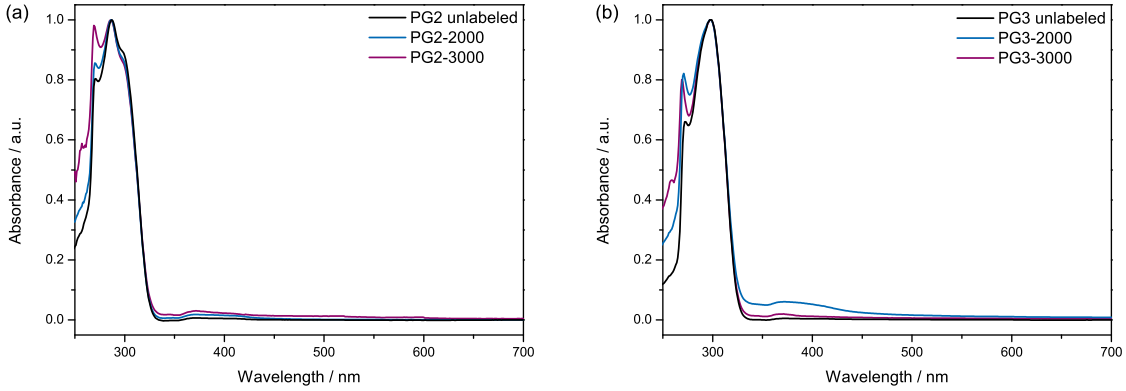

Figure 8-28: UV-Vis spectra of **PG2** (a) and **PG3** (b) $P_n \approx 2000, 3000$ recorded in TCE before and after labeling with Sanger's reagent.

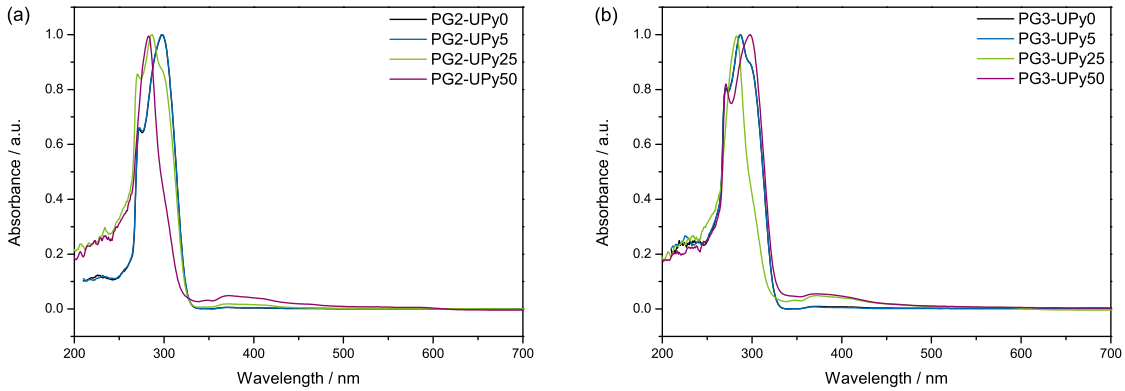

Figure 8-29: UV-Vis spectra of **PG2** (a) and **PG3** (a) with $P_n \approx 40$ and 0, 5, 25, and 50 mol% UPy recorded in TCE after labeling with Sanger's reagent.

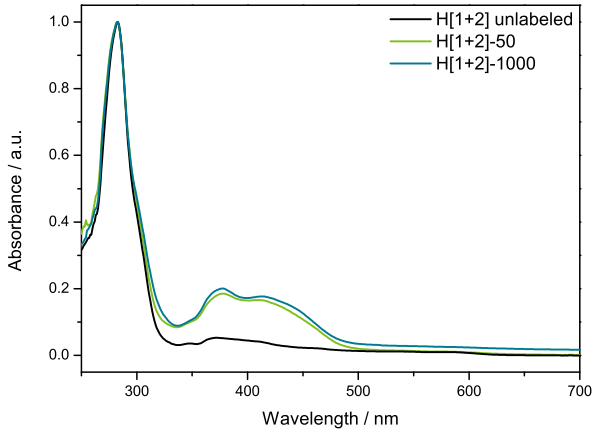

Figure 8-30: UV-Vis spectra of **H[1+2]** with $P_n \approx 50$, 1000 recorded in TCE before and after labeling with Sanger's reagent.